Understanding Primary Organic Aerosol Volatility at Atmospherically Realistic Concentrations for SIP Analysis

REPORT TO THE

California Air Resources Board Research Division

Project # 10-313

Prepared by:

Dr. Michael J. Kleeman[1]
Dr. Christopher D. Cappa[1]
Dr. Qi Zhang[2]
Dr. Timothy H. Bertram[3]

[1]Department of Civil and Environmental Engineering
[2]Department of Environmental Toxicology
University of California, Davis
One Shields Avenue, Davis, CA, 95616

[3]Department of Chemistry and Biochemistry
University of California, San Diego
San Diego, CA, 92093

February 19, 2014

DISCLAIMER

The statements and conclusions in this report are those of the contractor and not necessarily those of the California Air Resources Board. The mention of commercial products, their source, or their use in connection with material reported herein is not to be construed as actual or implied endorsement of such products.

Portions of this work were funded by US Department of Energy (DOE), Atmospheric System Research Program, Grant No. DE-FG02-11ER65293.

ACKNOWLEDGEMENTS

The measurements and analysis described in this report were largely conducted by graduate students and postdoctoral scholars with guidance from their faculty mentors. In many cases, these students and postdocs are the lead authors of individual chapters submitted for publication in peer-reviewed journals. The student and postdoc scholar team consisted of the following individuals:

Toshihiro Kuwaya – graduate student researcher, CEE Dept, UC Davis
Sara Forestieri – graduate student researcher, CEE Dept, UC Davis
Isabel Faria – postdoctoral research scholar, CEE Dept, UC Davis
Sonya Collier – postdoctoral research scholar, Etox Dept, UC Davis
James Brady – graduate student researcher, Chem Dept, UC San Diego
Timia Crisp – graduate student researcher, Chem Dept, UC San Diego

The authors would like to thank Nehzat Motallebi (CARB) for grant management support.

The authors thank Mang Zhang and the team of engineers at the Haagen-Smit Vehicle Testing Facility for help with vehicle procurement and testing as well as Sulekha Chattopadhyay for help with analysis of criteria pollutant emissions.

The authors thank Dr. Kyaw Tha Paw U (UC Davis) for lending us the Licor CO_2 analyzer.

TABLE OF CONTENTS

LIST OF TABLES

LIST OF FIGURES

LIST OF ACRONYMS

AB32 - California State Assembly Bill 32
ACPI - Accelerated Climate Prediction Initiative
AIM - Aerosol Inorganic Model
AMS – Aerosol Mass Spectrometer
BCs - boundary conditions
BenMAP - Benefits Mapping model from USEPA
BVOC - biogenic volatile organic compounds
CACM - Caltech Atmospheric Chemistry Model
CARB - California Air Resources Board
CCAQS - California Ambient Air Quality Standards
CCSM - Community Climate System Model
CI - confidence interval
CIT - California Institute of Technology
CMAQ - Community Multiscale Air Quality model from USEPA
DFP – Denuder Filter PUF
EC - elemental carbon
EMFAC - Emissions Factor Model maintained by CARB
HOA – Hydrocarbon-like Organic Aerosol
ICs - initial conditions
LAC - Los Angeles County
NH_4^+ / N(-III) - ammonium
NO_3^- / N(V) - nitrate
NOx - oxides of nitrogen
O_3 - ozone
OC - organic carbon
OH - hydroxyl radical
OOA – Oxygenated Organic Aerosol
PAS – PhotoAcoustic Spectrometer
$PM_{0.1}$ - Airborne particle mass with aerodynamic diameter less than 0.1 µm.
PM_{10} - Airborne particle mass with aerodynamic diameter less than 10.0 µm.
$PM_{2.5}$ - Airborne particle mass with aerodynamic diameter less than 2.5 µm.
PM - Airborne particulate matter
PN - particulate nitrate
PUF – PolyUrethane Foam
RMSE - Root Mean Square Error
RN - reactive nitrogen
SCAQMD - South Coast Air Quality Management District
SCAQS - Southern California Air Quality Study
SJV - San Joaquin Valley Air Basin
SO_4^{2-} / S(VI) - sulfate
SoCAB - South Coast Air Basin
SOP - Standard Operating Procedure

SV - Sacramento Valley Air Basin
UCB - University of California at Berkeley
UCD - University of California at Davis
UCSD - University of California at San Diego
USEPA - United States Environmental Protection Agency
UV - Ultraviolet radiation
VOC - volatile organic compounds

ABSTRACT

This report explores the volatility of primary organic aerosol (POA) emitted from light duty gasoline-powered vehicles at atmospherically relevant concentrations using state of the science instrumentation. Existing POA partitioning models were tested through analysis of emissions changes that result from perturbations to the dilution air used during vehicle sampling. Measurements were re-interpreted with the application of new theoretical models that can be extended to regional-scale modeling applications.

Emissions from a fleet of 8 gasoline vehicles operated on the UC driving cycle were characterized by (1) thermal-optical measurements of filter-collected organic carbon and elemental carbon, (2) GC-MS analysis of denuder-filter-PUF samples, (3) high resolution Aerosol Mass Spectrometer (HR-AMS) measurements for organic mass and the bulk and elemental compositions of organic species, (4) Time-of-Flight Chemical Ionization Mass Spectrometer (ToF CIMS) measurements of gas-phase concentrations and elemental compositions of carbonyls, alcohols, ketones and organic acids, and (5) multi-wavelength photoacoustic spectrometer (PAS) measurements of black carbon (BC). Vehicle exhaust was diluted to atmospherically relevant concentrations as different features of the dilution air were perturbed: temperature (25-100^{o}C), relative humidity (55-85%), and background black carbon particles concentrations (0-25±5 μg m^{-3}).

The majority (~75-80%) of the particle phase emissions from the vehicle fleet were categorized as non-volatile elemental carbon (EC) that will not evaporate in the atmosphere. Real-time measurements show that the highest EC emissions occurred during the cold-start portion of the test and/or during periods of hard acceleration. The remaining fraction (~20-25%) of the particle phase emissions was POA that could be broadly classified as a semi-volatile material (similar to motor oil) or an effectively non-volatile material (hypothesized to be fuel combustion products). The POA emissions were generally more volatile during the cold start portion of the driving cycle and less volatile after the engine and exhaust system reached operating temperature. Emissions of semi-volatile and non-volatile organic carbon from different vehicles could not be predicted a-priori. Half of the tested vehicles in the current study had emissions dominated by motor oil while the other half of the vehicles had emissions dominated by fuel combustion products. Further tests are needed using the methodology developed in this report to develop fleet wide characterization of the emissions of both types of POA for use in future regional modeling applications.

The prevalence of carbonyl species in the POA suggests that these species may be basic building blocks that are transformed into non-volatile POA as the vehicle exhaust ages. Carbonyl emissions increased with humidity suggesting an aqueous production pathway. Increased levels of black carbon in the dilution air scavenged carbonyl precursors and reduced total carbonyl production rates. The AMS may categorize the low-volatility POA (possibly associated with carbonyls) as refractory material that is not reported. Emissions of carbonyl oxidation products (acids) peaked during the cold-start portion of the driving cycle and had a strong correlation to NOx emissions.

EXECUTIVE SUMMARY

Background: Emissions tests have determined that primary organic aerosol (POA) generated from combustion sources behaves like a series of semi-volatile compounds when the particulate phase concentrations range between 100 – 10,000 µg m^{-3} [1]. More recent models fit to measurements of POA emitted from gasoline powered vehicles predict that POA is semi-volatile and will largely evaporate given sufficient time in the atmosphere. These conclusions are not supported by measurements of oxygenated organic species (carbonyls) emitted by gasoline vehicles. A follow-up study was needed to reconcile these differences.

Methods: Emissions from a fleet of 8 gasoline vehicles operated on the UC driving cycle were characterized by (1) thermal-optical measurements of filter-collected organic carbon and elemental carbon, (2) GC-MS analysis of denuder-filter-PUF samples, (3) high resolution Aerosol Mass Spectrometer (HR-AMS) measurements for organic mass and the bulk and elemental compositions of organic species, (4) Time-of-Flight Chemical Ionization Mass Spectrometer (ToF CIMS) measurements of gas-phase concentrations and elemental compositions of carbonyls, alcohols, ketones and organic acids, and (5) multi-wavelength photoacoustic spectrometer (PAS) measurements of black carbon (BC). The dilution air was perturbed by increasing the humidity from 55% to 85% and increasing the concentration of black carbon from 0 to 25±5 µg m^{-3} (Table 1). Temperatures were perturbed by amounts up to 100°C prior to sample collection. Multiple partitioning theories were applied to the results in order to better understand the portioning mechanisms for POA.

Table 1: Four unique experimental conditions tested.

Target Test Condition Matrix	
Base Condition RH = 55% Background EC = 0 µg m^{-3}	Adjusted RH RH = 85% Background EC = 0 µg m^{-3}
Adjusted EC RH = 55% Background EC = 25±5 µg m^{-3}	Adjusted EC+RH RH = 85% Background EC = 25±5 µg m^{-3}

Results: $PM_{2.5}$ mass emissions rates from the test fleet measured using the denuder-filter-PUF system had a median value of 0.44 mg $mile^{-1}$. $PM_{2.5}$ mass emissions rates measured using real-time instruments had a median value of 0.11 mg $mile^{-1}$. The discrepancy between the two measurement techniques largely stems from the classification of some emissions as refractory material by HR-AMS but as POA by the denuder-filter-PUF system.

The real-time instruments indicate that emissions rates varied strongly within a driving cycle and between vehicles. The majority (75-80%) of the emitted PM was classified as elemental carbon (EC) (Figure 1) with approximately 20-25% classified as OC (a component of POA) (Figure 2). Both EC and POA emissions were highest during the cold-start portion of the driving cycle and/or during periods of hard accelerations. Averaged across the entire test fleet, only 30% of the POA evaporated when the temperature was raised to 100°C during the cold-start and <20% of the POA evaporated under heating during other portions of the driving cycle (Figure 2). The chemical nature of the POA clearly changes during different phases of the driving cycle.

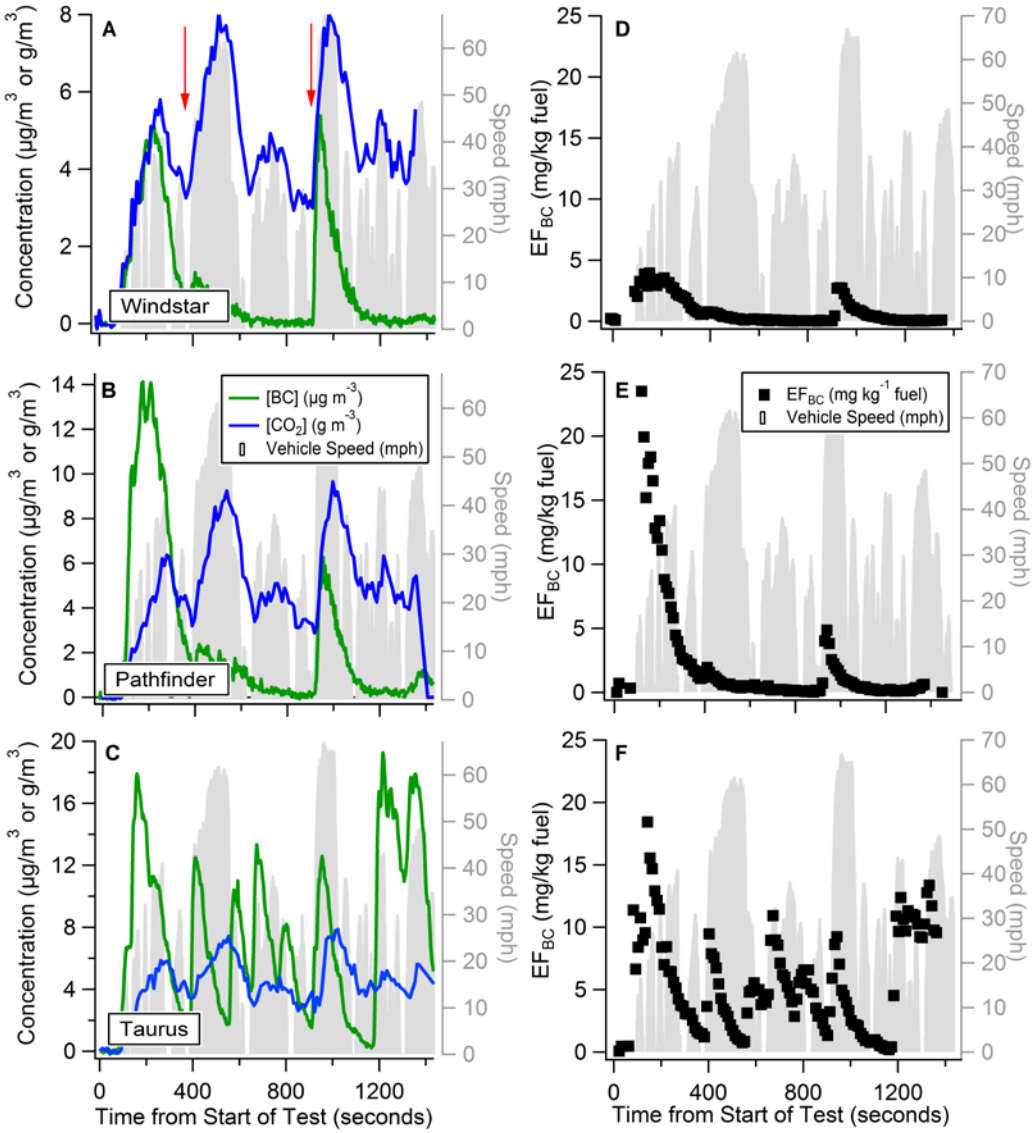

Figure 1: Real-time BC (green lines) and background-subtracted CO2 (blue lines) concentrations (A-C) and emission factors (black points; D-F) during a base case UC test on Sept. 20th for three LEVs: (A,D) Ford Windstar, (B,E) Nissan Pathfinder and (C,F) Ford Taurus.

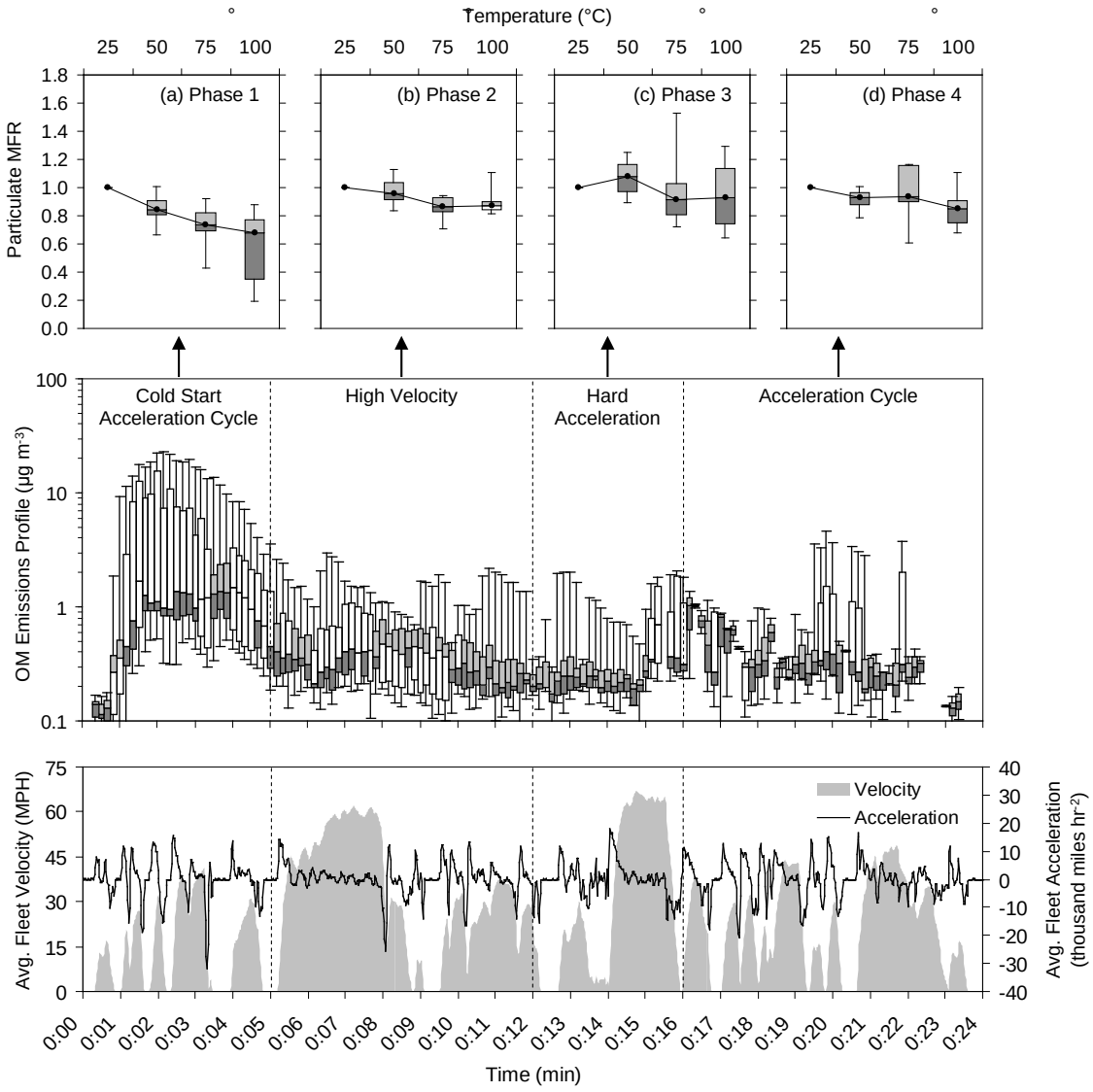

Figure 2: Top panel: mass fraction remaining of organic aerosol at different temperatures within different portions of the UC driving cycle. Middle panel: POA concentrations measured using HR-AMS. Bottom panel: driving cycle speed (gray regions) and acceleration (line).

A partitioning model based on a single component – similar to motor oil – fits the median POA partitioning behavior but does a poor job of explaining the full range of measured POA volatility (Figure 3, 4a). A partitioning model based on two components that have different volatility distributions – one similar to motor oil and one interpreted as non-volatile fuel combustion products – is able to explain the observed POA partitioning behavior with high accuracy (R^2=0.94 when intercept not fixed to zero) (Figure 4b). Measurements suggest that half the vehicle fleet tested had POA emissions dominated by

motor oil while the other half had POA emissions dominated by fuel combustion products.

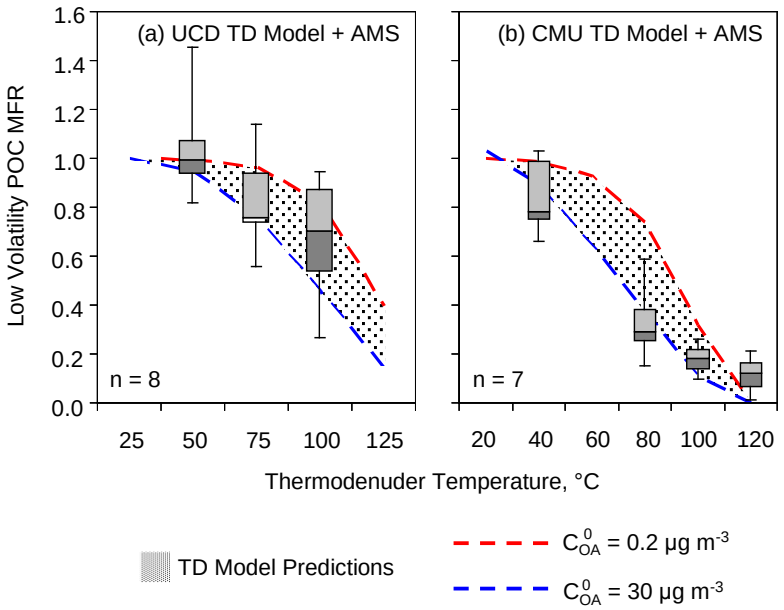

Figure 3: Thermal denuder model fit to measured OC mass fraction remaining (MFR) at increasing temperatures. Residence time in heated section is (a) 1 sec and (b) 30 sec. Scatter about the median response line accounts for the weak correlation coefficient.

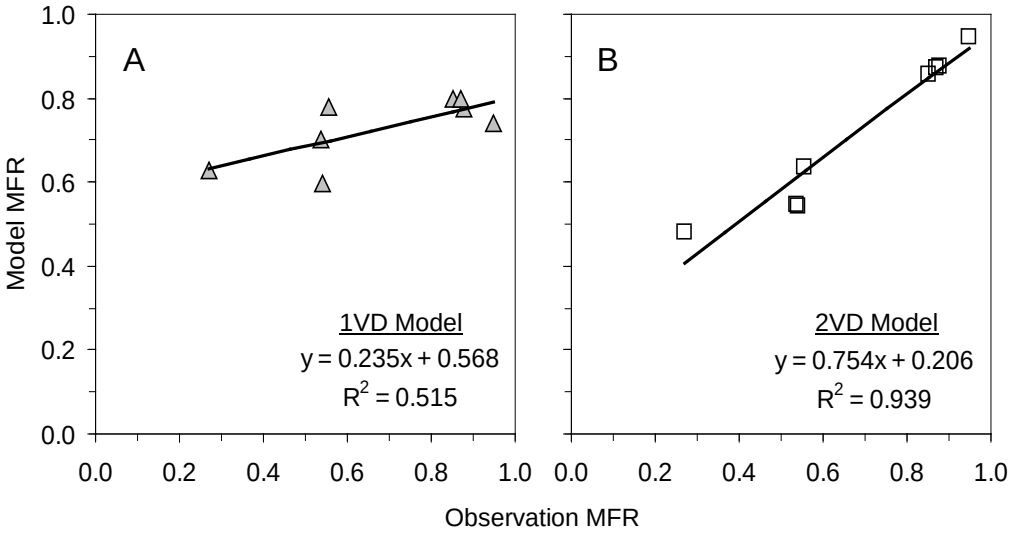

Figure 4: Predicted (vertical axis) vs. observed (horizontal axis) POA mass fraction remaining (MRF) for (a) a single volatility distribution and (b) two volatility distributions.

Speciation measurements show that 13-40% of the POA is composed of carbonyl species depending on test conditions. Higher humidity increased the total (gas+particle) carbonyl emissions rates due to increased aqueous reaction volume while higher EC in the dilution air lowered the carbonyl emissions rates due to scavenging of the precursor compounds (Figure 5). It is likely that carbonyls are related to the fuel combustion POA given their abundance in the emissions.

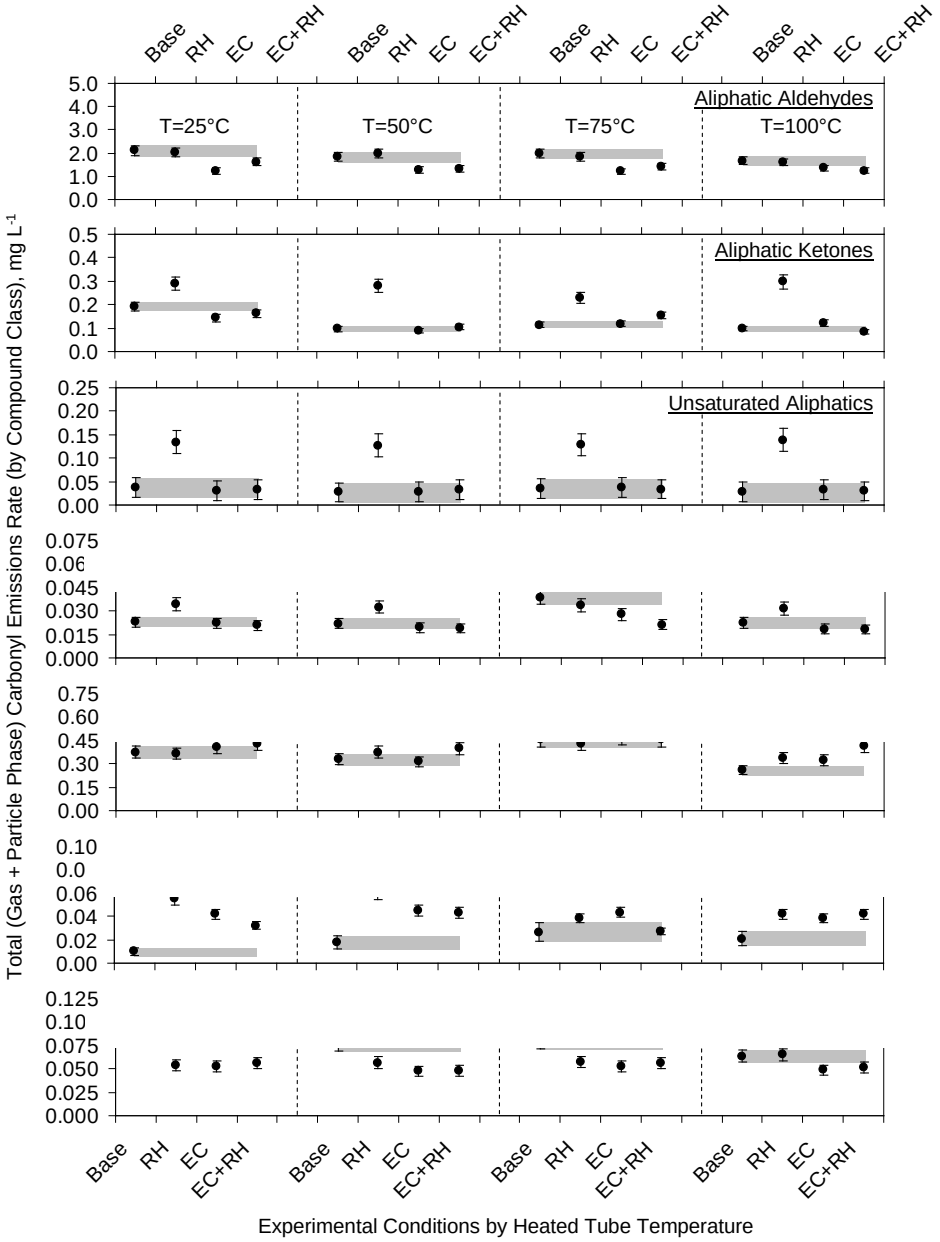

Figure 5: Total production trends for carbonyl compound classes under variable, atmospherically relevant conditions shown for sample legs heated to T = 25, 50, 75, and 100°C. Refer to Table 1 for experimental condition descriptors.

Total (gas+particle phase) carbonyl emissions rates decreased in 2011 vs. 2002 but condensed phase carbonyl emissions rates increased due to increased partitioning of aliphatic compounds to the condensed phase. The most abundant gas-phase carbonyl species detected was octanal. The most abundant particle-phase carbonyl species detected was propanal. It is very likely that propanal acts as the building block for a more complex form of condensed-phase POA.

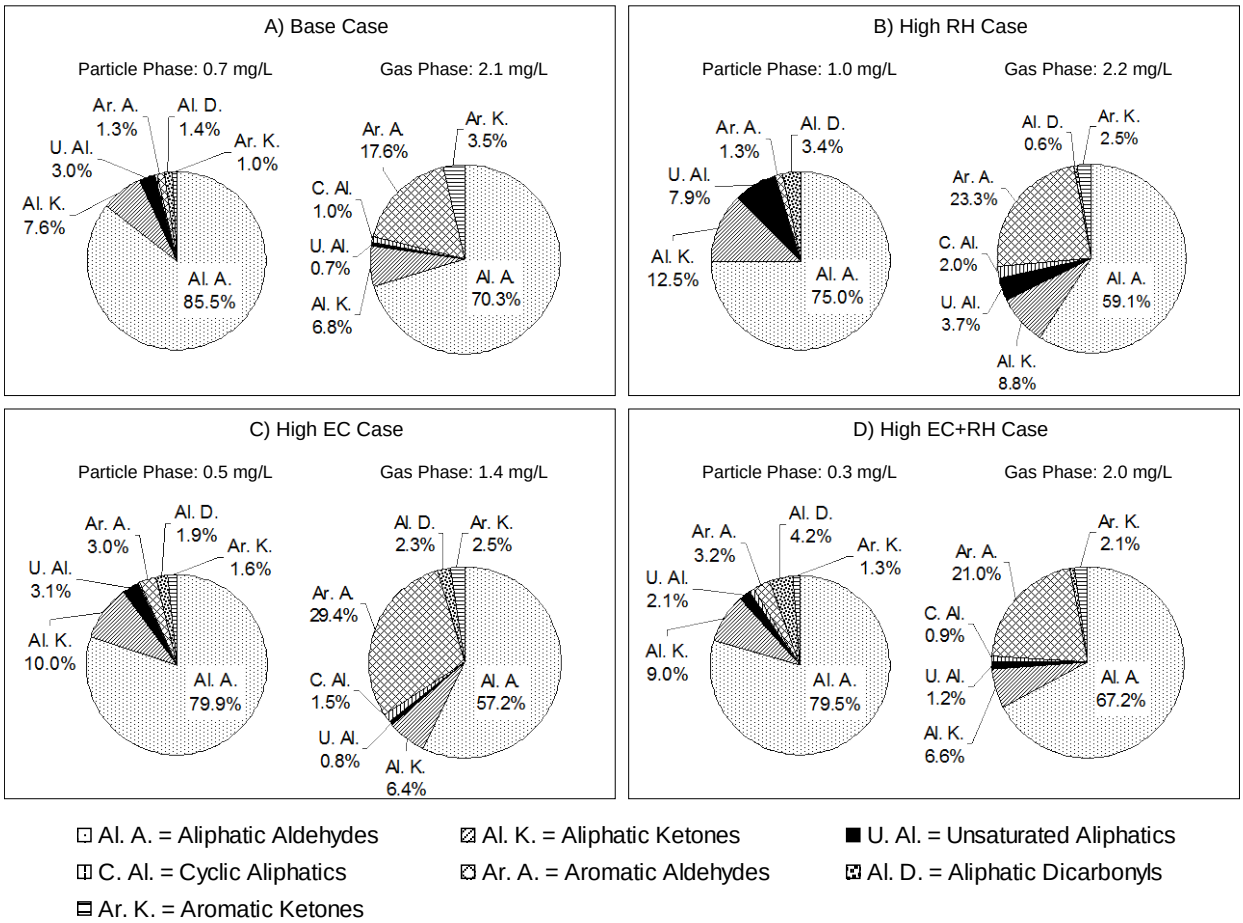

Figure 6: Gas-particle partitioning and speciation of gasoline carbonyl emissions at variable atmospheric conditions: (a) base case, (b) high RH, (c) high EC, (d) high EC+RH.

Real-time measurements quantified gas-phase propionic acid which is a direct oxidation product of propanal (the most abundant condensed-phase carbonyl building block). Emissions of propionic acid appear to peak during the cold-start portion of the driving cycle with a high correlation to NOx emissions (Figure 7).

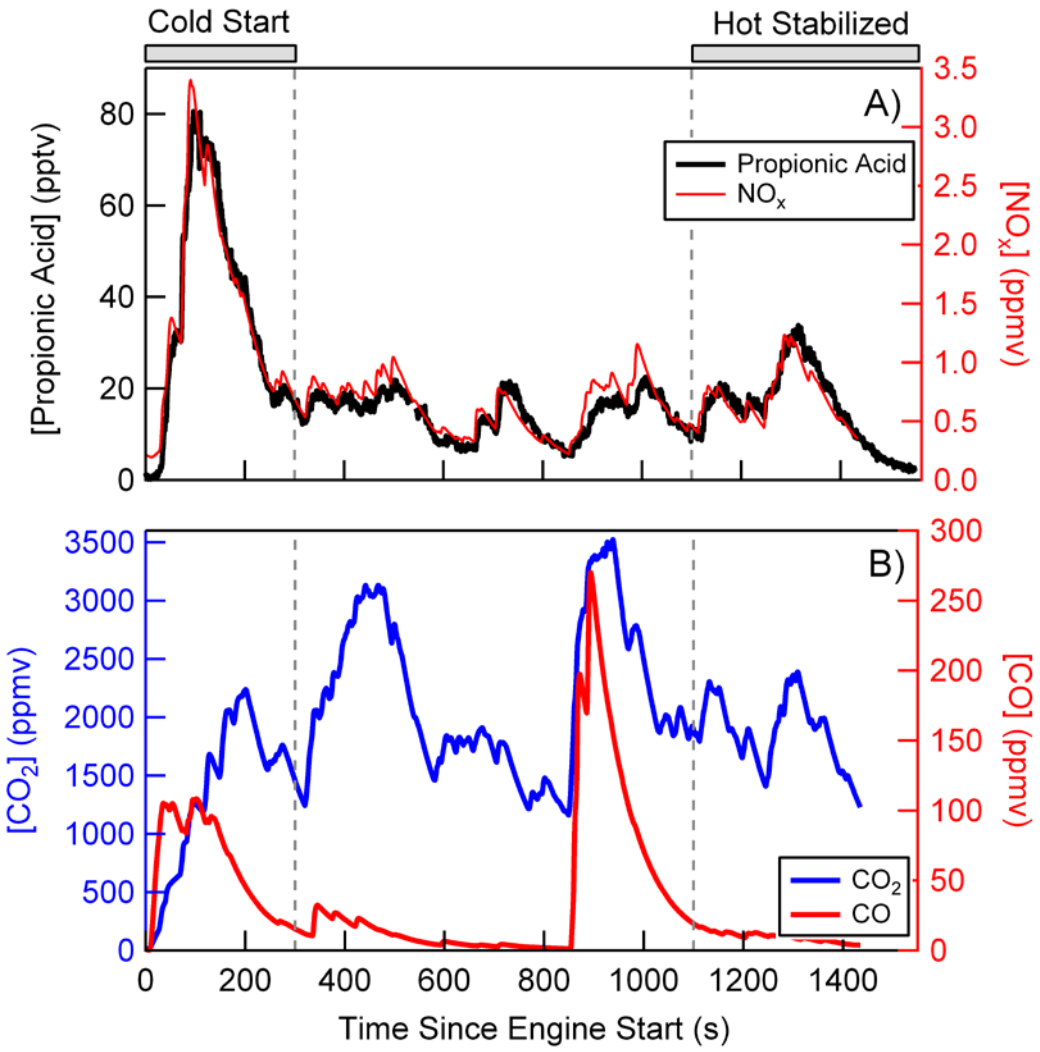

Figure 7: A) Real-time mixing ratios of propionic acid (black; detected at m/z = 73) for the first Cavalier test as measured after the secondary dilution system (SDS). Modeled NO_x mixing ratio, post-SDS, is shown in red. B) Mixing ratios of modeled CO (red) as well as modeled CO_2 (blue) post-SDS, for the first Cavalier test. The "cold start" period, defined as the first 300 s following engine start and the "hot stabilized" period, defined as the last 450 s of the test are shown with gray bars above panel A.

Conclusions: Primary organic aerosol (POA) emitted from light duty gasoline motor vehicles is not completely volatile at atmospherically relevant concentrations. Vehicles emit appreciable amounts of POA from fuel combustion that has very low volatility that can be characterized as effectively non-volatile under typical atmospheric conditions. The POA emitted during the cold-start portion of the driving cycle appears to have greater volatility than POA emitted during other phases of the driving cycle. A conceptual model composed of motor oil emissions and fuel-derived emissions of POA

can explain the observed partitioning behavior. The AMS, when operated at typical vaporizer temperature of 600^{o}C, may not be able to characterize all of this material due to difficulties vaporizing low-volatility POA at 600^{o}C under a vacuum. Carbonyl species may form some of the basic building blocks of low-volatility POA based on the prominence of carbonyls in the condensed phase. Increasing RH in the exhaust promotes carbonyl formation, indicating that chemical reactions are still taking place minutes after exhaust and dilution to atmospherically relevant concentrations. Real-time measurements of gas-phase carbonyl oxidation products show that their concentrations peak during the cold-start portion of the driving cycle.

Future Work: The motor oil and fuel combustion POA emissions should be characterized for +100 vehicles relevant for the California fleet. Further measurements should be made to explore the mechanisms of fuel-derived POA using carbonyl building blocks. The ability of the AMS to measure POA from light duty gasoline vehicles should be studied further. A clearer understanding on this issue is needed to avoid misinterpretation of results in current and future studies.

1 INTRODUCTION

1.1 Motivation

Emissions tests have determined that primary organic aerosol (POA) generated from combustion sources behaves like a series of semi-volatile compounds when the particulate phase concentrations range between 100 – 10,000 µg m^{-3} [1]. The behavior of the bulk organic aerosols can be represented using a general N-product absorption model in which the material is divided between N volatility bins. Figure 1-1 illustrates 2-product and 8-product versions of this representation as summarized by Kroll and Seinfeld [2].

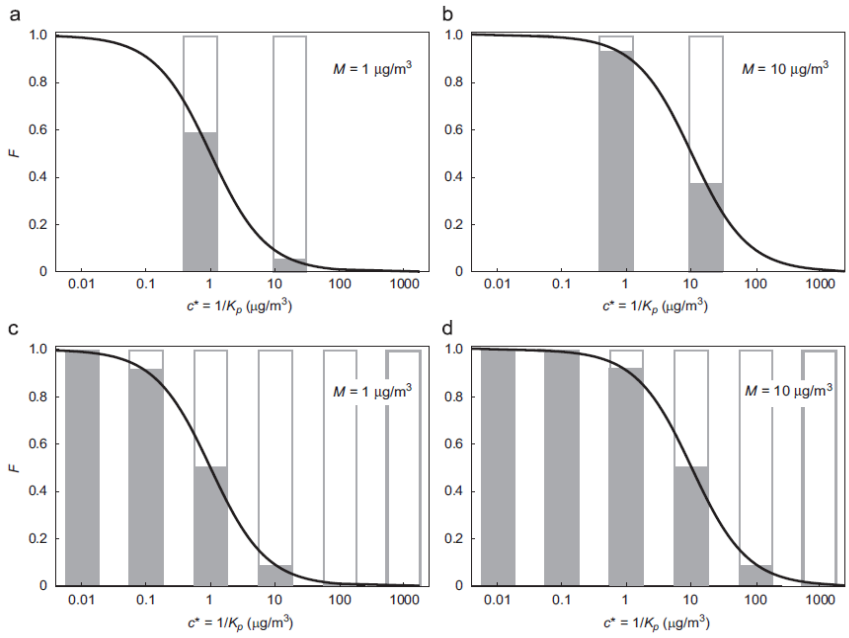

Figure 1-1: Representation of gas-particle partitioning of semi-volatile organic compounds using N-product absorption models. The partitioning of organic aerosol in each volatility bin depends on the Mass of existing organic aerosol (M). [2]

The N-product absorption model can be used to describe primary organic aerosol (POA) or it can be used to describe secondary organic aerosol (SOA) produced from the reaction of gas-phase organic compounds. Coupling of the N-product absorption model to traditional representations of gas-phase SOA formation generally under-predicts the amount of measured total organic aerosol (TOA) in the atmosphere. In most polluted areas where TOA concentrations range from 10-30 µg m^{-3} through most rural areas where TOA falls to 1-2 µg m^{-3} the traditional SOA models fail to predict sufficient production of low volatility products that partition to the condensed phase [3].

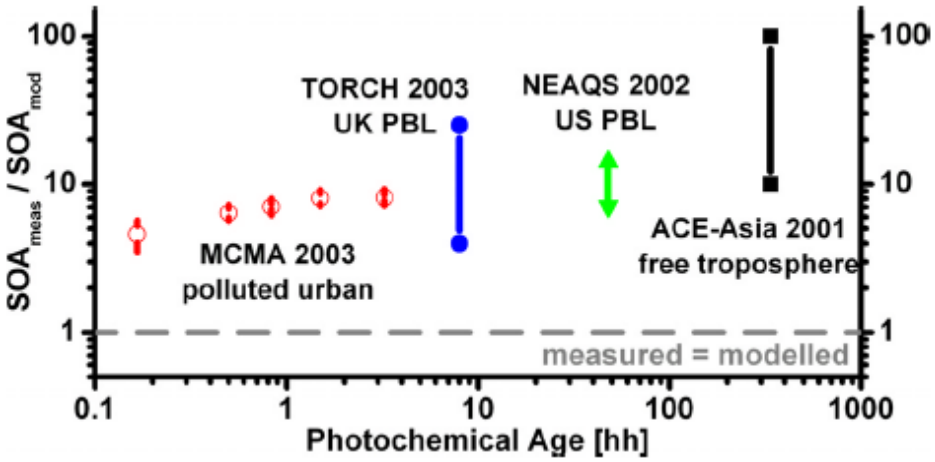

Figure 1-2: Comparison of measured to predicted SOA produced by N-product absorption models using traditional gas-phase SOA formation mechanisms. [3]

The failure of the N-product absorption + traditional SOA formation model to explain observed TOA concentrations has motivated numerous studies to identify the source of the missing carbon. One of the most popular recent theories to be put forward is the Volatility Basis Set (VBS). The VBS approach is based on the principal that organic compounds can be binned according to their vapor pressure or equivalently by C*, the saturation concentration. The exact VBS formulation varies with application, but in one common implementation the gas-phase portion of organic compounds in each volatility bin react with hydroxyl radical at a rate of approximately k=1.0E-11 cm^3 $molec^{-1}$ sec^{-1}. It is assumed that the products from these reactions fall into a volatility bin one order of magnitude less volatile than the parent compounds.

The organization of the VBS technique around volatility bins motivated the authors of the VBS theory to characterize the volatility of POA as inputs to their model. Thermal-denuder experiments have been conducted by passing motor vehicle exhaust through a heated denuder to characterize the volatility of the particles as a function of temperature [4]. The initial experiments were conducted at concentrations above 100 µg m^{-3} of organic aerosol (OA) with very few experiments conducted below 20 µg m^{-3}. Based on these high concentration thermodenuder experiments, along with related experiments in which isothermal dilution is used to alter the total OA concentration and the associated gas-particle partitioning, the VBS predicted that as OA concentrations decreased below 10 µg m^{-3} almost all compounds would have a very low particle-phase fraction with the majority of the material residing in the gas phase due to a lack of absorptive volume.

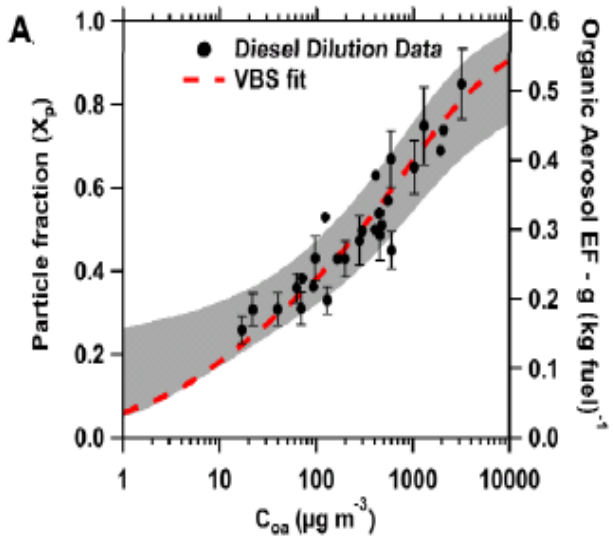

Figure 1-3: VBS extrapolation of OA volatility in high concentrations ranges (>100 µg m^{-3}) to low concentrations ranges (<10 µg m^{-3}). Note that the data below 100 µg m^{-3} appear to flatten but the curve extrapolated from the majority of the experiments conducted at C_{OA}>100 µg m^{-3} predict almost completely semi-volatile behavior for all OA compounds. Particle fraction (X_p) is measured relative to concentrations in undiluted exhaust. [4]

The data available to evaluate the VBS predictions under controlled conditions for atmospherically relevant concentrations below 30 µg m^{-3} are sparse. Despite the widespread adoption of these new theories by the research and regulatory community, much work remains to be done to constrain the many free parameters inherent in the volatility basis set (VBS) formulation of equilibrium partitioning theory and to demonstrate that these parameterizations represent POA partitioning at atmospherically relevant concentrations. Although there is no reason to think that the fundamental premise of the VBS is wrong (which posits that gas-particle partitioning is related to the vapor pressures of condensed phase species), there is no strong evidence to suggest that results obtained at concentrations well above ambient levels can be extrapolated with sufficient accuracy to ambient conditions. In fact, the results in Fig. 1-3 suggest that such extrapolations may be misleading.

Recent measurements of detailed organic species present in motor vehicle exhaust and their partitioning at atmospherically relevant concentrations suggest that the VBS theory may be incomplete at low concentrations, most likely because there are species that persist in the condensed phase at low concentrations whose properties cannot be well-explained from extrapolation from high-concentration experiments. Light duty vehicle emissions testing carried out at C_{OA} = 1-10 µg m^{-3} [5-8] at the CARB Haagan Smit Facility examined the partitioning of individual organic species. New analysis techniques

allowed for chemical characterization of ~20-30% of the POA present under these low concentration conditions. The majority of the identified POA was comprised of small oxygenated organic compounds that, as monomers, have sufficiently high vapor pressures that they would not be expected to exist to any appreciable extent in the condensed phase [5]. State-of-the-science absorption calculations that consider the possibility of multiple condensed phases and activity coefficients in each phase failed to predict the presence of these light oxygenated organic compounds in the condensed phase [9]. The measured presence of light oxygenated organic compounds in the exhaust PM contradicts the behavior predicted by the VBS (or any partitioning model that employs standard gas-particle absorption theory), suggesting that some other processes besides traditional absorption must account for the observed POA at atmospherically relevant concentrations.

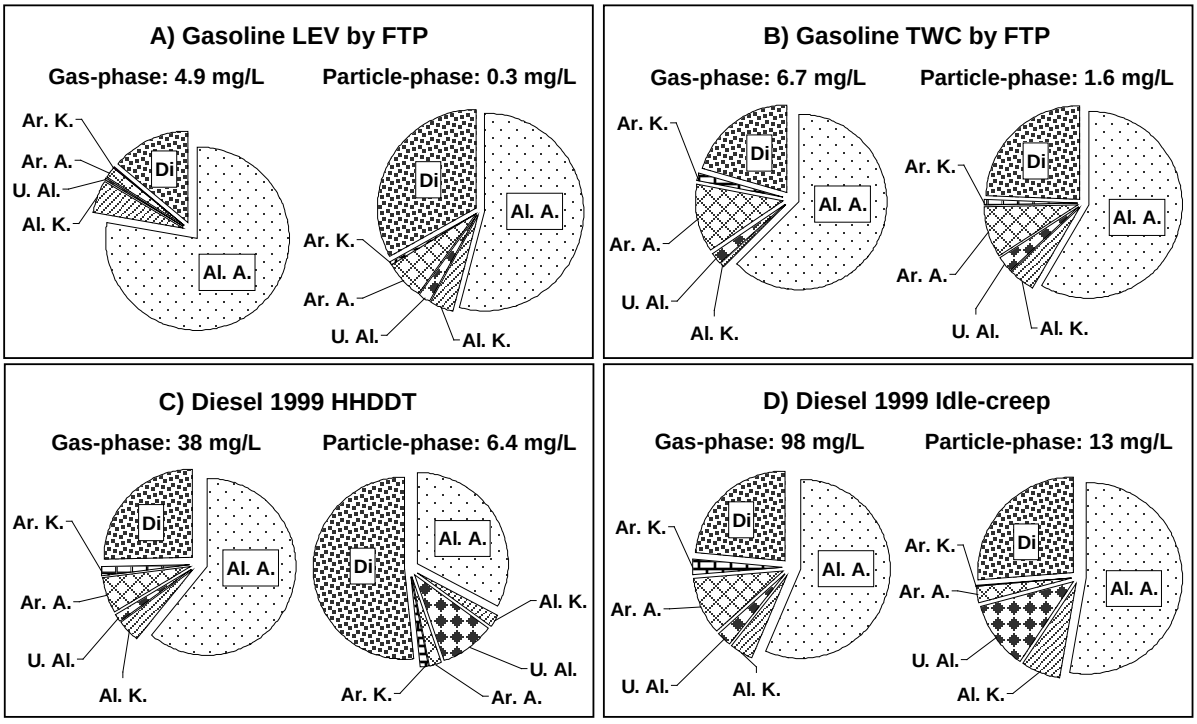

Figure 1-4: Carbonyl speciation for light-duty gasoline and heavy-duty diesel vehicles operated on chassis dynamometers [5].

The light oxygenated organic compounds in the particle phase are highly significant because they accounted for a large fraction of the total OA mass in the relevant concentration range (1-10 µg m^{-3}). Approximately 18% of the OA emissions from Low Emission Vehicle (LEV) gasoline-powered motor vehicles and 38% of OA emissions from three way catalyst (TWC) gasoline vehicles were composed of these light oxygenated compounds that do not appear to be controlled by absorption theory.

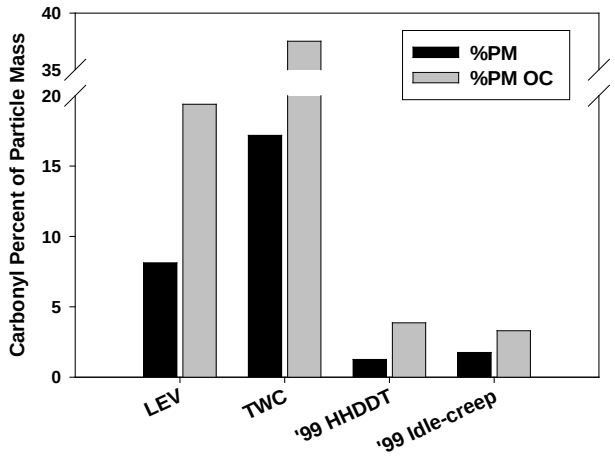

Figure 1-5: Particulate carbonyl emissions as a percentage of total particulate matter (PM) and particulate organic carbon (OC) emissions for light-duty gasoline (LEV, TWC) and heavy-duty diesel vehicles (99 HHDDT, 99 Idle-creep) [5].

Even when state-of-the-science thermodynamics models are employed that can predict the formation of multiple condensed phases with different activity coefficients in each phase, the predicted concentration of particle-phase organic aerosol is much lower than the measured concentration [9]. Actual partitioning for the 60 measured compounds that accounted for up to 38% of the OA mass from TWC vehicles was >3 orders of magnitude larger than predicted partitioning.

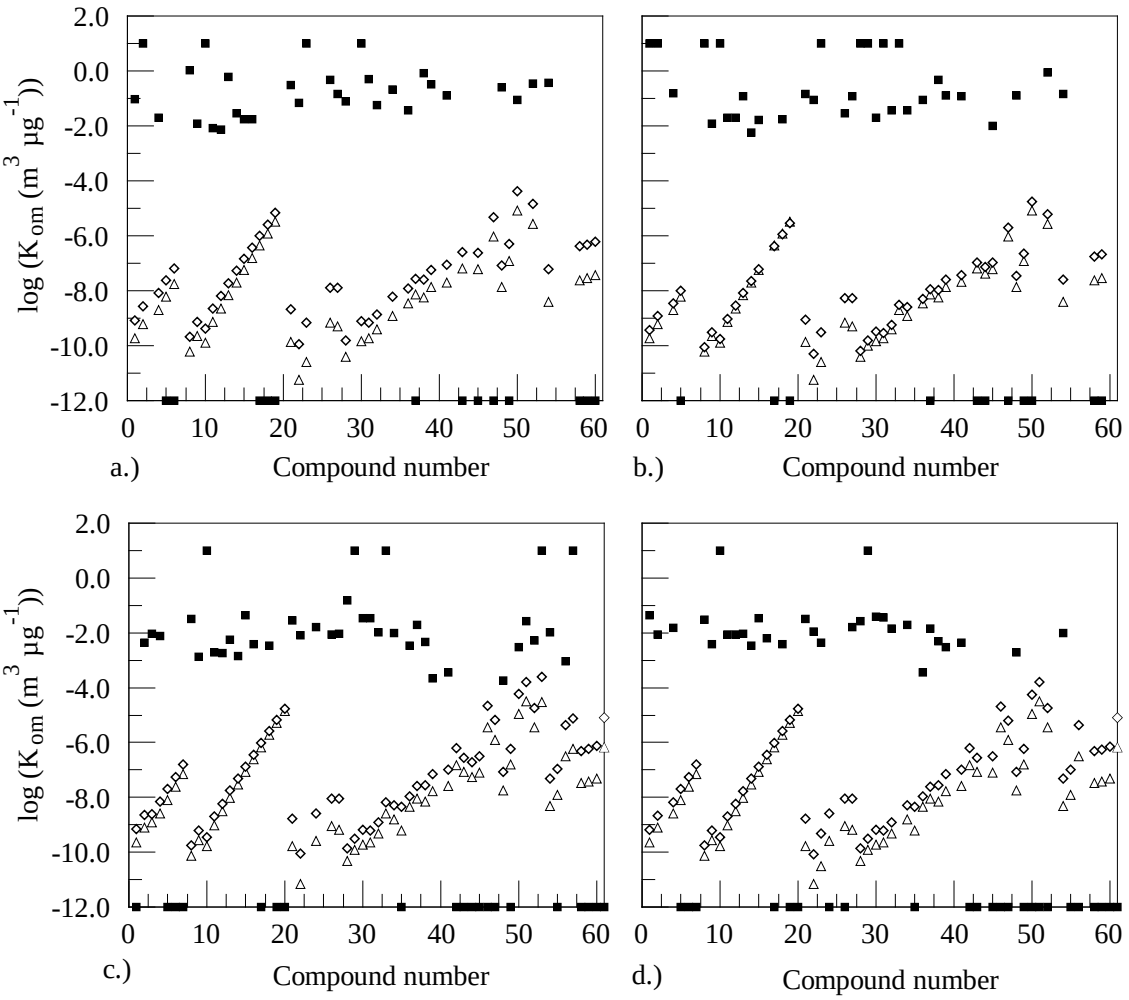

Figure 1-6: Observed (solid squares) and predicted (open triangle for POA assumption I and open diamond for POA assumption II) partitioning coefficients for carbonyl compounds in Table 1 of Ref [9]: a.) LEV; b.) TWC; c.) HDDV 5-Mode; d.) HDDV Idle.

1.2 Research Objectives

The objective of this project was to identify the dominant partitioning mechanism for primary organic aerosol emitted from gasoline-powered and diesel-powered vehicles at

atmospherically realistic concentrations in the range from < 5 – 30 µg m-3. A host of measurements were made to better understand the composition of the organic aerosol emissions including (1) thermal-optical measurements of organic carbon and elemental carbon, (2) GC-MS analysis of denuder-filter-PUF samples, (3) high resolution Aerosol Mass Spectrometer (HR-AMS) measurements for the exact composition of organic fragments, (4) Time-of-Flight Chemical Ionization Mass Spectrometer (ToF CIMS) measurements of gas-phase concentrations and elemental compositions of carbonyls, alcohols, ketones and organic acids, and (5) multi-wavelength photoacoustic spectrometer (PAS) measurements of black carbon (BC). Multiple partitioning theories were tested by manipulating the temperature, humidity, and background concentration of the dilution air used to reduce the tailpipe concentrations to atmospherically relevant levels. The following major hypotheses were tested at POA concentrations < 10 µg m^{-3}:

1. The concentration of EC in the background dilution air changes the partitioning of individual organic compounds in the exhaust emitted from gasoline and diesel engines.

2. The relative humidity of the background dilution air changes the partitioning of individual organic compounds in the exhaust emitted from gasoline and diesel engines.

3. The OA in motor vehicle exhaust does not behave like a completely semi-volatile material when comparing to a basecase with concentrations at atmospherically relevant levels.

1.3 Project Tasks

The following major tasks were identified to test the hypotheses described above:

Major Task 1: POA emissions from diesel-powered and gasoline-powered motor vehicles will be diluted to concentrations ranging from < 5 – 50 µg m^{-3}. The influence of changing temperature on the aerosol will be investigated using a thermal denuder system. Simultaneous measurements of gas-phase compounds will be made and related directly to the aerosol composition measurements. Dilution and heating can be used to independently adjust the final aerosol concentration and we will determine to what extent these provide equivalent results with respect to the observed partitioning. The dilution system will be modified so that the relative humidity of the system can be manipulated. The secondary dilution system will be further modified so that black carbon (BC) particles produced from a separate burner can be introduced into the dilution air with a final concentration between 0 – 10 µg m^{-3} to study the effect of adsorptive partitioning. The relative humidity (RH) will be adjusted between 50-90% to study the effects of aqueous partitioning.

Major Task 2: The organic aerosol concentrations produced during a series of gasoline and diesel vehicle tests will be measured as a function of dilution amount and thermodenuder temperature using a high-resolution Aerosol Mass Spectrometer capable of providing information about the size-resolved chemical composition of the particles

and the elemental composition (i.e., ratios of carbon, hydrogen, oxygen and nitrogen) of the POA. Simultaneously, gas-phase concentrations and elemental compositions of carbonyls, alcohols, ketones and organic acids will be determined using a Time-of-Flight Chemical Ionization Mass Spectrometer and BC concentrations will be monitored using a multi-wavelength photoacoustic spectrometer.

Major Task 3: The gas and particle phase organic compounds will also be captured separately for offline analysis using a denuder-filter-PUF sampling train and analyzed using GC-MS for the concentration of individual organic compounds. Partitioning calculations that consider absorption into organic aerosol, aqueous partitioning, and adsorption onto elemental carbon (EC) will be used to identify the dominant processes at atmospherically relevant concentrations.

In addition to measurements, absorption models will be applied to identify the dominant gas-particle partitioning mechanism at atmospherically realistic conditions. The absorption of carbonyl compounds into the OA phase will be calculated using the Extended Aerosol Inorganics Model (*E-AIM*), which is a state-of-the-science thermodynamic model that calculates the equilibrium partitioning for organic compounds between the gas phase, the particle aqueous phase, and the particle organic phase. The adsorption of carbonyl compounds onto EC will be modeled using the Langmuir and BET adsorption isotherm models. The Langmuir model was developed originally for systems with a monolayer adsorption on the surface of an adsorbent while the BET model was an extension of the Langmuir monolayer model to multilayer adsorption. Both the mass concentration and surface area of EC will be measured and combined with measured concentrations of individual oxygenated organic species to determine if adsorption controls partitioning.

1.4 Report Structure

This report is comprised of 10 chapters, including introduction (Chapter 1) and conclusions (Chapter 10).

Chapter 2 provides an assessment of black carbon emissions from light duty gasoline powered vehicles.

Authors note: The work in chapter 2 has been published in the journal Environmental Science and Technology and may be cited in any future studies as “S.D. Forestieri, S. Collier, T. Kuwayama, Q. Zhang, M.J. Kleeman, and C.D. Cappa. Real-time black carbon emission factor measurements from light duty vehicles. Environmental Science and Technology. 47(22), pp13104-13112 (2013), DOI: 10.1021/es401415a.”

Chapter 3 provides an assessment of gaseous CO2 subtraction from organic aerosol concentrations measured using HR-AMS.

Authors note: The work in chapter 3 has been published in the journal Environmental Science and Technology and may be cited in any future studies as "S. Collier and Q. Zhang. Gas-phase CO2 subtraction for improved measurements of organic aerosol mass concentrations and oxidation degree by Aerosol Mass Spectrometer. Environmental Science and Technology. 47(24), pp 14324-14331 (2013)."

Chapter 4 presents an analysis of hydrocarbon organic aerosol (HOA) emissions from light duty gasoline powered vehicles measured by HR-AMS.

Authors note: The work in chapter 4 is still under development and will be submitted for publication at a future date.

Chapter 5 summarizes the volatility of primary organic aerosol emitted from light duty vehicles.

Authors note: The work of chapter 5 is still under development and will be submitted for publication at a future date.

Chapter 6 reports on the effects of temperature, humidity, and black carbon concentration on the total emissions rate of carbonyls in light duty vehicle exhaust.

Authors note: The work of chapter 6 is still under development and will be submitted for publication at a future date.

Chapter 7 describes the effects of temperature, humidity, and black carbon concentration on the PM emissions of total POA and carbonyls emitted from light duty vehicles.

Authors note: The work in chapter 7 is still under development and will be submitted for publication at a future date.

Chapter 8 describes measurements of gas-phase organic acids emitted from light duty vehicles.

Authors note: The work summarized in chapter 8 is still under development and will be submitted for publication at a future date.

Chapter 9 summarizes measurements of gas-phase isocyanic acid (HCNO) emitted from light duty vehicles.

Authors note: The work summarized in chapter 9 has been submitted for publication in the journal Environmental Science and Technology and should be cited in any future studies as: "J.M. Brady, T.A. Crisp, S. Collier, T. Kuwayama, S.D. Forestieri, Q. Zhang, M.J. Kleeman, C.D. Cappa, and T.R. Bertram. Real-time emission factor measurements of isocyanic acid from light duty gasoline vehicles. Environmental Science and Technology, in review, 2013."

2 REAL-TIME BLACK CARBON EMISSION FACTOR MEASUREMENTS FROM LIGHT DUTY VEHICLES

2.1 Introduction

Black carbon (BC), the main refractory and strongly absorbing component of soot, constitutes a substantial fraction of primary particulate matter (PM) and is emitted by both anthropogenic and natural combustion sources. BC has adverse impacts on human health [10], contributes to visibility degradation [11], and influences climate by scattering and absorbing solar radiation [12] and acting as cloud condensation nuclei [13]. One important source of primary anthropogenic BC in urban areas is motor vehicles, with vehicular primary particulate emissions dominated by BC and particulate organic matter (POM, defined as the sum of particulate organic carbon and non-carbon components). Although light-duty gasoline vehicles (LDGVs) currently contribute less than 5% of $PM_{2.5}$ emissions, they can lead to high $PM_{2.5}$ concentrations near major roadways [14]. Current regulations, such as the low-emission vehicle II (LEV II) standards, focus primarily on particle mass, with less emphasis placed on composition and size of vehicle particulate emissions, even though the latter are important considerations when assessing the environmental and health effects of PM. Gasoline-fueled LEV II vehicles, which predominantly use port fuel injection technology, emit PM at a rate of approximately 1 mg $mile^{-1}$. The new national standards as well as the State LEV II-GHG standards encourage wider adoption of technologies that reduce CO_2 emissions, such as Gasoline Direct Injection (GDI). Vehicles based on GDI technology tend to have higher PM mass and particle number emissions than conventional PFI technology. Published reports suggest that GDI vehicles emit PM mass in the range of 2-20 mg $mile^{-1}$ [15, 16].

Accurate quantification of emission factors (EFs) or emission rates (ERs) of BC are central to development of composition-specific emissions inventories for use in models and future air quality regulations. To facilitate improvements in the spatial resolution of BC emissions modeling, accurate measurements of BC and ancillary species that are sufficiently fast (response times on the order of seconds) to capture the wide variations in emitted species concentrations throughout vehicle testing are necessary as these parameters change rapidly throughout a typical driving cycle. Such real-time measurements allow for the relation of broad aspects of driving behavior, such as acceleration, directly to emissions.

Here, results are reported from a study conducted in September 2011 in which eight LDGV's were tested on a Chassis dynamometer using the California Unified Cycle (UC) at the Haagen-Smit vehicle test facility at the California Air Resources Board (CARB) in El Monte, CA. The eight in use vehicles (requisitioned for this study) all met emission requirements for LEV I. Additionally, four different types of light duty vehicles (LEV I, ULEV, GDI and diesel) were tested on a constant velocity cycle. Real-time measurements of BC and other non-refractory PM (NR-PM) components and of gas-phase CO_2 concentrations were made, thereby allowing for quantification of EF_{BC}'s

throughout the driving cycle for each of the vehicles tested. Measurements here can be contrasted with most past measurements in which EF_{BC}'s were averaged over the entire driving cycle or specific subset periods, although there are a few studies [17, 18] that have quantified BC concentrations for individual vehicles in real-time during a cold-start driving cycle (see Table 4) and fast-response instruments (≤ 1 second) are often used during engine testing. The current study provides insights into the variability of not just BC concentrations, but of BC EFs throughout a driving cycle that bulk measurements cannot distinguish and also addresses some of the differences in EFs reported between previous field studies (e.g. on-road or tunnel sampling) and dynamometer studies.

2.2 Experimental

2.2.1 Vehicle Testing

Each full test day, the eight LEV vehicles (Table 2-1) were tested on a Chassis dynamometer, which mimics road load typically experienced by vehicles, following the UC. The UC is a predetermined driving cycle with a 300-second "cold start" phase followed by a 1135-second "hot stabilized running" phase. Cold start consists of starting the vehicle after letting it sit overnight at ~24 °C, followed by a period of small accelerations. Hot stabilized running has two periods of hard acceleration and a maximum velocity of 67.2 mph. In addition to the UC tests, four different types of light duty vehicles (LEV I, ULEV, GDI and diesel) were tested on a steady-state cycle, which begins with a cold-start (although not necessarily following the overnight conditioning) followed by a 30-minute 60 mph constant velocity phase.

Table 2-1: Summary of results for LEVs tested on the Unified Cycle

Model and Year	Phase	*N*	EF_{BC} (mg BC kg^{-1} fuel) Mean (±SE)	Median	ER_{BC} (mg BC $mile^{-1}$) Mean (±SE)	Median	SSA[%]	Max EF_{BC}[*] (±SE)
Ford Windstar 1998	Combined	5	1.5±0.4	0.94	0.21±0.06	0.14	0.30±0.04	7.8±1.3
	Cold Start		4.0±0.9	3.07	0.93±0.22	0.71	0.04±0.04	
	Hot Running		0.54±0.14	0.54	0.07±0.02	0.07	0.36±0.90	
Chevy Cavalier 2001	Combined	3	3.3±0.6	3.72	0.40±0.08	0.45	0.26±0.06	60.0±21.7
	Cold Start		14.3±5.0	10.19	2.7±1.0	1.93	0.05±0.04	
	Hot Running		0.42±0.13	0.35	0.05±0.01	0.04	0.24±11.8	
Toyota Tacoma 2003	Combined	6	8.1±1.2	8.49	1.24±0.20	1.21	0.10±0.02	35.3±6.0
	Cold Start		17.4±2.8	17.89	4.0±0.6	4.12	0.01±0.02	
	Hot Running		5.4±0.7	5.44	0.73±0.10	0.74	0.07±0.48	
Cherokee Laredo 2002	Combined	6	4.3±0.8	3.69	0.92±0.21	0.79	0.20±0.04	34.2±14.0
	Cold Start		11.2±4.2	7.56	3.6±1.4	2.44	0.05±0.02	
	Hot Running		1.83±0.35	1.58	0.35±0.07	0.30	0.22±0.89	
Nissan Pathfinder 2003	Combined	6	7.2±1.2	7.33	1.24±0.21	1.26	0.24±0.04	60.5±14.6
	Cold Start		26.4±6.0	26.29	6.7±1.5	6.64	0.03±0.02	
	Hot Running		1.07±0.14	1.03	0.17±0.02	0.16	0.29±0.93	
Chevy S-10 2002	Combined	6	1.92±0.25	2.01	0.25±0.03	0.26	0.20±0.02	11.8±5.7
	Cold Start		6.2±0.8	6.29	1.26±0.15	1.27	0.06±0.02	
	Hot Running		0.75±0.10	0.72	0.09±0.01	0.09	0.19±0.88	
Ford Taurus[$] 1997	Combined	5	24.1±8.1	18.16	3.5±1.2	2.57	0.09±0.05	79.9±27.4
	Cold Start		36±16	19.29	6.8±3.5	4.21	0.07±0.03	
	Hot Running		21.0±6.2	21.69	2.2±0.7	2.45	0.04±0.31	
Toyota Solara 2003	Combined	3	0.76±0.10	0.69	0.10±0.02	0.09	0.29±0.06	13.3±6.0
	Cold Start		2.8±0.7	2.34	0.61±0.16	0.51	0.09±0.05	
	Hot Running		0.29±0.04	0.32	0.03±0.00	0.04	0.44±4.37	

[$] Vehicle malfunctioned
[*] Maximum value observed during a test, typically during the cold start period
[%] SSA = single scatter albedo

Emissions from the vehicle tailpipe were sampled into a constant volume sampler (CVS), with an average dilution factor of 12.6 ± 3.4 and overall flowrate of 0.165 $m^3 s^{-1}$ (= 9,911 L min^{-1}). Ambient air and dilute exhaust air from the CVS were collected in Teflon bags over the entire driving cycle for subsequent analysis of concentrations of CO_2. The air was further diluted by a secondary dilution system (SDS) [8], which was generated by passing room air through a bed of activated carbon (to remove NO_x, O_3 and VOCs) followed by a HEPA filter (to remove PM). This resulted in a total dilution factor of ~60 (a factor of 12 in the CVS and an additional factor of 5 in the SDS). Since BC is non-volatile and since the real-time measurements were made under dry conditions, such modifications beyond the CVS will not affect the measured EF_{BC} values, although can influence POM measurement. As a result, of these post-emission modifications, real-time BC measurements are available for all test days, but POM and bulk BC measurements from only a subset of days are used here (specifically days without RH modification or non-vehicle soot addition). The diluted sample air was mixed under turbulent conditions

in a residence time chamber (RTC), with a residence time of ~70 seconds. The output flow from the RTC was split between the real-time instruments (5 L min^{-1}) and a denuder-filter-polyurethane foam (PUF) train. The real-time instruments sampled from the RTC through 0.25 in. (OD) copper tubing. The overall residence time through the CVS and the SDS+RTC was around 1.2 minutes. Because the RTC is turbulent, extremely rapid (seconds) fluctuations in concentrations associated with changes in driving conditions are smoothed out while slower (10s of seconds) variations are retained. Given this smoothing, the current study provides information as to how emissions of BC depend on general driving conditions during the UC, but does not capture very fast transients that can be seen during bench engine testing. The absolute average PM concentrations out of the SDS+RTC during UC tests ranged from 1-5 μg m^{-3}.

Most tests were conducted wherein the SDS dilution air was filtered room air. However, two alternative sampling configurations were considered in which the SDS dilution air either (i) was actively humidified or (ii) had non-vehicle BC added. Humidification had no discernible influence on the BC emission factors. Addition of a separate (non-vehicle) BC source required background subtraction in order to determine the vehicle-specific EF_{BC}.

Humidification was achieved by passing the dilution air over a heated ultrasonic nebulizer filled with MilliQ (18MΩ) water. The extent of humidification was controlled by altering either the speed of the ultrasonic nebulizer or the bath temperature. Typical (non-humidified) RH values in the SDS were 60%. For the humidified experiments the RH was typically 75%-85%.

The non-vehicle background BC, with concentrations ranging from 3-25±5 μg-m^3, was provided by an inverted methane co-diffusion flame [19]. The flame BC from was passed over a catalytic converter and through a thermodenuder (at 300 °C) to remove residual organic carbon. The SDS was under-pressured relative to the flame exhaust, and thus flame BC was sampled into the SDS through a variable valve. The amount of BC added was controlled by throttling the valve, and was monitored by the PAS. Over the course of a given test, the concentration of flame BC typically slowly decreased, likely as a result of clogging of the valve and pressure changes within the SDS. The time-dependent changes in the concentrations of flame BC throughout an individual test were estimated by measurement of the flame-only BC concentration (i.e. absorption) before and after the vehicle test and recognizing that for nearly all vehicles the vehicle-specific BC concentration usually fell to near zero during the period between the first and second hard acceleration. This background flame BC was subtracted from the total observed BC to determine the vehicle-specific BC concentrations throughout the driving cycle on test days. There was generally good correspondence between the time dependent behavior of the background corrected vehicle BC on flame days vs. non-flame days, indicating that the background correction is reasonable.

2.2.2 Instrumentation

Real-time measurements (i.e. response time ≥ 0.1 Hz) of particulate light absorption and light extinction coefficients (b_{abs} and b_{ext}, respectively), NR-PM concentrations and size distributions, gas-phase CO_2 and other specific trace gases (particularly organic acids and aldehydes), were made from the SDS+RTC for each vehicle tested throughout each driving cycle (Figure 2-1). Bulk PM from all vehicles tested over the course of a day was also sampled from the SDS+RTC onto a quartz-fiber filter for offline analysis. This study focuses only on the PM and CO_2 emissions, and mainly the BC component. Measurements directly from the CVS were made by CARB staff and included real-time gas-phase CO_2 and bulk sampling of particles from all vehicles onto a filter each test day for offline bulk chemical analysis.

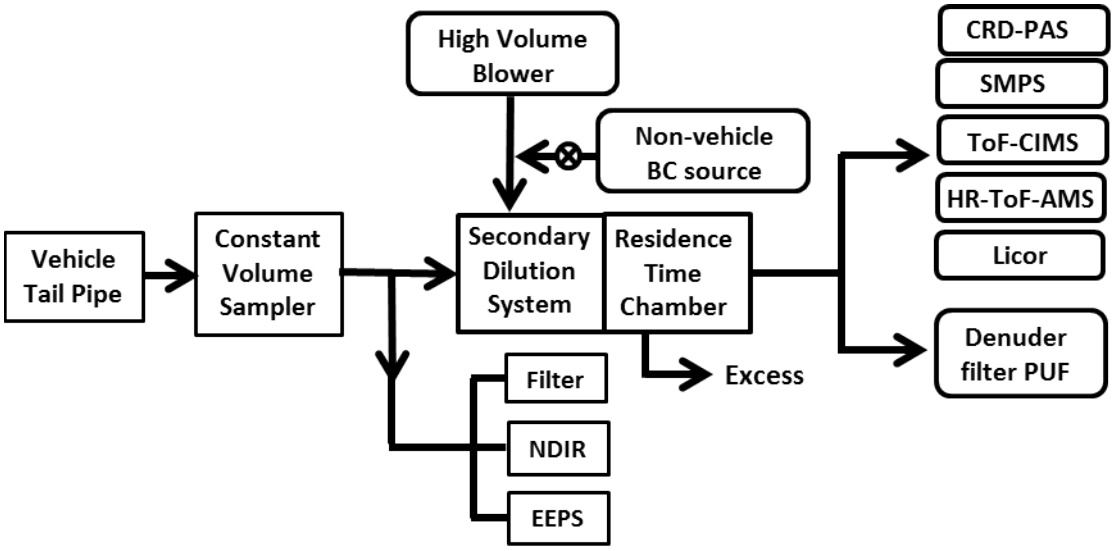

Figure 2-1: Schematic showing sampling configuration

Light Absorption and Extinction

The b_{abs} and b_{ext} (in Mm^{-1}) from the SDS+RTC were measured at 532 nm and 405 nm using a home-built cavity ring-down and photo-acoustic spectrometer (CRD-PAS). The UCD CRD spectrometer simultaneously measures light extinction for particles at low RH (< 20%) at both wavelengths and at two elevated RH's (~75% and 85%) at 532 nm [20]. Gas-phase interferences were measured in two filtered channels (one at each wavelength), although were negligible throughout this study. The air from the two dry CRD channels is sampled into the dual-channel PAS, where the absorption coefficients are measured [21]. Measurements were made at ~0.4 Hz, with a detection limit for the CRD of ~0.1 Mm^{-1} at 532 nm and 0.3 Mm^{-1} at 405 nm. The accuracy of the CRD system is <5% at both wavelengths. The detection limit of the PAS at 0.4 Hz was ~0.3 Mm^{-1} at

532 nm and 0.5 Mm^{-1} at 405 nm, with an accuracy of ±10% at 532 nm and ±15% at 405 nm.

BC concentrations are calculated from the measured aerosol absorption coefficients by dividing b_{abs} by the mass absorption coefficient (MAC), using MAC_{532nm} = 7.75 (±1.5) $m^2\ g^{-1}$ and MAC_{405nm} = 10 (±3) $m^2\ g^{-1}$ [22, 23], although only the 532 nm measurements are used here due to the better sensitivity and precision of the 532 nm channel. The MAC_{BC} is nearly constant over the range of particle sizes sampled here [22]. The PAS was calibrated daily by referencing the laser power normalized PAS signal response to ozone with the b_{ext} that was measured concurrently with the CRD [19]. For gases, extinction is equal to absorption in the absence of photolysis or fluorescence, which is the case here.

Aerodyne HR-ToF-AMS - Non-Refractory Particulate Matter

An Aerodyne high resolution time-of-flight aerosol mass spectrometer (HR-ToF-AMS) [24] was used to determine real-time concentrations of POM (Particulate Organic Matter, defined as POC + functional groups) and other components of non-refractory particulate matter (NR-PM), with an instrument accuracy of ± 20%. Non-refractory PM species are defined here as those that volatilize on time scale of a few seconds at ~600 °C under high vacuum (10^{-8} torr) conditions. NR-PM includes inorganic PM (such as SO_4^{2-} and NH_4^+) and POM, but not EC, the majority of sea salts or mineral dust. At the instrument inlet, a particle beam is created by an aerodynamic lens under vacuum conditions. The particles impact onto a hot plate and are immediately ionized by an electron impact ionizer. NR-PM measurements were made with an average time-resolution of 10 seconds. During each test, the HR-ToF-AMS was operated with the Ion Path in "V-mode" (higher sensitivity) for the first 23 minutes and in "W-mode" (higher mass-resolution) mode for the last minute. The data were analyzed using the analysis toolpacks Squirrel 1.51H and PIKA 1.10H, in IGOR Pro Version 6.22A (Wavemetrics, Inc.). The Ionization Efficiency was calibrated using size-selected monodisperse ammonium nitrate particles [25], which were atomized from solution, dried, sized with a differential mobility analyzer (DMA) and counted with a condensation particle counter (CPC).

Aerodyne HR-ToF-AMS - Carbon Dioxide

The HR-ToF-AMS was also used to determine real-time CO_2 concentrations. Typically, the HR-ToF-AMS is used only to measure concentrations of NR-PM. However, the HR-ToF-AMS is also sensitive to variations in the gas-phase concentrations of N_2, O_2 and CO_2. For ambient sampling, variations in gas-phase CO_2 concentrations are small, and thus a constant CO_2 correction is usually applied. When directly sampling from vehicles, as was done here, the variations in gas-phase CO_2 are significantly larger and the HR-ToF-AMS CO_2^+ signal can be used to quantitatively determine the gas-phase CO_2 concentration with 10 second time resolution. The Peak Integration by Key Analysis (PIKA) 1.10H toolpak, was used to fit and separate the CO_2 and N_2 peaks in the high-

resolution spectrum. Gas-phase CO_2 concentrations (in ppm) were determined from the HR-ToF-AMS by quantifying the real-time CO_2 -N_2 ratio and, using the equation:

$$[CO_2] = \left(\frac{CO_2}{N_2}\right) \times \left(REI_{CO_2}\right) \times f_{N_2}^{-1} \times CF_{m/z=15} \times 10^6 \qquad (1)$$

where REI_{CO2} is the relative ionization efficiency of CO_2, f_{N2} is the fraction of N_2 in the atmosphere and $CF_{m/z=15}$ is the correction factor for m/z=15 N_2 fragmentation. The estimated accuracy of [CO_2] using this method is estimated as 10% [26].

In addition to the CO_2 from the PIKA analysis of HR-ToF-AMS data, CO_2 was measured for a subset of tests in real-time using a Licor instrument at 1 Hz. The agreement between the Licor CO_2 and the PIKA CO_2 measurements is excellent, as seen in Figure 2. This validates the use of the HR-ToF-AMS in this non-traditional way to determine gas-phase CO_2, which was necessary because the Licor was not available for the entire campaign. The CO_2 from the PIKA analysis also compared well with ARB's real-time CO_2 data. The agreement between these two tests is shown in Figure 3. The ARB's real-time CO_2 data was smoothed using a box smoothing algorithm.

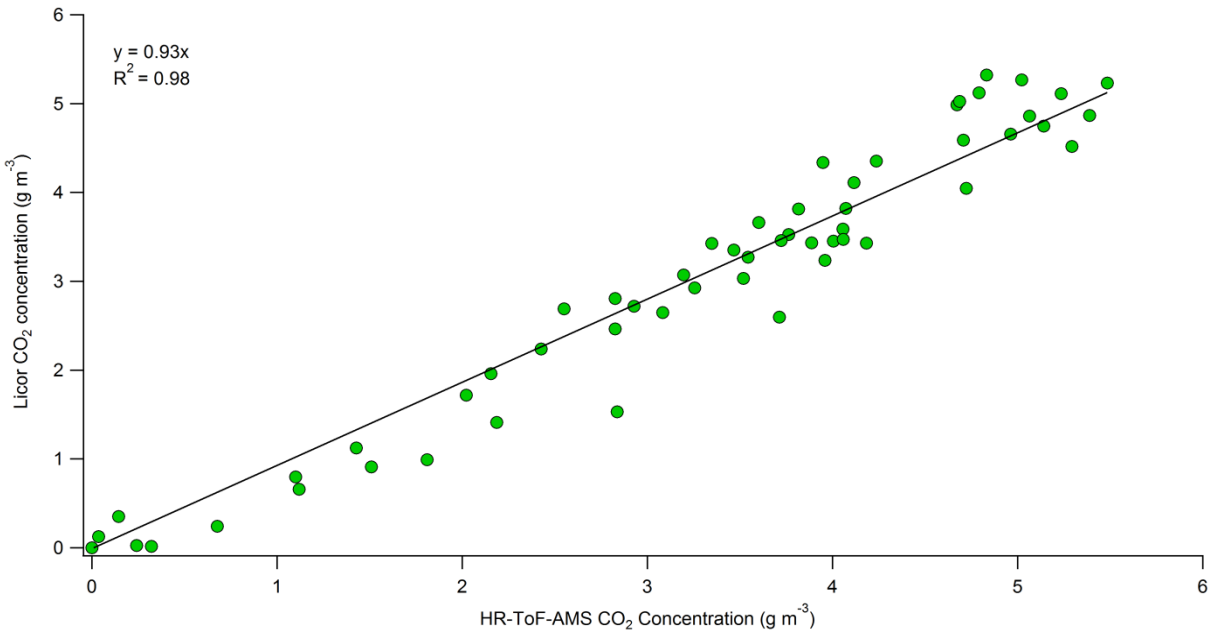

Figure 2-2: Comparison of Licor CO2 concentrations with CO2 from the HR-ToF-AMS

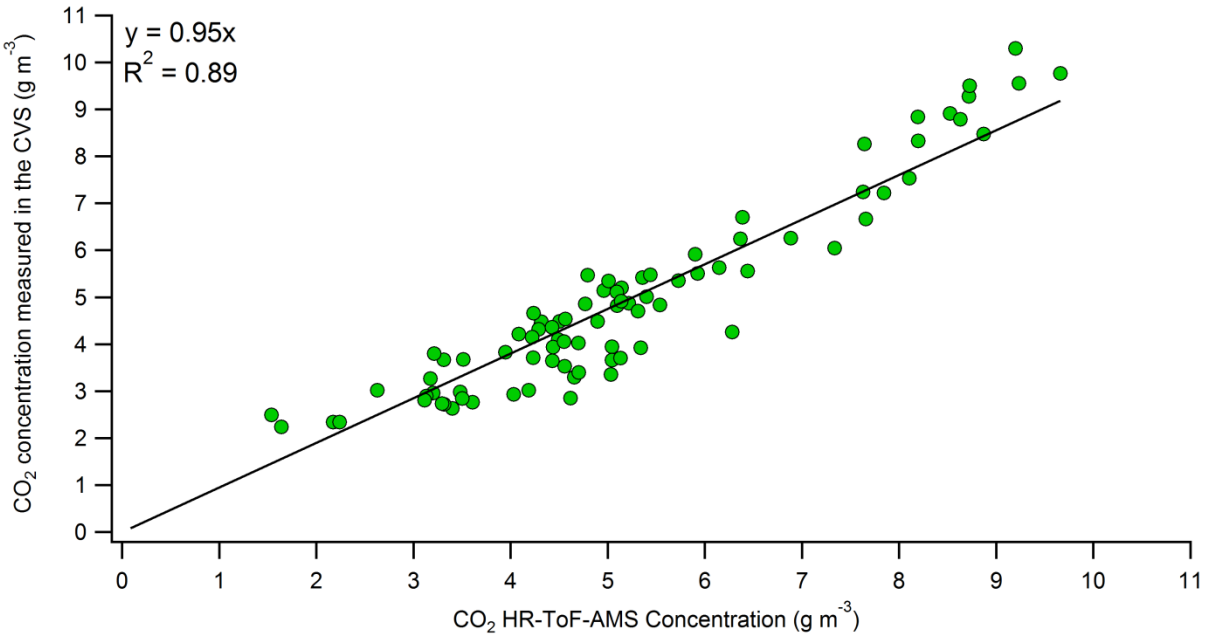

Figure 2-3: Comparison of real-time dilution-adjusted CO2 concentrations for a single vehicle in the CVS with CO2 from the HR-ToF-AMS PIKA analysis

ARB also measured the CO_2 concentration in the CVS airstream using a non-dispersive infrared instrument [27]. From this, the CO_2 emission rate (ER) for each vehicle test was determined as:

$$ER_{CO_2} = \frac{V_{mix}\rho_{CO_2} f_{CO_2}}{VMT} \quad (2)$$

where V_{mix} is the total volume of dilute exhaust sampled (m^3 sample), ρ_{air} is the density of air at the sampling conditions (kg m^{-3}), and f_{CO2} is the volume fraction of CO_2 in the dilute exhaust in the CVS. To relate the ARB CO_2 to the real-time measurements, the additional dilution in the SDS was accounted for to determine the CO_2 concentration, as seen by the real-time instruments.

Importantly, the real-time [CO_2] from the AMS compared well with the Licor, within 6%, on average (Figure 2-2). CO_2 was measured from the CVS using a non-dispersive infrared (NDIR) spectroscopy method. The dilution-adjusted AMS [CO_2] agreed with the all-test average CVS NDIR [CO_2] within 8%, providing confidence that the use of the AMS in this non-conventional manner is justified.

Filter-based EC/OC

Elemental carbon (EC) is operationally defined as carbonaceous material that combusts at high temperatures in an oxygen-containing atmosphere, whereas BC (black carbon) is

defined as light absorbing components of soot. For this analysis EC and BC are considered to be equivalent.

Bulk, daily average elemental carbon (EC) and particulate organic carbon (POC) concentrations and relative fractions were determined from the collected filter samples from either the CVS or SDS+RTC using a Thermo-Optical Analyzer (Desert Research Institute) and the IMPROVE_A protocol [28], with overall precisions of ± 5-10% for POC and ± 20% EC [29]. EC is operationally defined as carbonaceous material that combusts at high temperatures in an oxygen-containing atmosphere, whereas BC is defined as light absorbing components of soot. For this study EC and BC are considered to be equivalent. PM in the CVS was collected on pre-fired, quartz fiber filters by ARB, and the extracted samples were analyzed for EC and OC mass using a Thermo-Optical Analyzer (Desert Research Institute). Only one composite sample was collected for each test day. The EC/OC analysis followed the IMPROVE_A protocol [30]. The OC and EC concentrations are corrected for pyrolysis (charring) of OC by monitoring sample light reflectance. The estimated uncertainty in the EC and OC measurements using this method is ± 10% for OC and ± 20% for EC [29].

2.2.3 Emission Factor Calculations

Emission factors are defined here as the amount of BC emitted (in mg) per kg of fuel burned and emission rates are the amount of BC emitted per mile driven. Vehicle emissions models, such as the EPA's Motor Vehicle Emission Simulator (MOVES), rely on accurate quantification of EFs and ERs. Real-time EF_{BC} values were calculated as:

$$EF_{BC} = w_C \left[\frac{b_{abs}}{MAC \cdot [CO_2]} \right] 10^6 = w_C \left[\frac{[BC]}{[CO_2]} \right] 10^6 \qquad (3)$$

where w_c is the mass fraction of carbon in fuel (assumed to be 0.85) [31] and [BC] (in µg m^{-3}) and [CO_2] (in g-C m^{-3}) are the background corrected concentrations, which have been synchronized in time and where the [BC] has been averaged to the same time-base as the [CO_2] (0.1 Hz). Equation 3 assumes the majority of fuel carbon is converted to CO_2, consistent with observations. The background [BC] was zero, except for the tests that added non-vehicle soot, in which case the added [BC] was subtracted.
Emission rates were calculated as:

$$ER_{BC} = \frac{EF_{BC}}{MPG \times \rho_{gasoline}} \qquad (4)$$

where MPG is the vehicle-specific fuel economy (in miles per gallon with an assumed gasoline density, $\rho_{gasoline}$, of 720 kg m^{-3}). The overall uncertainty in EF_{BC} comes from uncertainty in the *MAC* (± 19%), b_{abs} (± 10%), [CO_2] (± 10%) and the carbon content of the gasoline fuel (± 5%). An additional uncertainty for tests with added non-vehicle

background BC results from baseline subtraction and is estimated to be ± 5% for high emitting vehicles and ± 23% for low emitting vehicles over the entire UC. (Note that "high" and "low" are used here to characterize the range of EF_{BC} and ER_{BC} from the tested vehicles, and splits the 8 vehicles into two groups). The propagated uncertainty is ± 24% for days without background BC, ± 25% for high emitting vehicles on days with non-vehicle BC, and ± 33% for low-emitting vehicles on days with non-vehicle BC.

2.3 Results

2.3.1 Average BC Emission Factors

All-test averages and box-and-whisker plots of EF_{BC} and ER_{BC} (averaged from real-time data) for each LEV tested on the UC are shown in Figure 2-4. The box and whisker plots show the mean (■), median (-), lower and upper quartile (boxes) and 9th and 91st percentile (whisker). The test vehicles are organized from lowest to highest overall emission factors. The Taurus malfunctioned after only one test; the gray circle indicates the EFBC prior to the malfunction.

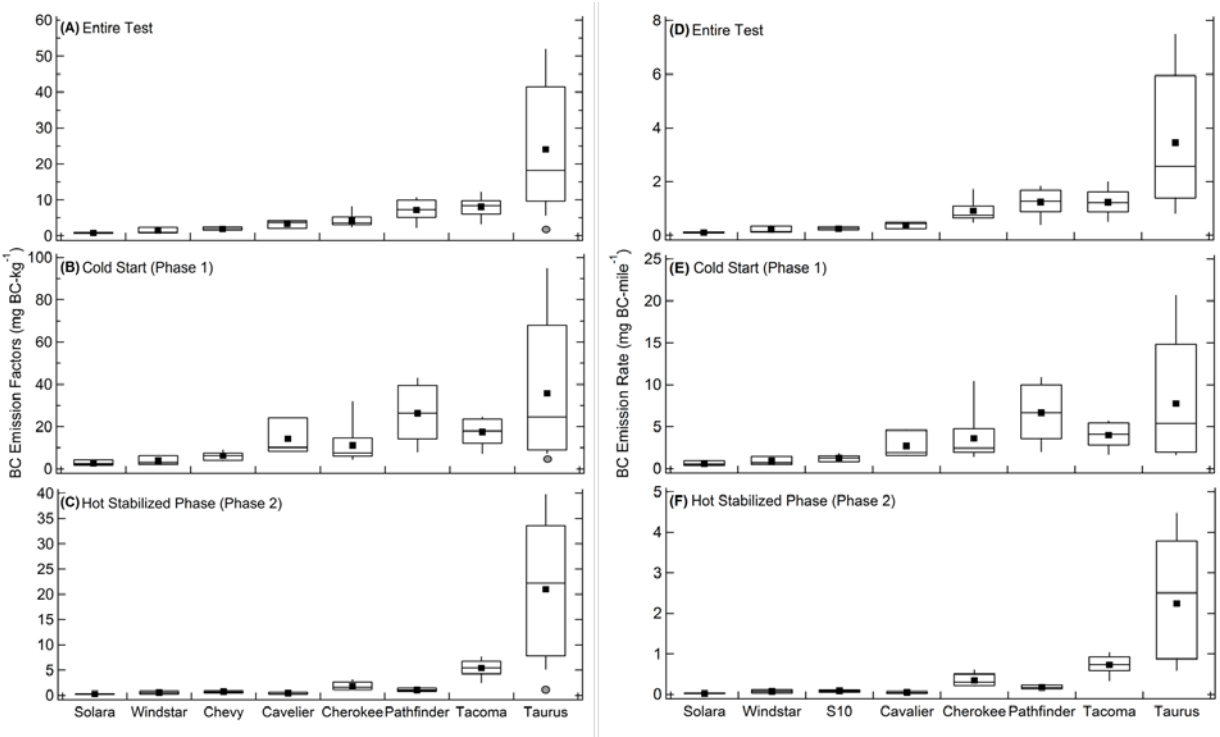

Figure 2-4: Black carbon emission factors (left panels) and emission rates (right panels) for all LEVs tested using the Unified Cycle. Results are shown for (A and D) overall, (B and E) Cold Start/Phase 1 and (C and F) Hot Running/Phase 2 EFs and ERs.

The daily (all tests) average real-time [BC] from the SDS+RTC compared well with the [EC] in the CVS, agreeing on average to within 12% (excluding one anomalous test day

when one vehicle malfunctioned during testing, thus strongly affecting the bulk EC measurement) (Table 2-2). The consistency between the thermal [EC] measured in the CVS and the daily averaged [BC] indicates that particle mass losses in the CVS and the SDS+RTC were minimal.

Table 2-2: Comparison of BC from thermal optical analysis and averaged real-time BC

Date	PAS ($\mu g\ m^{-3}$)	ARB ($\mu g\ m^{-3}$)
9/9/2011	4.79	6.11
9/13/2011	4.64	4.95
9/20/2011[#]	3.55	10.3
9/22/2011	8.21	7.15
9/23/2011	6.11	5.89

[#] an anomalous test day when one vehicle malfunctioned during testing

Typically, BC emissions are largest during the cold start phase, consistent with previous dynamometer studies [17, 31-34]. For example, the averaged ER_{BC} ranged from 0.61 – 5.3 mg $mile^{-1}$ during cold start but only 0.03 – 0.7 mg $mile^{-1}$ for hot stabilized. Reasons for this difference may include reduced volatilization and wall impingement of gasoline fuel during cold start.

2.3.2 Real-time BC Emissions Factors

A key aspect of this study is the ability to quantify EF_{BC} and ER_{BC} throughout the UC driving cycle. Figure 2-5 shows that there is a great deal of variability in the EF_{BC} during a given phase. The vehicle speed is shown for reference (grey lines). The red arrows indicate the occurrence of the first and second hard accelerations. The delay in at the beginning is due to the residence time in the CVS and the SDS+RTC; the speed profile has been shifted accordingly. Consistent with the average EF_{BC} and ER_{BC} values, the vehicle-specific maximum in the real-time EF_{BC} for properly functioning vehicles occurred during the cold start phase (60-360 seconds; Figure 2-5), ranging from 7.8 to 75.5 mg-kg^{-1}. Two additional peaks in EF_{BC} occurred during the hot-stabilized phase (360-1435 seconds), the first concurrent with a "hard" acceleration (at ~400 seconds) and the second, typically larger peak, with another hard acceleration (at ~920 seconds). This is consistent with the second acceleration during the hot stabilized phase being more rapid than the first (by 43%) and suggests that the EF_{BC} is most sensitive to the air-to-fuel ratio in the engine, with peaks corresponding to fuel-rich conditions (i.e. during the cold start phase and during hard accelerations). Unlike EF_{BC} (and [BC]), the [CO_2] peaked during all accelerations (not just hard accelerations), and overall exhibited greater consistency between tests that occurred on different days for a given vehicle.

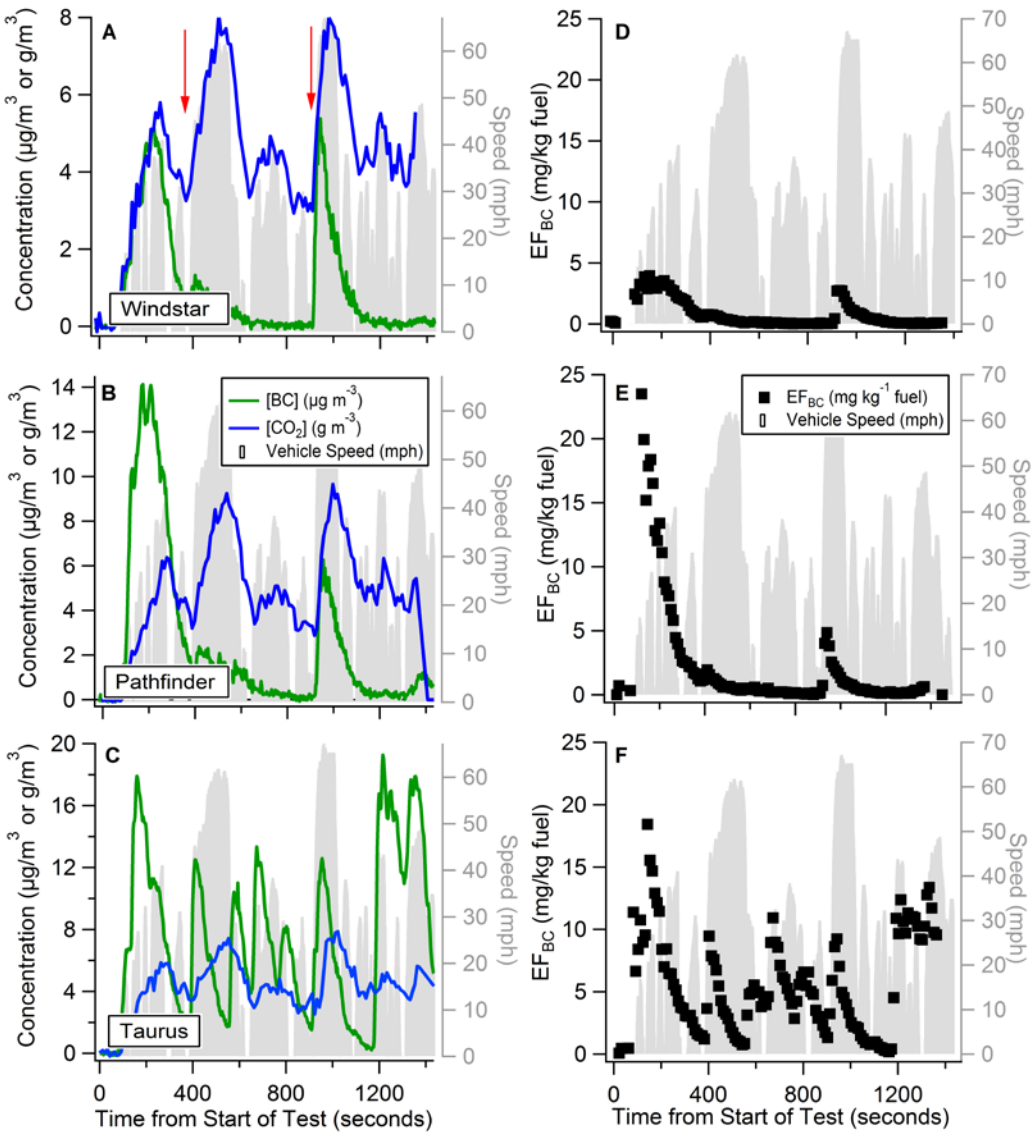

Figure 2-5: Real-time BC (green lines) and background-subtracted CO2 (blue lines) concentrations (A-C) and emission factors (black points; D-F) during a base case UC test on Sept. 20th for three LEVs: (A,D) Ford Windstar, (B,E) Nissan Pathfinder and (C,F) post-malfunction Ford Taurus.

The timing and magnitude of maximum EF_{BC}'s during a typical driving cycle may be used to inform spatially resolved models. The real-time EF_{BC}'s reveal that a major proportion of BC emissions would likely occur in the morning within approximately the first five minutes of driving (i.e. cold start) and in locations prone to hard accelerations (e.g. freeway entrances). Although modeling tools (such as MOVES) take increased PM emissions into account during cold start, the models could benefit from the enhanced time resolution provided by these real-time EF_{BC} or real-time ER_{BC} measurements since primary PM emissions tend to have sharp spatial gradients [35]. The real-time behavior

implies that local air quality of neighborhoods adjacent to major roadways and freeway entrances will be most affected by LDGVs in the morning driving commute.

2.3.3 Malfunctioning Vehicle

Results from the Taurus provide for an interesting case study because the Taurus engine began malfunctioning on 9/15 (after 3 sampling days), as indicated by the "check engine" light turning on. Although engine diagnostics that would elucidate the nature of the engine malfunction are not available, it is evident that after at this point the Taurus EF_{BC} increased substantially and became more variable (Figure 2-5c). However, despite this malfunction, the ER_{BC} values for the Taurus are still well below the expected range of "smoker" vehicles [8, 36-38]. Before malfunctioning, the Taurus exhibited the typical three peak structure in [BC], reaching a maximum of 10 μg m^{-3} (Figure 2-6). Just after malfunctioning, there were many more peaks in [BC] and the maximum concentration after the SDS+RTC reached 200 μg m^{-3}. Later tests (Figure 2-5c and 2-5f) similarly evidenced greater variability and higher [BC] than the properly operating vehicle, with an average EF_{BC} that was a factor of 6 higher than the other vehicles (Figure 2-4). In contrast to properly functioning vehicles, the post-malfunction Taurus BC emissions did not depend on the driving phase and were more sensitive to all periods of acceleration in the hot running phase, not just the two hard accelerations. This indicates that malfunctioning vehicles might not only have higher peak *EF* and *ER* values compared to properly functioning vehicles, but that they will emit BC throughout a typical drive cycle. This would in turn alter the spatial pattern of BC emissions for such vehicles.

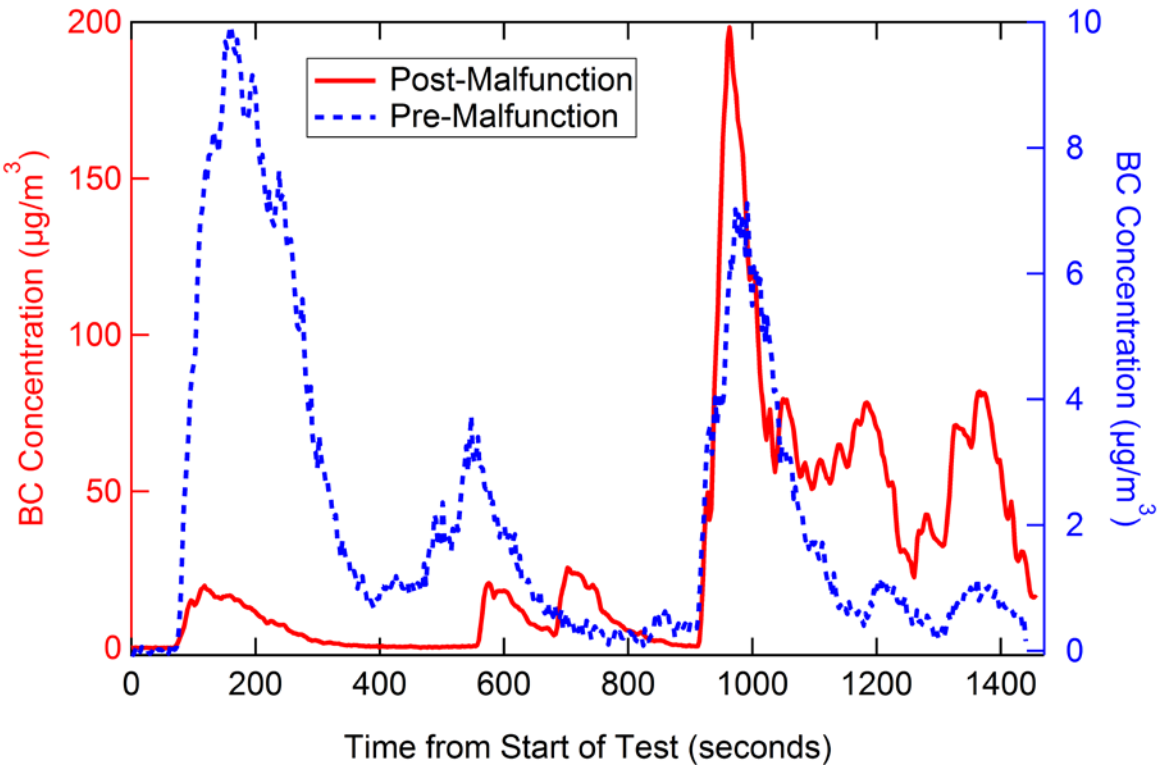

Figure 2-6: Real-time BC concentrations from the Ford Taurus (LEV) during the UC before (Sept. 9th; blue line) and after (Sept. 15th; red line) malfunctioning. Note the difference in scales for the two axes.

2.3.4 BC/TC and EC/TC

The real-time measurements (for tests performed with no added non-vehicle soot) demonstrate that BC dominates the total carbon (TC = BC + POC or EC + POC), with an all-vehicle full test average BC/TC = 0.75 ± 0.14 (1 SD) (Figure 2-7) and cold start and hot running values of 0.83 and 0.73, respectively. The very large BC fraction is consistent with the observation of very small average particle single scatter albedo (SSA) values (0.05 and 0.23 during cold and hot phases, respectively, and where SSA is the fraction of total light extinction due to scattering). The BC/TC (from the AMS and PAS and sampled from the SDS+RTC) compared well with the EC/TC (from thermal optical analysis and sampled from the CVS), with EC/TC = 0.80 on the single day where the measurements could be directly compared. The campaign average EC/TC from the CVS was similarly high (0.79). The slightly higher BC/TC could result from the additional dilution in the SDS relative to the CVS and consequent increased partitioning of semi-volatile POM species into the gas phase [39], although the difference is small and within uncertainties, suggesting minimal influence of this additional dilution on the POM. The BC/TC ratio was relatively consistent between driving cycles for most vehicles, although the Pathfinder and Solara had somewhat large, although highly variable bursts of POM during cold-start, with an average cold-start BC/TC for these vehicles of 0.64 to 0.68, respectively. The relatively high BC/TC ratios observed here are consistent with some

previous dynamometer studies [8, 33, 34], but not with others [17, 32, 37] (Table 2-4). Further, these dynamometer results can be compared with recent (post-2000) on-road and tunnel studies in which BC/TC or EC/TC ratios have been reported for LDGVs specifically, with values of 0.40±0.05 [31], 0.16±0.05 [40], 0.50±0.1 [41], and 0.5±0.6 [42] (most on-road studies are unable to clearly distinguish the LDGV contribution). The discrepancy between the relatively high EC/TC values in some dynamometer studies (including this one) but not others for similar model years could be in part due to the relatively small number of vehicles tested, although the consistently high BC/TC values for all vehicles tested would argue against this. The comparably large BC/TC ratio observed here could result from the relatively high dilution ratios used here, although the similarity of the SDS (total dilution factor ~60) and CVS (dilution factor ~12) EC/TC suggests this is not the case. Nonetheless, the possibility that the comparatively low EC/TC ratios in some studies result from smaller dilution factors cannot be ruled out. It is possible that our observations differ from the on-road studies because of substantial contributions from older, high-emitting vehicles in on-road studies, which often emit more unburned lubricating oil [43], or from contributions from non-tailpipe sources (e.g. organic compounds from road dust) [44].

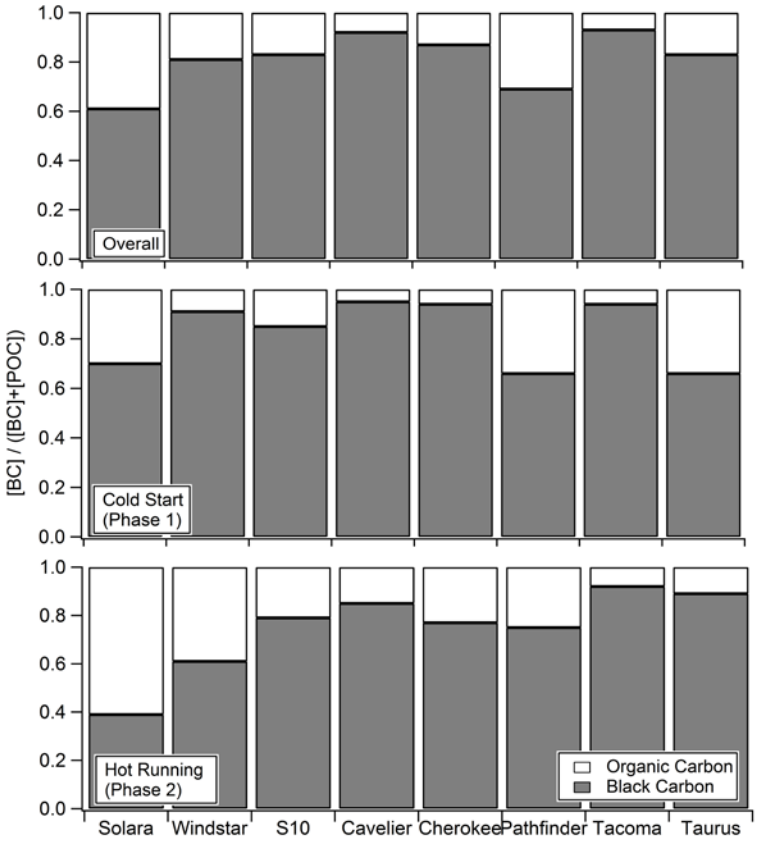

Figure 2-7: Average BC to total carbon (=BC + POC) ratios for LEVs determined from the real-time instrumentation (i.e. PAS and AMS), excluding the days on which non-vehicle BC was added to the SDS.

2.3.5 Constant Velocity (Steady State Operation)

EF_{BC}'s and ER_{BC}'s for the constant velocity tests were averaged from the start of the constant period until the end of the test (Table 2-3). Average ER_{BC}'s for LEVs are much lower during the steady state test than during either the cold start or hot stabilized phases of the UC, consistent with Schauer et al. [33], and likely as a result of vehicles operating at stoichiometry (i.e. low load) during steady-state operation even at high speeds. Interestingly, steady-state EF_{BC}'s for the SULEV GDI were substantially larger than for the other LEVs equipped with standard multi-port fuel injection, consistent with previous studies [45]. As expected, EF_{BC} for the diesel vehicle, which was not equipped with a diesel particle filter, was substantially larger than the GDI, ULEV, and LEV vehicles.

Table 2-3: Results from the constant velocity tests

Make/Model	Model Year	MPG	RH	Times previously started on test day	EF_{BC} (mg kg^{-1})	ER_{BC} (mg $mile^{-1}$)	EF_{OM} (mg kg^{-1})	ER_{OM} (mg $mile^{-1}$)
Chevy Cavalier (LEV)	2001	37	Ambient	0	0.50	0.04	0. 11	$9.0x10^{-3}$
Chevy Cavalier (LEV)	2001	37	Ambient	1	0.18	0.01	0.06	$4.6x10^{-3}$
Hyundai Sonata (GDI, SULEV)	2011	50	High RH	0	33	1.80	1.9	0.11
Hyundai Sonata (GDI, SULEV)	2011	50	Ambient	0	36	1.97	1.6	0.09
Hyundai Sonata (ULEV)	2008	39	Ambient	0	0.93	0.07	0.13	$9.3x10^{-3}$
Hyundai Sonata (ULEV)	2008	39	High RH	3	0.45	0.03	0. 39	0.03
Volkswagen Jetta (Diesel)	2004	47	Ambient	0	120	6.9	7.1	0.41

The average PM emission rate (BC + POM) from the GDI was 2.0 mg mile^{-1}, comparable to previous studies [45, 46]. The observed GDI ER_{PM} meets current PM standards (10 mg mile^{-1}) and the first phase of proposed PM standards under LEV III (3 mg mile^{-1}), but exceeds the second phase of proposed PM standards (1 mg mile^{-1}) [14]. Even though the GDI ER_{PM} meets current standards, the substantially larger ER_{PM} values for the GDI compared to the LEV suggests that any shift towards GDI vehicles (driven by their increased fuel economy relative to multi-port fuel injection) could lead to an increase in PM emissions from gasoline vehicles.

2.4 Discussion

2.4.1 Comparison with Dynamometer Studies

The average ER_{BC} values for all vehicles from this study compare reasonably well with results obtained from the majority of previous dynamometer studies, both for individual phases and averaged over the entire cycle [8, 17, 32, 33, 47] (Table 2-4). For example, the overall ER_{BC} reported in Fujita et al. [32] of 1.2 mg mile^{-1} is between the high and low emitters tested here. However, the ER_{BC}'s from high and low emitters are lower than those reported in Schauer et al, [33] likely because their vehicles started at lower cold start temperatures.

Table 2-4: Comparison of BC emission factors and rates for LEVs with other studies

Study & Type	Year of Measurements or Vehicle Model Years	BC Emission Factor (mg kg^{-1})	BC Emission Rate (mg $mile^{-1}$)	BC/TC or EC/TC ratio
Dynamometer Studies				
This Study (Low)[#] Combined[%]	1998 - 2003	1.90 (± 0.52)	0.24 (± 0.06)	0.75 (±0.14)[°] 0.80 (±0.08)[&]
This Study (High)[$] Combined	1997-2003	10.47 (± 3.98)	1.65 (± 0.51)	
This Study (Low)[#] Phase 1[^]	1998-2003	6.82 (± 2.59)	1.38 (± 0.46)	
This Study (High)[$] Phase 1	1997-2003	21.7 (± 2.29)	5.33 (± 0.88)	
This Study (Low)[#] Phase 2[+]	1998-2003	0.5 (± 0.05)	0.06 (± 0.01)	
This Study (High)[$] Phase 2	1997-2003	7.03 (± 2.19)	0.87 (± 0.47)	
Fujita et al. (2007) Combined[32]	1990-2001		1.2	0.23
Schauer et al. (2008) Combined[33]	1995-1999		3.9	0.34-0.84
KCS (2006) Phase 1[17]	1990-2000/ 2000-2003		4.4/3.6	0.36 – 0.38[°]
KCS (2006) Phase 2[17]	1990-2000/ 2000-2003		0.7/0.3	
Robert et al. (2007) Overall[8]	1996-2003		0.40	0.68
Geller et al. (2006) (New European Driving Cycle)[47]	2001		0.76	0.28
On-road and Tunnel Studies				
Kittelson et al. (2006)[34]	1984-1999		2.0	0.64
Grieshop et al. (2006) (tunnel)[42]	2002	26.6		0.46
Zielinska et al. (2004)[37]	1982-1996		4	0.40
Ning et al. (2008) (on road)[40]	2004-2005	20.5		0.16±0.05
Liggio et al. 2012 (on road)[48]	2010	115 (Median = 59)		
Strawa et al. 2010 (tunnel)[41]	2006	22		0.50±0.1
Park et al. 2011 (on-road)[49]	2007	60 (Fast Acc.) (Median = 20)		
Miguel et al. 1998 (tunnel)[50]	1996	30		
Geller et al. 2005 (tunnel)[51]	2004	30.4		
Kirchstetter et al. 1999 (tunnel) [31]	1997	35		0.40±0.05

[%] Averaged over the entire UC.
[#] Average for the 4 vehicles with the lowest average EF_{BC}.
[$] Average for the 4 vehicles with the highest average EF_{BC}.
[°] BC/TC single-day average over all vehicles, sampled from the SDS (N_{days}=2).
[&] EC/TC single-day average over all vehicles, sampled from the CVS (N_{days}=1).
[^] Phase 1 = cold start
[+] Phase 2 = Hot running

2.4.2 Comparison with On-Road and Tunnel Studies

The average EF_{BC} values here are substantially smaller than the mean EF_{BC} values reported in on-road and tunnel studies that distinguish LDVs, by factors of 2-10 (for the high emitters here) and 10-60 (for the low emitters here) (Table 2-4). This is true even though the vehicles sampled in the on-road and tunnel studies typically do not operate under cold-start conditions and therefore should, in principle, emit less BC. Our EF_{BC}'s are, in particular, much lower than the median values reported in Park et al. [49] and Liggio et al. [48] The average EF_{BC} here is 5.2 mg kg^{-1} for properly functioning vehicles, compared with a median EF_{BC} = 61 mg kg^{-1} from Liggio et al. [48] for a highway dominated by gasoline-powered vehicles (or ~75 mg kg^{-1} extracted for just the LDGVs) and a range of 10-30 mg kg^{-1} from Park et al. for LDGV vehicles operating under various conditions (e.g. idling vs. fast acceleration vs. high speed cruising).[34]

A possible reason for these differences is that the mean EF_{BC} values in on-road and tunnel studies are skewed towards higher values by very high-emitting vehicles, including older vehicles and malfunctioning vehicles. Dynamometer studies indicate that the ER_{BC}'s of vehicles with older model years are substantially higher than those from newer vehicles. For example, in one study the average ER_{BC} from vehicles with model years 1980-1990 was around 4 times higher than from vehicles with model years 1990-2000, but with a much smaller decline in going from 1990-2000 to 2000-newer [17]. This is likely due to implementation of improved emission control technologies in newer vehicles, allowing for more ideal fuel-to-air ratios. Thus, the oldest vehicles sampled in the on-road studies (with median vehicle ages of ~10 years) [52] likely push the average EF_{BC} upwards. However, most of the on-road/tunnel studies in Table 2-4 report measurements from the mid-2000's, and thus most of the vehicles sampled should have been from the mid-1990's into the 2000's, not all that different from the vehicles tested in the current study. It is possible that the small fleet of vehicles sampled in the current study happened to have emissions substantially lower than a typical on-road vehicle, although this seems unlikely since the vehicles tested were actual in-use vehicles (requisitioned for this study) and since the average EF_{BC} from even the malfunctioning vehicle was only 24 mg kg^{-1}. However, since the tested vehicles were all classified as LEV I it is possible they have lower EF_{BC}'s than some in-use vehicles.

On-road malfunctioning vehicles, including smokers [8, 36-38], may also drive up the average EF_{BC}. Interestingly, the average EF_{BC} of the malfunctioning, high-emitting vehicle tested in this study was at the lower end of reported mean and, for the few studies that report it, median on-road EF_{BC} values. It seems unlikely that there would be enough malfunctioning vehicles on the road to substantially influence the median (especially for studies conducted in locations that require periodic vehicle emissions testing, such as California). Additionally, studies that report both the mean and the median [48, 49] indicate that the mean is only around 2-3 times higher than the median. The median should be more characteristic of the behavior of the average vehicle, and thus there remains an apparent inconsistency between our dynamometer results on the on-road and tunnel studies.

Notably, the GDI vehicle tested in this study emitted substantially more BC than the LEVs tested in this study and exceeds the proposed LEV III standard.. However, the influence of GDI vehicles is likely minimal for the on-road and tunnel studies because the fraction of GDI vehicles in the U.S. fleet is negligible for model years 2007 and older [53], and most on-road and tunnel studies listed in Table 2-4 took place before 2007.

The real-time observations demonstrate that BC emissions are sensitive to driving behavior, in particular acceleration, and it is possible that the UC may not accurately reflect the driving behavior (i.e. the frequency of aggressive accelerations) observed in on-road studies. However, Liggio et al. measured emissions from vehicles traveling on a straight stretch of highway. We observed that, for a given vehicle, the EF_{BC} was substantially lower during steady, high velocity operation compared to the cold start or hard accelerations during the hot running phase. Thus, it seems reasonable to expect that the median EF_{BC} values from Liggio et al. should, in principle, be lower than that measured during the UC here, which is not the case.

3 GAS-PHASE CO2 SUBTRACTION FOR IMPROVED MEASUREMENTS OF ORGANIC AEROSOL MASS CONCENTRATION AND OXIDATION DEGREE BY AEROSOL MASS SPECTROMETER

3.1 Introduction

The Aerodyne Aerosol Mass Spectrometer (AMS) has become a prevalent tool for analyzing the non-refractory (NR) components of submicron particulate matter (PM_1) sampled in real-time from both ambient and controlled-laboratory environments [54]. The instrument relies on decoupled vaporization (600 ° C) and electron impact (EI) ionization for particulate matter detection where parent molecules are fragmented and the data yields bulk chemical information [54, 55]. The analysis of such data relies on comparisons with reference EI mass spectra, representative tracer ions, and extensive laboratory characterization to allow for realistic interpretation of ambient aerosol data [56]. The High Resolution Time-of-Flight AMS (HR-ToF-AMS) allows for isobaric ions collocated at the same integer mass-to-charge ratio (*m/z*) to be distinguished, yielding more detailed chemical information [24]. In addition, the AMS has the ability to provide size-resolved chemical information using the particle time-of-flight (PTOF) function [55]. The size distribution of a mass spectral signal is a useful indicator of its sources [e.g., 56, 57, 58, 59].

The inlet of the AMS acts as a particle concentrator, stripping away a substantial portion of the gas, and concentrating the particles to an order of up to 10^7 relative to the gases in the air sampled at the inlet [60]. However, the gas phase ions detected by the instrument can still dominate the raw signal, making them an important component of the mass spectrum. For example, the *m/z* calibrations are typically done using some of the gas phase ions and the nitrogen signal (N_2^+, *m/z* 28) is used as an internal standard to track the real-time sensitivity of the instrument [58]. For ambient sampling, signals produced by air components such as nitrogen (N_2), oxygen (O_2), water vapor, argon (Ar), and CO_2 can interfere with the signals produced by PM since they either overlap with isobaric ions originating in the particle phase or the ion signal in question can originate from both the gas phase or be a fragment of parent molecules originating from the particle phase. The gas phase signals may interfere with quantification of particle size distributions as well [56, 61]. For example the O^+ (*m/z* = 16) signal needs to be properly removed to determine the size distribution of ammonium in ultrafine particles, which was found to be important for unraveling the chemistry of new particle growth [62].

The *m/z* 44 (CO_2^+) signal coming from gas phase CO_2 is indistinguishable from signals resulting from the fragmentation of oxygenated organic species, thus can significantly influence the oxygen-to-carbon ratio (O/C) of the bulk signal [63] and interfere with factor analysis of the AMS mass spectra [64]. Properly subtracting the gas phase components is therefore crucial for accurately assessing the O/C and the oxidation state of the sampled aerosol, as well as for quantification of organic aerosol mass. By default gas-phase CO_2 is determined by scaling the N_2^+ signal to an assumed background

atmospheric mixing ratio of CO_2 in air. Hence the signal at *m/z* 44 is broken up into gas-phase and particle-phase CO_2^+ where the gas-phase signal is determined as the N_2^+ signal times the assumed mixing ratio of CO_2 and all remaining signal at this *m/z* is assigned as an organic particle-phase signal (i.e., Org44) [56]. During field campaigns periodic filter tests, where no particulate matter is sampled into the AMS, are performed to determine the background gas phase mixing ratios of CO_2 in ambient air, and these values are incorporated in the fragmentation table to determine Org44.

In cases when the gas phase components that interfere with PM signal vary significantly, collocated, real-time gas phase measurement data are needed to adjust the fragmentation table that is used for processing the AMS data. An example of this application can be found in Setyan [64], which describes the results of a rural-remote sampling campaign where an HR-ToF-MS measured ambient aerosol in conjunction with various gas-phase measurements. It was found in this case that the gas-phase CO_2 had a strong diurnal pattern where concentrations varied by approximately 8% and accounted for as much as 75% of the total signal at *m/z* 44 during low organic mass loading periods. A real-time gas-phase measurement of CO_2 was utilized to subtract the varying gas-phase portion in order to properly account for Org44. This study also found that this correction was important for properly extracting organic factors via factor analysis of the organic mass spectral matrix [64].

In addition to relying on collocated gas phase measurements, internal checks utilizing built-in AMS features can be advantageous in determining the gas-phase to particle-phase ratio for a given ion signal. For example, the signal ratio for gas-phase to particle-phase for an ion such as NH_2^+ or CO_2^+ can be derived by examining the signal distribution of the ion in question in PTOF space. Signal showing in the size range corresponding to the so-called PTOF air-beam region will be treated as gaseous and the rest which appears in the PM region will be assigned to particle phase [61]. This ratio can then be applied to the fragmentation table for proper gas-phase subtraction. In addition, multivariate analysis such as positive matrix factorization (PMF) [65] can be used to separate the gas-phase and particle-phase contribution in cases where an ion has significant contributions from both phases and where their time-dependent signals are varying uniquely.

Here we present a detailed discussion on utilizing all three methods mentioned above for the determination of the real-time gas-phase particle-phase division of the signal for the CO_2^+ ion at *m/z* 44 and illustrate these methods by examining vehicle emissions. Vehicle emissions are comprised of a mix of gas-phase and particle-phase components [66]. The gas-phase components include typical combustion products such as CO_2, volatile organic compounds (VOCs), CO, NO_x, and others [67]. The particle-phase compounds are a complex mixture of elemental carbon and semi-volatile and low-volatility organic compounds mostly comprised of hydrocarbon-like organic species which mainly come from unburned fuel and lubricating oil [68, 69]. In sampling this type of aerosol using the AMS, the important gas-phase components, e.g., CO_2, vary widely on a fast time-scale and therefore may interfere severely with the particulate compounds of interest.

In this study, an HR-ToF-MS was used to sample vehicle emissions in real-time where the vehicles were running on a chassis dynamometer. A collocated LI-COR instrument was used to sample real-time gas phase CO_2. The real-time measurement of both organic PM loading and gas-phase emissions allowed for analysis of emission factors as a function of engine load. It was found generally that changes in the CO_2 emissions correlated with velocity and the variation of emissions of particulate matter correlated with engine load and that there is a non-negligible portion of the CO_2^+ signal which is particle bound. In order to properly define what portion of the *m/z* 44 signal belongs to gas-phase, the collocated LI-COR data was utilized and the resulting gas-phase subtraction was verified using both PMF and the size-resolved PTOF information. The motivation of this study is to report the various tools used to subtract a varying gas-phase CO_2 signal for proper quantification of organic PM concentrations and O/C ratios, illustrated by closely examining vehicle emission measurements where gas-phase contribution to total *m/z* 44 signal is large and variable. The methods presented in detail here can be applied to any situation where gas-phase components may influence the PM signal of interest.

3.2 Experimental Methods

A fleet of in-use vehicles was chosen for emissions sampling at the California Air Resources Board (ARB) Haagen-Smit facility in El Monte, CA in September of 2011. Eight Light duty gasoline vehicles (LDV), ranging in year from 1997-2003, were driven under the first two phases of the unified drive cycle (UC) driving cycle where the first phase consists of a 300 second cold-start and the second phase consists of 1135 seconds of hot running with various accelerations and periods of constant high velocity. A sample of 3 types of alternative vehicles, including an ultra-low-emissions vehicle (ULEV; Hyundai Sonata 2010), gas direct inject (GDI; Hyundai Sonata 2008), and diesel passenger vehicle (VW Jetta 2008), were driven under a constant velocity driving cycle which consists of a short hot-start and rapidly accelerated to an extended period of constant velocity. In order to measure vehicle emissions at atmospherically relevant concentrations, a secondary dilution system (SDS) described elsewhere [70] and shown schematically in Figure 1, was installed to further dilute vehicle emissions from ARB's in-house constant volume sampler (CVS) tunnel. The SDS consisted of a sampling volume where vehicle emissions were injected. Dilution air was introduced via an orifice plate after it was filtered and denuded. The diluted emissions then passed through a residence time chamber (RTC) followed by a manifold which led to various real-time instruments including an HR-ToF-AMS (Aerodyne Research Inc., USA) and a LI-6262 CO_2/H_2O gas analyzer (LI-COR Inc., USA). The flow through the SDS was kept within the transition/turbulence regime to promote mixing mimicking that of emissions in the atmosphere. The first stage dilution was on average 18 in the CVS and the average dilution applied in the SDS was 4.8, leading to a factor of ~ 86 dilution to the tailpipe emissions. The dilution was adjusted to maintain a total PM loading within 2-30 $\mu g/m^3$.

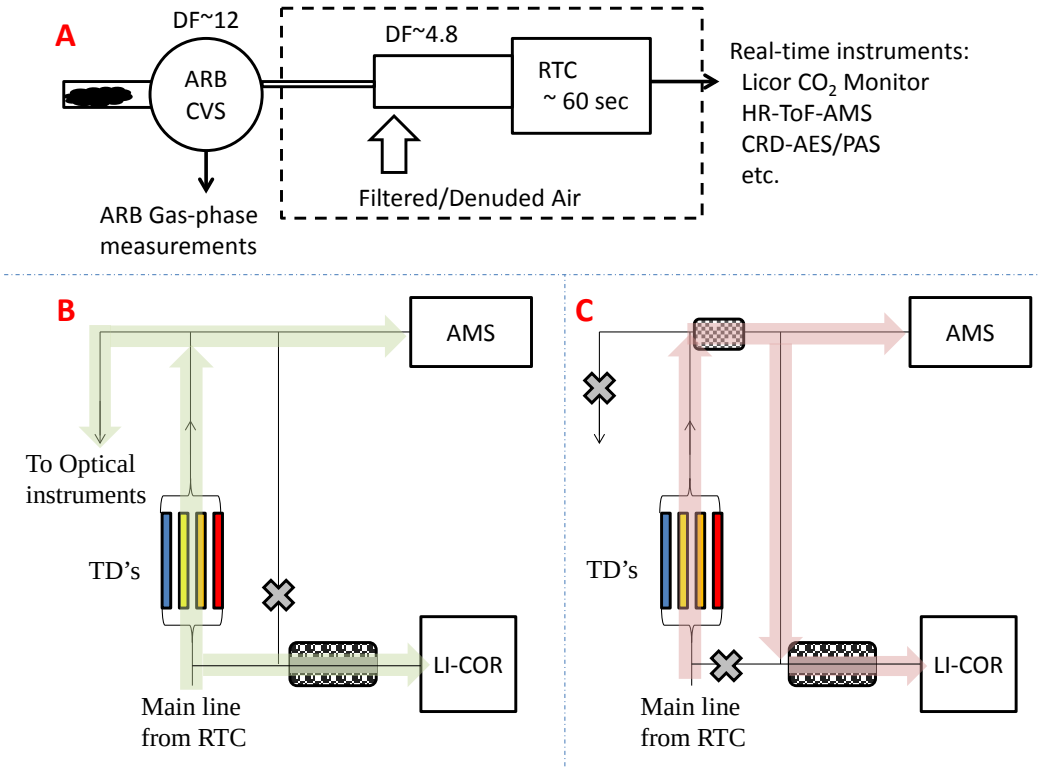

Figure 3-1: Panel A shows a simplified schematic of the vehicle emissions sampling scheme where vehicle emissions undergo an initial dilution in the constant volume sample tunnel (CVS) and undergo a second dilution in the secondary dilution system (SDS) which includes a residence time chamber (RTC) eventually leading to a suite of real-time instruments. Panel B shows a schematic of the AMS and LI-COR configurations in regular vehicle sampling mode and Panel C shows the filter sampling mode.

The HR-ToF-AMS was operated at 10 second averaging in V-mode with both MS and PTOF modes, utilizing the ToF-AMS DAQ version 4.0.1 software. The LI-COR instrument was placed upstream of the manifold system to maintain sufficient residence time through the thermal tubes and its signal was recorded by the Measurement Computing USB-AI-Temp block terminal using a LabView v10 application with 1 second averaging. In order to calibrate the AMS gas-phase CO_2^+ ion signal reading to that of the LI-COR CO_2 reading, daily filter tests were performed where a particle filter was placed upstream of a tee which branched to both the AMS and the LI-COR system. Figure 1 illustrates the vehicle emission sampling mode versus the filtered air sampling mode. In addition, ARB provided real-time gas-phase measurements that were taken directly from the CVS tunnel. A more detailed description of the vehicles and test types conducted and the analyses of the HR-ToF-AMS data is given in a related manuscript (Collier et.al., in preparation).

3.3 Methods of Subtracting Gaseous Contributions to AMS CO2+ Signal

Gas-phase subtractions and fragmentation table adjustments are a necessary step when analyzing NR-PM_1 data, particularly for species that exert a strong influence on the mass spectra of an aerosol signal. There are many situations in which this type of analysis is critical. In the case of vehicle emission sampling during the UC drive cycle described above, the gas-phase CO_2 levels are varying rapidly and with a large range of concentration, particularly during cold-start tests where the vehicle undergoes various accelerations and differing cruise velocities. If no modification is done to the fragmentation table, the particle signal at m/z 44 can be significantly influenced by the signal from gaseous CO_2^+, leading to substantial overestimation of the O/C ratio in particles, especially for low particle loading situations. An example of this can be found in Figure 2, which shows the time series and mass spectra of two adjacent vehicle tests, V1 and V10, during the first 300 seconds since ignition. V10 has a particle phase signal that is almost an order of magnitude larger than V1 yet both have comparable gas-phase CO_2 concentrations as measured by the LI-COR instrument. If the default gas-phase correction, which assumes a background CO_2 concentration of 370 ppm (see section 3.1), is used for both cases, the portion of particle phase signal at m/z 44 is more dramatically overestimated in the mass spectrum of V1 (Figure 2d) compared to V10 (Figure 2b), due to the relatively larger gas-phase contribution of CO_2^+ at m/z 44 for V1 compared to V10.

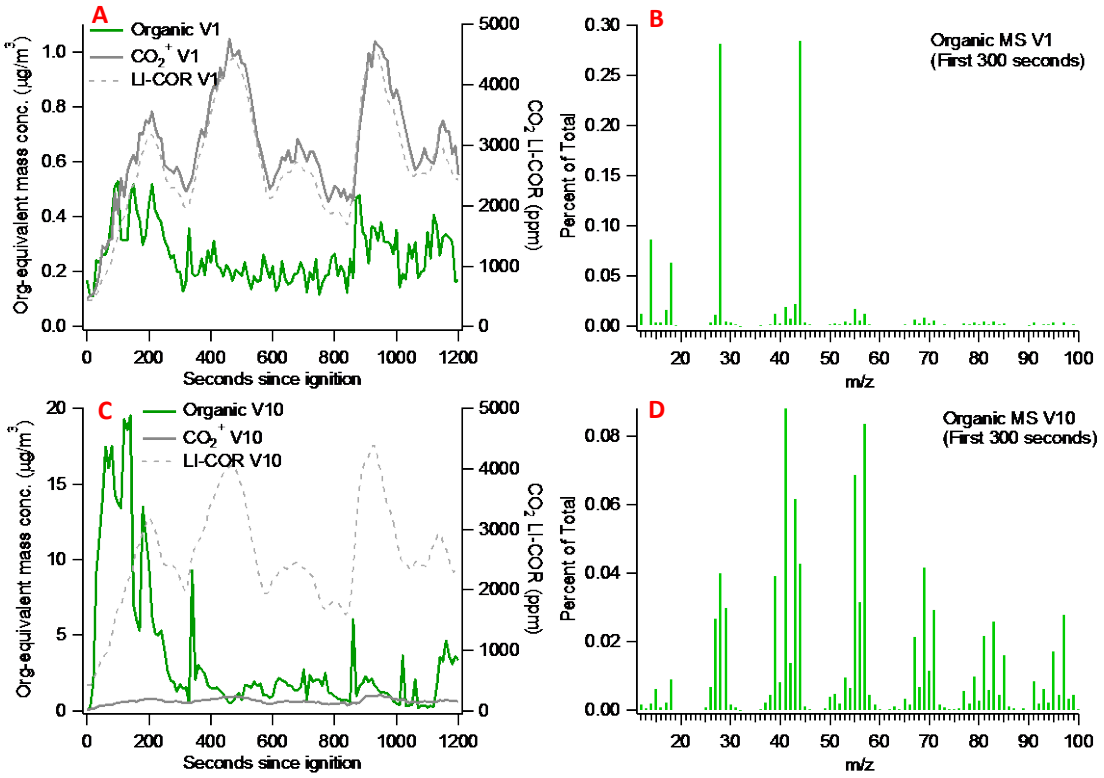

Figure 3-2: An example of the time-series of organic loading (signal contribution from *m/z* 44 not included in the time trace) and total signal at *m/z* 44 (mostly CO_2^+) of two contiguous cold-start gasoline light-duty vehicle tests. The normalized mass spectrum of each vehicle test is an average of the first 300 seconds of the cold-start test. Default fragmentation values used for gas-phase subtraction **[56]**).

Figure 3 shows a comparison between the signal ratio of total CO_2^+/N_2^+ as measured by the AMS during both filter tests and vehicle tests and the LI-COR CO_2 mixing ratio. A linear function was fit through the filter data points. All other vehicle test data lie close to the fit function or above it. Data points representing higher loading tend to lie farther from the linear fit, indicating there is a particle-phase portion in the CO_2^+ ion signal. The fraction of the signal at *m/z* 44 that is gaseous clearly varied substantially and must be removed properly for proper quantification of organic PM. The default approach that assumes a constant CO_2^+ to N_2^+ ratio cannot be relied upon under these circumstances and may lead to errors in oxygen-to-carbon ratio as well as the overall organic mass loading.

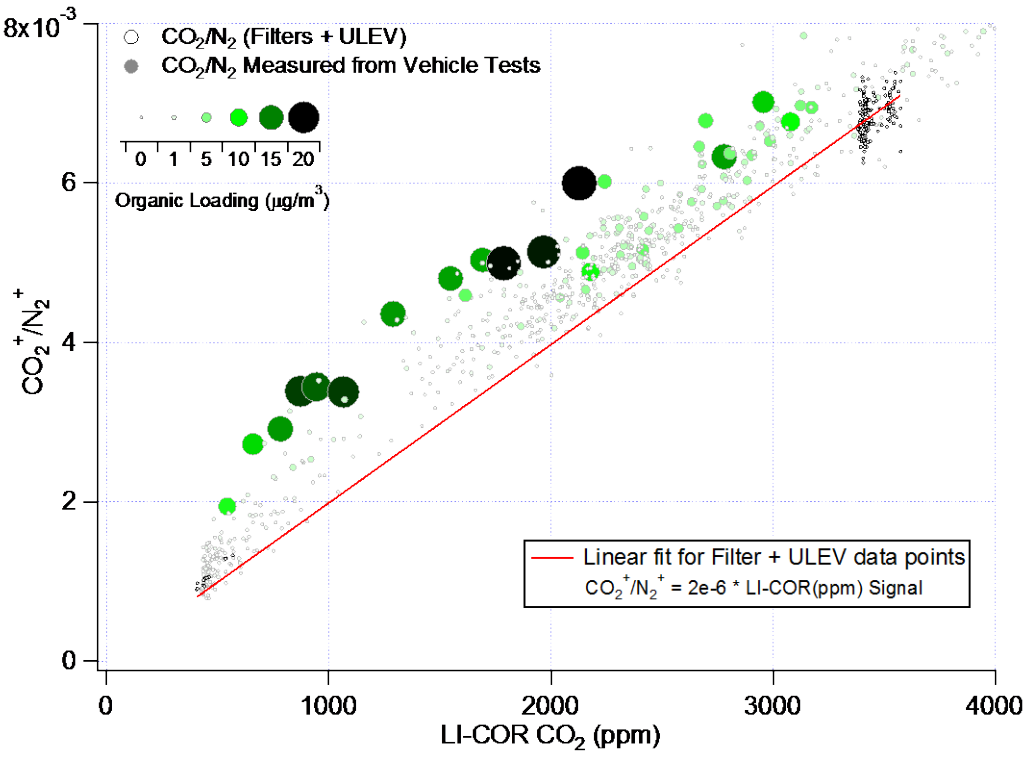

Figure 3-3: AMS ratio between CO_2^+ and N_2^+ ion signals vs. gas phase CO_2 concentration. The markers with the black stroke are comprised of filter and ULEV test data points. The red fit line defines the relationship between LI-COR measured concentration and AMS measured concentration of gas-phase CO_2. The markers with grey stroke represent vehicle test data points. All individual data points are colored by overall organic mass loading with increasing loading denoted by a darker green color as well as increasing size.

This illustrates the importance of developing a robust method for subtracting the real-time CO_2 gas phase signal in situations where gas-phase signals may vary widely, such as sampling vehicle or biomass burning emissions. Table 1 delineates detailed steps recommended for a rigorous gas-phase subtraction and hence proper quantification of AMS data. Each method is explained in more detail below.

Table 3-1: Gas-phase subtraction standard procedure

Method 1: Utilization of collocated gas phase measurements 1. Include a collocated gas-phase analyzer sampling at similar or higher time-resolution 2. Calibrate to AMS using filtered air 3. Apply all IE, REI, CE values to data and filter test data a. Analyze all filtered air runs in single Squirrel/Pika pxp b. Plot average filtered air load for given ion versus average reading from collocated instrument for a given filter period 4. Modify fragmentation table to reflect subtraction based on real-time gas-phase data from collocated instrument
Method 2: Performing PMF on combined PM and gas-phase signals 1. Include gas-phase ion in organic family and generate 2-D matrix 2. Input matrix and error matrix into PMF Evaluation Toolkit 3. Perform all recommended preparation steps 4. Setup PMF calculation with varying fpeak 5. Verify that resulting factors separate gas-phase signal from PM signal
Method 3. Analysis of PTOF data 1. Plotting individual ion in PTOF space 2. Find percentage in so called PTOF airbeam space compared to that found in PM space

3.3.1 Utilization of collocated gas phase CO2 measurements

Collocated gas-phase measurements and filter tests are recommended practices for quantifying gas phase signals in AMS data. Filter tests have a two-fold purpose. They help determine average background concentrations of important gas-phase ions which may interfere with particle-phase ions of interest. Secondly, when comparing AMS data to collocated gas-phase measurements the filter periods act as a calibration between the gas instrument signal and the loading reported by the AMS for the gas-phase ions of interest. In this case the mass loading at *m/z* 44 was found for all filter tests and plotted versus the average signal output of the corresponding LI-COR results (Fig. 3). In the fragmentation tables for AMS data analysis the gas-phase CO_2 is apportioned based on the concentration ratio of CO_2 to N_2 in the atmosphere [56]. The default apportionment equation for signal at *m/z* 44 is,

$$Frag\_CO_2 = 0.00037*1.36*1.28*1.14*frag\_N_2 \quad [1]$$

Where Frag_CO_2 is the gas-phase CO_2 contribution to the mass spectrum signal at *m/z* 44, 0.00037 is 370 ppm, 1.36 is the relative ionization efficiency of CO_2 with respect to nitrate, 1.28 is the reciprocal of the fraction of N_2 in air, 1.14 is a correction for the fragmentation of N_2 at *m/z* 15, and frag_N_2 is the N_2 contribution to the mass spectrum signal at *m/z* 28 [56]. 0.00037 may need to be adjusted based on filter tests conducted during an experiment. The organic PM contribution at *m/z* 44 (i.e., Org44) is simply the total signal at *m/z* 44 (mz44) minus the Frag_CO_2 value.

In the case of a rapidly varying signal, the 0.00037 value in equation 1 has to be substituted with a time series of the real-time gas-phase CO_2^+/N_2^+ ratio. In this study, the CO_2^+ and N_2^+ signals during the filter tests were used to calculate the slope of the function defining the ratio of CO_2^+ to N_2^+ as a function of the collocated LI-COR signals:

$$CO_2^+/N_2^+ \text{ (Filter)} = m*\text{LI-COR Signal(Filter)} \quad [2a]$$

The slope *m* is then used to calculate a new wave describing the real-time mixing ratio of CO_2^+/N_2^+ as a function of the real-time LI-COR signal during vehicle tests:

$$CO_2^+/N_2^+ \text{ (Vehicle)} = m*\text{LI-COR Signal(Vehicle)} \quad [2b]$$

A reference to the real-time CO_2^+/N_2^+ mixing ratio data is placed in the cell belonging to the gas-phase CO_2^+ in the fragmentation table [56]. Now the organic PM signal at *m/z* 44 is redefined as:

$$\text{Org44} = \text{mz44} - CO_2^+/N_2^+ \text{ (Vehicle)} * \text{frag\_}N_2 \quad [3]$$

It is important that filter test conditions are representative of actual test conditions. In this case, since the filter tests were conducted during ambient conditions as opposed to during vehicle tests, they represented only a narrow range of low gas-phase CO_2 concentrations compared to the dynamic range of the vehicle test CO_2^+ signal loading (Fig. 3). In order to define the linear relationship between the LI-COR signal and the AMS gaseous CO_2^+ value with larger dynamic range which reflects the vehicle test conditions, the data points acquired with the ULEV vehicle were included in order to define *m* in equation 2b (Fig. 3). The particle loading during ULEV tests was substantially lower than standard LEV vehicles whereas the CO_2^+ signal was close to the average levels emitted by all the vehicles tested. CO_2^+ signals from ULEV tests were therefore used as a proxy for particle-free air in the present study. However, we recommend that future experiments perform filter tests that represent the entire concentration range of CO_2. Henceforth this particular gas-phase subtraction method will be referred to as varying CO_2 subtraction method.

A case study was chosen to illustrate the effect of this subtraction method and is depicted in Figure 4. The organic PM concentrations determined using the default fragmentation table settings were clearly overestimated compared to those determined after proper CO_2 subtraction (Fig. 4a). Indeed, during the period between approximately 350 to 550

seconds since ignition, the total CO_2^+ signal is elevated and the loading difference is more pronounced. The organic PM trace determined after proper CO_2 subtraction is not influenced by the gas-phase CO_2^+ signal fluctuations and yet is elevated above the broken brown trace (i.e., organic PM determined without counting the signals at *m/z* 44; Fig. 4a), indicating it is not being over-subtracted. As shown in Figure 4b, the average mass spectrum for this vehicle with default fragmentation settings where the CO_2^+ and CO^+ signals clearly dominate the spectrum and CO_2^+ accounts for greater than 10% of the total signal. In contrast, the mass spectrum after applying the varying CO_2 subtraction shows less than 2% CO_2^+ contribution (Fig. 4c).

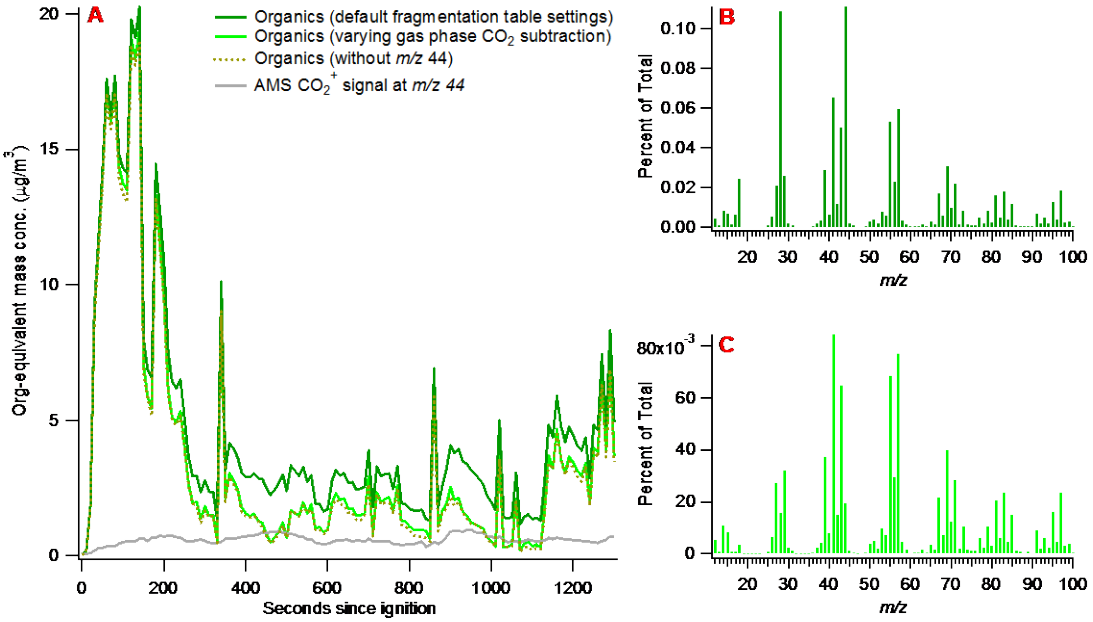

Figure 3-4: Panel A shows a comparison of organic PM signal for vehicle 10 (Ford Taurus 1997) before and after the final CO_2 subtraction method is applied. Panel B depicts the mass spectrum of organics using the default fragmentation setting. Panel C depicts the mass spectrum of organics using varying gaseous CO_2 subtraction.

3.3.2 PMF Analysis

In atmospheric aerosol sampling and data analysis, particularly with the AMS, a powerful mathematical tool, Positive Matrix Factorization (PMF) [65], is often used to estimate the number of factors contributing to the overall AMS organic signal sampled in real-time [71, 72]. Factors can be attributed to different sources or different physical-chemical processes and can typically be correlated with tracer species, diurnal patterns, and air-mass trajectory information. PMF is not limited to aerosol source apportionment and can be used to separate any factors that have varying contributions to any matrix which is the linear combination of these factors. For the purposes of this study PMF was used as a tool to separate the gas-phase and particle phase contributions at *m/z* 44. The capability to separate the signal contribution hinges upon the fact that gas-phase and particle-phase

signals of CO_2^+ have distinct temporal variations (Fig. 2). In this case gas phase CO_2 tends to correlate more strongly with fuel consumption while organic aerosol correlates more strongly with engine loading and engine temperature.

To generate the 2D matrices of high resolution organic mass spectra and corresponding error spectra for PMF analysis, the fragmentation table was modified so that the organic fragment included the entire *m/z* 44 signal, i.e. no gas-phase subtraction was performed. The PMF Evaluation Tool (PET) [72] version 2.05 Beta was used for this analysis. The preparation of the mass spectral and error matrices was performed following the procedures given in Table 1 of Zhang et al (2011) [71], which include down-weighting weak *m/z*'s, down-weighting *m/z* 44 and related *m/z* values, applying a minimum error to the error matrix, and removing all isotopic ions. A range of FPEAK values was set from -1 to 1 with increments of 0.1 and the number of factors was set from 1 to 4.

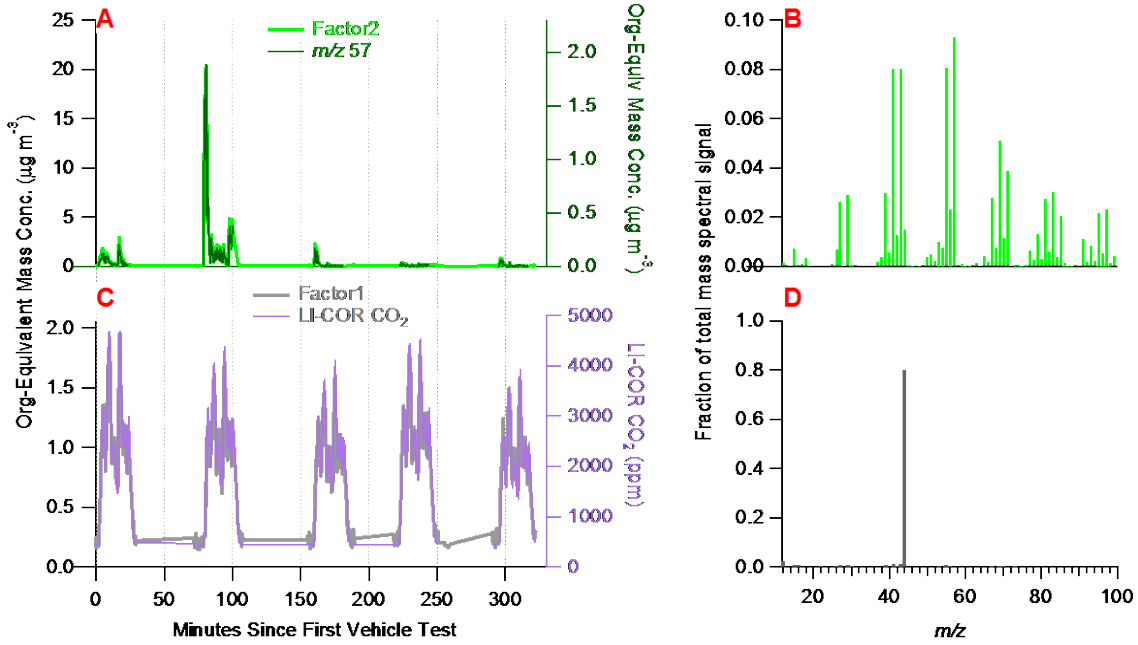

Figure 3-5: PMF results for the 2-factor solution. Panel A shows the time trace for Factor 2 with the signal contribution from *m/z* 57 superimposed. Panel C shows the time trace for factor 1 with the time series of LI-COR CO_2 mixing ratio superimposed. Panel B shows the mass spectrum of Factor 2 and panel D shows the spectrum of Factor 2.

A solution with up to four factors was explored but the two-factor solution yielded the best results. As shown in Figure 5, the two-factor solution presented minimal "mixing" and "splitting" of factors where factor 1 and factor 2 have very little correlation with each other in terms of both their time dependences and their mass spectra. The higher factor solutions show apparent indications of mixing and splitting of factors. The two-factor solution yielded a factor 1 corresponding clearly to gas-phase CO_2 and a factor 2 corresponding to vehicle emission organic PM (Fig. 5). Figure 5d depicts the mass spectrum of factor 1 where the largest signal is the CO_2^+ ion at *m/z* = 43.997. Figure 5b

shows the mass spectrum of factor 2, which looks like a typical hydrocarbon-like organic aerosol (HOA) spectrum, and where the percent contribution of the CO_2^+ ion is 1.42%. In addition, the time series of factor 1 correlates very well with that of CO_2 mixing ratios measured by LI-COR (Fig. 5c) whereas the time series of factor 2 and $C_4H_9^+$ (i.e., an AMS tracer ion for HOA [73]) correlate tightly (Fig. 5a).

It is also interesting to point out that the rotational ambiguity for the 2-factor solution was minimal where FPEAK had very little effect on the percent contribution of the 2 factors. This is an indication that the two factors are almost orthogonal, reflecting the fact that CO_2 and organic PM have completely different mass spectra and that their time series from this vehicle test are poorly correlated. The same analysis was performed on other tests as well. For the diesel vehicle the 2-factor solution yielded similar factors to those of the gasoline vehicle PMF results. There was a clear gas-phase CO_2 factor and an HOA factor that has a CO_2^+ ion contributing 4.6% of the total signal. For both the GDI vehicle test and the ULEV vehicle test, the 2-factor solution yielded a gas-phase factor and an HOA factor in which the CO_2^+ ion contributes ~ 6-7% of the total signal. However, since the alternative vehicle tests were not run in the cold-start drive cycle, but rather under constant velocity conditions, the time-dependent loading for organic PM and CO_2 did not vary significantly and were not uniquely variable with respect to each other. As a result, the PMF results are more ambiguous for the constant velocity conditions.

3.3.3 Subtracting gas phase contributions using PTOF data

The third option for determining what percentage of the overall *m/z* 44 signal corresponds to particle-bound CO_2 is to utilize the PTOF information. In the signal distribution of individual *m/z*'s plotted as a function of particle size, the portion attributable to PM is well separated from the gas-phase signal. The segregated portion of the *m/z* 44 signal can be used to calculate f44, defined as the fraction of PM signal at *m/z* 44 with respect to overall organic PM loading. This can be directly compared to the same ratio derived using the other two methods discussed above. Figure 6 shows AMS signal for N_2^+, *m/z* 44, and *m/z* 57 in PTOF time space and corresponding to an average of all runs on a test day with overall organic loading > 5 μg/m^3. The area under the curve was calculated for *m/z* 44 between PTOF sizes 30 –1500 nm. The transmission efficiency for the aerodynamic lens of this instrument drops off rapidly below 30 nm (the ideal range is 60 nm-600 nm [60]). The f44 averaged over all gasoline vehicle data points on this day is approximately 3.5% when using the PTOF method. When the average PTOF size distribution is averaged using data points corresponding only to overall organic PM loads > 2 μg/m^3 the f44 is approximately 2%. However, due to low chopper duty cycle (2%), the AMS PTOF size distribution data has much lower signal-to-noise ratio than the data acquired under the mass spectral mode, which has a duty cycle of 50%. For this reason, using PTOF data to calculate f44 for low PM mass loading conditions could give unreliable results.

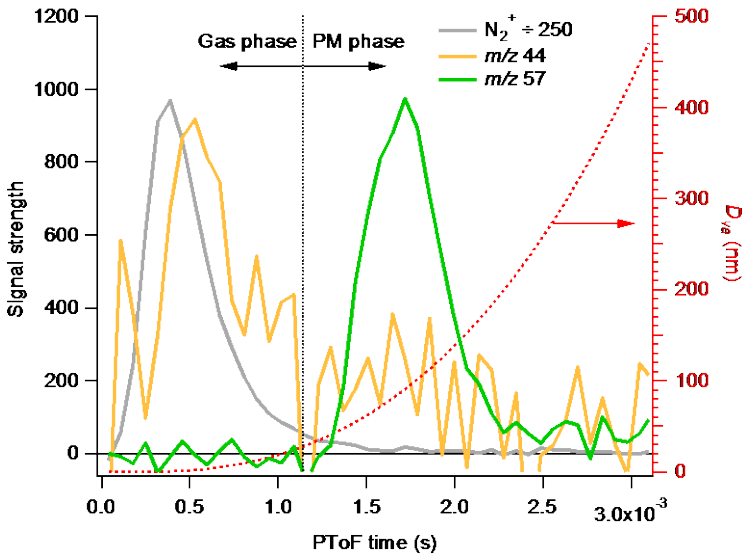

Figure 3-6: Average signal acquired by AMS in PTOF mode for all vehicles on September 20th (Base Case test day) with loading > 5 µg/m^3 and plotted in PTOF space. The grey trace depicts the N_2^+ ion signal which dominates the gas-phase or air beam portion of PTOF space. The light green trace depicts the signal at *m/z* 57 ($C_4H_9^+$) which is completely in the particulate matter portion of PTOF space. The signal at *m/z* 44 has a relatively large portion in gas-phase space and a small but non-negligible portion in the PM portion of PTOF space.

3.4 Discussion

After applying the subtraction described in section 3.3.1, new organic PM data was generated for all vehicle emissions tests. Figure 6 shows the statistics for the fraction of total organic signal at *m/z* 44 (f44) for all LDV test data. The f44 values derived via separating gas-phase and particle-phase signal at *m/z* 44 using the collocated gas-phase CO_2 measurement was binned according to overall organic loading. The average f44 values derived using the other two methods, i.e., the PTOF method (section 3.3) and the PMF method (section 3.2), are also shown for reference. The f44 value derived using the varying CO_2 subtraction method appears to converge to approximately 1% at higher organic aerosol loading for the LDV data. Mohr, Huffman [74] report a similar f44 range of 0.5-2.5% for vehicle emissions sampling utilizing an HR-ToF-AMS. In the present study, at the lowest loading the mean value of f44 is 9%, however these values are likely to be more uncertain due to the decreased signal-to-noise ratio at such low PM loading, which is also illustrated by the wider spread of the f44 values as depicted by the error bars. The higher signal-to-noise and the decreased spread in f44 at higher loading makes the converging value of ~ 1% a more preferable choice to represent an overall average vehicle emissions mass spectrum. The f44 values determined by the PMF and PTOF method give consistent results, i.e., ~ 1% (Figure 7).

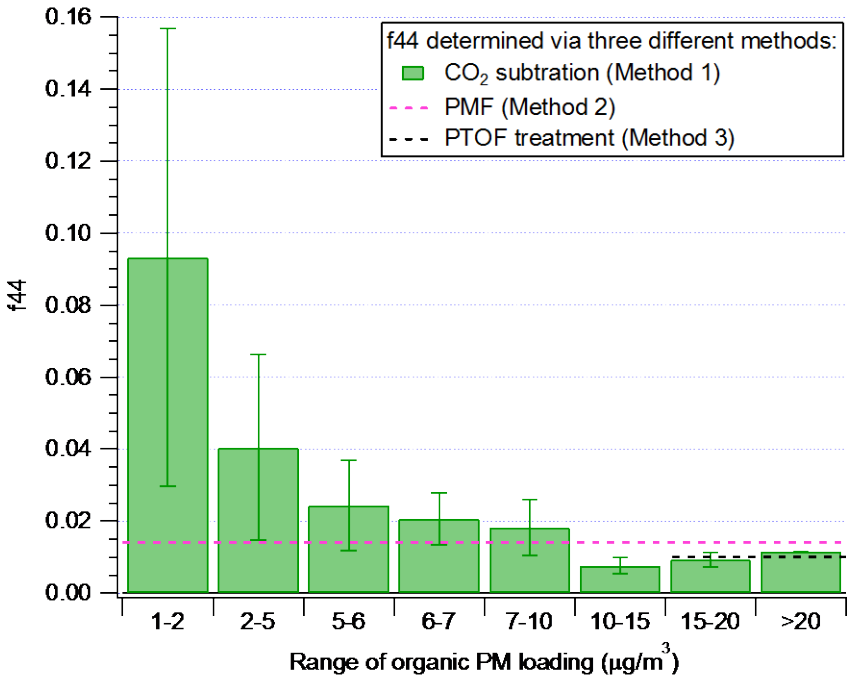

Figure 3-7: Average f44 values for all vehicle test data of LDV under Base Case conditions where f44 was derived using the varying gas-phase CO_2 subtraction method, and is depicted by the green bars. The error bars indicate the 1 standard deviation of the means. f44 derived using PMF and PTOF (for loading > 15 µg m^{-3}) are shown as dashed lines for reference.

Figure 7 clearly indicates a general trend of increased f44 with decreasing of organic aerosol loadings. This trend may have a physical interpretation. Partitioning of less oxidized PM components to the gas-phase would increase the O/C ratio of the remaining PM which would be reflected by a higher signal in the PM portion of the CO_2^+ ion. The f44 derived using the collocated gas-phase measurements show similar trends for GDI and ULEV tests and the values converge at 1.5% and 5%, respectively. However, these values are not reproduced well by either PTOF or PMF, in part due to the test conditions where these alternative vehicles were operated under a constant velocity test condition, as a result the gas-phase and particle phase behavior did not vary uniquely.

By contrast, in the diesel case there is no clear converging value, rather the f44 appears to be relatively flat over the entire loading range (0 - 60 µg/m^3). The lower bound for diesel f44 is approximately 4.5% and the upper bound is approximately 7.5% although most of the data lies within a mean f44 envelope of 4.5 and 6%. These values are consistent with the results from the PTOF and PMF methods where f44 was found to be ~ 5%. The f44 value for diesel is consistent with that found by Schneider, Weimer [68] whose results show a slope of 0.048 between total particle signal at *m/z* 44 vs. the total mass loading of organics.

Our results indicate that these three different approaches yield internally consistent values for the gas/particle apportionment of CO_2^+ when certain data quality parameters are met, however the subtraction method using the collocated gas-phase measurement gave the most reliable results and is the most rigorous method under these test conditions. The consistency among these 3 methods, in particular for the gasoline vehicle tests, which were the main focus of this study, give confidence in the data after the proper gas-phase subtractions have been applied.

4 CHARACTERIZING PM EMISSIONS FROM VEHICLES: DYNAMOMETER TESTS USING A HIGH-RESOLUTION AEROSOL MASS SPECTROMETER

4.1 Introduction

The transportation sector continues to be an important source of anthropogenic primary organic aerosol (POA) and plays a significant role in the air quality of an urban environment. In the paper by Zhang, et.al. (2007) [75] the concentration and mass fraction of hydrocarbon-like organic aerosol (HOA), a surrogate for vehicle POA, is reported for multiple locations and its fraction relative to the more oxygenated organic aerosol (OOA), a surrogate for secondary organic aerosol (SOA) varies between 20-60%. The relative contribution from heavy duty vehicles (HDV) and light duty vehicles (LDV) to urban particulate matter (PM) pollution has also been studied extensively. POA is traditionally viewed as non-volatile and condensed to the particle phase, but more recent studies suggest that it is far more dynamic and may play a larger role than previously suspected in the formation of secondary organic aerosol (SOA) [76]. Heavy duty vehicles such as diesel trucks tend to emit much higher amount of PM dominated by black carbon (BC) while light duty vehicles, although far more numerous, contribute a relatively smaller portion to the overall mass from vehicle emissions yet can dominate in the emission of low-volatility organic species such as polycyclic aromatic hydrocarbons (PAH's) [77] and semi-volatile organic species which may be a substantial contributor toward the formation of SOA. The importance of LDV emissions in urban SOA formation has been posited by a recent study [78]. This conclusion, however, has been challenged by another study, which found that the emissions of diesel vehicles had a higher potential for SOA formation [79]. Understanding the chemical and physical properties of POA and the mechanisms that transform volatile and semi-volatile organic compounds into SOA is necessary for taking steps toward improving regional air quality.

Various approaches using real-time instrumentation have been taken in studying vehicle emissions including on-road vehicle chase studies [59, 80] measurements from tunnels [81-83] measurements near roadways or vehicle sources [84-86] and directly from the tail-pipe while running vehicles on chassis dynamometers [87]. Using real-time instruments is preferred because they afford us a look into the complex chemical and physical processes taking place as primary emissions are emitted into a diluted and well-mixed ambient environment. Soot and metallic ash particles form in the combustion engine along with a release of hot gases which come from fuel and lubricating oil [67]. This mix of particles and hot gases rapidly cool and dilute during which various processes may occur. Depending on the available surface area of pre-existing particles, the rapidly cooling gases may nucleate to form new and small particles or may condense onto the pre-existing particles [86]. In the case of diesel vehicles, sulfate is a major component of the exhaust and since it has a relatively low volatility it readily forms new particles and therefore provides a surface for other semi-volatile and less-volatile gases to condense upon [88].

Particulate and gaseous pollutants emitted from vehicles also undergo quick transformations once released into ambient air. For example, near roadway studies by as shown that the PM in vehicle emissions is composed of ultrafine modes which rapidly grow in size and decrease in number downwind of major roadways with a quick increase of the oxygen-to-carbon (O/C) ratio [84, 86]. In addition, the downwind urban and remote organic aerosol concentrations still remain high and progressively more dominated by oxygenated organic aerosol (OOA) farther from major anthropogenic POA sources like urban centers [75]. The chemistry and morphology of vehicle emissions is complex and understanding these processes is important for various reasons. If a clear connection between these primary emissions and the ubiquitous SOA can be made, it may lead to changing public policy on the methodology of vehicle emission controls. The need for better vehicle emission control standards has already been identified where currently these controls are based on mass and size cut-off, with no method for mitigating the potentially important role the ultrafine organic aerosol component plays in health related issues.

Understanding the detailed chemistry of vehicle emissions will also allow the community to evaluate its prevalence when analyzing regional air quality samples. For example, many urban air quality measurement campaigns yield data that is an aggregate of all the primary and secondary sources and these different components have to be identified and their relative contributions estimated. Finding the correct molecular markers or characteristic mass spectra of vehicle emissions is important for source apportionment.

The Aerodyne Aerosol Mass Spectrometer (AMS) has been used extensively for source apportionment of ambient aerosol as detailed in the review paper by Canagaratna, et.al. (2007) [54] and Zhang, et.al. (2005) [73]. Positive Matrix Factorization (PMF) [65] is one of the prevalent tools used to decompose the aggregate aerosol into the various factors which contribute to the overall chemical composition of ambient aerosol and PMF as applied to AMS data has helped to identify a number of key factors where the two main factors are hydrocarbon-like organic aerosol (HOA) and oxygenated organic aerosol (OOA) (Ulbrich [72], Zhang, Jimenez [71]): HOA is typically characterized by a low O:C, correlates well with m/z = 57 and is generally understood to come primarily from POA such as vehicle emissions; OOA has a high O:C and correlates well with SO_4^{-2} and is generally understood to be a proxy for SOA. Each of these factors can be further subdivided into more identifiable factors. In order to use PMF reliably, reference mass spectra can be utilized for comparison with the derived factor mass spectra and sampling directly from a POA source can provide the information required to constrain ambient data for more reliable source apportionment.

In the past the Aerodyne High Resolution Time-of-Flight AMS (HR-ToF-MS) has been used for combustion emission sampling [Schneider, Weimer [68],Mohr, Huffman [74]] and significant differences have been found among different sources such as biomass burning, vehicle emissions, cooking aerosol, etc. Here we report on the results collected by an HR-ToF-AMS sampling vehicle exhaust from a specially designed secondary

dilution system (SDS) where vehicles were running on a chassis dynamometer both under typical commuter driving behavior and under constant velocity. The SDS was used primarily to dilute the emissions to atmospherically relevant loading but was also used to perturb the environment into which the emissions were sampled and simulate differing environmental conditions. The HR-ToF-AMS sampled at high time resolution (10 seconds) and was run concurrently with other real-time instrumentation providing complimentary information such as real-time BC loading and real-time gas phase CO_2 concentration. Furthermore, the host facility retained gas-phase information taken upstream of the SDS for further analysis. This report intends to provide emission ratios for POA / HOA which can be tied to engine load or ambient conditions and detailed mass spectra of various gasoline light duty vehicles running on a chassis dynamometer. The motivation for this particular method is to effectively isolate the vehicle emissions, have control over the dilution in order to obtain atmospherically relevant conditions and to observe the variations among vehicles. The mass spectra reported will be useful for comparison against HOA-type factors or sources identified in ambient aerosol data. The effects of overall loading on detailed chemistry will be explored.

4.2 Experimental Methods

4.2.1 Overview of Vehicle Emission Sampling Experiments

In September of 2011, an extensive month-long vehicle sampling experiment was performed at the California Air Resources Board (CARB) Haagen-Smit Facility in El Monte, CA. This particular experiment consisted of installing a secondary dilution system (SDS) which sampled from the CARB Constant Volume Sampler (CVS) tunnel, and drew vehicle emissions from the tail-pipes of a representative fleet of 8 spark-ignition gasoline passenger vehicles. The experiment was divided in two major parts. First the fleet of 8 vehicles was tested under the first 2 major portions of the California Unified Cycle (UC) which consisted of a 300 second cold start phase followed by 1135 seconds of a hot phase. Each day the same driving cycle was applied to all 8 vehicles (in random order) and different ambient conditions were applied in the SDS. The second major half of the experiment consisted of using a constant velocity driving cycle where a short hot acceleration was followed by approximately 20 minutes of 60 mph driving. For this driving cycle various atmospheric conditions were changed such as dilution or residence time. Other alternative vehicles were also tested under these conditions such as a passenger diesel vehicle, and ultra-low-emissions vehicle (ULEV) and a gas-direct-inject (GDI) vehicle.

4.2.2 Secondary Dilution System

The SDS was designed to mimic the dilution and mixing that occurs when emissions leave the tail-pipe on the open road and can be exposed to varying conditions such as pre-existing background particles or elevated relative humidity. For a description of a previous study using a similar system refer to Robert, VanBergen [89] and for a more

detailed description of the current study refer to Forestieri *et al*. (2013). Figure 1 below shows a diagram of the SDS. Vehicle emissions undergo an initial dilution of a factor of approximately 18 in the CVS tunnel. Downstream of the emissions input CARB sampled gas-phase components such as total hydrocarbon (THC) using flame ionization detection (FID), CO/CO_2 using non-dispersive infra-red detection (NDIR) and NO_x using chemical-luminescence detection (CLD). The diluted emissions were sampled from the CVS tunnel by the SDS where filtered and denuded air provided the second step in dilution (on average by a factor of 4.8) and the mixed and diluted emissions then traveled from the primary SDS chamber into a residence time chamber (RTC) where the residence time was approximately 60 seconds. From the RTC a manifold led to two major sections, the first leading to four temperature legs (25, 50, 75 and 100 °C) where each leg had a denuder-filter-polyurethane foam (PUF) stack. The second major part of the manifold led to a hydraulically controlled valve switching manifold so that emissions were switched among 4 hot tubes (temperatures were also 25, 50, 75 and 100 °C) where the chosen hot tube led to a suite of real-time instruments including the HR-ToF-MS, a Time-of-Flight Chemical Ionization Mass Spectrometer (ToF-CIMS), a Cavity Ring-Down Aerosol Extinction Spectrometer (CRD-AES) [90] combined with a Photo-acoustic Absorption Spectrometer (PAS) [91] and a TSI model 3081 Scanning Mobility Particle Sizer (SMPS). Upstream of the thermal tubes which lead to the real-time instruments a LI-COR LI6262 CO_2 gas phase analyzer sampled the emissions for real-time CO_2 gas phase subtraction. The pump placed downstream of the denuder/filter/PUF system and the pumping action of the real-time instruments provided the total flow through the SDS system.

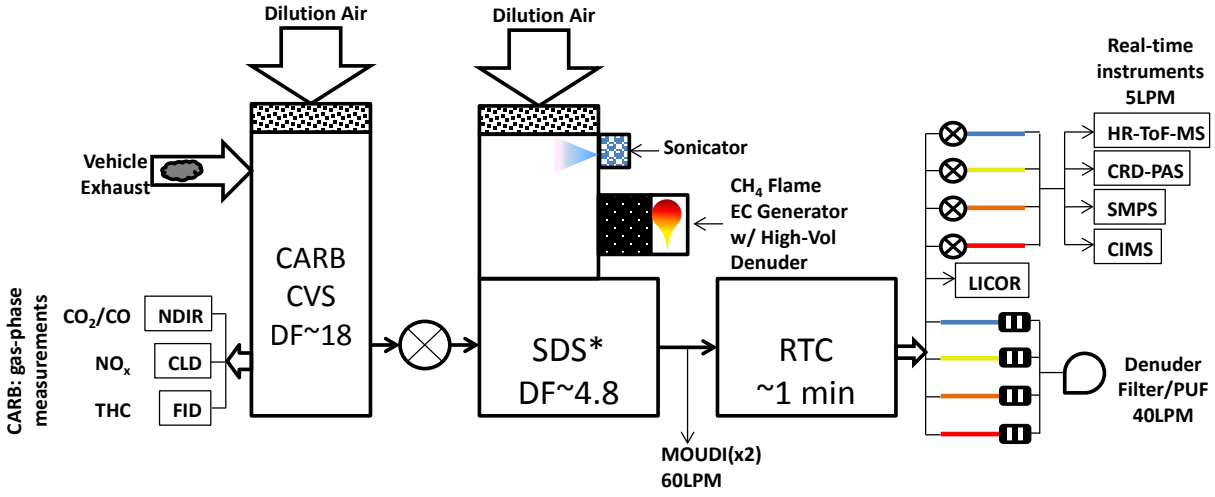

Figure 4-1: Schematic of experimental set up. Vehicle emissions undergo an initial dilution of ~18 in the CVS tunnel and where gas-phase components are measured. Emissions undergo a secondary dilution in SDS followed by passage through RTC. Several ports draw emissions into the thermodenuder-filter-polyurethane foam (PUF) system or are sampled by a suit of real-time instruments including the High-Resolution Time-of-Flight Mass Spectrometery (HR-ToF-MS), a Cavity-Ring-Down and Photo-Acoustic Spectrometer (CRD-PAS), a Scanning Mobility Particle Sizer (SMPS) and a Chemical Ionization Mass Spectrometer (CIMS). The portion of the emissions traveling to the real-time instruments is shifted every 30 seconds through 4 temperature legs (25,50,75,100°C). Additionally a LI-COR instrument sampled gas-phase CO_2 concentration.

4.2.3 Test Conditions

The cold start has a characteristic “stop and go” type driving profile. The beginning of the hot phase has a large acceleration followed by an extended period of constant speed. Later in the hot phase a second hard acceleration is followed by an extended period of constant speed. This is meant to be representative of typical commuter driving behavior combining surface-street and freeway driving. The UC was used to test the 8 SI gasoline vehicles on a daily basis where each day the atmospheric conditions in the SDS were changed to modify relative humidity or dilution where the relative humidity was controlled by sonicating milli Q water just downstream of the SDS dilution air input. For the purposes of this report only the base case will be discussed. There were two base case test days (09/15/2011, 09/20/2011). In this report the base case test which occurred on 09/20/2011 will be emphasized. For the base case test day the average relative humidity and temperature of the SDS dilution air were 49.79±0.51% and 25.94±0.35°C respectively. For the constant velocity driving cycle the alternative vehicles were also tested under varying atmospheric conditions. Table S1 summarizes the conditions for each of the test cases. Sampling of the background was performed before and after vehicle tests.

4.2.4 Real-time Measurement of Aerosol Chemistry

The HR-ToF-MS [24, 54] was used to quantify and characterize the non-refractory sub-micron aerosol species including organics and inorganic species such as SO_4^{2-}, NO_3^-, Cl^- and NH_4^+. The inlet of the HR-ToF-MS consists of an aerodynamic lens which concentrates particles to the axisymmetric centerline and due to vacuum expansion into the main chamber and strips away a large portion of the ambient gas. The particle beam then passes by a chopper wheel with a 2% opening which modulates the particle beam and allows for mass spectra to be resolved in terms of vacuum aerodynamic diameter (D_{va}) in PTOF mode [92]. The chopper can also be operated to subtract the background signals (chopper completely blocks the particle flow) from the un-modulated particle beam (chopper completely away from the particle path) and calculate an ensemble mass spectrum (MS mode). The particle beam impacts on a temperature controlled (600°C) oven for thermal vaporization and the newly formed gas phase molecules are ionized by electron impact (EI) with an energy of 70 eV. The resulting, fragmented ions are driven toward a mass spectrometer for orthogonal extraction where two paths are possible, V-mode for high sensitivity and W mode for high resolution sampling. For this experiment the instrument was set to average every 10 seconds where 4 seconds the instrument averaged the aggregate PM mass spectrum in MS mode and for 6 seconds the instrument ran in PTOF mode. Due to the low aerosol concentration, the instrument was operated primarily in V-mode. As mentioned earlier, the vehicle emissions underwent thermal conditioning where the valve system switched to each temperature leg every 30 seconds alternating elevated temperatures with ambient temperatures. This yielded 3 HR-ToF-MS data points for each temperature section. In this report only the data points corresponding to ambient temperatures will be analyzed. Before the campaign onsite ionization

efficiency calibrations were performed using atomized and size selected ammonium nitrate particles and size calibrations were performed using atomized polystyrene spheres. The LI-COR LI6262 instrument sampled at 1 Hz and regular filter samples were performed for calibration with the HR-ToF-MS.

4.3 Data Analysis

4.3.1 HR-ToF-MS data processing: Gas-phase subtractions and fragmentation and batch table adjustments

All data was processed using SQUIRREL ToF-AMS Data Analysis Toolkit version 1.51H and PIKA ToF-AMS HR Analysis version 1.10H (downloadable from http://cires.colorado.edu/jimenez-group/ToFAMSResources/ToFSoftware/index.html) programs in Igor Pro 6.22A, where each major test day was processed in a separate file. A collection efficiency of 0.5 was assumed for all PM, which is a reasonable assumption given that the PM was neither acidic nor composed in large fraction by nitrate [93]. Typically relative ionization efficiencies (RIE) of the various non-refractory aerosol components are adjusted according to RIE tests performed with the IE calibration test. In this case pure ammonium sulfate was atomized after the ammonium nitrate IE calibration test which is used to calculate the relative ionization efficiency of sulfate ions. The RIE value for organic PM is typically assumed to be 1.4 under atmospheric conditions, but different types of organics can have differing RIE values. In this case pure hydrocarbons are being sampled and so the RIE was set to 2.1 [55]. In order to apportion the individual m/z signals to their proper sources (air-related, organics, sulfate, etc.) the so-called fragmentation table [56] is used to represent the total mass spectrum as an aggregate of mass spectra where each fragment may contribute to every m/z being analyzed. The default fragmentation table is most suitable for atmospheric aerosol and must be modified according to the best judgment of the user. In this case some of the most important ions to adjust are the gas-phase ions which have high concentrations and interfere with organic PM signals. An extensive CO_2 subtraction analysis has been performed and reported elsewhere (Collier, et.al. submitted) and the details will not be discussed here. Briefly, it was found that for the SI gasoline vehicles, the CO_2^+ ion contributed ~1% of the overall organic PM mass spectrum, for diesel 4.5%, for GDI 1.5% and for ULEV 5%.
The detection limit of the non-refractory species was calculated as three times the standard deviation of the average signal during filter tests [24]. The values are given in Table 4-1.

Table 4-1: Detection limits calculated for non-refractory species as 3 x the standard deviation of the average signal during 10-s averaged filter tests.

	Detection limits (ng m^{-3})
Organics	6
Nitrate	22
Chloride	106
Ammonium	2
Sulfate	31

The results presented in this report were all derived from the high resolution peak fitting analysis. An ion list of 589 ions were fitted and applied to all SI gasoline vehicles and the list was modified slightly for the diesel, GDI, and ULEV vehicle tests. In order to report the high resolution mass spectrum, certain ions were removed after post-processing due to their proximity to air-related ions.

4.3.2 Removal of Signals from Silicone Contamination

During the field campaign a contamination source was identified in the vehicle tests, where occasionally a prominent and distinct mass spectrum consisting of peaks at m/z = 73, 149, 207, 221, 276, 355, 401 where m/z = 207 was the most prominent peak, would dominate the HOA mass spectrum. Later the source was identified and removed from the system. These contamination peaks have been reported before in relation to silicone rubber tubing [94]. The peaks were fit using Si containing ions. The contamination was not prominent during periods of low loading and the m/z = 207 ion was used as a tracer for the contamination. All data presented here has been screened for data points with prominent contamination peaks. During base case days the percent of signal removed due to contamination was less than 5%. For other test dates, for example during days where background EC particles were added using the methane flame, the added contribution from contamination was estimated to be up to 8.6% of the detectable total organic signal.

4.4 Results

4.4.1 Emissions of organic PM from Vehicles: time dependent mass loading

A repeatable structure was observed for the time-dependent loading of the organic PM for all vehicles in response to the UC. As was described earlier, the drive cycle consists of two major parts: the cold start and the hot phase. The resulting time-series can be broken up into four major sections and are clearly correlated to the engine loading. The lowest panel in Figure 2 shows the time-dependent loading for all vehicle runs on 09/20/2011 as a function of time since ignition, plotted on the left axis, and the average speed (MPH) is plotted on the right axis. The running average for all vehicles is superimposed on the individual vehicle runs. A 1-minute time delay is expected between

the recorded speed and the HR-ToF-MS signal response due to the RTC. During the cold-start phase all vehicles consistently emit a higher loading with respect to the average organic PM loading. The burst of organic PM during the cold start phase makes up anywhere from 30 to 87% of the total mass emitted during the vehicle run. Following the cold-start phase the organic PM loading signal reaches a steady state for all vehicles, except for vehicle 10, which continues to vary significantly. It was determined during the campaign that this vehicle began to malfunction (Forestieri, et.al. (2013)). Directly after cold start there is a hard acceleration followed by constant speed where some of the vehicles emit a small burst of particles in response to the elevated engine load, the signal of which sometimes blends in with the cold-start response curve. The lower loading period which occurs after appears to correspond to the extended period of constant speed, where the engine loading is not fluctuating significantly. Directly after the constant velocity portion a “stop and go” period follows but the POA loading remains stable due to the elevated engine temperature and presumably due to after-treatment devices beginning to reach equilibrium temperatures. At approximately 840 seconds after ignition a second hard-acceleration followed by high speed leads to an elevated signal response though never reaching the same levels as during the cold-start phase. The UC ends with more “stop and go” driving behavior where the signal response is again at a lower level. Despite the wide range of overall organic loading among the 8 vehicles, they all display this similar behavior. A similar trend is reported by Kittelson, Watts [66] where various vehicles were driven under the UC on chassis dynamometers but at different dilution levels. In summation, there is a phase 1 where the POA loading is highest due to cold-start, phase 2, where the vehicle POA levels off, phase 3, a second slight elevation due to the second hard acceleration and a final phase 4, where the POA levels off a second time. These four major response phases will be used later when comparing the chemistry of the emissions at different portions of the drive cycle.

The alternative vehicles were driven on a constant velocity drive cycle and therefore do not display the same structure as the gasoline SI-vehicles on the UC. Figure 3 depicts the time trace of the POA loading for each of the alternative vehicles under base case conditions. The diesel vehicle was diluted to a higher degree in order to avoid overwhelming the real-time instruments and avoid break-through in the denuder/filter/PUF stacks. Vehicles under constant velocity have an initially high loading of organic PM, where the magnitude depends on the engine temperature, and eventually levels out toward the end of the vehicle test. The vehicles were not cold-started for the constant velocity tests.

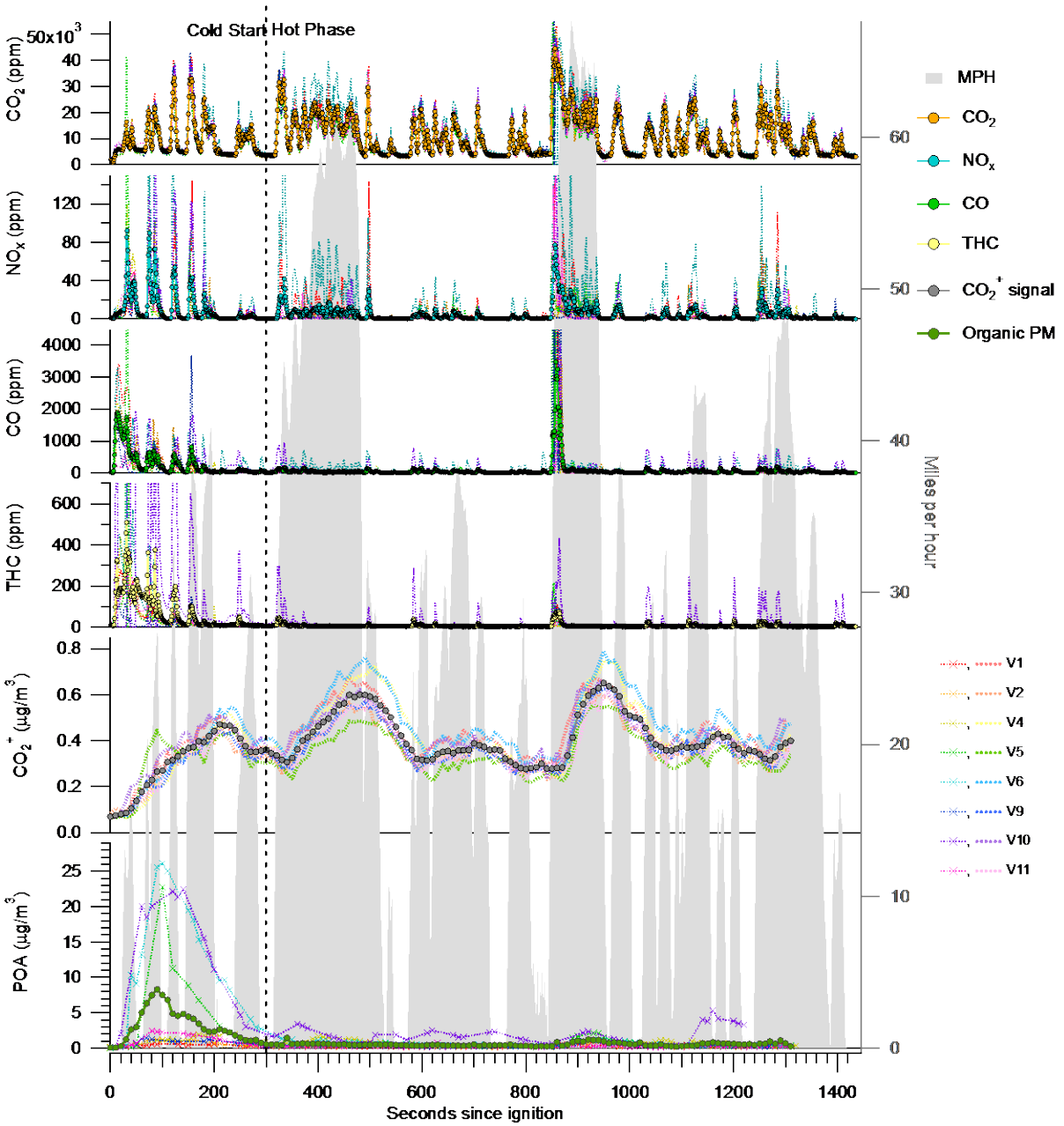

Figure 4-2: Summary of time traces for various components for all 8 SI-LEV under UC on 09/20/2011 where dashed lines are the traces for each individual vehicle and round markers are the funning average of all 8 vehicles. Top four panels include gas-phase components measured by CARB at dilution factor of ~12 including CO_2, NO_x, CO and total Hydrocarbons (THC). The fifth panel includes the total signal at CO_2^+ (*m/z* 44) as measured by the AMS with a dilution factor ~60. The bottom panel shows the total organic PM mass loading. The right axis shows the miles-per-hour of the UC and where the vertical black dashed line represents the division between the cold start phase and the hot running phase.

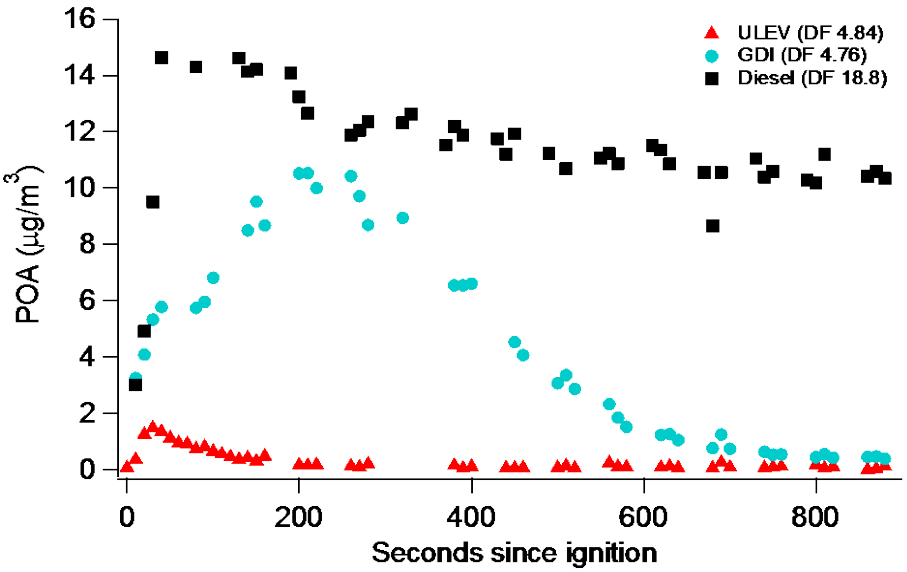

Figure 4-3: Organic PM loading time traces for the 3 alternative vehicles tested under constant velocity. Note that the vehicle emissions underwent different dilution factors.

4.4.2 Size Distribution of POA in Vehicle Emissions

The AMS provides chemically resolved, mass-weighted size distributions in vacuum aerodynamic diameter. The size distribution of the organic PM is shown below in Fig. 4. The dominant size mode is centered at a D_{va} = 90 nm with some evidence of larger particles at sizes greater than 200 nm. Vehicle emissions are characterized by large quantities of small particles in the 30-60 nm range *[66]* and tend to be fractal. During vacuum expansion fractal particles will appear larger due to drag experienced in the expansion process *[86]*. Fig. 4 shows size distributions averaged over all vehicle runs as well as segregating only the first phase of the UC drive cycle. The phase 1 size distribution coincides well with the overall size distribution and is clearly the dominant factor as discussed in the previous section. The size distributions for m/z = 57 (mostly $C_4H_9^+$), which is a marker ion for long chain hydrocarbon *[95]*, also coincide with the overall organic distributions indicating that particles of all sizes are composed primarily of hydrocarbons. Although the size distribution in the larger sizes is noisy, there seems to be some evidence of larger accumulation mode particles.

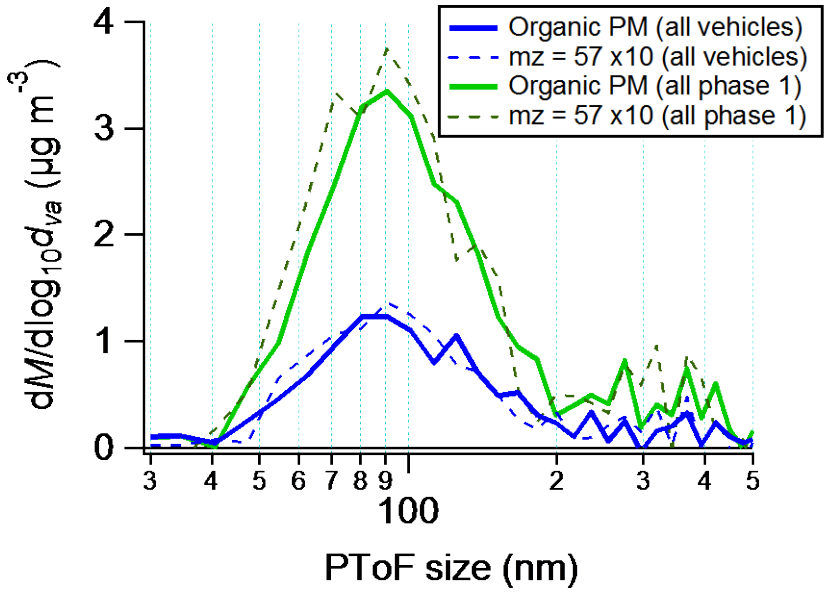

Figure 4-4: Size distribution of organic PM and *m/z* = 57 (x 10) averaged over all vehicle runs and averaged over phase 1 of the UC for all vehicles

4.4.3 POA mass spectra

The chemistry of the organic PM from the vehicle emissions is reported here as an average POA high resolution mass spectrum. Figure 4 represents the average of 8 vehicles tested on 09/20/2011. The spectrum is divided into 5 major ion fragment families: $C_xH_y^+$, $C_xH_yO_1^+$, $C_xH_yO_2^+$, HO^+, $C_xH_yN^+$. The majority of the mass spectrum is composed of $C_xH_y^+$ ion fragments. The spectrum exhibits the so-called "picket-fence" fragmentation pattern which is typical of long-chain hydrocarbons. The HR MS also exhibits oxygenated ion fragments (light pink bars). Other vehicle emission sampling tests have found strong evidence of light oxygenated compounds in the form of carbonyls [96], and the POA focused study by Mohr, Huffman [74], also using the HR-ToF-MS, identified oxygenated ions such as $C_2H_3O^+$ at *m/z* 43 and $C_3H_5O^+$ at *m/z* 57 in engine exhaust. These and other oxygenated ions have been identified in this new standard POA MS. Higher order oxygenated ion fragments are also present, the most significant one being CO_2^+ at *m/z* 44. As was mentioned earlier, the CO_2^+ signal has two sources, gas phase and particle phase, and statistical analysis of this data set found that at higher loading the fragment of the overall POA signal belonging to CO_2^+ converged at 1% for gasoline SI-LEV. The other major $C_xH_yO_2^+$ ion is $C_2H_4O_2^+$ at *m/z* = 60 although several ion series containing 2 oxygen atoms are present to high m/z in a small fraction of total signal values. The average O/C ratio of this averaged POA MS is 0.057, the H/C is 1.79 and the OM/OC is 1.23. The prevailing interpretation of vehicle exhaust mass spectra is that it is composed mainly of fuel and lubricating oil and the relative contribution from each may depend on engine load and type. Schneider, Weimer [68] found that the mass spectra of atomized diesel fuel, and the fumes from a diesel vehicle running on a chassis dynamometer were very similar.

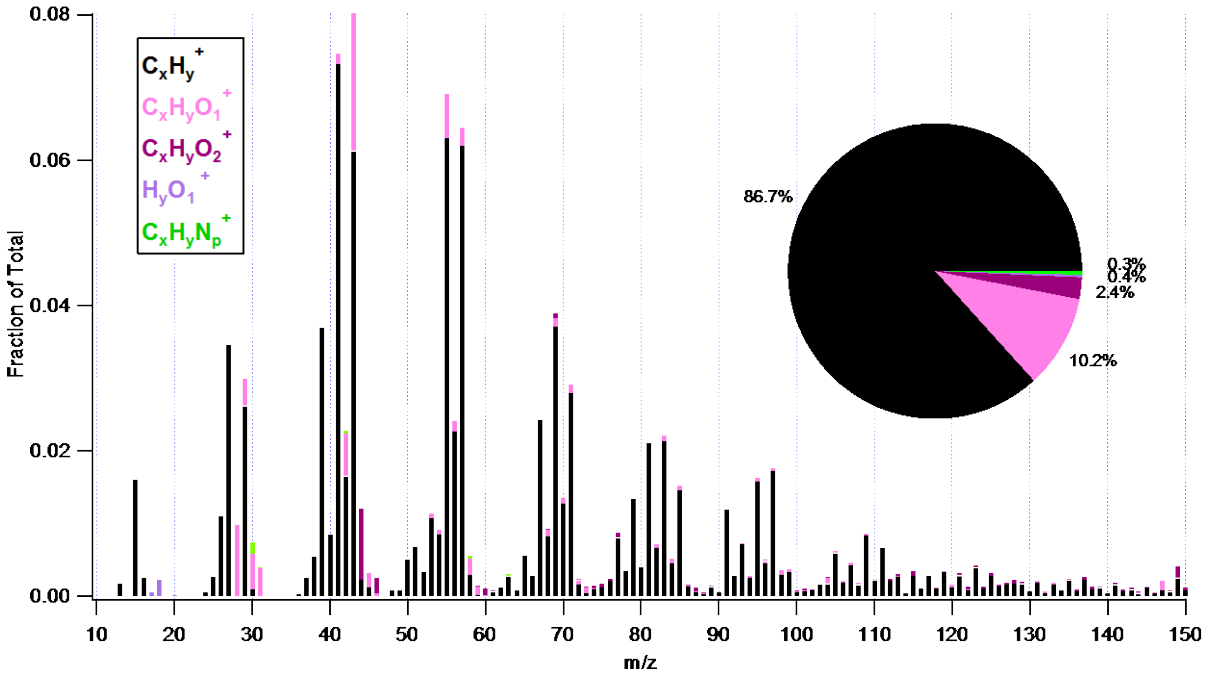

Figure 4-5: Average mass spectrum of 8 vehicles broken down by ion family and displayed in unit mass resolution. The pie chart depicts the relative contribution of each ion family to the overall mass

One possible reason for this is that fuel evaporates and re-condenses on soot particles. The similarity among all 8 vehicles here can be explained by the fact that all 8 vehicles were ran on the same CARB approved gasoline fuel (CA summer blend).

When comparing this mass spectrum to atmospherically derived HOA spectra a high R^2 correlation can be reported. The HOA spectrum derived through PMF from a New York city near-roadway sampling campaign has an O/C ratio of 0.06, OM/OC = 1.24 and H/C = 1.83. The R^2 correlation between the atmospheric HOA and the POA averaged over 8 vehicles reported here is 0.938. A meta-comparison between this average mass spectrum and that of various HOA mass spectra derived through PMF from atmospherically sampled aerosol shows that this mass spectrum correlates highly with the derived HOA spectra. Figure 5 depicts an image plot showing a cross-correlation analysis between the mass spectrum derived here and that of various ambient sampling studies. The spectra included in this image plot were downloaded from the AMS unit mass resolution (UMR) spectral database (http://cires.colorado.edu/jimenez-group/AMSsd/).

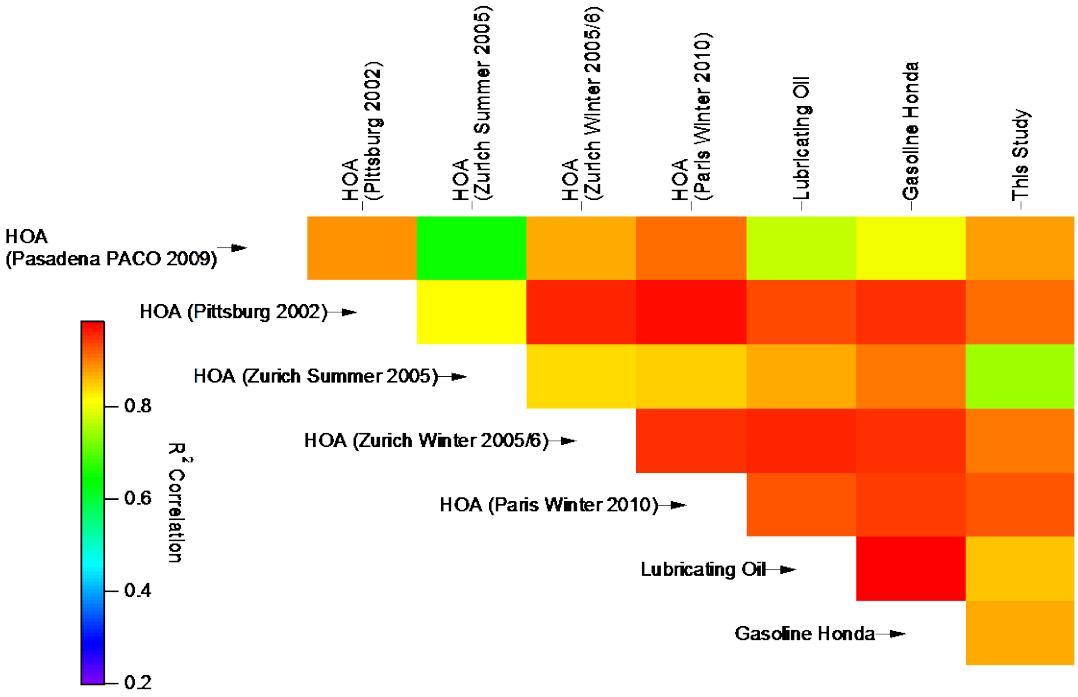

Figure 4-6: Image plot depicting a cross correlation between the averaged mass spectrum derived for 8 SI gasoline vehicles and the HOA mass spectrum derived through PMF from various ambient aerosol sampling studies. Additionally standard mass spectra of atomized fuel and lubricating oil are included. Boxes are colored by R^2 correlation.

The ambient studies include HOA spectra from urban sampling sites [95, 97-100], as well as controlled experiment derived mass spectra such as atomized lubricating oil [80] and sampling directly from the exhaust of a gasoline vehicle [74]. The lowest correlation between this study and all other studies (see right-most column of image plot Fig. 5) was 0.74 between this study and the HOA factor derived from the summer Zurich study. The best correlation was found between this study at the HOA factor derived from the Paris study and was calculated to be 0.92. The mass spectrum derived here correlated fairly well with both the lubricating oil spectrum (R^2 = 0.85) and the gasoline vehicle (R^2 = 0.87). These two factors correlate very well with each other (R^2 = 0.98) suggesting the emissions from the Honda vehicle were dominated by lubricating oil. This also suggests lubricating oil may be an important component of the exhaust sampled during this study. The relative importance of lubricating oil will be discussed further in section 4.4.

As discussed in section 5.1 the 8 vehicles tested during this study emit a wide range of POA mass loading. The overall loading affects the composition of the condensed phase emissions where generally low loading periods lead to higher fraction of oxygenated

compounds. Figure 7 below illustrates this behavior where the fraction of individual ions with respect to overall organic mass are plotted versus organic mass.

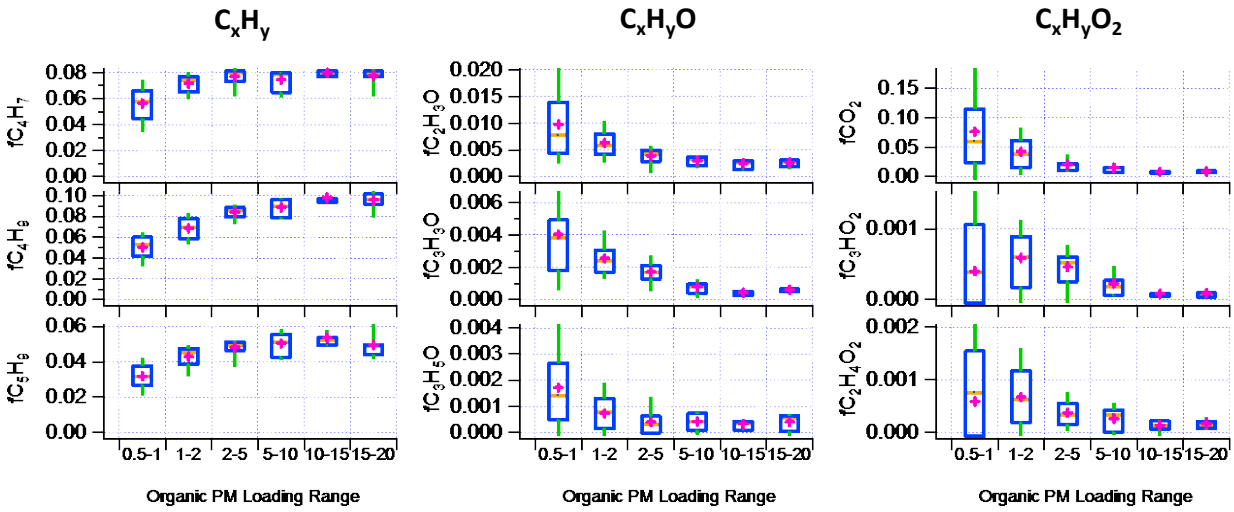

Figure4-7: Statistical distribution of the fraction of a given ion with respect to overall organic mass plotted as a function of total organic mass using box plots. The pink crosses represent the mean, the yellow bars represent the median, the top and bottom of the blue box represents the 75th and 25th percentile respectively and the top and bottom green whiskers represent the 90th and 10th percentile respectively. The ions represented are grouped by ion type from left to right C_xH_y, C_xH_yO and $C_xH_yO_2$. The above data is for the base case test (09/20/2011).

In the left column of Fig 7 the primary hydrocarbon ions are depicted (C_4H_7 (*m/z* 55), C_4H_9 (*m/z* 57), C_5H_9 (*m/z* 69)) and their fractions tend to increase with increased organic PM loading. The middle column depicts the primary oxygenated ions (C_2H_3O (*m/z* 43), C_3H_3O (*m/z* 55), C_3H_5O (*m/z* 57)), some of which are collocated with the C_xH_y ions shown, and their fraction with respect to organic PM mass tends to decrease with increasing organic PM mass. The same can be said of the $C_xH_yO_2$ ions depicted in the right column. The top right box plot shows the distribution for the fraction of particle phase CO_2 which tends to plateau at 1% at higher organic PM loading. This behavior was well documented in a separate manuscript (Collier, submitted).

Figure 8 below shows the O/C ratio of each vehicle versus the averaged PM loading, and where the size of the markers are proportional to the R^2 correlation between the individual vehicle MS and the overall averaged MS. Although the O/C ratio values have a relatively wide range, the R^2 values are all above 0.88, which can be explained by the overall dominance of the $C_xH_y^+$ ion family of each vehicle averaged MS. There is also a trend in evidence between the O/C and the overall PM loading, where an inverse correlation exists. Oxygenated compounds tend to be less volatile and therefore remain in the condensed phase. In this case, the fraction of oxygenated compounds is increasing as

the overall POA loading is decreasing. One exception is the MS for the diesel passenger vehicle, which has a very high relative mass loading but an average O:C value.

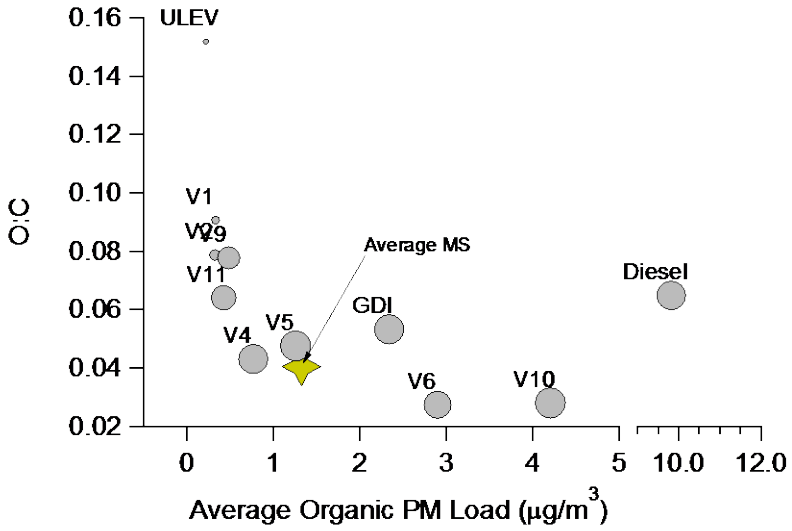

Figure 4-8: O:C versus average organic PM loading for each vehicle (ambient, base case conditions). Yellow star denotes mass weighted average MS of all vehicles (except Diesel vehicle test).

Similar results are observed when examining the chemical change among UC phases. Figure 4-9 depicts the ion family pie charts for each distinct phase for the vehicle 6 test where the majority of the POA mass was emitted in phase 1. For phase 1 O/C = 0.023, for phase 2 O/C = 0.066, for phase 3 O/C = 0.068 and for phase 4 O/C = 0.11. For phase 1 the average POA mass loading is 9.7 µg/m^3 whereas the loading is well below 1 µg/m^3 for the rest of the phases.

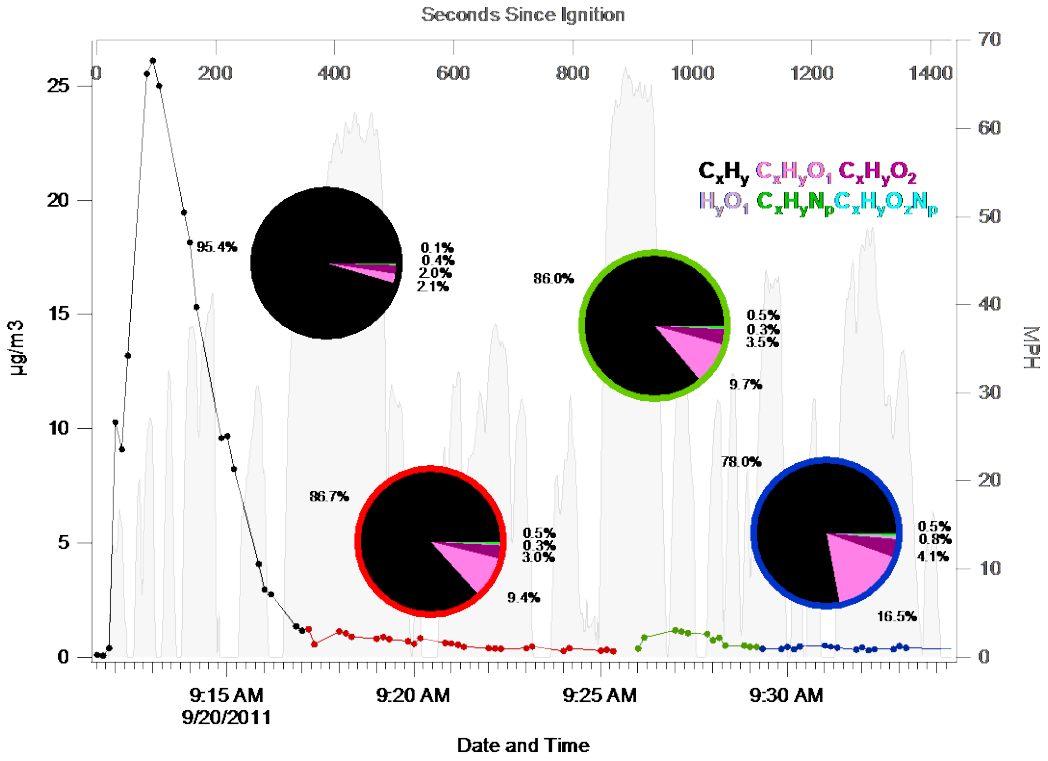

Figure 4-9: Comparison of the ion family breakdown for each phase of vehicle 6 test. The traces correspond to the POA loading for vehicle 6 where the black portion is phase 1 or cold start, the red portion is phase 2 which includes a hard acceleration and constant high speed, the green portion corresponds to phase 3, which includes a second hard acceleration and the blue portion is phase 4 corresponding to the final portion of the hot-phase. The pie charts are color-coded by phase colors and depict the average contribution of each ion family to the average MS for the given phase.

The average mass spectrum for the alternative vehicles is provided in Figure 9. The diesel vehicle has an O/C ratio of 0.12, an H/C of 1.76 and an OM/OC of 1.31. Although the overall fraction of the $C_xH_yO_1^+$ ion family contributes less than 10%, the $C_xH_yO_2^+$ is relatively high, primarily due to the higher CO_2^+ particle phase contribution. The ULEV vehicle has the highest O/C ratio at 0.21, an H/C of 1.7 and an OM/OC of 1.44. Here the contribution of the $C_xH_yO_1^+$ ion family is the highest among all the vehicles tested. The GDI vehicle is similar to the gasoline vehicles with an O/C of 0.06, H/C of 1.84 and an OM/OC of 1.24.

A comparison of the mass spectrum for each of these vehicle tests, including the alternative vehicles can be made. It has been found that when taking an average mass spectrum for all base case vehicle tests the chemistry is still remarkably similar. Despite having a substantially higher average POA loading, the Diesel vehicle MS has an R^2 correlation greater than 0.98.

4.4.4 Apportionment of Lubricating Oil and Fuel

The apportionment of lubricating oil and fuel-combustion aerosols to overall vehicle emissions affects the estimates of vehicle emission ratios and may inform policy on how emission control technologies are implemented [43]. A common tracer for lubricating oil is Zinc. Zinc has an exact mass of 63.9292 and is slightly smaller than the SO_2^+ ion which has an exact mass of 63.9619. The difference in mass is sufficient for separation and therefore quantification by HR-ToF-AMS. The next most abundant isotope of Zinc is ^{66}Zn which is well separated from other ions in V-mode. In PIKA the ^{66}Zn ion was unconstrained in order to verify that the AMS was indeed detecting a real Zn signal. The linear fit in the scatter plot of Fig. 10 shows that the relative abundance of the two isotopes matches with the theoretical value. The time series of Zinc as a function of seconds since ignition is shown in Fig. 11 for each vehicle on the base case day.

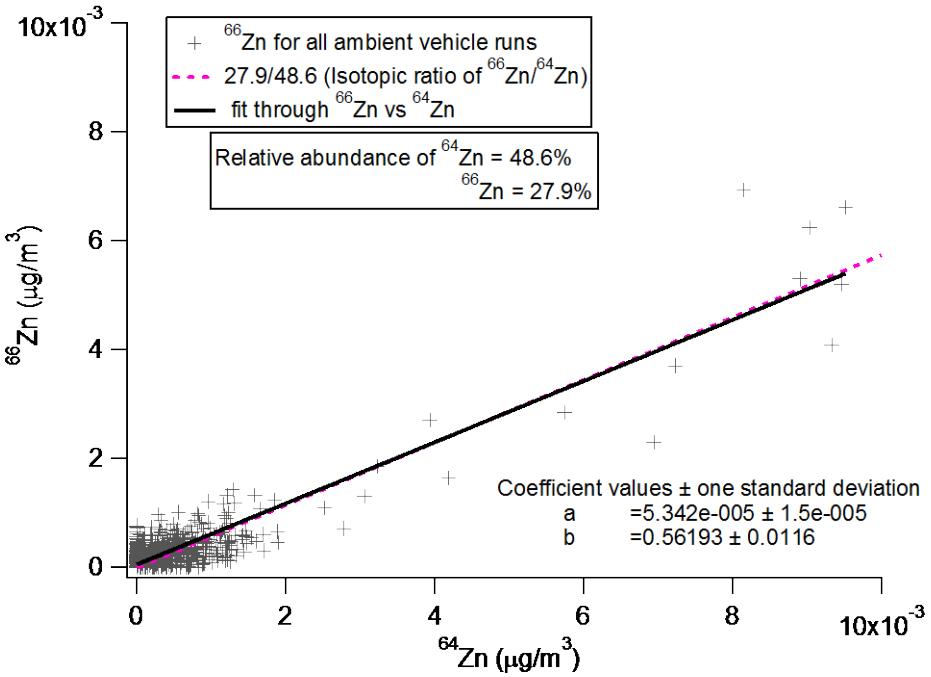

Figure 4-10: Scatter plot of ^{66}Zn vs ^{64}Zn where the black line is the linear fit through the data points and the pink dashed line is the slope of the theoretical relative abundance between 66Zn and 64Zn.

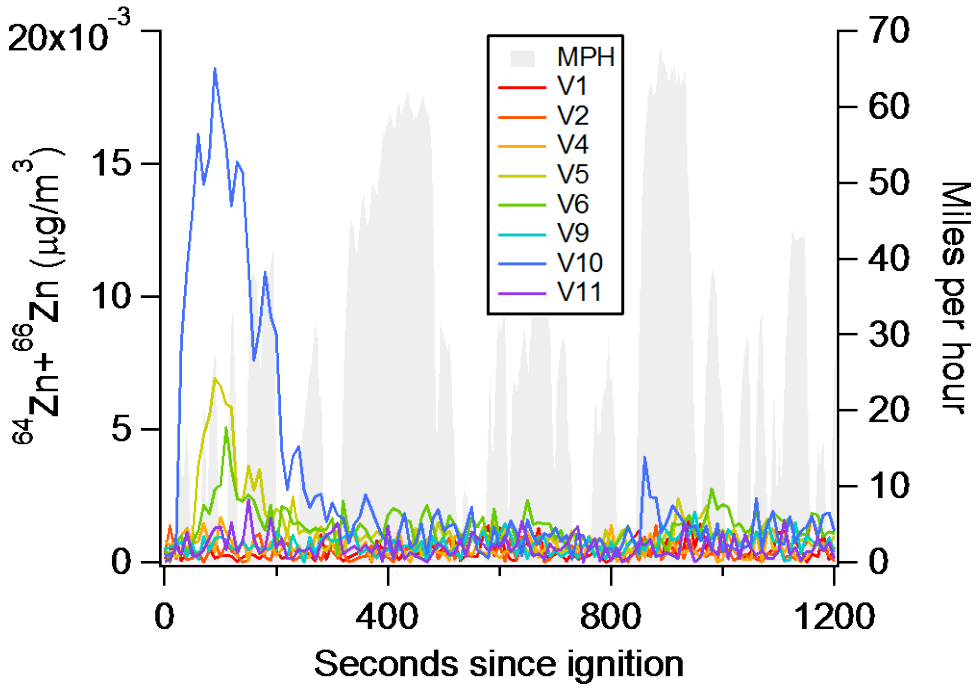

Figure 4-11: Time series of Zinc for each vehicle as a function of seconds since ignition. Velocity profile of UC shown in the background for reference

The mass loading of Zn tends to be higher during the cold start phase 1 portion of the drive cycle and it is particularly high for V10. As is discussed in Forestieri et.al. (2013), V10, which is the Ford Taurus, became a malfunctioning vehicle during the measurement campaign. It consistently shows higher EC emission ratios as well as high organic PM loading relative to the other vehicles in the test fleet. Although all 8 vehicles used the same fuel provided by ARB, the lubricating oil was left as is. Different lubricating oils will have different quantities of additives such as Zinc and so the above information cannot be used to calculate relative abundance of lubricating oil in the emissions in a quantitative way. However, it is clear that lubricating oil plays an important role during the cold-start portion of the UC and that it makes a large contribution in the emissions of malfunctioning vehicles.

4.5 Conclusions

A comprehensive vehicle emissions experiment has been carried out using various on-road LEV's running on a chassis dynamometer while diluting and mixing the exhaust in a secondary dilution system. The dilution was controlled in order to attain atmospherically relevant conditions (0.5-30 µg/m^3). Various real-time instruments were used to monitor the composition and mass loading of the gas-phase and particle-phase emissions as a function of engine load and other atmospheric factors. In this report the results acquired with an Aerodyne HR-ToF-MS have been presented. The time-dependent organic PM mass loading was found to behave in a consistent way across all vehicles despite having a

wide range of overall mass loadings. The average mass spectrum of each vehicle was determined and an overall average spectrum was reported. The average mass spectra for the individual vehicles was found to have high correlation with the average, giving high confidence that this POA MS can be used as a LEV standard for comparison with ambient aerosol sampling data. The overall O/C ratios of vehicle POA were low, but were found in this study that they are dependent on overall loading. The lowest loading mass spectra tended to have higher O/C values, due to partitioning of the more volatile fraction to the gas-phase. When comparing the mass spectra of the alternative vehicles with the gasoline vehicles the correlations still remained high suggesting the chemical composition of POA is remarkably similar for all LEV. Vehicle organic PM has been shown to be dynamic in its partitioning behavior, where chemistry is affected by the overall mass, and responds to environmental factors such as dilution. Further analysis of these test results will shed light on other aspects of vehicle emissions.

5 VOLATILITY OF PRIMARY ORGANIC AEROSOL EMITTED FROM LIGHT DUTY GASOLNE VEHICLES

5.1 Introduction

Emissions tests have determined that primary organic aerosol (POA) generated from combustion sources behaves like a series of semi-volatile compounds when the particulate phase concentrations range between 100 – 10,000 μg m^{-3} [1]. Recent tests of light duty gasoline-powered motor vehicles performed by May et al. [101] suggest that more than 90% of the POA emitted from this source is semi-volatile [101] with the implication that it would evaporate given sufficient time in the atmosphere. These findings are based on measurements from a fleet of vehicles recruited in California with exhaust diluted to near-atmospheric concentrations ranges in a Teflon reaction chamber followed by POA measurements using a Q-AMS. This experimental design is far more realistic than original tests used to establish the potential volatility of POA [4], but it still suffers from several potential weaknesses. May et al. infer a portion of the POA volatility through a comparison of traditional thermal optical OC measurements made after the first stage of dilution and Q-AMS OA measurements made after the second stage of dilution. May et al. made the bulk of their measurements from high emitting vehicles and then extrapolated their results to the lower emitting vehicles. Finally, May et al. assume that the composition of all particles are uniform (internal mixture assumption) and the same between all vehicles tested which yields a large amount of scatter in the POA volatility prediction vs. measurement. This basic assumption then allowed them to assume that all POA could be approximated as having a single, vehicle- and time-invariant volatility distribution.

The present study provides an additional set of measurements for the volatility of POA emitted from light duty motor vehicles that attempts to address the questions left unanswered in the previous studies. Vehicle emissions in the current study underwent two stages of dilution with measurements by thermal optical EC/OC analysis at each stage, and parallel measurements of thermal optical OC and AMS OA measurements at the second stage of dilution. The vehicle fleet selected for study had emissions rates in the lower third of the California fleet within the Low Emitting Vehicle (LEV) category so that, after dilution, results did not need to be extrapolated outside the tested range. A key update, both conceptually and from a practical standpoint, is that the observations were interpreted within the context of a model that allows for variable amounts of two distinct types of POA emissions that have different volatility distributions. This conceptual picture is consistent with POA from motor vehicles being a balance between unburned lubricating oil and products of the combustion process, which may have very different properties. The results of these measurements provide a more accurate estimate of POA volatility for the California fleet of light duty vehicles with LEV emissions technology.

5.2 Experimental

5.2.1 Vehicle Test Fleet and Driving Cycle

A fleet of eight light duty gasoline-powered vehicles equipped with LEV technology was recruited from the California public and/or group of vehicles maintained by the California Air Resources Board (CARB) for emissions testing purposes (Table 2-1). The average vehicle model year was 2001 (age of 12 yrs) which is close to the average age of vehicles in the US (11.4 years). Vehicle gas tanks were drained and filled with summer-blend gasoline procured by CARB. All vehicles were pre-tested prior to use in the study to ensure proper operation and representative emissions rate (< 10 mg/mile). Vehicles were operated on a chassis dynamometer over the Unified Cycle (UC) driving cycle from a cold-start condition.

5.2.2 Testing Procedure

Vehicle exhaust underwent a first stage of dilution with filtered ambient air using a constant volume sampler (CVS) operated at either 9.9×10^3 lpm (350 scfm) (for vehicles with smaller engines) or 1.7×10^4 lpm (600 scfm) (for vehicles with larger engines). The relative humidity of the exhaust in the first stage of dilution was maintained below 100% to avoid water condensation in the sampling train. Approximately 60 lpm of exhaust from the first stage of dilution was further diluted with ambient air pre-cleaned by passing it through a bed of activated carbon and a HEPA filter to remove background gases and particles. All the components of the secondary dilution system were stainless steel pre-washed with organic solvents to remove background organic contamination. The fleet-average dilution factor after stage 1 was approximately 12 and after stage 2 was approximately 60.

A size-resolved sample of the emissions aerosol was collected immediately after the second stage of dilution using a Micro Orifice Uniform Deposit Impactor (MOUDI) equipped with aluminum substrates. One composite MOUDI sample was collected for each set of 8 vehicles (standard test day).

After the second stage of dilution, emissions were aged approximately 1.2 min in a dark residence time chamber (RTC) to allow for equilibration of semi-volatile material between the gas and particle phases. Emissions were then split into 8 parallel sampling trains (two sets of 4) that were heated to different temperatures (25^{o}C, 50^{o}C, 75^{o}C, and 100^{o}C) to perturb the equilibrium condition (Figure 4-1 right side). All heated sections of the sampling train had a residence time of approximately 1 sec.

Each set of 4 sampling trains served different instrument packages. One set provided emissions to a high resolution Aerosol Mass Spectrometer (HR-AMS), a photoacoustic spectrometer (PAS), and a time-of-flight chemical ionization mass spectrometer (ToF-CIMS) at a flow rate of approximately 5 lpm. Instruments scanned each sampling

sequentially using an automated valve system following a pattern of 30 sec leg 1, 30 sec leg 2, 30 sec leg 1, 30 sec leg 3, 30 sec leg 1, 30 sec leg 4.

Emissions in the second set of 4 sampling trains were collected using media in 4 dedicated denuder-filter-PUF (DFP) arrangements. Composite samples were collected from all 8 test vehicles during a standard sample day. Two eight-channel annular denuders (URG, Chapel Hill, NC) were placed in series for each sampling train to prevent breakthrough of gases. The annular denuders were coated with XAD-4 polystyrene resin [102] that was extracted at the end of each standard sample day. One set of filters and PUF samples were collected on each sample day. The flow rate through each DFP sampling train was 17 lpm.

The fleet of 8 test vehicles (Table 4-1) was driven through the UC driving cycle once each test day (including a cold start). Multiple test days were carried out to (1) perform replicate measurements and (2) to explore the effects of humidity and black carbon concentration in the second stage of dilution air.

5.2.3 Analytical Procedures

The quantification methods for BC emissions measured using PAS are summarized in Chapter 2. The quantification methods for OA emissions measured using HR-AMS are summarized in Chapters 3 and 4. Real-time measurements for BC and OA were investigated as function of time during the driving cycle and were averaged over the entire test day to enable comparisons to off-line measurement techniques.

Quartz filters were collected after the first stage of dilution according to CARB protocols for emissions measurements. The EC/OC content of each quartz filter was measured using a Thermo-Optical Analyzer (Desert Research Institute) following the IMPROVE_A temperature ramp [30].

MOUDI samples were collected immediately after the second stage of dilution at the basecase temperature on aluminum foil substrates. All aluminum sampling media was baked at 500^{o}C for 48hrs prior to use and stored in petri dishes lined with aluminum foil that had been similarly pre-cleaned. Petri dishes were sealed with Teflon tape and stored in a freezer at -30^{o}C when samples were not being collected.

Emissions were aged in the RTC after the second stage of dilution and then passed through heated sampling legs before collection on quartz filters in a denuder-filter-PUF (DFP) sampling train. Filters were pre-baked at 500^{o}C for 48hrs prior to use and stored in petri dishes lined with aluminum foil that had also been baked at 500^{o}C. All filters were handled with metal tweezers pre-cleaned with solvents.

The concentration of EC and OC on each aluminum substrate and quartz filter collected after the second stage of dilution was measured using thermal optical analysis with a Sunset Labs EC/OC analyzer [103] following the NIOSH temperature protocol [104].

The official transition between OC and EC measured on quartz filters was identified as the point after the introduction of oxygen in the sample when the brightness of the filter returned to the value at the start of the temperature ramp. In practice, pyrolysis of carbon from motor vehicle emissions is negligible, and the transition to EC effectively begins at the point when oxygen is introduced into the thermal optical analysis. MOUDI samples employed this latter definition of the transition point between OC and EC since the foil substrates do not permit the measurement of light transmittance through the sample.

5.3 Results

5.3.1 Measurement Intercomparison

Co-located measurements of EC and POA collected on quartz filters (stage 1 and 2 of dilution), MOUDI (stage 2 of dilution), HR-AMS (stage 2 of dilution), and PAS (stage 2 of dilution) were compared to determine reproducibility and reliability of the individual measurement techniques. POA measurements made after the first and second stages of dilution, respectively, were not compared due to the possibility that semi-volatile material was still present in the condensed phase after dilution by a factor of 12, which would bias comparisons with POA made at a dilution factor of +60. EC is non-volatile and can be compared at any point in the sampling train after accounting for intermediate dilution factors.

The comparison in the right panel of Figure 5-1 shows good agreement between thermal optical measurements of EC/OC made at different locations in the dilution system with different collection media, different analysis temperature ramps, and different carbon analyzers. All EC/OC measurements are in agreement within experimental uncertainty.

The comparisons in the left panel of Figure 5-1 indicate differences between the thermal optical measurements of EC vs. the PAS measurements of BC, and the thermal optical measurements of OC vs the HR-AMS measurements of OA. In both cases, the real-time measurements detect less carbon than the offline instruments. A comparison of CO2 measurements made after the first stage of dilution by CARB and the CO2 measurements made alongside the HR-AMS and PAS measurements confirms that the flow rate through the real-time instrument sampling lines was correct (Figures 2-2 and 2-3). The differences between the HR-AMS vs. filter-based measurements (33-89%) are larger than the differences between the PAS vs. filter-based measurements (12-69%), ruling out the possibility of a systematic bias.

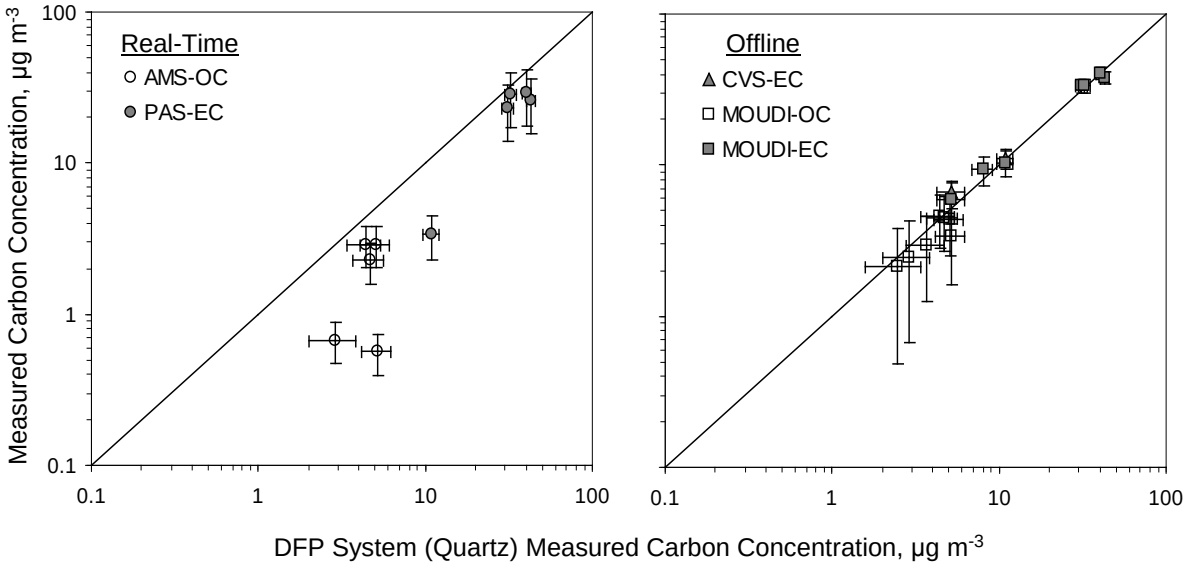

Figure 5-1: Comparison of EC and particulate OC measured using real-time instruments (AMS and PAS) and filter based instruments (MOUDI and CVS) to Quartz filter measurements from DFP system. Five points were used for real-time comparisons, seven points were used for MOUDI comparisons, and two points were used for CVS comparison. Numbers of comparable points were based on data availability.

The EC/BC differences between the thermal optical technique and the PAS have been discussed in Chapter 2. One of the cars in the test fleet had an elevated emissions rate of EC/BC on the day when the disagreement between the thermal optical measurement and the PAS is largest. This emissions rate did not overwhelm the detection limits of either technique and should not have resulted in a difference in the measured concentrations. It is possible that some low-volatility carbon emitted during this test was not black but detected as EC, leading to differences in the EC and BC measurements. Further research on this topic is ongoing.

The OC/OA differences between the thermal optical technical and the HR-AMS are significant. Figure 5-2 illustrates the difference between the two measurements under basecase conditions, when EC was injected into the second stage of dilution air, and when EC was injected in the background air and the humidity of the background air was increased from a nominal value of 70% to 85%. The HR-AMS measurements are lower than the thermal optical measurements at all temperatures in each one of these tests. Statistical analysis using a paired t-test indicates the HR-AMS measurements are lower than the thermal optical measurements with 95% confidence.

One possible explanation for the discrepancy illustrated in Figure 5-2 is that filter-based measurements are biased high due to the presence of gas-phase adsorption artifacts. This explanation is not consistent with the trends shown in Figure 5-2 because heating the

sample by 50^{o}C does not substantially reduce the OC concentration measured on the filter even though a gas-phase adsorption artifact would presumably be susceptible to partitioning back to the gas phase at these temperatures. It is likely that the two upstream denuders stripped all of the semi-volatile gas-phase OC compounds out of the sample stream prior to reaching the filter.

A second possible explanation for the discrepancy between the thermal optical and HR-AMS measurements is that the HR-AMS does not classify low-volatility carbonaceous material as OC while the thermal optical method does classify this material as OC. The HR-AMS defines any material that doesn't volatilize after a few seconds at 600^{o}C under vacuum as "refractory". A typical thermogram from the EC/OC analysis shows that a significant amount of OC emitted from motor vehicles evaporates at temperatures well above 600^{o}C, anywhere from 15-30% of the total OC (Figure 5-3). An example of a specific carbon-containing compound that evolves at these temperatures in an inert He atmosphere is calcium carbon ($CaCO_3$) [105] which would have been classified as OC by the thermal optical analysis in the current study. The amount of OC that evolves at temperatures greater than 600^{o}C during thermal optical analysis is shown as the dark portions of the bars in Figure 5-2. This material does not completely account for the differences in the thermal optical vs. HR-AMS measurements. Additional factors appear to be at work which prevent quantification of some fraction of the carbonaceous material emitted from light duty gasoline vehicles using HR-AMS.

It is noteworthy that Q-AMS was the principle method employed by May et al. [101] in their measurement of LDV exhaust volatility. A fraction of the POA volatility between the first and second stages of dilution was attributed to the differences in the thermal optical vs. Q-AMS measurements but the current comparison suggests that some of that difference could be explained by differences in the measurement techniques. Co-located measurements between Q-AMS and a thermal-optical analyzer were not reported by May et al.

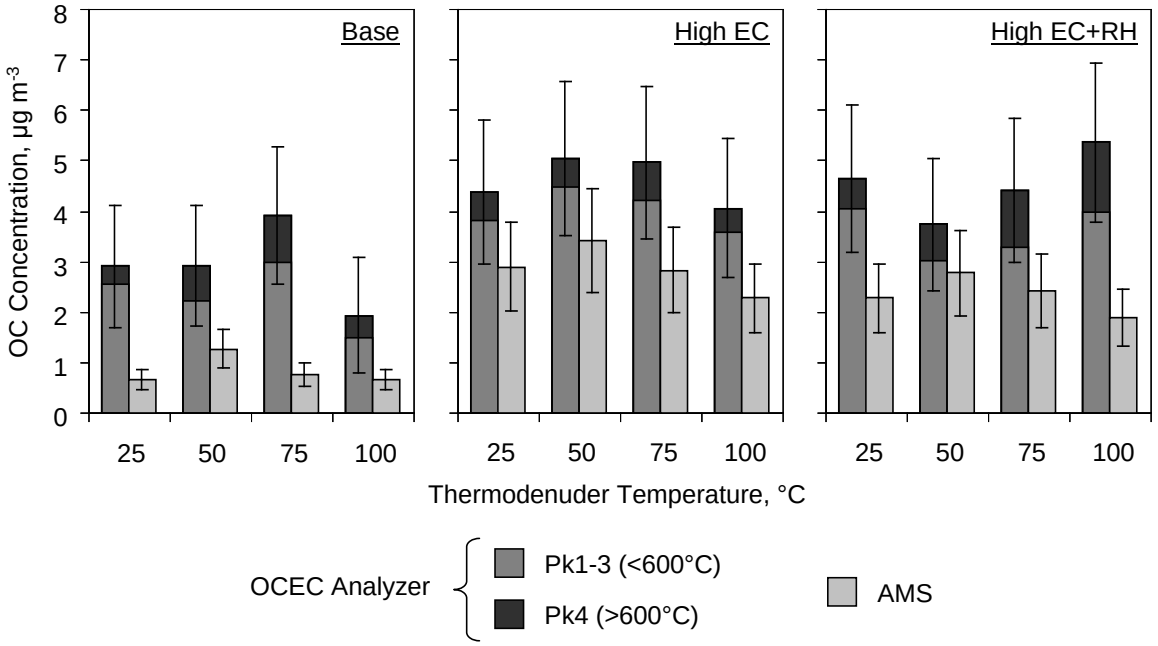

Figure 5-2: Measured OC concentration from DFP train Quartz filter (thermal optical OCEC) and HR-AMS during three of the core tests (base, high EC, and high EC+RH) at four temperatures. Pk1-3 indicates OC that volatilized in a He atmosphere at temperature below 600°C in and Pk4 indicates OC that volatilized at temperatures above 600°C. Uncertainty bars represent handling and/or instrumental uncertainty.

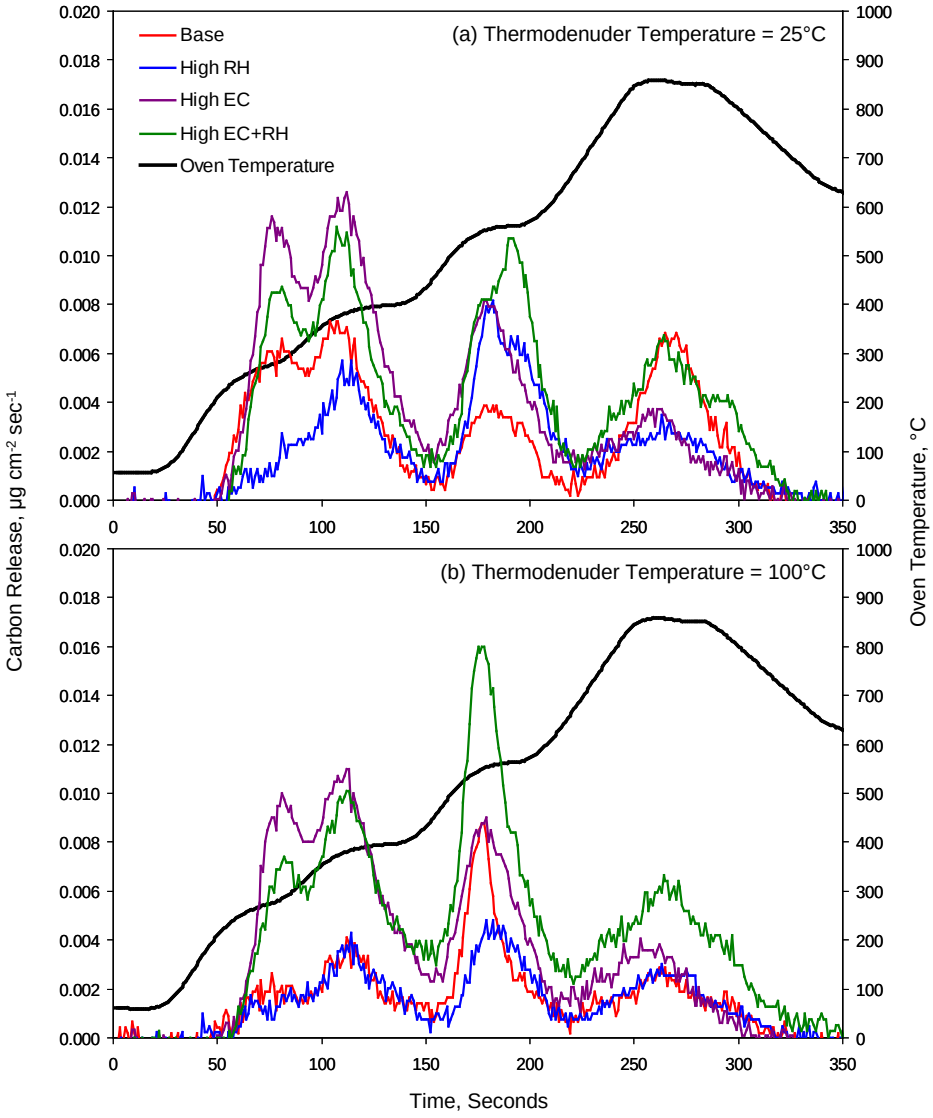

Figure 5-3: Thermogram of DFP Quartz filters in He atmosphere obtained at (a) T = 25°C and (b) 100°C for all experimental conditions: base case, high RH case, high EC case, and high EC+RH case.

5.3.2 Test Fleet Emissions Characteristics

The PM and POA emissions rates from the 8 vehicles utilized in the current study for the chassis dynamometer tests were compared to the emissions rates from the 7 vehicles used to measure POA volatility reported by May et al. [101]. The distribution of emissions rates from +200 vehicles tested by the US EPA as part of a comprehensive emissions characterization program carried out in Kansas City [106] were used as an indicator of typical fleet behavior in this comparison. The Kansas City fleet included vehicles with many different ages spanning a range of emissions control technologies, most of which

were pre-LEV. As shown in panel 1A of Figure 5-4, 4 out of the 7 vehicles used to measure POA volatility in the May et al. (CMU) fleet had PM emissions rates > 10 mg/mile which would have excluded them from the current testing as "high emitting vehicles". Panel 2A of Figure 5-4 shows that the highest emitting vehicle used in the current study (which had LEV emissions control technology but was malfunctioning) emitted PM at a rate of only 3.2 mg/mile. May et al. selected the representative vehicles to use in their thermodenuder-based POA volatility analysis based on the need to have sufficiently high concentrations of POA in their Teflon reaction chamber so that their Q-AMS measurements produced reasonable signal to noise ratios. This experimental limitation appears to make their results most relevant to vehicles with emissions rates greater than 10 mg/mile.

Figure 5-4 panels 1B and 2B illustrate the POA emissions from the vehicle fleet used by May et al. (CMU fleet) and the fleet used in the current study. Note that the results shown the left panels of Figure 5-4 are based on a reanalysis of the raw data provided in the supplemental information of the May et al. study. May et al. [101] did not create these figures or plot the data in this manner. POA emissions from the May et al. (CMU) fleet are orders of magnitude higher than POA emissions from the fleet recruited for the current study, likely because the total PM emissions rates from these vehicles were also much higher. Both sets of POA measurements are based on AMS and presumably have the same bias relative to thermal-optical OC (see Figure 5-2 and associated discussion). These POA measurements likely under-estimate the absolute concentration of low volatility POA in the emissions, but the comparison between the different fleets is not affected by this issue.

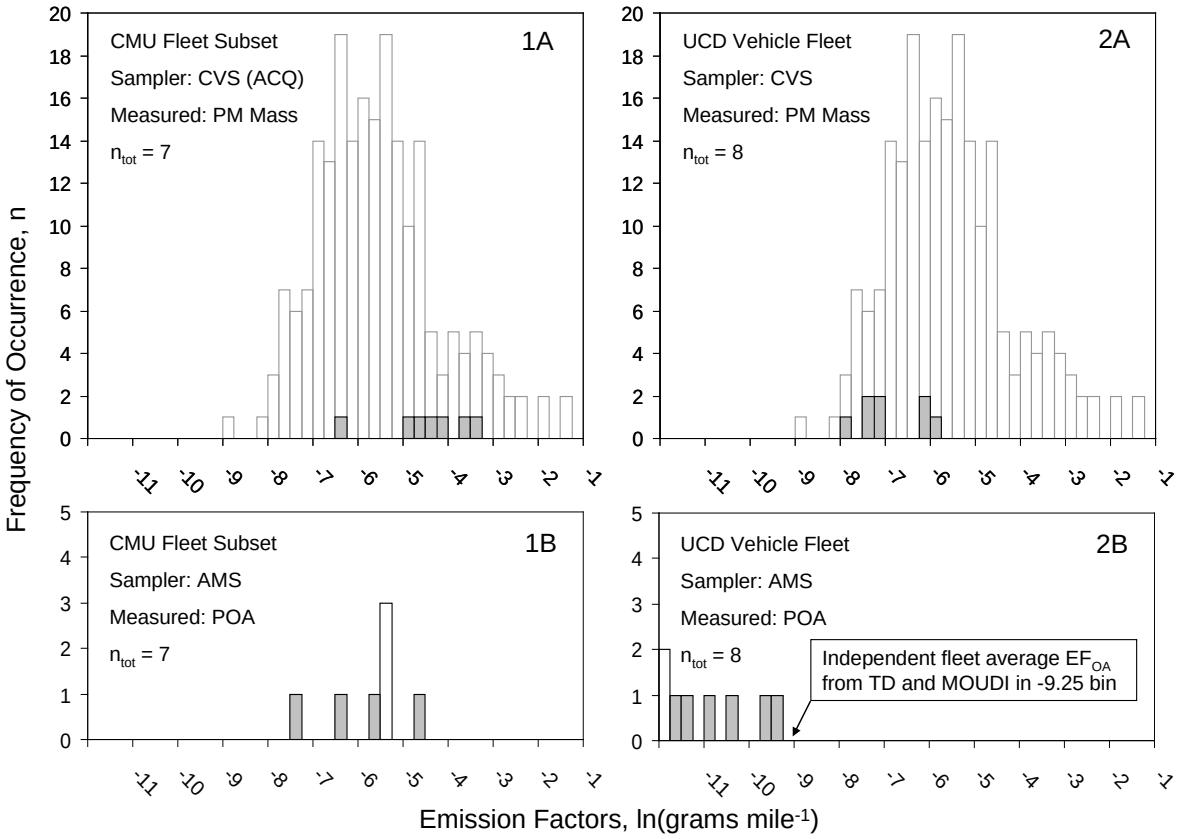

Figure 5-4: Emission factors of PM measured after the first phase of dilution (panel 1A and 2A) and POA measured using HR-AMS after the second stage of dilution (panel 1B and 2B). Final dilution ratio ~300-1500 for CMU and ~ 61 for UCD. White bars are the EF from the Kansas City study and the overlaid gray bars are CMU and UCD fleet EF. EF of POA from offline filter measurements are shown in panel 2B. ACQ = adsorption corrected Quartz. n_{tot} is the number of vehicles in each fleet.

Figure 5-5 shows the distribution of the emissions rates from the entire fleet tested by May et al. [101] alongside the Kansas City fleet. Note that the results shown the upper panel of Figure 5-5 are based on a reanalysis of the raw data provided in the supplemental information of the May et al. study. May et al. [101] did not create these figures or plot the data in this manner. Emissions from the May et al. fleet have a mode at 11.1 mg/mile while the EPA fleet has a mode at approximately 2.5 mg/mile. The reason for the higher emissions rate from the May et al. fleet vs. the Kansas City fleet is not known. The May et al. fleet did contain vehicles with emissions rates similar to the vehicles employed in the current study, but these lower emitting vehicles were not used to estimate the POA volatility from thermodenuder experiments due to limited signal to noise ratios from Q-AMS measurements in their Teflon reaction chamber.

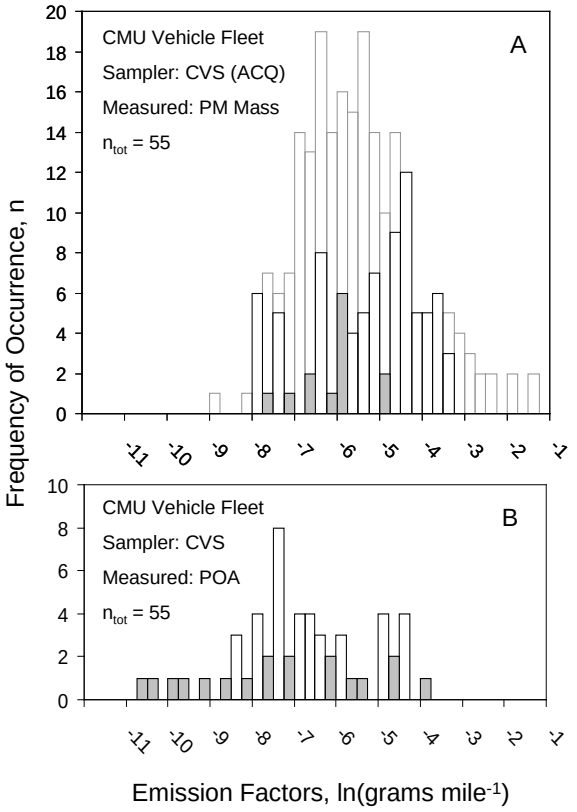

Figure 5-5: Emission factors of PM and POA from CMU's full vehicle fleet tested in 2011 overlaid on the distribution of emission factors representative of vehicle population in Kansas City, MO.

5.3.3 POA Volatility Measurements

The apparent volatility of OA at elevated temperature is one of the primary measures that have been used to estimate how POA might evaporate when diluted downwind of emissions sources. Figure 5-6 shows the mass fraction ratio (MFR) calculated for POA emitted from light duty vehicles after heating to different temperatures as measured using HR-AMS and the thermal optical technique in the current study. In general, POA concentrations increase as temperature is increased from 25 to 50°C. This increase in POA concentrations due to mild heating is inconsistent with the absorption theory typically used to explain POA partitioning. One potential explanation for this increase is that ongoing chemical reactions that produce POA in the vehicle exhaust speed up at increased temperatures, thereby leading to increased POA concentrations. Further increases in temperature lead to a decrease in the POA MFR, with a median MFR value of approximately 0.8 at 100°C as determined from either the HR-AMS or the thermal optical technique. The relatively large MFR at 100°C suggests that POA emissions have

relatively low volatility compared to the results of May et al. which predicted much greater POA volatility, although direct visual comparison between the current study and May et al. cannot be performed because of the differences in residence times of the thermodenuders employed (see Section 5.3.4). Given the differences in the test vehicle fleets, dilution ratios, and residence time at elevated temperatures, additional analysis is required to interpret these results.

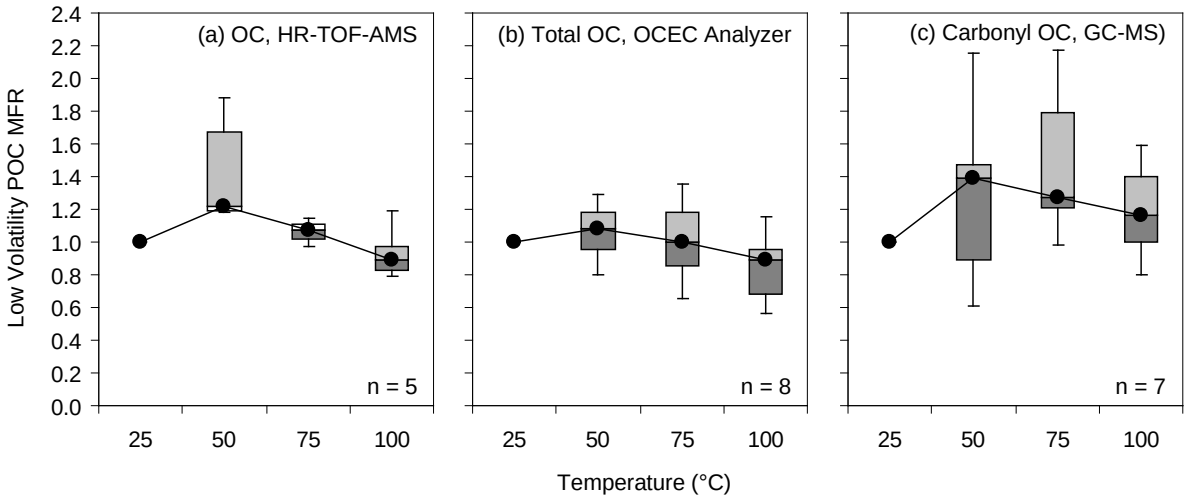

Figure 5-6: MFR of POC emitted from the fleet of light-duty gasoline vehicles as a function of temperature. n represents the number of sampling events used in each statistical analysis. Box-whisker plots represent volatility for: (a) sum of OC from 37 carbonyl compounds measured using GC-MS, (b) sum of organics (< 300 m/z), converted to OC using OM/OC=1.23, measured using HR-TOF-AMS, and (c) Total filter based OC measured using OCEC Aerosol Analyzer.

The real-time HR-AMS measurements made in the current study can examine the volatility of POA emitted from the test fleet during different phases of the UC driving cycle. Figure 5-7 shows the POA MFR measured during the phases of the UC: (1) cold start acceleration, (2) high velocity, (3) hard acceleration, and (4) hot running acceleration. All of the data shown in Figure 5-7 represents basecase conditions (no changes to background humidity or introduction of background EC). POA emissions during the cold start portion of the driving cycle appear to be higher than during other portions of the driving cycle, and they appear to be more semi-volatile. The cold starts often emit larger amounts of VOCs, CO, and NOx because the emission control equipment has not reached its optimal operating temperature. POA appears to be less volatile during the phases of the driving cycle after the cold start. This result indicates that there is a greater fraction of very low-volatile POA in the diluted gasoline vehicle exhaust when the vehicle has reached a stead state operating temperature. The median of POA MFR at all temperature ranges fluctuates above 0.7. It can be noted, however, that the uncertainty bounds of MFR dips below 0.4 during the cold start acceleration cycle at T = 100°C.

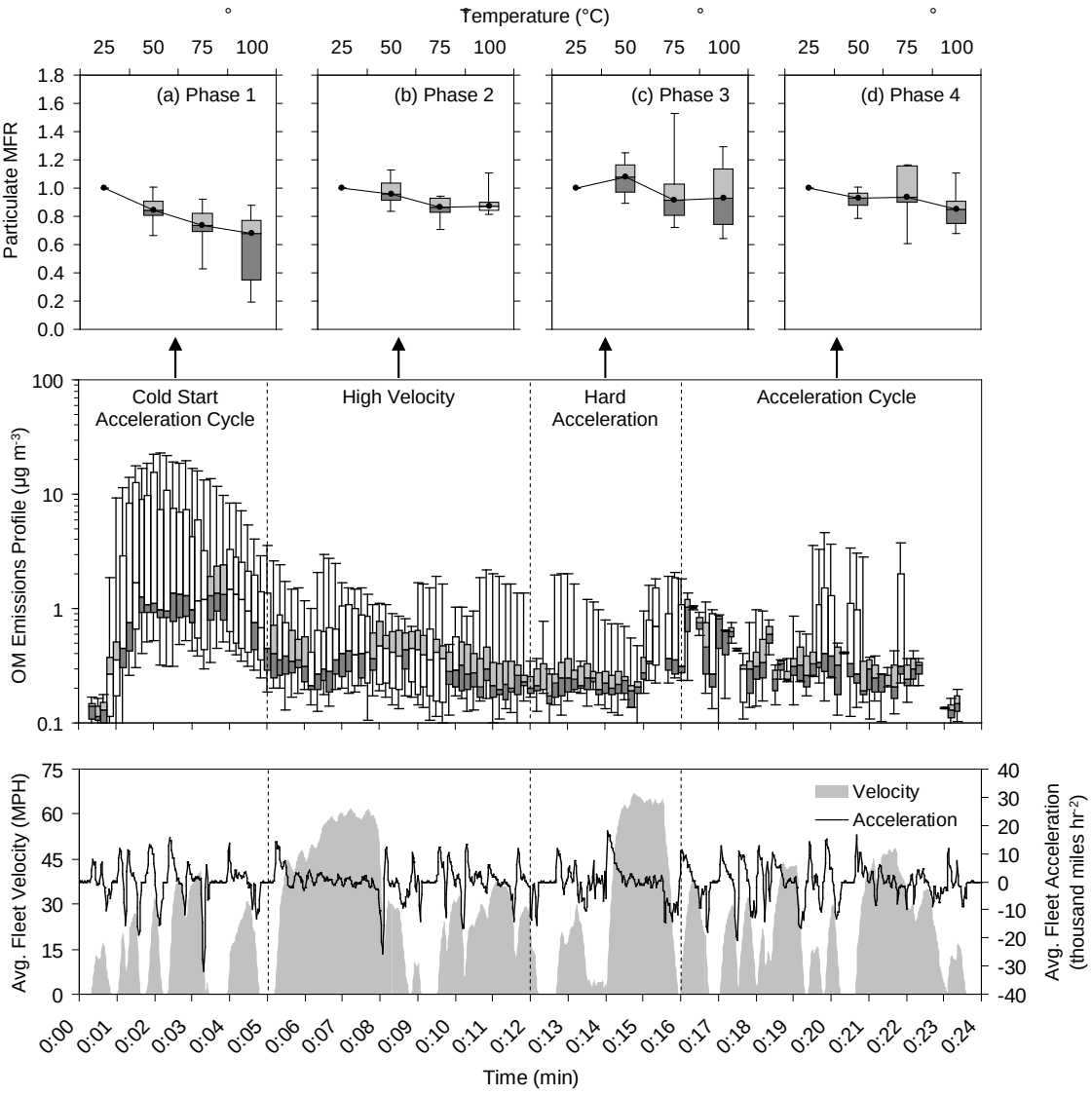

Figure 5-7: MFR of POC at different UC driving schedule phases during base case (8 individual vehicles): (a) Phase 1, cold start acceleration, (b) Phase 2, hard acceleration and stop-and-go, (c) Phase 3, second hard acceleration, (d) Phase 4, stop-and-go.

5.3.4 POA Volatility Modeling

May et al. interpreted the results from the light duty vehicle POA MFR at elevated temperatures using a single volatility distribution fit to a thermal denuder (TD) model [101]. The calculation assumed that the OA is mono-disperse with a particle diameter Dp = 200 nm. A diffusion coefficient of 5 x 10^{-6} m^2 s^{-1} was used along with an

accommodation coefficient of 1. The Kelvin effect was also considered in the model with surface tension of 60 dynes cm^{-1}. A similar model [107] was used to fit the POA volatility measured in the current study (Figure 5-8). The model fit was calculated at two OA concentrations (0.2 µg m^{-3} and 30 µg m^{-3}) to reflect the range of dynamic conditions experienced during each test. The median mass fraction remaining (MFR) in the current study falls between the two model predictions at the two concentrations when the POA volatility distribution recommended by May et al. [101] is used. The difference in the median MFR in the current study (~0.8) vs. the May et al. study (<0.2) results mainly from differences in the residence time at elevated temperature between the two studies and the assumed mono-disperse OA particle diameter. May et al. heated the POA samples for ~30 sec while the current study heated samples for ~1 sec. The difference in residence time is explicitly accounted for in the model.

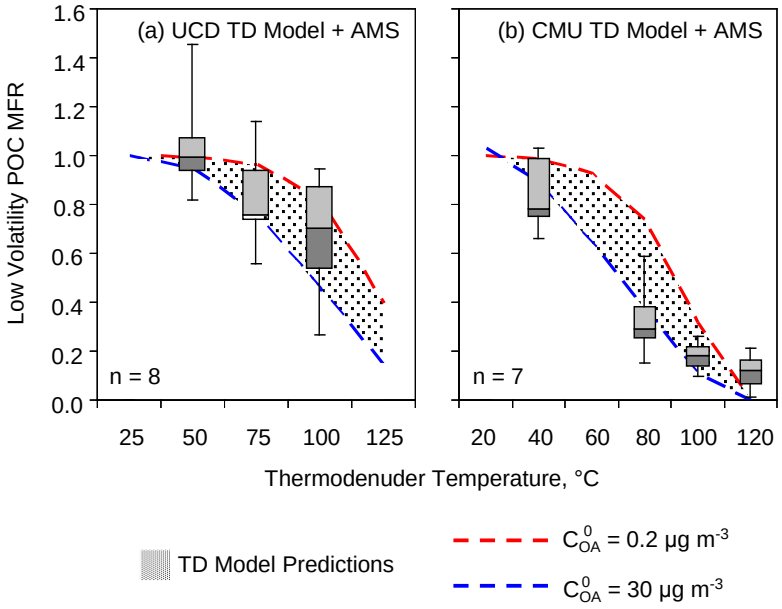

Figure 5-8: MFR derived from UCD-AMS and CMU-AMS data fit to respective TD model parameters. The red and blue dotted lines indicate sensitivity of the MFR based on the organic aerosol model input.

Although the TD model captures the behavior of the median POA volatility distribution it does a poor job capturing the scatter of individual vehicle MFRs about the median value. This scatter is obvious in the box and whisker plot shown in Figure 5-8 (May et al. data or UCD data). The lack of model skill when using this single volatility distribution formulation is also illustrated in the scatter plot of predicted vs. observed MFRs shown in Figure 5-9A (UCD data only). The Pearson correlation coefficient (R^2) for the regression line without forcing the intercept to zero is 0.52 (weak correlation) and considerably lower when an intercept of zero is required. This finding suggests that the TD model does not explain all the variability in the observed data.

The TD model developed by May et al. assumes that a single volatility distribution describes motor vehicle POA. Previous studies based on detailed chemical analysis of emissions from gasoline powered motor vehicles have determined that lubricating oil and fuel make separate and distinct contributions to the POA emissions [6]. The fuel contribution to POA uses heavy PAHs (MWt>300amu) as a fuel indicator. It is likely that fuel contributes strongly to the POA that evolves at elevated temperatures in the thermal optical analysis (Figure 5-3). Building on this framework, a new TD model was developed based on an assumption that there are two types of POA with distinct volatility distributions that make up vehicle POA: motor oil and combusted fuel products. The latter will be referred to as fuel-derived POA. The volatility distributions for each of these components are shown in Figure 5-10. The motor oil volatility distribution is based on direct measurements of motor oil evaporation at elevated temperature from May et al. [101]. The fuel volatility distribution is selected to ensure essentially non-volatile behavior (the exact distribution of material into volatility bins with $C^*<0.1$ μg m^{-3} is not critical). The relative amounts of these two POA types is varied to produce an optimal match with the observed MFR at 100°C from each individual vehicle. The ability of this two component volatility distribution model to fit the observed MFRs of individual vehicles is shown in Figure 5-11 and in the scatter plot shown in Figure 5-9B. The skill of the two component model is greatly improved; the R^2=0.94 when the regression line is not forced through zero or R^2=0.8 when the regression line is forced through zero.

The remaining scatter evident in Figure 5-9B is caused by the vehicles for which the absolute POA concentration increased slightly with temperature (especially at 50°C), which likely reflects the action of continued chemical reactions in the diluted exhaust. The TD model is based on absorption partitioning and is unable to predict increasing MFR as temperature increases. Despite these limitations, the 2 component volatility distribution combined with the TD model explains the majority of the scatter in the measured MFRs from individual vehicles.

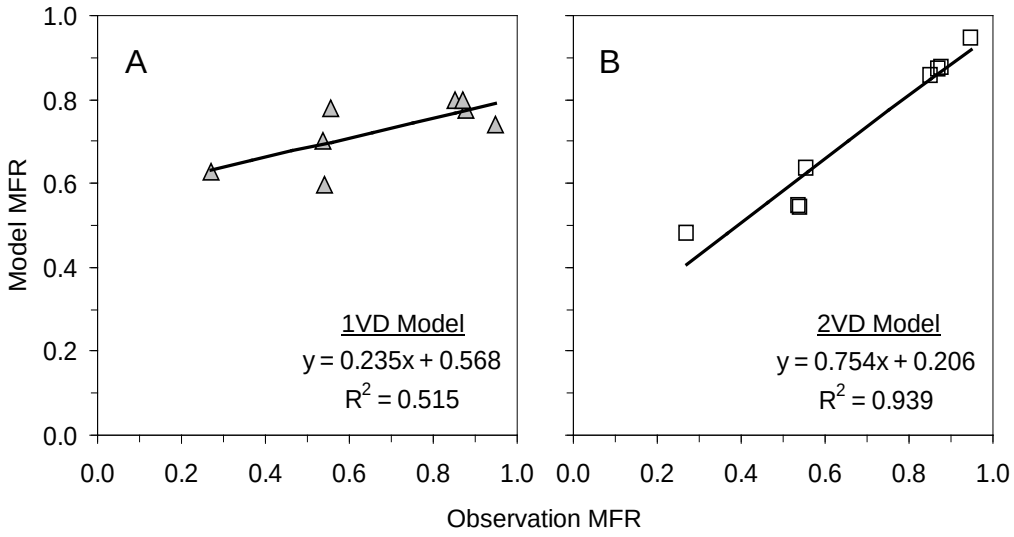

Figure 5-9: Predicted vs. observed POA mass fraction remaining using (A) a TD model with a single volatility distribution and (B) a TD model with two volatility distributions.

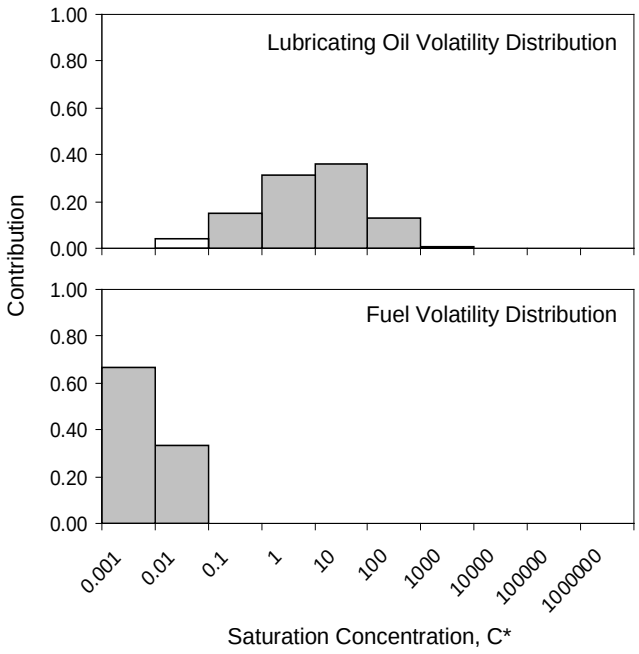

Figure 5-10: Volatility distribution of lubricating oil and fuel utilized in the Fuel-Oil Split UCD TD model to fit the observations. C^* is in units of $\mu g\ m^{-3}$.

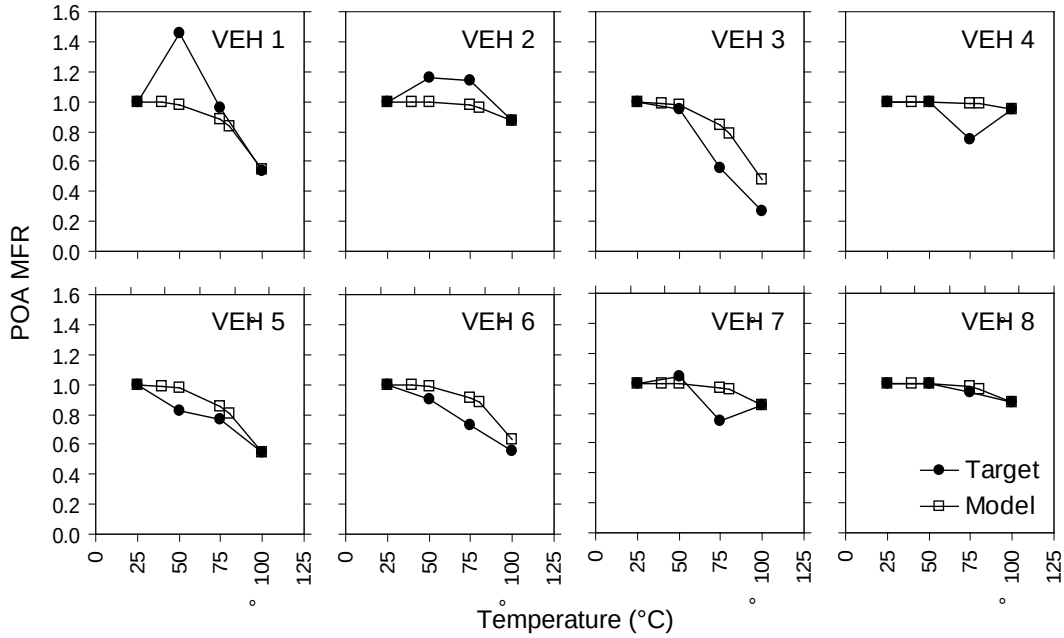

Figure 5-11: Two-Phase UCD TD model fit for MFR obtained using daily average AMS OA concentration for individual vehicles.

5.3.5 Fuel and Oil Contributions to POA Emissions

The 2-POA type volatility distribution fits illustrated in Figure 5-11 were determined by iteratively adjusting the relative amounts of motor oil and fuel-derived POA in the TD model with the goal of minimizing the residual error. Figure 5-12 shows the relative amount of oil POA and fuel-derived POA calculated for each of the 8 vehicles tested in the current study. Three vehicles had emissions dominated by oil POA, one vehicle had emissions dominated by fuel-derived POA, and the remaining four vehicles had a mixture of fuel-derived and oil POA. The total POA emissions rate was not a predictor of either dominant fuel-derived or oil POA emissions. Each vehicle appears to emit variable amounts of both material.

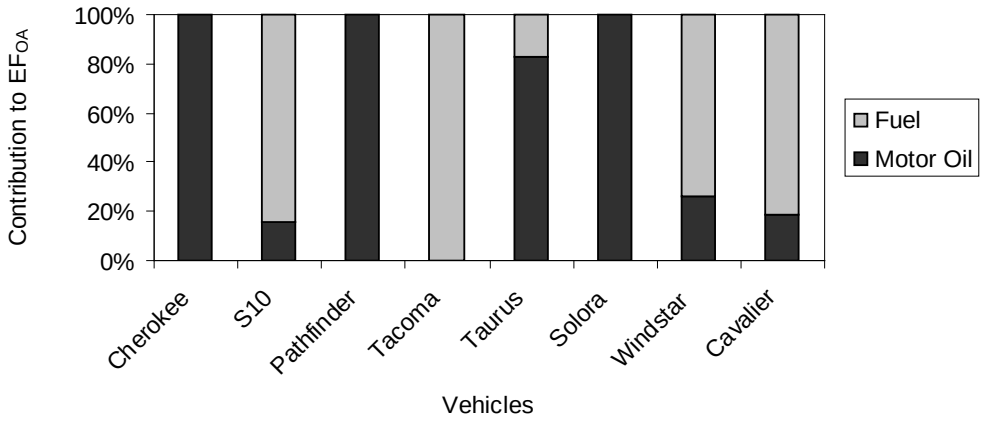

Figure 5-12: Emissions of OA attributed to fuel-derived and motor oil derived POA (UCD vehicle fleet).

The real-time measurements available in the current study make it possible to measure the oil and fuel-derived product contributions to POA during different portions of the UC driving cycle. Figure 5-13 shows the fraction of POA attributed to oil during each UC phase for each vehicle used in the current study. The three highest POA emitters were vehicles 1 (Cherokee), 3 (Pathfinder), and 5 (Taurus) at OA loading of 4.13 μg m^{-3}, 2.82 μg m^{-3}, and 1.17 μg m^{-3}, respectively during the cold starts. Each of these vehicles emitted essentially 100% oil POA during the cold start but much lower proportions of oil POA during other portions of the driving cycle. Vehicle 4 (Tacoma) and 6 (Solara) exhibited very high oil contributions to POA during the final phase of the driving cycle.

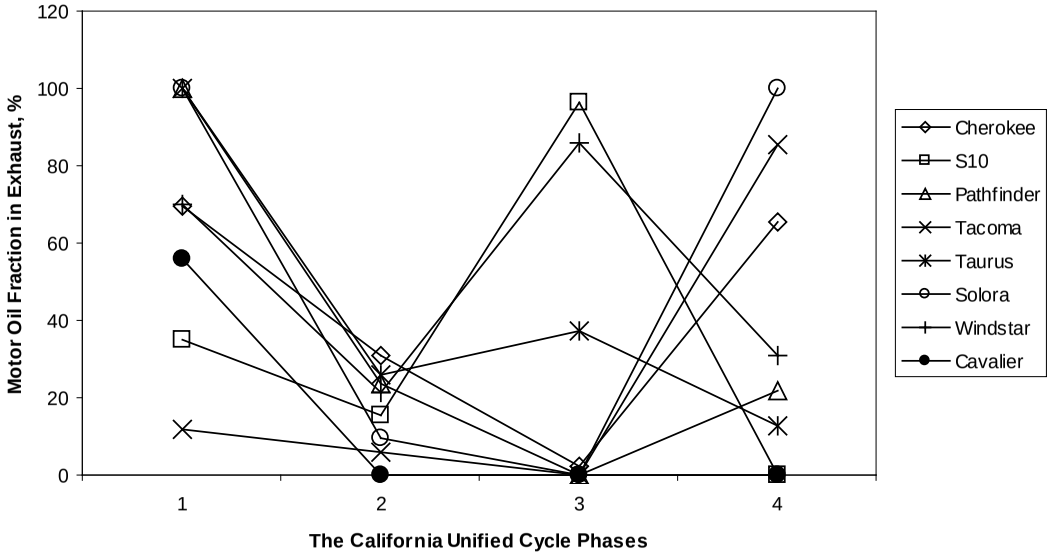

Figure 5-13: Motor oil contribution to vehicle OA emissions separated by driving cycle phases.

5.3.6 Fuel and Oil Volatility Distributions Fit to Previous Data

The 2 component volatility distribution TD model was applied to the measurements of May et al to determine the fraction of oil vs. fuel-derived contributions to POA. Figure 5-14 shows that the large fraction of the May et al. fleet have POA dominated by oil contributions. The larger emissions rates from the May et al. fleet vs. the fleet tested in the current study likely contribute to this finding (see Section 5.2.1).

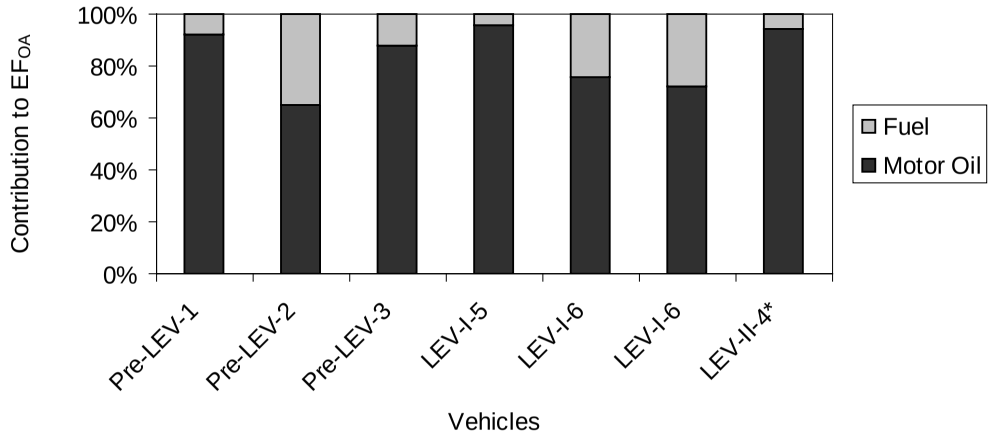

Figure 5-14: Emissions of OA contributed to fuel and motor oil derived POA (CMU vehicle fleet).

5.4 Discussion

Figure 5-15 describes the distribution of fuel-derived and oil POA emissions measured in the current study (8 vehicles) and by May et al. (7 vehicles) calculated using the techniques discussed above. Vehicles that emitted negligibly small amounts of either fuel-derived or oil POA were not plotted on the histograms for that component. The EF_{OA} contribution measured in the current study from the fuel-derived products in all phases of the UCD cycle are more consistent than the oil contributions which span several orders of magnitude between vehicles in the same portion of the cycle or between the same vehicles in different portions of the cycle. Motor oil POA emissions are generally higher from all vehicles during the cold-start portion of the driving cycle.

Both the fuel-derived and oil POA emissions rates measured in the current study are lower than the corresponding emissions rates measured by May et al. This finding largely stems from the different vehicle fleets that were tested (see Figure 5-4 and associated discussion). The differences in oil POA emissions factors are larger than the differences in the fuel-derived POA emissions factors when comparing the two studies.

The extrapolation of the single volatility distribution proposed by May et al. to the ambient atmosphere will result in almost complete evaporation of POA emitted from motor vehicles. This prediction does not fully match the POA volatility measured by May et al. (see divergence of predictions vs. measurements at 120^{o}C in Figure 5-8b). The two component (fuel-derived + motor oil) volatility distribution more accurately predicts the volatility of POA emitted from light duty vehicles because it better captures the physical processes involved. This framework should be incorporated into future regional modeling applications that consider the volatility of POA. However, further measurements are needed to construct reasonable histograms of the fuel-derived/motor oil POA split that are representative of on-road fleet characteristics before regional modeling calculations are warranted.

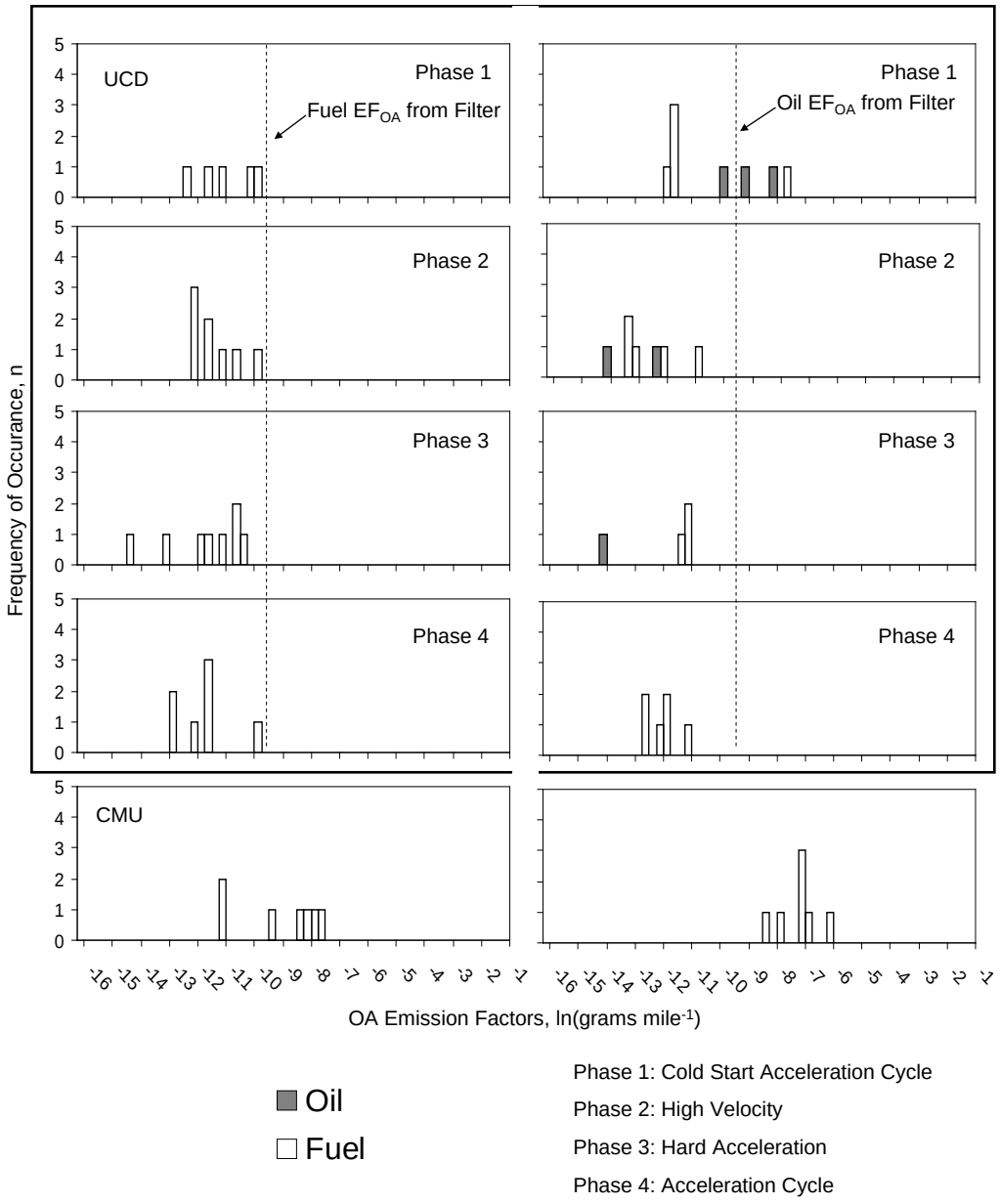

Figure 5-15: Apportioned EF_{OA} from fuel and oil. Boxed histograms represent UCD fuel-oil split for individually separated phases while the unboxed histograms represents CMU fuel-oil split. Data includes 8 vehicles from UCD and 7 vehicles from CMU.

5.5 Conclusions

A partitioning model based on a single volatility distribution similar to motor oil roughly explains the median partitioning behavior of POA emitted from a fleet of 8 light duty gasoline motor vehicles but the error in the model fit is unacceptably large (R^2=0.52). A model incorporating two volatility distributions – one similar to motor oil and one composed largely of effectively non-volatile material – explains the measured behavior of the POA volatility much more accurately (R^2=0.94). The two volatility distributions can be interpreted as motor oil with intermediate volatility and fuel combustion products with low volatility. Of the 8 vehicles in the test fleet, 4 vehicles emitted POA predominantly composed of motor oil and 4 vehicles emitted POA predominantly composed of fuel-derived products. Motor oil emissions were generally highest during the cold-start portion of the UC driving cycle with reduced emissions rates during the phases when the engine and emissions control equipment reached operating temperature. Emissions of POA associated with fuel-derived products were roughly equal during all segments of the driving cycle. A larger fleet of vehicles should be tested to determine accurate rates for motor oil and fuel-derived POA emissions for the fleet of light duty gasoline vehicles in California.

6 EFFECT OF DILUTION AIR TEMPERATURE, HUMIDITY, AND BLACK CARBON CONCENTRATIONS ON TOTAL CARBONYL EMISSIONS FROM GASOLINE FUELED MOTOR VEHICLES

6.1 Introduction

Organic aerosol (OA) accounts for a significant fraction of $PM_{2.5}$ in the atmosphere where it affects both the environment and human health. The majority of the primary organic aerosol (POA) observed in urban regions is emitted from combustion sources such as on-road diesel and gasoline vehicles [108-110]. POA directly contributes to the total OA burden and/or provides material for subsequent chemical reaction leading to the formation of secondary organic aerosol (SOA). Understanding and characterizing the behavior of anthropogenic POA in the real atmosphere is necessary to correctly assess the direct and indirect impacts of mobile sources for future epidemiological studies and control programs.

Recent measurements have determined that carbonyl compounds are an abundant component of POA emissions from gasoline vehicles [5]. A follow-up study was unable to explain the partitioning of light carbonyl compounds to the condensed phase using a state of the science model based on absorptive partitioning theory [9]. Further research is needed to better understand the conditions that promote carbonyl formation in the exhaust from gasoline vehicles and the conditions under which these carbonyls partition to the condensed phase. The insights gained from these studies may benefit our general understanding of POA and SOA associated with this important source of $PM_{2.5}$.

The purpose of the current study is to examine how the emission rate of total (=gas+particle) carbonyls from light duty gasoline vehicles has evolved in response to changing fuel composition between 2002 and 2001. The change in total carbonyl emissions in response to the temperature of the dilution air, the relative humidity of the dilution air, and the concentration of black carbon (BC) particles in the dilution air will also be quantified in order to gain greater insights into carbonyl production mechanisms in the exhaust stream from vehicles. Table 6-1 summarizes the test matrix used in the measurement campaign.

Table 6-1: Four unique experimental conditions tested.

Target Test Condition Matrix	
Base Condition RH = 55% Background EC = 0 μg m^{-3}	Adjusted RH RH = 85% Background EC = 0 μg m^{-3}
Adjusted EC RH = 55% Background EC = 25±5 μg m^{-3}	Adjusted EC+RH RH = 85% Background EC = 25±5 μg m^{-3}

6.2 Experimental Methods

6.2.1 Vehicle Fleet and Driving Cycle

Table 6-2 summarizes the fleet of vehicles used in the current study in comparison to the fleet of vehicles used for previous emissions characterization tests. All vehicles were selected from the Low Emissions Vehicle (LEV) emissions control technology which limits their model years to the range ~1997-2002. The average age of the vehicle fleet used in the present study was 12 years which is representative of the US average vehicle fleet age of 11.4 years. The average mileage of the LEV vehicles predictably increased between the testing conducted in 2002 (46,678 miles) vs. 2011 (90,257 miles). All vehicles used in the current study were pre-screened to ensure they had emissions rates < 10 mg $mile^{-1}$. The fleet emissions characteristics are discussed by Robert et al. [70] and in Chapter 5 of the current report.

All vehicles were tested on the Unified Cycle (UC) driving cycle in the current study whereas previous tests used the Federal Test Procedure (FTP-75) driving cycle. Both cycles involve a cold start followed by a series of accelerations, decelerations, and constant velocity segments. The UC driving cycle is generally recognized as more aggressive (greater acceleration, higher top speed) resulting in higher PM emissions [111].

Table 6-2: Vehicle fleet composition of the past (2002) and the present (2011) dynamometer study that represents on-road gasoline vehicle fleet emissions.

Vehicle Fleet Comparison

2002

Category	Year	Make	Model	Mileage	Engine Information
LEV PC	1996	Honda	Civic	77,703	4 cylinder
LEV PC	1998	Honda	Accord	97,811	4 cylinder
LEV PC	1999	Toyota	Camry LE	43,160	6 cylinder
LEV PC	1999	Nissan	Sentra GXE	52,630	4 cylinder
LEV PC	2002	Chevrolet	Monte Carlo	20,230	6 cylinder
LEV LDT/SUV	1998	Ford	Explorer	82,513	8 cylinder
LEV LDT/SUV	2000	Jeep	Grand Cherokee	31,751	6 cylinder
LEV LDT/SUV	2000	Toyota	Tacoma	51,554	6 cylinder
LEV LDT/SUV	2002	Nissan	Pathfinder	8,169	6 cylinder
LEV LDT/SUV	2003	Chevrolet	Silverado	1,264	8 cylinder

2011

Category	Year	Make	Model	Mileage	Engine Information
LEV PC	1997	Ford	Taurus	130,092	6 cylinder
LEV PC	1998	Ford	Windstar	90,519	6 cylinder
LEV PC	2001	Chevrolet	Cavalier	52,666	4 cylinder
LEV PC	2003	Toyota	Camry Solara	97,304	6 cylinder
LEV LDT/SUV	2002	Chevrolet	S10 Pickup	57,690	4 cylinder
LEV LDT/SUV	2002	Chrysler	Grand Cherokee	83,200	8 cylinder
LEV LDT/SUV	2003	Toyota	Tacoma	100,535	4 cylinder
LEV LDT/SUV	2003	Nissan	Pathfinder	110,055	6 cylinder

6.2.2 Vehicle Fuel

The vehicle fleet in both 2002 and 2011 was fueled with California summer blend gasoline but the specifications of that fuel changed between the two measurement campaigns. Fuel in 2002 contained the additive methyl tert-butyl ether (MTBE) to increase oxygen content while the fuel in 2011 contained ethanol (EtOH) for the same purpose. MTBE was banned in California in 2003 due to potential ground water contamination problems. A survey of fuel characteristics from all refineries in southern California showed that median total aromatic content of gasoline increased from 22% to 23.5% by mass between 2002 and 2011, while Reid Vapor Pressure (RVP) decreased from 6.8 psi to 5.8 psi. The second phase of California's reformulated gasoline (CaRFG) program in 1996 called for a more stringent Reid vapor pressure (RVP) requirement in efforts to reduce evaporative losses of reactive compounds in gasoline [112].

6.2.3 Vehicle Test Procedure and Dilution Sampling

The source sampling campaign was conducted using a chassis dynamometer at California Air Resources Board's (CARB) Haagen-Smit Laboratory in El Monte, California. Vehicle emissions were diluted in two stages. A constant volume sampler (CVS) operated by CARB provided a primary dilution ratio of ~12.7 while the secondary dilution system shown in Figure 6-1 provided a dilution ratio of ~4.8, achieving total dilution ratio of approximately 61 to replicate atmospherically relevant mobile emissions concentrations. The base case concentration of $PM_{2.5}$ in the final diluted sample was 13.8 $\mu g\ m^{-3}$. Air flow rates in the secondary dilution system were adjusted to ensure turbulent mixing in the stack dilution tunnel (SDT) with Re >> 4000.

The system that provided the second stage of dilution in the current study was able to manipulate the properties of the dilution air to study the effect on carbonyl emissions rates (Figure 6-1). Second stage dilution air passed through a pre-filter, an activated carbon bed, and a HEPA filter to remove background gases and PM. The humidity of the dilution air was then adjusted between 55-85% by introducing water droplets that evaporated into the air stream. Water droplets were generated using three sonicators in series upstream of the sample injection port. The water bath for each sonicator contained milli-Q water (Millipore Corporation) with < 5 ppb total organic carbon (TOC) to minimize organic contamination (water OC << vehicle OC).

Background elemental carbon (EC) particles (also referred to as soot) were introduced into the diluted sample stream at the same time as vehicle emissions to provide additional surface area for the study of carbonyl partitioning processes (see Chapter 7). An inverted co-flow diffusion flame generator was used to produce EC through controlled methane combustion followed by removal of gaseous pollutants using a catalytic converter and removal of OA using a full sized thermal denuder [19]. Generated soot was injected into the secondary dilution system to achieve background EC concentrations ranging between 0 and 25±5 $\mu g/m^3$ in the dilution tunnel, as determined from in situ measurement with the PAS (see Chapter 2).

Carbonyl samples were captured using four denuder-filter-PUF (DFP) sampling trains operated at varying temperatures (25, 50, 75, and 100°C) after approximately 1.2 minutes of aging in the residence time chamber (RTC). Two eight-channel annular denuders (URG, Chapel Hill, NC) were placed in series for each sampling train to prevent breakthrough of gases. The annular denuders were coated with XAD-4 polystyrene resin [102] that was extracted at the end of each standard sample day. One set of filters and PUF samples were collected on each sample day. Quartz filters were baked at 500°C for +12 hrs before use to remove background OA. All sampling media were stored at -30°C in carbon-free containers when not in use. The flow rate through each DFP sampling train was 17 lpm.

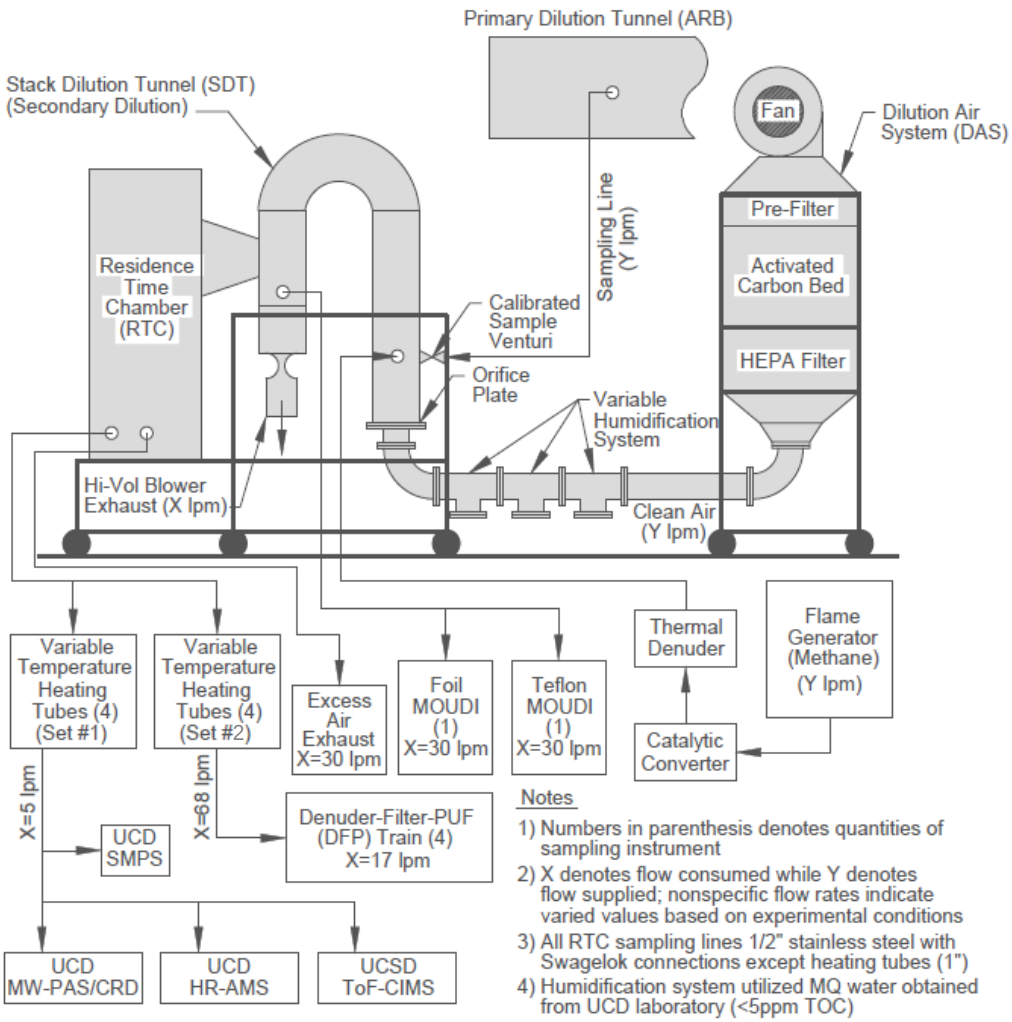

Figure 6-1: Schematic of the secondary dilution system that is able to manipulate relative humidity, background EC concentration, dilution ratios, and retention times of the dilution air stream.

6.2.4 Analytical Procedures

Samples captured on annular denuders coated with XAD-4 resin, Quartz filters, and PUFs were individually extracted in separate methanol and hexane dichloromethane (DCM) solutions while using O-(2,3,4,5,6-pentafluorobenzyl)hydroxylamine (PFBHA) as a derivatizing agent [5]. Samples were spiked with recovery standards to correct for losses during the analytical procedures involving gas chromatography mass spectrometer (GC-MS). The compound 2-F-benzaldehyde was used as a recover standard for compounds with carbon count below 7 (C < 7) and 8-F-1-benzosuberone was used as a recovery standard for compounds with C > 7. Backup recovery standards of 4-F-benzophenone and 5-F-1-Indanone were also used as a quality control measure. A detailed description of the sample preparation techniques is provided by Jakober et al. 2008 [5].

6.3 Results

6.3.1 Accuracy of Replicate Measurements

Quality control measures employed in the study compared measurements from replicated (or near-replicate) experiments to assess the daily fluctuations of vehicle fleet emissions. Emission comparisons between core and back-up test cases, as shown in Figure 5-2, were made for days with elevated RH with no background EC adjustments and days with both elevated RH and background EC adjustments. Slight differences between the test conditions can be considered marginal due to inherent deviations in the day-to-day fleet emissions rate.

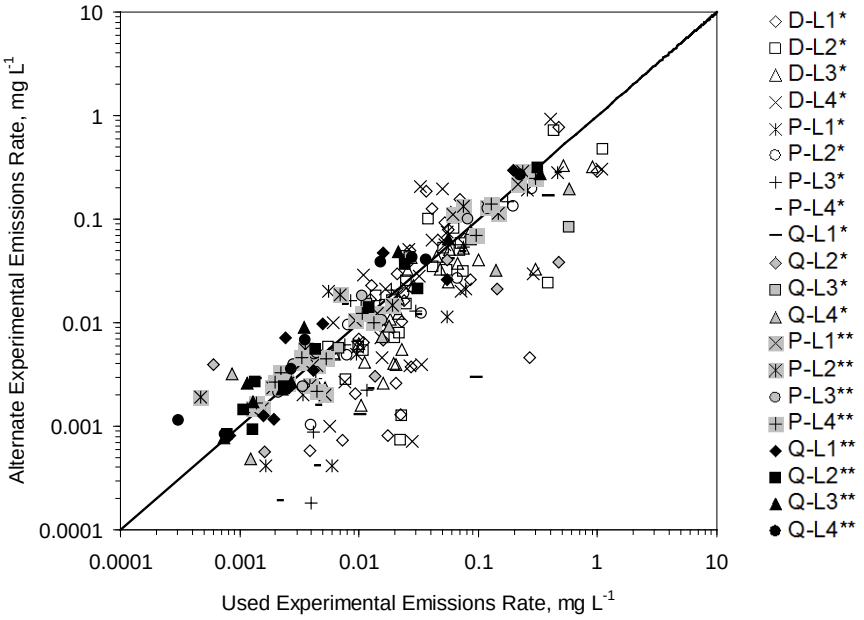

Figure 6-2: Scatter plot for quality control measures comparing concentrations measured on different days. D, P, and Q denote denuder, PUF, and Quartz filter, respectively, as collection methods. L1, L2, L3, and L4 denote different temperature legs. * indicates comparison between RH = 85% days with no EC adjustments and ** indicates comparison between alternate test day with RH = 75% and background EC = 15 $\mu g/m^3$ and core test day with RH = 85% and background EC = 20 $\mu g/m^3$.

6.3.2 Comparison Between Carbonyl Emissions Characteristics in 2002 and 2011

The vehicle fleet used in 2011 was similar to the fleet used to characterize carbonyl emissions in 2002 [5, 8] based on year, make model, engine, and emissions control

technology (Table 6-1). Figure 6-3 shows the relative amount of different classes of carbonyl species emitted in 2011 and 2002 and the total carbonyl emissions rate in those years. Total carbonyl emissions decreased by 44% in 2011 vs. 2002, presumably due to changes in the fuel composition but possibly also due to the changes induced by the different vehicle fleet and different driving cycle. Despite these shifts, the composition of the carbonyl emissions was similar between tests conducted in 2002 and 2011. Aliphatic aldehydes account for the majority of the measured carbonyl mass at roughly 75% in both studies. Contributions from other carbonyl compounds also show similarities: aliphatic ketones (0.7% past, 2.7% present), unsaturated aliphatics (0.4% past, 1.0% present), cyclic aliphatics (0.1% past, 0.6% present), and aromatic ketones (5.7% past, 5.5% present).

The most notable change between 2011 and 2002 is that the later emissions lack the 14.4% aliphatic dicarbonyl contribution observed in 2002 but instead have a higher fraction of aromatic aldehydes (2.3% past and 13.1% present). In absolute terms, emissions of aromatic aldehydes increased by a factor of ~3-4 in 2011 vs. 2002. As of January 1, 2003, California banned the use of MTBE as an oxygenate additive to gasoline fuels due to hazards involving groundwater contamination from underground storage tank leaks along with its potential as a carcinogen [113]. MTBE was replaced with EtOH as a continued effort to reduce carbon monoxide emissions during fuel combustion. EtOH molecules can decompose into methyl radicals in the combustion process that can propagate further to produce aromatics more efficiently over aliphatic dicarbonyls [114]. The increase in median refinery fuel aromatic content between 2002 and 2011 may have also contributed to the increase in aromatic aldehyde emissions.

Increasing RH from 55% to 85% in the second phase of dilution air enhanced the overall production of carbonyl compounds by 10% with more notable contributions from unsaturated aliphatics and aliphatic ketones. This finding shows that the vehicle emissions are undergoing continued chemical reaction even after dilution by a factor of 60. Elevated humidity in the real atmosphere shows evidence of enhanced SOA production through gas-particle partitioning and photochemistry [115, 116]. Photochemical reactions were not allowed in the current sampling strategy meaning that other chemical reactions must have influenced carbonyl concentrations. The major effect of increased RH may have been production of larger aqueous volumes where carbonyl production reactions can take place.

Introduction of background EC into the second phase of dilution air quenched the production of carbonyls by 34%, likely due to heterogeneous radical quenching on soot surfaces. The addition of EC into the system also increased the surface area available for gas phase adsorption of semi-volatile hydrocarbons (carbonyl precursors) which may have prevented those compounds from partitioning to the aqueous phase where they could have undergone conversion to carbonyl products, under the assumption that water uptake by the EC was negligible. The increase of dilution air RH from 55% to 85% mitigates the effects of the EC addition but still yields a carbonyl production rate that is 17% below the basecase value.

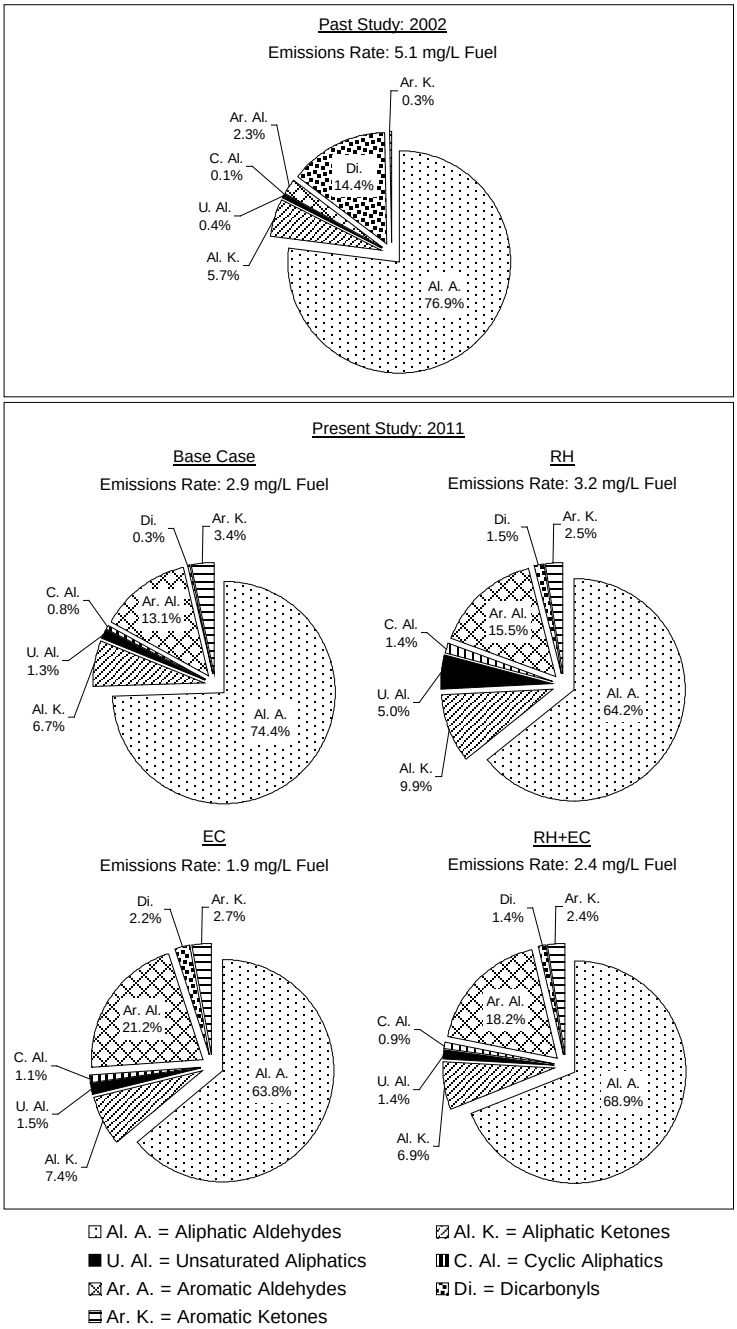

Figure 6-3: Total emissions rate of carbonyl compound classes (gas and particle phase) from 2002 and 2011 dynamometer study at ambient temperature (25°C). Each chart represents the total emissions rate under variable experimental conditions.

6.3.3 Detailed Carbonyl Speciation

Table 6-3 describes the total (gas and particle phase) carbonyl speciation for each of the four unique test conditions (Table 6-1). Aliphatic aldehydes were the most abundant carbonyl class despite the change in the gasoline fuel content which suggests that the emissions that derive from the oxygenate additive do not account for large fraction of the carbonyl emissions. Propanal and nonanal dominate the aliphatic aldehyde mass contributing to > 80% of the speciated mass. In contrast to measurements made in 2002, aliphatic dicarbonyl compounds no longer make large contributions to the total organic mass with 2,3-hexanedione missing entirely in the 2011 measurements. The removal of aliphatic dicarbonyls from the emissions are likely due to the replacement of MTBE with EtOH as the oxygenate additive as suggested in previous discussion.

Table 6-3: Total carbonyl emissions rates (gas and particle phase) from representative on-road vehicle fleet. Near detection limit emissions rates are labeled det.

Emissions Rate (μg L^{-1}) for Measured Gas and Particle Phase Carbonyls

Compounds	T = 25°C				T = 50°C				T = 75°C				T = 100°C			
	Base Case	RH	EC	RH+EC	Base Case	RH	EC	RH+EC	Base Case	RH	EC	RH+EC	Base Case	RH	EC	RH+EC
Aliphatic Aldehydes																
propanal	525	677	230	117	416	703	197	145	411	510	158	153	250	545	261	148
butanal	79	236	6.7	41	105	228	6.3	12	81	152	22.4	47	36	181	50	27
pentanal	7.8		0.8	2.1			0.2	6.6	7.7				4.8			
hexanal	31	42	4.2	29	8.6	39	10	4.5	8.8	30	11	36	11	2.5	18	17
heptanal	15	25	17	14	10	21	10	8.7	15	28	24	21	3.6	5.9	12	11
octanal	91	107	82	101	81	97	78	84	105	113	109	116	76	74	91	97
nonanal	1267	837	771	1200	1150	774	897	980	1207	880	795	937	1197	697	818	847
decanal	62	53	74	69	48	54	37	33	83	63	43	57	46	43	63	51
undecanal	15	19	18	21	13	21	17	17	25	27	22	21	14	16	14	17
dodecanal	24	39	23	26	23	37	22	24	32	38	30	28	23	39	22	26
Aliphatic Ketones																
2-butanone	47	64	41	14	17	99	19	8.2	17	61	25	8.4	16	96	30	6.7
3-pentanone	det.	11	2.3			17	1.1		det.	12	3.8		det.	19	4.2	
2-pentanone		24	7.9	1.7		34	0.4			23	0.2	0.7		35		0.1
2-hexanone	130	167	71	132	70	140	57	91	80	104	71	127	72	112	74	75
2-heptanone	4.9	20	8.1	10	0.3	14	3.7	0.4	9.3	23	10	13		7.4	2.8	1.8
2-octanone	8.0	10	11	3.5	8.8	10	5.4	3.0	6.5	10	6.7	3.3	8.4	12	11	2.2
3-nonanone		12				6.5				6.0				9.3		
2-undecanone		7.5	1.5	1.9		6.6	1.5	1.6		7.2	1.6	2.2		9.4		
Unsaturated Aliphatics																
methacrolein		58	1.3	2.5		64	2.3	3.7		44	2.3	3.3		49	1.7	2.8
crotonaldehyde		5.4				4.7				6.2						
5-hexen-2-one	3.3	48	3.1	2.5	2.3	61	3.7	4.5	4.9	39	2.6	3.5	2.5	60	4.5	3.6
2,4-hexadienal									6.8		8.0					
4-hexen-3-one						2.2										
3-Me-2-butenal	20	42	17	28	15	50	16	24	15	35	16	27	18	47	17	23
trans-2-hexenal		4.4				4.0				5.3						
trans-4-decenal	14		9.5		10		6.0		8.3		8.1		7.4		9.3	
Cyclic Aliphatics																
2-Me-2-cyclopenten-1-one		3.6		0.1		3.1				4.5	0.9	0.7				
2-cyclohexen-1-one	0.3	3.3	5.5	4.5	0.2	2.9	3.9	4.9	0.5	4.1	6.6	4.3	det.		3.3	4.1
3-Me-2-cyclopenten-1-one	0.5	7.3	1.4	1.5	det.	4.0	1.0	0.6	1.0	6.4	2.0	1.8		6.4	0.8	0.5
3,5-Me-2-cyclohexen-1-one	2.2		2.2	2.6	1.6		2.4	2.5	2.3		2.3	2.3	2.4		2.4	2.5
pinonaldehyde	20	31	13	12	20	33	12	11	35	33	16	12	20	39	12	11
Aromatic Aldehydes																
benzaldehyde	97	94	131	136	61	93	77	109	125	127	150	128	31	66	60	107
o-tolualdehyde	60	60	60	52	68	63	46	55	51	70	69	61	34	59	49	65
m-tolualdehyde	80	112	92	94	74	110	79	97	109	126	106	117	65	101	87	100
p-tolualdehyde	53	82	46	56	47	82	43	51	63	98	55	62	48	83	49	57
4-Et-benzaldehyde	31	80	26	31	29	81	26	28	41	88	29	33	32	81	28	29
2-Et-benzaldehyde	31	38	29	36	31	38	27	33	40	42	33	36	30	47	30	33
5-NO2-2-furaldehyde	21	27	24	22	20	24	16	25	24	26	24	16	20	28	19	22
mesitaldehyde		16				16				16				23		
1-naphthaldehyde	5.8	9.2	4.4	4.4	5.8	9.3	4.0	4.5	6.9	9.1	5.1	3.9	5.9	14	4.0	4.1
2-naphthaldehyde	7.0	15	5.3	4.9	7.1	15	4.5	5.3	8.4	15	5.9	4.6	7.0	22	4.8	4.9
Aliphatic Dicarbonyls																
2,3-hexanedione			28	18			19	24			25	12			19	29
glyoxal		16				12			0.6	15	0.3			17	0.1	
methylglyoxal	9.9	30	14	14	18	28	26	19	26	17	18	15	21	20	19	13
Aromatic Ketones																
benzophenone	6.5	6.8	2.4	4.4	2.7	7.0	2.0	2.3	3.0	6.8	2.5	2.4	2.7	11	2.1	2.3
acetophenone	24	31	20	24	21	29	17	21	26	31	21	27	19	24	20	23
9-fluorenone	34		2.7	2.0	18		2.1	1.8	16		3.5	5.3	13		1.9	6.4
1-indanone	19	18	18	16	23	25	18	13	19	25	15	13	16	25	16	11

6.3.4 Variation of Carbonyl Emissions Rate with Temperature, RH, and Background EC

Elevated Temperature - Figure 6-4 compares the carbonyl emissions rates in different classes at 25°C, 50°C, 75°C, and 100°C under all four test conditions (Table 6-1). The total (gas+particle) emissions rates respond weakly to the temperature perturbation, with far greater effects related to humidity and EC concentrations. Atmospherically relevant temperature perturbations (25°C vs. 50°C) generally produced slightly reduced emissions of carbonyl compounds in the majority of the classes. Increased temperature may have enhanced chemical reaction rates leading to increased production of certain individual carbonyl compounds. Emissions rates of butanal and methylglyoxal increased as temperature rose from 25°C to 50°C.

Elevated Relative Humidity – Figure 6-4 describes the changes in the overall production rates of the carbonyl compounds under various RH conditions. In general, injecting water vapor into the air stream caused increased production of aliphatic ketones, unsaturated aliphatics, cyclic aliphatics, and aliphatic dicarbonyls in comparison to the base case under all temperature ranges. As shown in Table 3, lighter, more water soluble aliphatic aldehyde compounds such as propanal and butanal increased in production while larger, less water soluble compounds like nonanal reduced at all temperature ranges in comparison to the base condition test. However, the sum of the mass contribution from aliphatic aldehydes remained relatively unchanged at all temperature legs (see previous discussion).

Certain carbonyl compounds were only emitted at rates above the study detection limits at increased RH conditions, including 3-pentanone, 2-pentanone, 3-nonanone, 2-undercanone, methacrolein, crotonaldehyde, trans-2-hexanal, 2-Me-2-cyclopentenone, mesitaldehyde, and glyoxal. In a complimentary fashion, certain carbonyl compounds were not emitted above study detection limits at increased RH conditions, including pentanal, trans-4-decanal, 3,5-Me-2-cyclohexenone, and 9-fluorenone.

Background EC – Introduction of background EC inhibited the production of certain specific carbonyl compounds including propanal, pentanal, hexanal, nonanal, 2-hexanone, pinonaldehyde, p-tolualdehyde, and 9-fluorenone. In a complimentary fashion, addition of EC into the background air led to emissions of 2,3-hexanedione at concentrations above the study detection limits (this compound was not detected in the base condition). The appearance of new species at low concentrations may be related to the adsorption of vapors onto the walls of the RTC followed by continued release after the elevated RH test. Species such as 3-pentanone, 2-pentanone, 2-undercanone, methacrolein, and 2-Me-2-cyclopentenone may also be influenced by this effect.

Competition between elevated RH and EC – Introducing both elevated RH and background EC further suppressed production of species such as propanal and 2-butanone below what was observed during the background EC injection test. In theory, elevated RH increases production of certain carbonyl species (refer to section above). However, as shown in Figure 6-4, the adjusted RH+EC test still produced carbonyl emissions below the basecase level due to the dominant effect of the EC. 3-nonanone, crotonaldehyde, trans-2-hexenal, mesitaldehyde, and glyoxal are present only during elevated RH but not during elevated RH+EC test. This pattern suggests that adsorption effects counter the effects of increased water volume, likely due to the scavenging of carbonyl precursors.

2,3-hexedione appears whenever EC is injected and trans-4-decenal is removed whenever water is introduced to the secondary dilution air. However, these compounds are suppressed when both background EC and RH are increased. The cause for this synergistic effect is unknown.

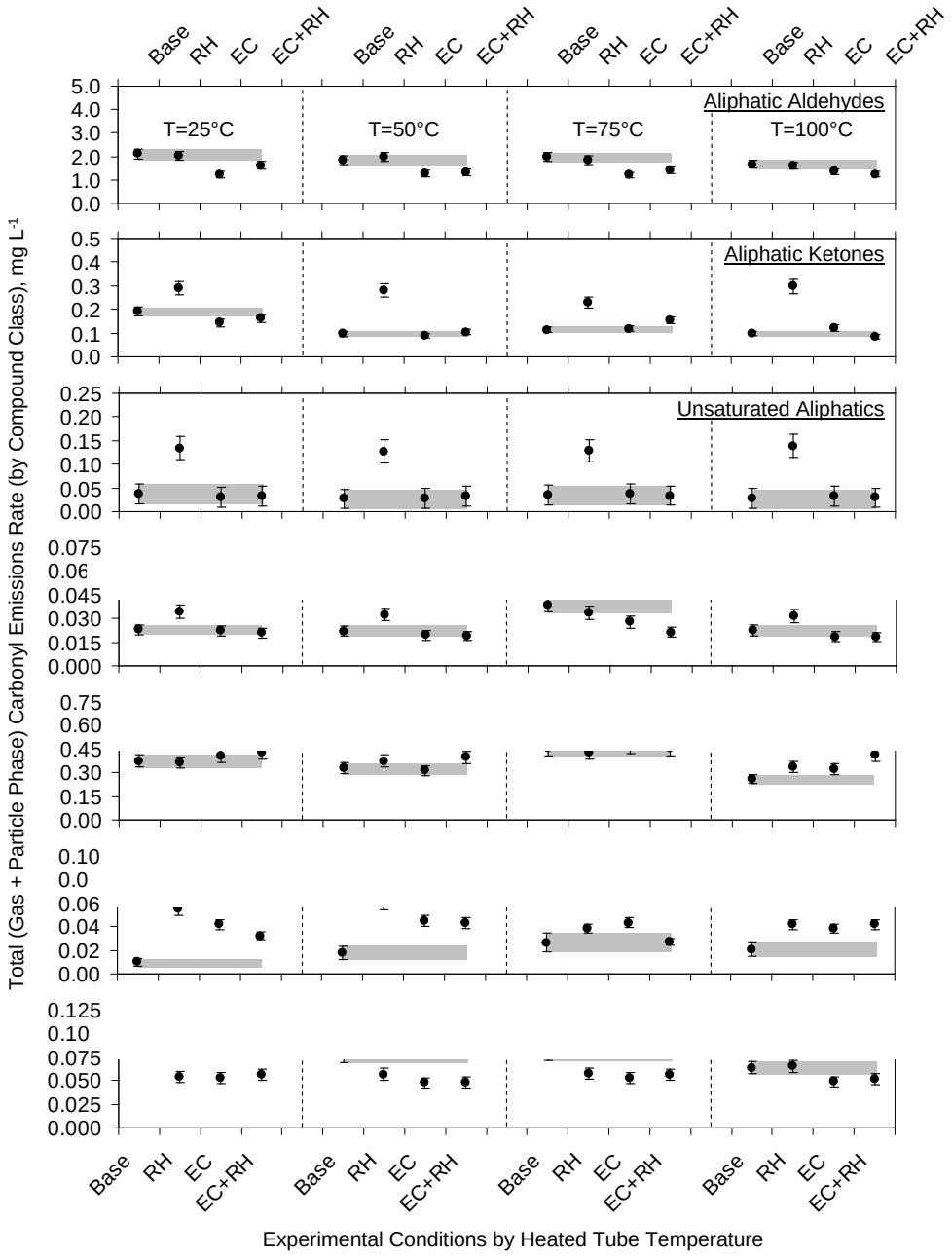

Figure 6-4: Total production trends for carbonyl compound classes under variable, atmospherically relevant conditions shown for sample legs heated to T = 25, 50, 75, and 100°C. Refer to Table 1 for experimental condition descriptors.

6.4 Discussion

The increased water volume at higher RH affected the chemistry carbonyl emissions both in terms of total production rates and speciation. Changes to the yields of carbonyl species suggest aqueous reaction pathways. Since Milli-Q was used for the humidification process, the aqueous phase chemistry should have had minimal interference from the presence of electrolytes that may otherwise reduce production efficiency. A laboratory study that measured SOA yields from α-piene/ozone reactions determined that environments containing only OA and water produced higher yields at 50% RH in comparison to dry conditions when the seed aerosol was not inorganic [117]. Given the relatively fresh nature of the emissions in the current study (~60 sec aging) and the lack of an introduced oxidant, it is unclear if the carbonyl reaction products apparent in the emissions should be described as primary or secondary in nature. The previous study only observed the behavior of the SOA precursors (carbonyls) under a relatively clean environment at RH of ~45-55%. Water content in the atmosphere is extremely variable depending on location, season, ventilation, and time of the day. It is important to update the SOA formation mechanisms in models to account for the changes SOA yields due to changes in humidity.

EC provides large surface area that can act as adsorption / condensation sites. Adsorption behavior of a surface can be described by the simple Langmuir isotherm which assumes that the volume of gas adsorbed is a function of gas partial pressure. Abundant compounds such as propanal and nonanal had lower contribution to the mass during this experiment likely because of the adsorption / condensation of precursor compounds onto the inert EC surface that reduced the production rates. However, competitive adsorption of the organic compounds are difficult to assess and their behaviors are not still fully understood [118]. A recent study also suggested that the condensational uptake of semi-volatile organic compounds (SVOCs) is a function preexisting sulfate and nitrate seed particles in the vehicle exhaust (Liggio et al. 2011).

6.5 Conclusions

Organic carbon emissions from light duty gasoline vehicles diluted by a factor of ~60 and aged in the dark for 1.2 min continue to undergo chemical reactions that are influenced by changes to temperature, humidity, and the presence of background concentrations of black carbon in the dilution air. Concentrations of total (=gas+particle phase) carbonyls decreased in 2011 vs. 2002 for comparable vehicle fleets, most likely due to changes in summer blend gasoline composition in California. Total carbonyl emissions generally increased as relative humidity increased, suggesting production via an aqueous phase mechanism. Concentrations of total carbonyl emissions generally decreased as black carbon was added to the dilution air most likely because the black carbon scavenged the precursor species for carbonyl production. Temperature had a weak impact on total carbonyl production rates under the current experimental design.

7 EFFECT OF DILUTION AIR TEMPERATURE, HUMIDITY, AND BLACK CARBON CONCENTRATIONS ON THE GAS-PARTICLE PARTITIONING OF CARBONYL EMISSIONS FROM GASOLINE FUELED MOTOR VEHICLES

7.1 Introduction

Airborne particulate matter significantly impacts human health across the world. Particulate matter (PM) emissions at urban centers in the US are dominated by anthropogenic sources with major contributions from light duty gasoline-powered motor vehicles. Carbonaceous compounds broadly classified as elemental carbon and organic compounds make up the majority of the primary PM emissions from gasoline vehicles [119]. Once emitted to the atmosphere, organic compounds continue to react leading to higher oxygen content and repartitioning between the gas and particle phase. Several parameterizations of this process have been proposed but a complete explicit understanding of these chemical reactions is still lacking. Furthermore, the parameterized chemical models have trouble predicting observed concentrations of organic aerosols in the atmosphere, with the majority of models under-predicting concentrations [3]. New studies into the reaction pathways for carbonaceous emissions from motor vehicles (and other major combustion sources) are needed to better understand PM formation from these sources.

Many experiments have been performed to characterize organic aerosol formation pathways from individual volatile organic compounds (VOCs) or VOC mixtures but observations of the OA chemical evolution of real-world gasoline vehicle emissions under controlled conditions have not been studied to the same extent because of the associated experimental difficulties. Real-world emissions in ambient air are mixed with fluctuating concentrations of background aerosols with chemical reaction rates influenced by meteorological patterns that cannot be reproduced on demand. Dilution of direct emissions from gasoline vehicles to atmospherically relevant concentrations at atmospherically representative conditions under controlled conditions may act as a more practical method to understand the chemical evolution of OC and OC precursors that will provided insights into atmospheric behavior.

In the present study, a representative fleet of on-road light duty gasoline-powered vehicles was operated on a dynamometer under the California Unified Cycle (UC) driving cycle to measure emissions of carbonyl species in the gas and particle phase. The tailpipe exhaust was diluted by a factor of 61 and aged for approximately 1 minute to reduce concentrations to atmospherically relevant concentrations. The dilution air was manipulated to adjust relative humidity (RH) between 55 to 85% and black carbon particles produced by a soot generator were introduced into the dilution air at concentrations between 0 and 25±5 $\mu g\ m^{-3}$. The temperature of the resulting emissions mixtures were perturbed between 25-100^{o}C. Samples were collected on an annular denuder-filter-polyurethane foam (PUF) sampling train (DFP) and followed by derivatization and analysis by GC/MS. The concentrations of gas-phase and particle-phase carbonyl species under various experimental conditions are studied to better understand the partitioning mechanisms for these compounds.

7.2 Experimental Methods

7.2.1 Methods and Material

Chapter 6 provides a comprehensive description of the experimental methods and so only a brief summary is provided in the current Chapter. A set of 8 representative on-road light duty gasoline vehicles (see Table 6-2) with LEV emissions control technology were tested at the California Air Resources Board (CARB) Haagen-Smit Laboratory in El Monte, California, using summer-blend gasoline. Vehicles ranged in model year between 1997-2003 with an average odometer reading of 90,257 miles. Vehicles were operated on a dynamometer under the California Unified Cycle (UC) which is more aggressive (harder acceleration, higher top speed) than the Federal Test Procedure (FTP) driving cycle used in a previous carbonyl emissions characterization study [5].

The first stage of emissions dilution by a factor of ~12.7 was provided by a Constant Volume Sampler (CVS) operated by CARB. A second stage of dilution by a factor of ~4.8 was provided by the Secondary Dilution System (SDS) (see Figure 6-1). The humidity of the secondary dilution air was manipulated between 55-85% and the concentration of background EC in the secondary dilution air was adjusted between 0-25±5 μg m^{-3} (see Chapter 6) to observe how these changes affected the partitioning of carbonyl species (see Table 6-1 for the matrix of test conditions).

Air samples were collected on annular denuder (D) –filter (F) -polyurethane foam (PUF) sampling train (DFP) after a residence time of ~1.2 min at the full dilution factor of ~60 to allow aging of the primary emissions. The annular denuders were coated using ground XAD-4 polystyrene resin (Sigma-Aldrich, St.Louis, MO) to increase adsorption surface necessary to collect organic gases from the sample stream. XAD-4 was ground using the SPEX Sampleprep 8000 Mixer/Mill prior to application with target discharge granularity in the micron range. Quartz filter (QAO47; Pall Corp., Port Washington, NY, USA) and PUF (URG) filter media downstream of the annular denuders collected low-volatile and semi-volatile carbonyl compounds. The denuder, filter, and PUF samples were extracted using methanol and a hexane:dichloromethane (DCM) solution with 1:1 ratio. The samples were derivatized using O-(2,3,4,5,6-pentafluorobenzyl) hydroxylamine (PFBHA) to stabilize the carbonyl functional groups during the extraction and analysis. Details of the individual extraction methods are described by Jakober et al (2006).

7.2.2 Recovery of Internal Standards

Internal standards were used to evaluate the recovery of the carbonyl compounds during the extraction process. Figure 7-1 shows the % recovery of the internal standards across 64 samples from all measurement in the current study. Median extraction efficiency was approximately 80%.

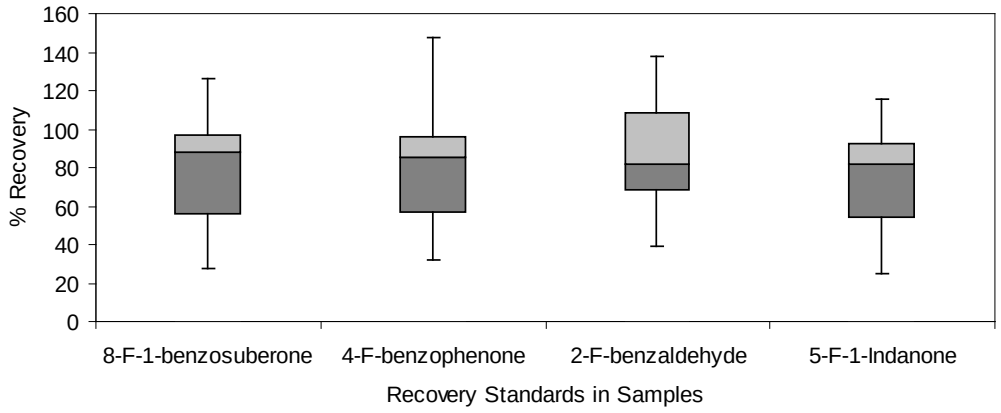

Figure 7-1: Carbonyl recovery performance based on internal standards. Correction using 2-F-benzaldehyde was applied to carbonyls C6 and below with 5-F-1-indanone as backup and correction using 8-F-1-benzosuberone was applied to carbonyls >C6 with 4-F-benzophenone as backup.

7.2.3 Denuder Capacity Analysis

Gas phase carbonyls in the current study were defined to be those measured from the two blank subtracted annular denuders used in series in the DFP sampling trains. The first and second denuders were extracted separately to determine if a significant amount of gas-phase carbonyl breakthrough mass was detected on the second denuder. Figure 7-2 compares the amount of each carbonyl captured on denuder 2/denuder 1. The denuders had different surface areas, and so the maximum theoretical ratio for a compound that breaks through completely would be 0.35 based on standard equilibrium partitioning via absorption theory or Henry's Law. The compounds illustrated in Figure 7-2 do not asymptotically approach the value of 0.35 as molecular weight is decreased (simple volatility is increased). Furthermore, the detection of some compounds on the downstream denuder but not others is not consistent with the saturation of surface sorption sites that would affect all compounds in a similar fashion. As discussed below, some other partitioning mechanism involving a reversible sequence of condensed phase reactions must occur in the sample stream between denuder 1 and 2 in order to explain the observed trends. Collection of the compounds on the first denuder perturbs the system and draws more of the material back through the reversible chemical reactions towards the gas-phase. In this fashion, the denuders coated with XAD behave similarly to the PFBHA derivatization agent that pulls the compounds towards their elementary building blocks. Given the complexity of this system, the definition of the gas-phase concentrations as those measured on the denuders will be used in the remaining analysis presented below.

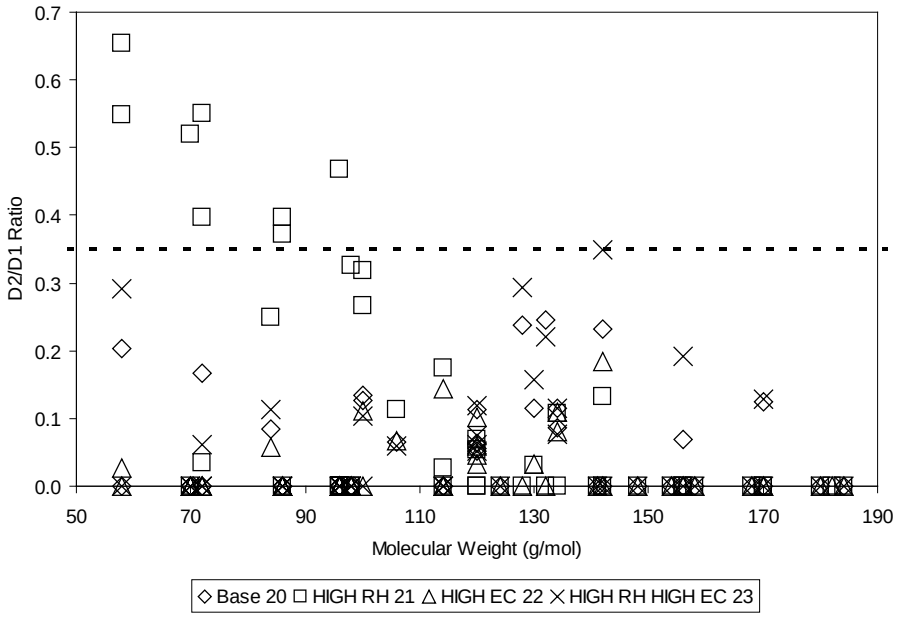

Figure 7-2: Denuder capacity ratios, D_2/D_1, for all measured carbonyl species.

7.3 Results

7.3.1 Comparison to Previous Measurements

A total of 37 carbonyls were detected in the present study during the base case test at 25°C (no manipulation of background RH or EC). The gas and particle-phase emissions rates of these compounds were compared to previous tests of light duty gasoline vehicle exhaust conducted in 2002 by Jakober et al. in 2002. The test fleet composition in the current study and in the Jakober et al. study was similar (see Table 6-2). The inherent differences between the two studies are the driving cycles (UC vs. FTP), odometer readings (~90K miles vs. 45K miles), condition of the vehicle (one vehicle with mild malfunction in the current study), and advancement in the gasoline fuel technologies (summer blend 2011 gasoline vs. summer blend 2002 gasoline).

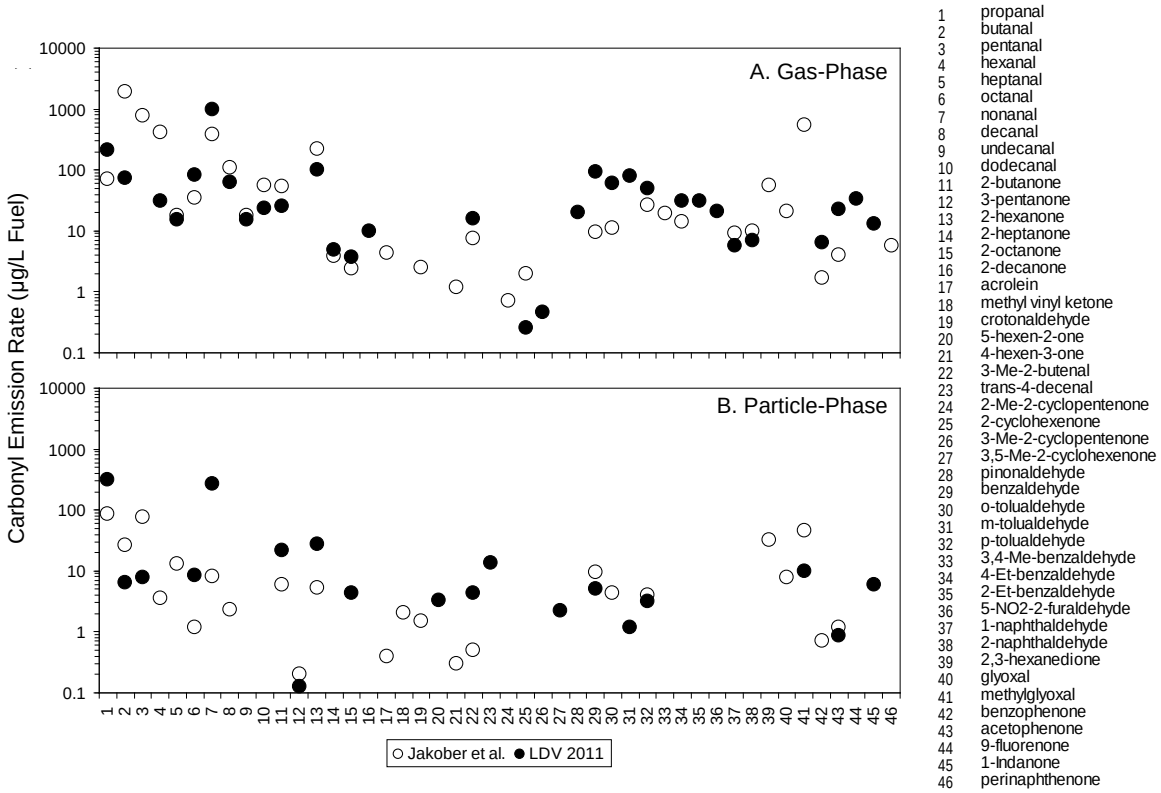

Figure 7-3: Carbonyl emission rates from representative on-road vehicle fleet tested in 2002 and in 2011 separated by gas and particle phase.

Total (gas + particle phase) carbonyl emission rates measured in the current study are typically lower than the values measured in 2002 [119-122] (see Chapter 6). Figure 7-2 generally shows that the particle-phase carbonyl emission rates generally increased over the entire spectrum of measured compounds with offsetting decreases in gas-phase emissions. Gas phase aliphatic aldehyde emissions decreased between 2002 and 2011 while gas-phase aromatic aldehydes increased. The ratio of the summed gas phase aliphatic aldehyde and aromatic aldehyde emission rates between the two studies (2011:2002) are 0.4 and 3.8, respectively. The decrease in one category and increase in another category may be related to changes in fuel composition. Regulation adopted by the state of California in 1991 require the gasoline refiners to control the Reid Vapor Pressure (RVP) based on the atmospheric temperature variations between seasons to reduce evaporative emissions from gasoline fuel [112]. RVP is monitored by the test method ASTM-D-323 and is essentially the measure of the volatility of the fuel source[112]. RVP is also controlled to ease the vaporization of gasoline during engine combustion to maintain optimum combustion conditions in the engine. Higher levels of RVP are optimal during the winter while lower levels of RVP are desired during summer. The variability in the gasoline formulations and the apparent emissions differences between the 2002 and 2011 tailpipe emissions are shown in Figure 3.

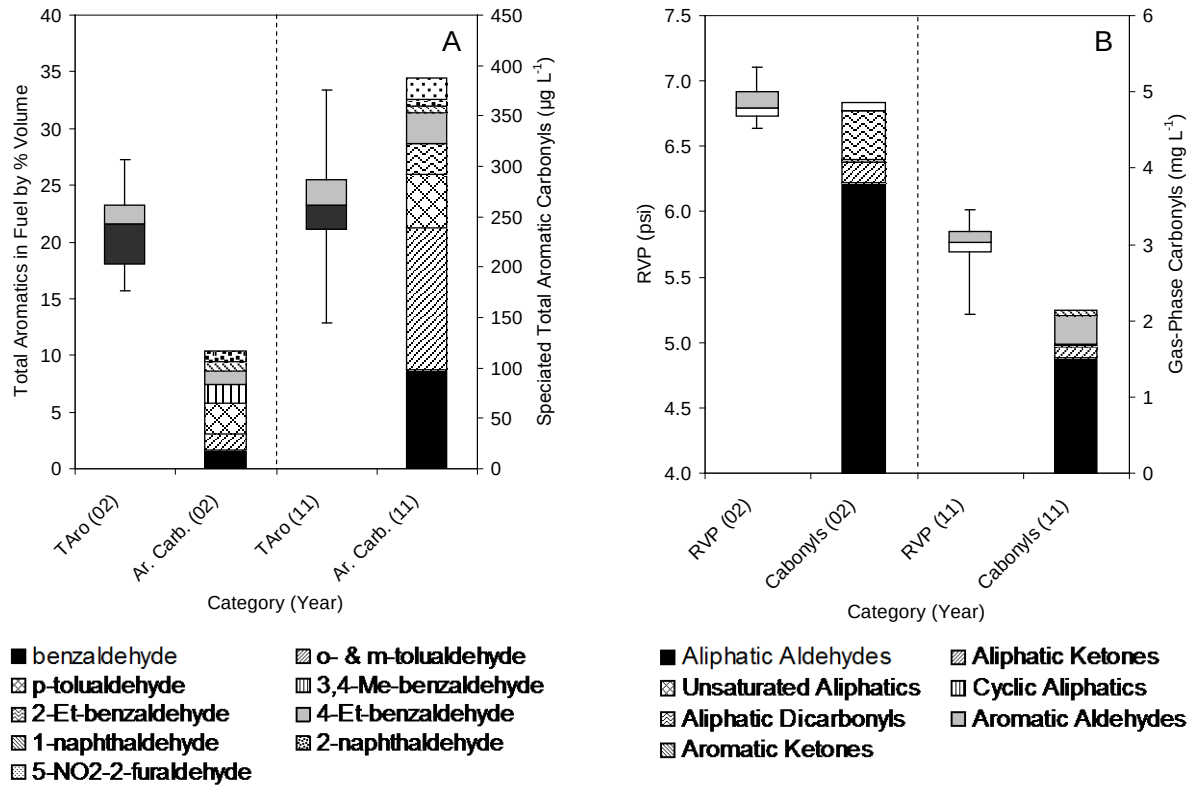

Figure 7-4: Comparison of composition and RVP of gasoline blends between 2002 and 2011 fuels used in source testing campaigns.

As shown in Figure 7-4, the relative aromatic content in the gasoline blends increased between 2002 and 2011. The simplest method to decrease the RVP of gasoline fuels is to remove volatile components of the fuel and replace them with less volatile (higher molecular weight) components. As apparent from the panel 7-4B, the gas phase emission rates of the aliphatic aldehydes and aliphatic dicarbonyls decreased significantly while aromatic aldehyde emission rates increased. The 99.9% reduction in gas phase aliphatic dicarbonyls is likely due to the removal of methyl tert-burtyl ether (MTBE) from the fuel and the introduction of ethanol (EtOH). California Reformulated Gasoline Regulation (CaRFG) prohibited MTBE as a gasoline fuel oxygenate in 2003 due to the contamination of water supplies by leaking storage tanks. EtOH was selected as a more environmentally friendly oxygenate alternative.

7.3.2 Influence of Humidity and Background EC on Carbonyl Partitioning

As shown in Figure 7-2, particle phase carbonyl emissions rates from gasoline powered LEVs have generally increased by a factor of ~2.6 between 2002 and 2011. Particulate carbonyls accounted for approximately 20% of the POA emitted from gasoline powered LEVs in 2002 [5]. The current measurements indicate that particulate carbonyls account for approximately 28% of the total POA emissions under basecase conditions. Figure 7-4 summarizes the carbonyl contributions to the total POA measured on the Quartz filter under various experimental conditions where the second stage of dilution air was manipulated. Measurements in 2002

showed that approximately 54% of the particulate carbonyls were aliphatic aldehydes whereas the current study shows that 85% of the measured particulate carbonyls are aliphatic aldehydes. It is plausible that the reduction in the gas phase aliphatics (Figure 7-3) was due to the additional partitioning of these compounds to the particle phase. The partitioning mechanism generally does not follow absorption theory [9]. Aliphatic carbonyls with high pure-compound vapor pressures such as propanal and butanal appeared in the low/semi-volatile particle phase as shown in Table 7-1. The effects of manipulating the RH and background EC concentration of the second stage of dilution air will provide additional insights into the partitioning mechanisms.

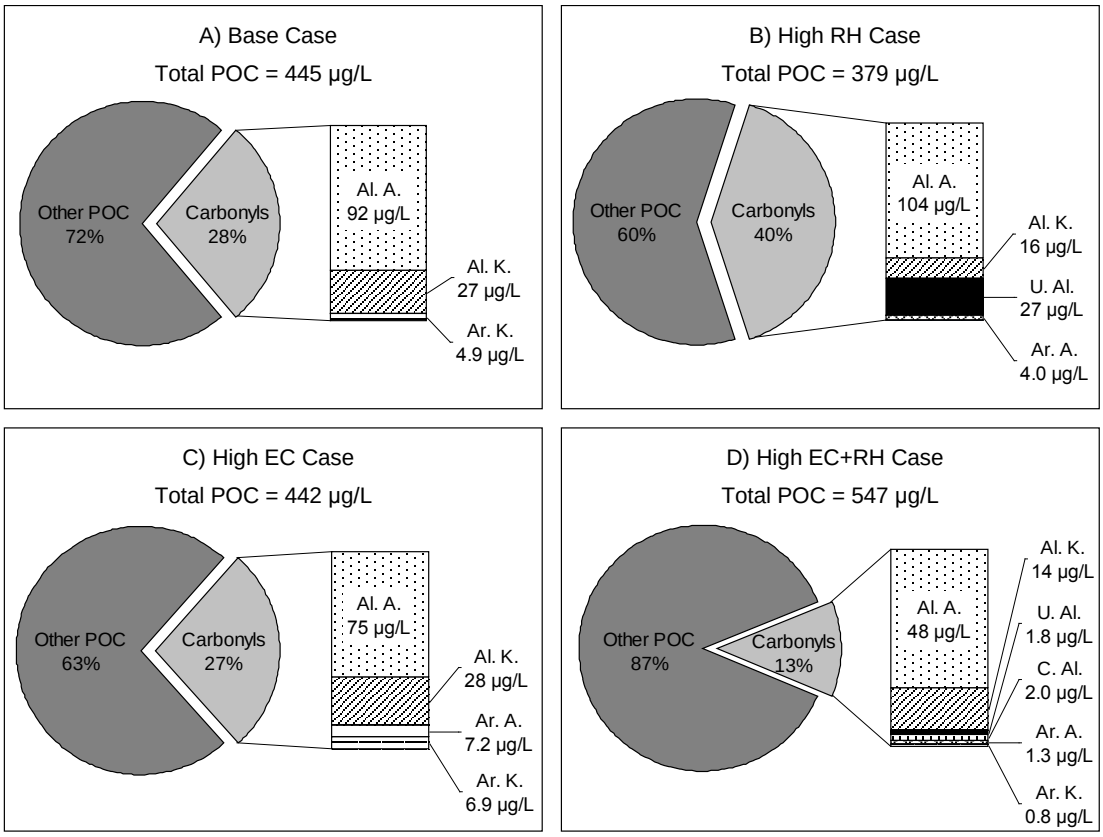

Figure 7-5: Speciated contribution of particulate carbonyl emission rates to total POC measured from gasoline based PC/LDV at atmospherically relevant dilution (Quartz filter measurements). All of the emission rates listed here are in mass carbon (µg C) per liter of fuel consumed. POC emissions used in this figure are organic contamination corrected POC during externally generated black carbon injection days.

Total POC decreased when humidity in the secondary dilution air was increased to 85% but the carbonyl emissions rate increased by approximately 22% resulting in 40% of the POA mass composed of identified carbonyls under this condition. The enhancement of the condensed phase carbonyl concentrations as humidity increases suggests a condensed aqueous reaction pathway. The majority of the increased carbonyl production in the case with higher RH can be attributed to the production of unsaturated aliphatics that accounted for 27 µg C/L fuel. Again, classic portioning of carbonyls to the aqueous phase using a Henry's Law approach cannot explain the

condensed phase concentrations of these aliphatic compounds [9]. It is likely that some additional complexation of aliphatic carbonyls takes place in the aqueous phase. The PFBHA derivatization pulls some of the carbonyls back through a reversible reaction sequence when samples are extracted prior to analysis. The measured carbonyl concentration therefore represent the concentrations of the building blocks within each of the compound classes that have not yet undergone an irreversible reaction leading to some other form of condensed phase POA. The measured concentrations do not represent the actual chemical form of this material in the exhaust particles.

The POC contribution during the high EC case is characterized by reduction in aliphatic aldehyde contribution (17 μg C/L fuel or ~20% reduction from base case) and production of aromatic aldehydes (7.2 μg C/L fuel) that is not observed in the base case. The 20% reduction of aliphatic aldehydes is largely due to the reductions of both propanal and butanal contributions in the particulate phase. It is plausible that the elevated black carbon concentrations in the air stream scavenged the precursors to propanal and butanal before they could partition to the aqueous phase. The presence of the EC may have also provided a reaction surface for the production of aromatic aldehydes. It has been observed that adsorption onto EC dominates the partitioning of organic vapors when EC/OC ratio is > 0.5 [123]. The EC/OC ratio in the SDS during this study was > 3 for non-EC injection tests (base case and high RH case) and > 6 for EC injection tests (high EC case and high EC+RH case).

Manipulation of both the RH and the background EC introduces additional chemical transformations in the reaction pathways as evident from the increased contributions from carbonyl compounds not present in the base case conditions. Large reduction (48%) of particulate aliphatic aldehydes were observed for this test condition while carbonyls such as unsaturated aliphatics, cyclic aliphatics, and aromatic aldehydes were detected in the emissions. Elevated RH seem to be encourage unsaturated aliphatic carbonoyl production while elevated EC seems to enhance the production of aromatic aldehydes in the particle phase. The combination of both increased EC and RH inhibits the individual enhancement effects but also produces cyclic aliphatics not observed previous cases. It is plausible that reduction of aliphatic aldehydes corresponds to production of other carbonyl species.

Table 7-1: Speciated gas-phase and particle-phase carbonyl emissions rate from a fleet of gasoline PC/LDV at variable atmospheric conditions. Samples were collected at ambient temperature of 25 degrees Celsius.

Emission Rate (µg L^{-1}) for Measured Gas and Particle Phase Carbonyls

Compounds	Base Case		RH Case		EC Case		EC+RH Case	
	Gas	Particle	Gas	Particle	Gas	Particle	Gas	Particle
Aliphatic Aldehydes								
propanal	212	315	262	413	27	203	53	64
butanal	73	6.4	99	137	6.7		26	15
pentanal		7.8				0.8		2.1
hexanal	31		28	13	2.9	1.3	27	2.3
heptanal	15		25		17		14	
octanal	83	8.3	102	5.0	73	9.4	95	5.0
nonanal	999	273	685	148	542	229	1028	171
decanal	62		53		74		69	
undecanal	15		19		14	3.2	20	
dodecanal	24		39		23		26	
Aliphatic Ketones								
2-butanone	26	22	41	24	14	27	10	4.2
3-pentanone		0.1	9.0	2.0	2.3			
2-pentanone			17	6.7	7.9		1.7	
2-hexanone	102	28	87	79	50	21	107	25
2-heptanone	5.0		18	1.9	8.1		10	
2-octanone	3.8	4.3	9.8		3.5	7.9	3.5	
3-nonanone			6.2	5.8				
2-undecanone			7.5		1.5		1.9	
Unsaturated Aliphatics								
methacrolein			28	29	1.3		2.5	
crotonaldehyde			5.4					
5-hexen-2-one		3.3	21	28		3.1		2.5
2,4-hexadienal								
4-hexen-3-one								
3-Me-2-butenal	16	4.3	23	18	9.9	4.8	22	4.3
trans-2-hexenal			4.4					
trans-4-decenal		14				9.5		
Cyclic Aliphatics								
2-Me-2-cyclopenten-1-one			3.6				0.1	
2-cyclohexen-1-one	0.3		3.3		5.5		4.5	
3-Me-2-cyclopenten-1-one	0.5		7.3		1.4		1.5	
3,5-Me-2-cyclohexen-1-one		2.2				2.2		2.6
pinonaldehyde	20		31		13		12	
Aromatic Aldehydes								
benzaldehyde	93	5.2	82	12	127	4.1	129	6.6
o-tolualdehyde	60		60		51	9.1	52	
m-tolualdehyde	79	1.2	111		91	1.0	92	1.9
p-tolualdehyde	50	3.1	81		43	2.7	54	1.8
4-Et-benzaldehyde	31		80		26		31	
2-Et-benzaldehyde	31		37		29		36	
5-NO2-2-furaldehyde	21		26		24		22	
mesitaldehyde			16					
1-naphthaldehyde	5.8		9.2		4.4		4.4	
2-naphthaldehyde	7.0		15		5.3		4.9	
Aliphatic Dicarbonyls								
2,3-hexanedione					28		18	
glyoxal			9.1	7.2				
methylglyoxal	0.1	9.9	4.2	25	3.1	11	0.4	14
Aromatic Ketones								
benzophenone	6.5		6.8		2.4		4.4	
acetophenone	23	0.9	31		19	0.7	22	2.1
9-fluorenone	34				2.7		1.9	0.1
1-indanone	13	6.0	18		9.5	8.5	14	2.0

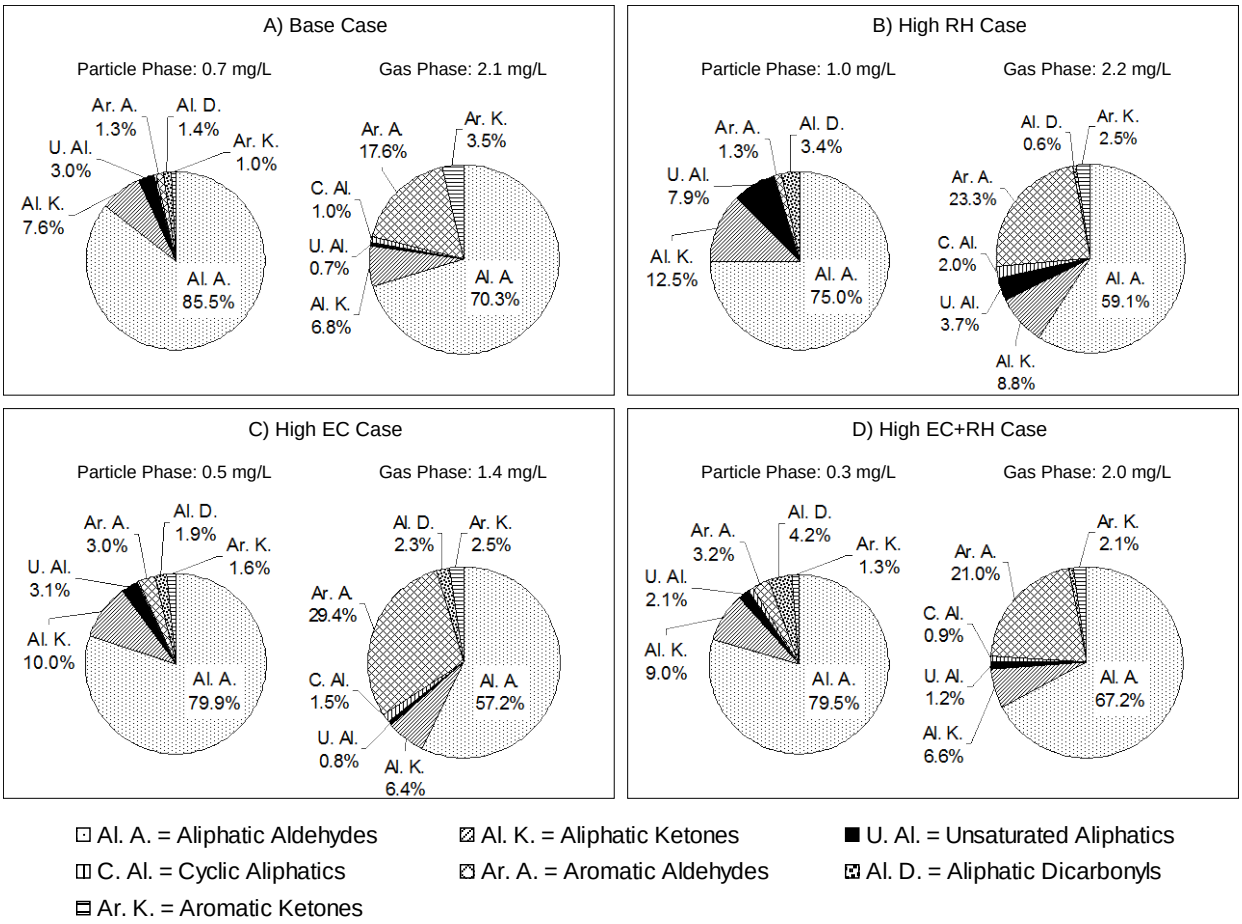

Figure 7-6: Gas-particle partitioning and speciation of PC/LDV gasoline carbonyl emissions at variable atmospheric conditions: (a) base case – 55% RH and 0 additional EC, (b) high RH case – 85% RH and 0 additional EC, (c) high EC case – 55% RH and additional 25±5 μg m^{-3} EC, and (d) high EC+RH case – 85% RH and additional 25±5 μg m^{-3} EC.

7.4 Conclusions

Total (=gas+particle phase) emissions rates of carbonyl species from light duty gasoline vehicles decreased in 2011 vs. 2002 for comparable vehicle fleets. The most likely explanation for this trend is changes to the speciation of gasoline over this time period. Gas phase carbonyl emission rates are reduced by 57% (from 4.8 mg/L to 2.1 mg/L) and the particle phase carbonyl emission rate are increased by 133% (from 0.3 mg/L to 0.7 mg/L). Much of the trend for increasing particle-phase emissions is associated with additional transfer of gas-phase aliphatic species to the condensed phase. Particle-phase carbonyl species accounted for 28% of total OC in the current study under basecase conditions, compared to 18% of OC in 2002. Increasing RH from 55% to 85% increased particle-phase carbonyl concentrations by 43% and gas-phase carbonyl concentrations by 5%, consistent with the hypothesis of an aqueous phase production mechanism for carbonyl species. Increasing concentrations of black carbon concentration in the dilution air decreased particle-phase concentrations by 39% and gas-phase concentrations by 33%, consistent with the hypothesis that the black carbon scavenges the carbonyl precursors, preventing them from entering the aqueous phase. Temperature perturbations up to 100^{o}C had little effect on the partitioning of carbonyl species, consistent with the hypothesis that these compounds do not partition to the condensed phase via classic absorption into an OC absorbing matrix.

8 ON THE PRIMARY EMISSION OF ORGANIC ACIDS FROM LIGHT DUTY GASOLINE VEHICLES AND OCEAN-GOING VESSELS

8.1 Introduction

Field measurements have demonstrated that organic acids are ubiquitous in the troposphere and are present in both the gas and aerosol phase [124-127]. Gas-phase organic acids can contribute to particle acidity and have been shown to be a major component of secondary organic aerosol (SOA) mass loadings [128], thus impacting particle hygroscopicity. As a result, there is renewed interest in determining the relative importance of primary and secondary sources of organic acids and the importance of anthropogenic and biogenic processes. Laboratory measurements, confirmed by field observations indicate that short chain carboxylic acids are directly emitted to the atmosphere from terrestrial vegetation [129] and as a by-product of both biomass burning [130] and fossil-fuel combustion [131, 132]. In addition, carboxylic acids have been shown to be produced in the atmosphere from ozone-alkene reactions, $RC(O)O_2$ reactions with HO_2, and heterogeneous and multiphase reactions involving SOA [133].

At present, fuel-based organic acid emission factors from mobile vehicles and commercial shipping vessels are not available to properly constrain organic acid emission inventories. The early measurements of Kawamura et al. [131, 132], describe primary emissions of organic acids from fossil fuel combustion, but do not provide quantitative values for input into chemical transport models. Current constraints on formic (FA) and acetic acid (AA) emissions from mobile vehicles are derived from measurements of the emission ratios of FA and AA relative to carbon monoxide (CO) in the Hampton Roads Bridge Tunnel studies of Talbot et al. [134], where formic acid emission was measured to be 2.1×10^{-4} FA per CO and acetic acid emission ratios were measured at 4.2×10^{-4} AA per CO. However, it is important to note that these measurements were made prior to 1988 and it is more than likely that emission from the current fleet of automobiles is significantly different. In comparison, there currently are no constraints on the emission rates of organic acids from ocean-going vessels.

In what follows we report the first measurements of real-time, fuel-based, organic acid emission factors from light duty gasoline vehicles (LDGV). In this study, a representative fleet of LDGVs were driven under the California Unified (UC) cycle at the California Air Resources Board's Haagen-Smit Laboratory, where C1-C10 carboxylic acids (excluding acetic acid), carbon monoxide (CO) and carbon dioxide (CO_2) were detected in real-time in the diluted exhaust. The study was conducted on eight LDGVs (Table 1 of supporting information (SI)) sequestered by the California Air Resources Board from the current on-road vehicle fleet. Organic acid mixing ratios were determined *via* chemical ionization, time-of-flight mass spectrometry (CI-TOFMS) at 2Hz, allowing for real-time measurement of organic acid mixing ratios throughout the drive cycle. In addition, simultaneous measurements of carbon monoxide (CO) and carbon dioxide (CO_2) allow for real-time fuel based emissions factors (FBEFs) to be calculated for the overall drive cycle, as well as for specific phases of the UC cycle.

Emission ratios from mobile vehicles are compared directly with fuel-based emission factors for ocean-going vessels as determined from sampling of plume intercepts during the 2010 CalNex

project that took place aboard the R/V Atlantis in coastal Southern California. Using the sample CI-TOFMS instrument, direct measurements of organic acid emission factors were made both during day and night sampling of 23 ship plumes, most of which were sampled within five minutes of emission.

8.2 Experimental

8.2.1 Test vehicle selection and operation at the Haagen-Smit Laboratory

Eight LDGVs were sequestered by the California Air Resources Board from the current on-road vehicle fleet. All eight vehicles met the current California vehicle emissions standards set by the LEV II emission requirements. Before each day of testing, the eight LDGV were left sitting overnight with a nominal cold soak engine temperature of 24 °C. The vehicles were then placed on a chassis dynamometer and driven according to the UC cycle. The UC cycle is representative of a typical twenty minute trip taken by a California driver and is more aggressive than the current federal testing protocols urban drive cycle, FTP-75 (Austen et al., 1993). Each vehicle was driven under ambient conditions twice, with the exception of the Ford Windstar which was driven through the entire drive cycle only once due to a malfunction during the first day of testing.

8.2.2 Vehicle exhaust handling and dilution systems at the Haagen-Smit Laboratory

The vehicle exhaust was sampled directly from the vehicle tailpipe and diluted in two stages prior to measurement. The exhaust dilution system has been described in detail elsewhere, and is only described briefly here. The primary dilution stage consisted of a constant volume sampler (CVS) which fed directly into the secondary dilution system (SDS) [8], achieving a total dilution factor of 60. The exhaust dilution was achieved using secondary dilution air passed through a pre-filter, high-efficiency particulate air (HEPA) filter, and activated carbon. Following dilution, the sample was mixed under turbulent mixing conditions in a 0.10-m^3 residence time chamber (RTC) and then sub-sampled by the CI-TOFMS through a 2.24 meterlong piece of perfluoroalkoxy (PFA) tubing with a 3.175 millimeter inner diameter. The transit time of the vehicle exhaust from tailpipe to instrument was 80 seconds.

8.2.3 Measurements of NOx, CO and CO2 mixing ratios at the Haagen-Smit Laboratory

Real-time mixing ratios of nitrogen oxides ($NO_x \equiv NO + NO_2$), CO, and carbon dioxide (CO_2) were measured in the CVS using a Horiba 7200-SLE. Subsequent measurements of CO_2 were made after the SDS by an Aerodyne High Resolution Time-of-Flight Aerosol Mass Spectrometer (HR-TOF-AMS) using the Peak Integration by Key Analysis (PIKA) 1.10H toolpak. Utilizing the CO_2 mixing ratios measured in the CVS and post-SDS sampling line as constraints, dilution and mixing in the SDS were modelled with a continuously mixed flow reactor model. The same

model was applied to the concentrations of CO and NO_x measured in the CVS to give post-SDS mixing ratios for both CO and NO_x.

8.2.4 CIMS measurements of organic acids

C1-C10 (C2 excluded) organic acids were detected in real-time using a chemical ionization time-of-flight mass spectrometer (CI-TOFMS). The instrument used here has been previously described for the detection of gas-phase formic acid [135] and details of acetate ion chemistry for the detection of other organic acids can be found in Veres et al. [136]. Here, we briefly describe this instrument as applied to the detection of a wider suite of organic acids. The sample flow entering the ion-molecule reaction region (IMR) was restricted to 1.7 L min^{-1} using a critical orifice, with the remaining flow pulled through a sample bypass line. Utilizing acetate reagent ion chemistry, organic acids (HA) are detected as A^-, following negative ion proton transfer. The acetate reagent ion was generated by mixing 10 sccm of ultra-high purity (UHP) nitrogen that was bubbled through a reservoir of acetic anhydride with 1.5 slpm of UHP N_2 and passing the mixture through a ^{210}Po ionization source (NRD P-2021) orthogonal to the IMR. The CI-TOFMS duty cycle was held at 66 kHz for the duration of the study where the raw spectra were time averaged and saved at a rate of 2 Hz.

The CI-TOFMS was calibrated twice daily at the start and finish of each testing run using a calibrated formic acid (HCOOH) permeation source (Kin-Tek, SRT-2, 21.6 ng min^{-1} at 50º C) as a relative reference compound. Here, we apply the same calibration constant determined for formic acid to all of the organic acids detected in the study.

8.2.5 Ship Intercepts During CalNex 2010

During the California Research at the Nexus of Air Quality and Climate Change (CalNex) Study, we made measurements in 23 plumes from ocean-going vessels in coastal California. Measurements discussed here were made aboard the *R/V Atlantis* as part of the CalNex 2010 multi-platform field campaign [137]. The *Atlantis* provided a platform to measure the outflow of pollution in the marine boundary layer (MBL) along the coast of California during May and June 2010. Here, we concentrate on determining fuel based organic acid emission factors for each of the individual ship plumes. Of the 23 plumes encountered, 19 were sampled at night. The collection of vessels include: 1 Tug Boat, 3 Passenger Ships, 10 Cargo Ships, and 9 Tankers. The same CI-TOFMS used for vehicle testing was used during CalNex. The primary difference being the inlet manifold. During CalNex, ambient air was pulled through a 7.6 m, 0.64 cm ID PFA heated inlet (temperature controlled to 35ºC) at 10 standard L min^{-1} (slpm) at 933 mbar, resulting in an average residence time of 1.5 seconds. Calibrations to formic acid were conducted every 90 minutes for a total of 293 calibrations during the campaign. Background determinations were conducted every 30 minutes by overflowing the inlet with UHP N_2 (882 total). Simultaneous measurements of CO_2 permit calculation of fuel-based emission factors for each plume sampled.

8.3 Real-time emissions factor measurements from light duty gasoline vehicles

8.3.1 Real Time Mixing Ratios

A typical time series of the mixing ratio of propionic acid (C3 carboxylic acid), NO_x, CO, and CO_2 over the UC cycle is shown in Figure 1. Through matching both vehicle speed and converter temperature data with the post-SDS gas-phase measurements, all gas-phase measurements were time adjusted by 80 seconds to account for residence time in the dilution system. Here we concentrate on two specific regions of the UC drive cycle: 1) The first "cold start" phase is characterized by an increase in the catalytic converter temperature to stable temperature (300 °C) at which the TWC should be operating efficiently. Operationally, this is the first 300 seconds of the drive cycle. 2) The final "hot stabilized" phase, which occurs as the car has come out of the hard acceleration and the catalytic converter temperature begins to stabilizes again. Operationally, this is the last 300 seconds of the drive cycle. Mixing ratios of nine mono-protic carboxylic acids were measured above the CI-TOFMS detection threshold for each of the eight cars studied.

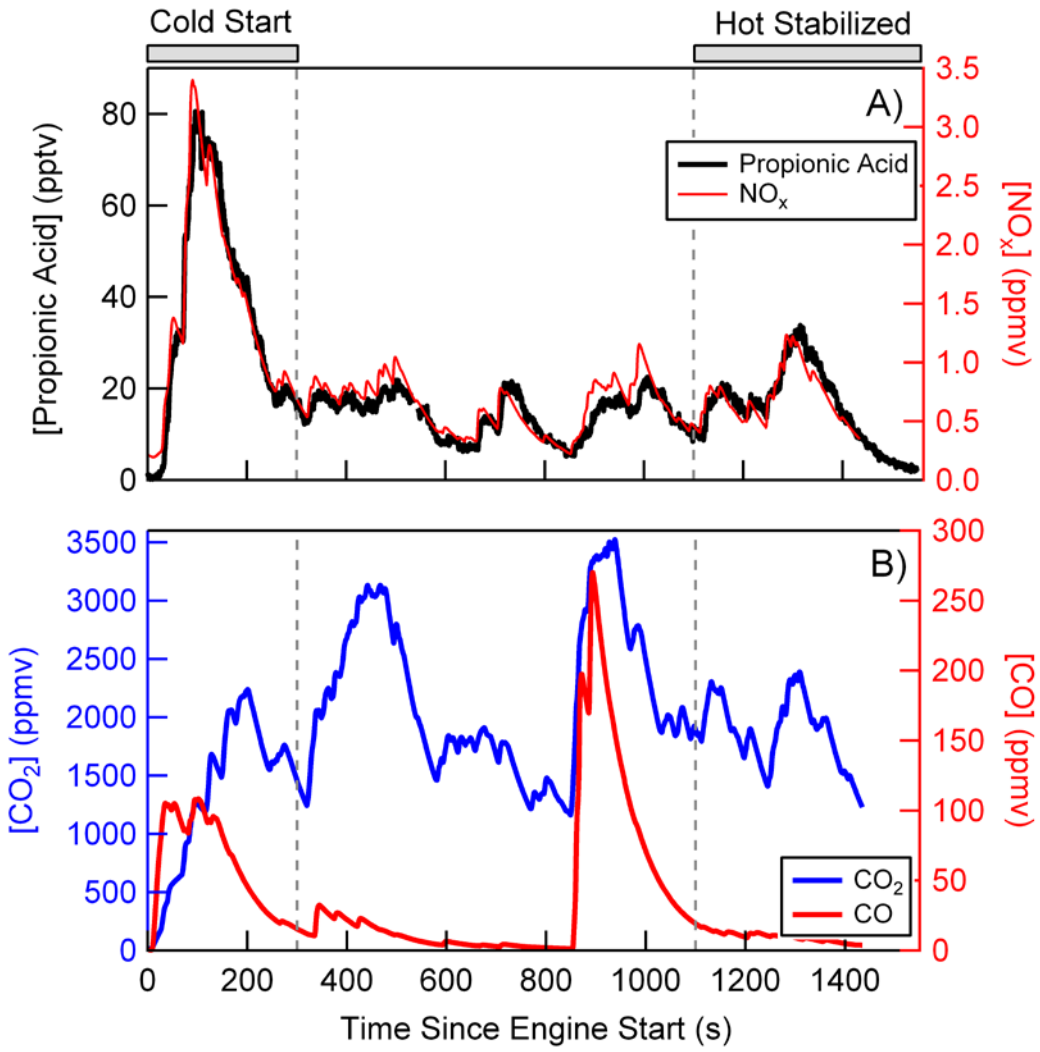

Figure 8-1: A) Real-time mixing ratios of propionic acid (black; detected at m/z = 73) for the first Cavalier test as measured after the secondary dilution system (SDS). Modeled NO_x mixing ratio, post-SDS, is shown in red. B) Mixing ratios of modeled CO (red) as well as modeled CO_2 (blue) post-SDS, for the first Cavalier test. The "cold start" period, defined as the first 300 s following engine start and the "hot stabilized" period, defined as the last 450 s of the test are shown with gray bars above panel A.

8.3.2 Real-time organic acid fuel based emission factors

Here, we define Fuel Based Emission Factors (FBEF) for individual organic acids as the mass of the select organic acid (milligram) emitted per kilogram of fuel burned by the LDGVs. The FBEFs were calculated using the following equation:

$$FBEF_{HNCO} = \frac{[HA]}{[CO_2]} \times \frac{MW_{CO_2}}{MW_C} \times W_C \qquad \text{(E1)}$$

where [HA] is the mass concentration of the organic acid of interest, [CO_2] is the mass concentration of CO_2, MW_{CO_2} and MW_C are the molecular weights of CO_2 and carbon, and W_C is the mass fraction of carbon in the fuel, assumed to be 0.85 [31]. The FBEFs are calculated under the assumption that the carbon present in the fuel is converted to CO_2 with unit efficiency, where the contributions from other carbon species are negligible. The mass concentrations of CO_2 were calculated using the real-time measurements of CO_2, measured by the HR-TOF-AMS after the SDS, constrained by CO_2 measurements in the CVS as discussed in Chapter 3.

FBEFs for the nine organic acids measured are shown in Figure 2A as a function of carbon chain length for both the cold start and hot stabilized periods of the drive cycle for the Cavalier. As shown, emission rates decrease with increasing organic acid chain length and are generally higher during the cold start period as opposed to the hot stabilized period. For comparison the enhancement ratio of select organic acids, relative to CO is shown in Figure 2B, again indicating decreasing organic acid emissions with increasing carbon chain length. For comparison, vehicle emissions as determined from the tunnel studies of Talbot et al. indicated formic acid/carbon monoxide ratios ranging between 161.5 and 352.6 pptv/ppmv (mean ± 1σ of 232.7 ± 71). For comparison measured HCOOH/CO ratios determined here for the Cavalier were 5.36 ± 3 pptv/ppmv for the cold start phase and 47.93 ± 32 pptv/ppmv for the hot stabilized phase of the drive cycle. Given the driving conditions in the Hampton Roads Bridge Tunnel, it is most reasonable to compare the results of Talbot et al. (232.7 ± 71 pptv/ppmv) to the measurements made during the hot stabilized phase of the UC drive cycle (47.93 ± 32 pptv/ppmv). The results presented here would further reduce the contribution of primary organic acids to global emissions estimates (from 2% to < 0.5 % of the total primary emissions), if we scale them linearly with CO.

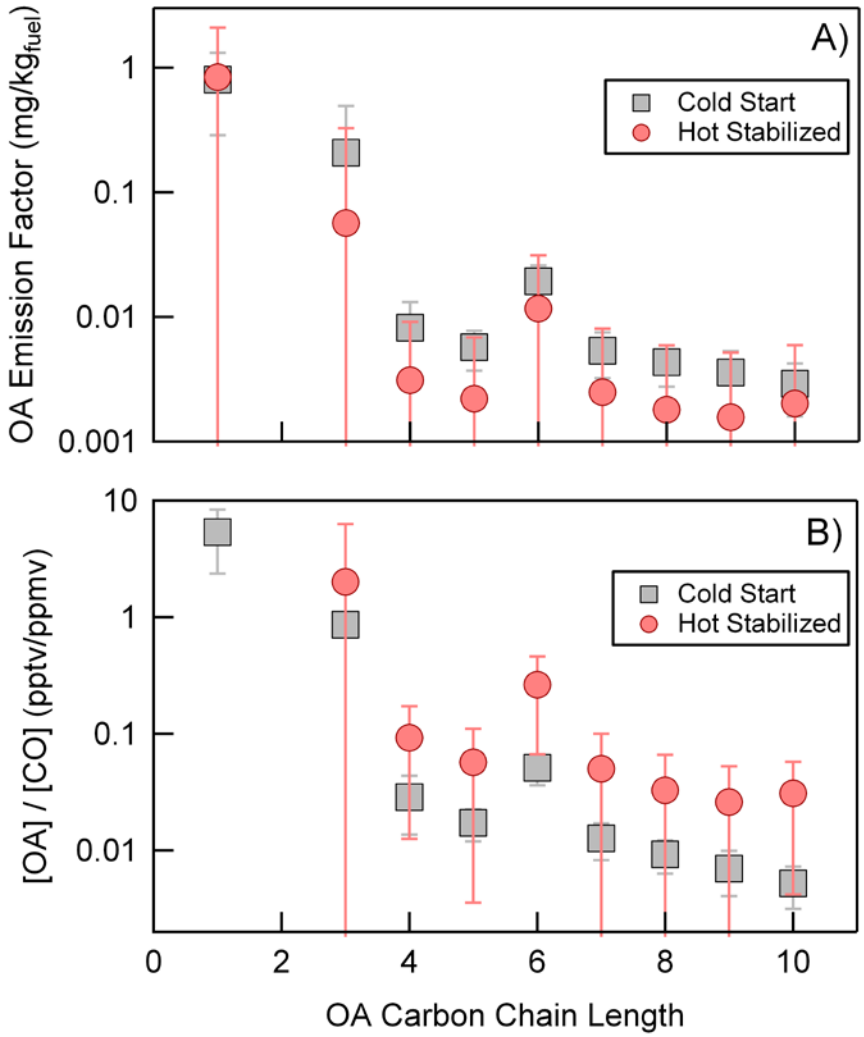

Figure 8-2: A) Average fuel-based emission factors for gas-phase organic acids as a function of the carbon chain length for both the cold start and hot stabilized periods of the drive cycle. B) Average organic acid to carbon monoxide (CO) ratio, in pptv/ppbv, for the cold start and hot stabilized periods of the drive cycle. Note that OA refers to organic acid (not organic aerosol).

8.3.3 Partitioning of organic acids between the aerosol and gas phase

As part of the 2011 measurements, mixing ratios of organic acids were measured behind three heated inlets (50, 75, and 100°C), in addition to an unheated inlet line (25°C). This experimental configuration permits assessment of the partitioning of organic acids between the gas and aerosol phase. The ratio of the observed mixing ratio sampled through each of the three heated channels is shown as referenced to the unheated inlet line in Figure 8-3. Equilibrium absorptive partitioning theory can be used to predict the fraction of organic acids in the particle-phase (F_p) as a function of the organic aerosol mass concentration (C_{OA}), the molecular weight of the

organic acid (MW), the activity coefficient of the acid in the OA matrix (ζ), the vapor pressure of the organic acid (P_v), and temperature, *via* E2:

$$F_P = \left(1 + \frac{MW\ 10^6\ \zeta\ P_V}{760 RT\ C_{OA}}\right)^{-1} \qquad \text{(E2)}$$

For the C1-C5 organic acids measured here and the temperatures and organic mass concentrations routinely sampled in the diluted auto-exhaust, it is expected (based on E2) that greater than 95% of the organic acids should be in the gas-phase. As shown in Fig. 8-3A-D, gas-phase organic acid mixing ratios increase with increasing temperature on average. However, the increase is less than 5% for all acids measured at temperatures between 25 and 100°C, suggesting that the organic acids in primary vehicle exhaust are concentrated in the gas phase, a likely result of the acidity of primary aerosol particles combined with the relatively high equilibrium vapor pressures for the organic acids sampled here.

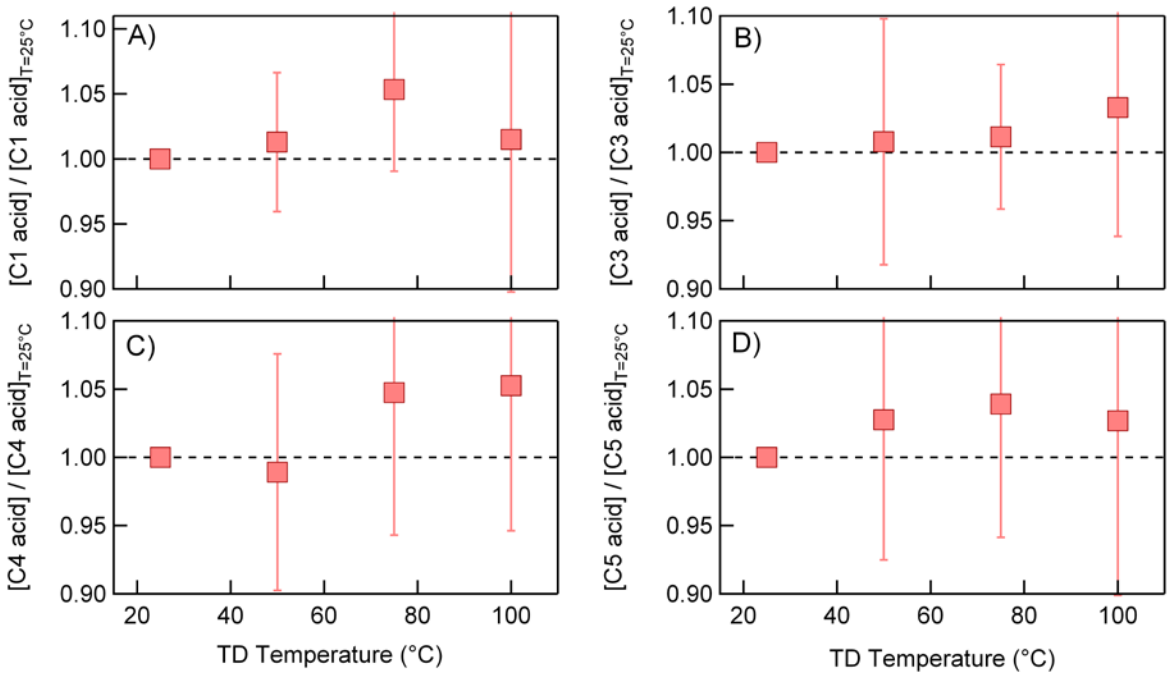

Figure 8-3: Observed enhancement in the organic acid gas-phase concentration as a function of the thermal denuder temperature for C1, C3, C4, and C5 organic acids (A-D, respectively).

8.4 Determination of formic acid fuel-based emission factors from ocean-going vessels

During the CalNex 2010 field campaign fuel based emission factors were derived from 23 plume intercepts of ocean-going vessels. The spatial location of these plume intercepts is shown in Figure 4, where each marker represents an individual plume intercept, ranging from less than one minute in duration to over six minutes in duration. The markers are color coded by the formic

acid fuel based emission ratio determined *via* E1. A sample ship plume intercept is shown in Figure 5 for the Mathilde Maersk, a 367 m container ship. Formic acid mixing ratios are shown in Figure 5A and the corresponding CO_2 mixing ratio is shown in Figure 5B. Fuel based emission ratios were calculated from both the slope of the correlation plot between CO_2 and HCOOH as well as from the ratio of the respective plume areas as shown by the colored regions in Figure 5. For all 23 plumes sampled, calculation by the regression and plume area method agreed to within 20%.

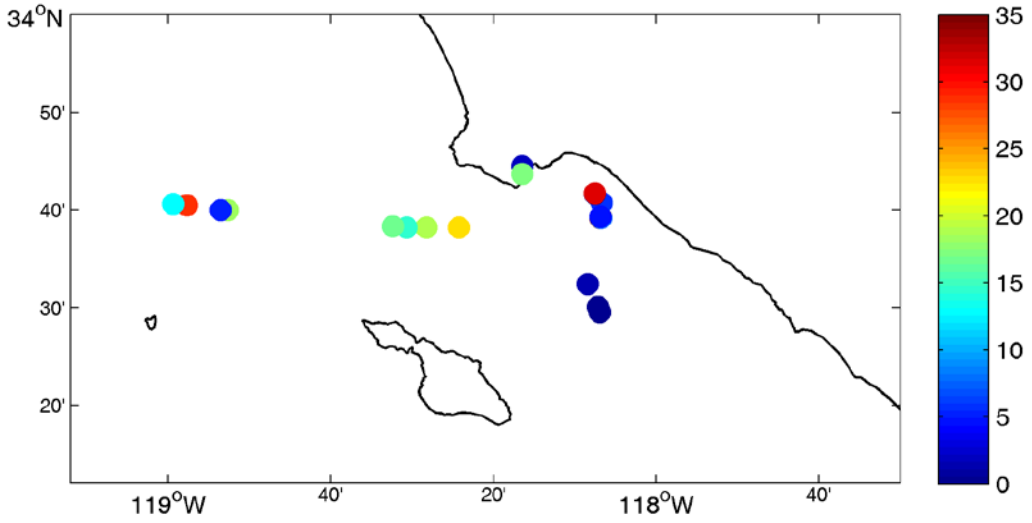

Figure 8-4: Location of ship plume intercepts during the CalNex 2010 field campaign as measured from the RV Atlantis. The color shading on each marker represents the formic acid fuel based emission ratio (mg/kg_{fuel}) for each plume intercept.

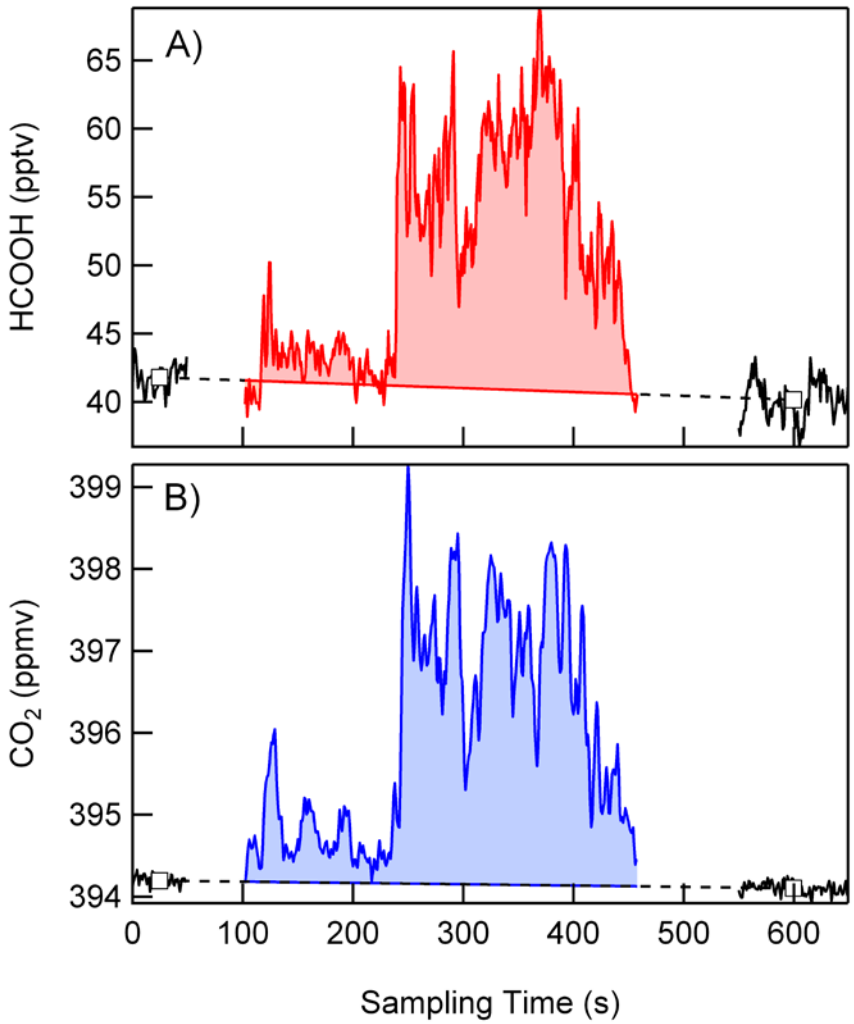

Figure 8-5: Formic acid (A) and CO_2 (B) mixing ratios during a plume intercept of the Mathilde Maersk container ship of the coast of Southern California.

The mean fuel-based emission factor for the 19 ship plumes sampled during daylight hours was determined to be 9.8 mg/kg_{fuel} and 14.3 mg/kg_{fuel} for nighttime plume samples. The variability in the measured emission factor is shown both in Figure 4, as well as in Figure 6, as a function of the estimated plume age. Future work in this area will focus on determining the sources of the variability in the measured FBEFs.

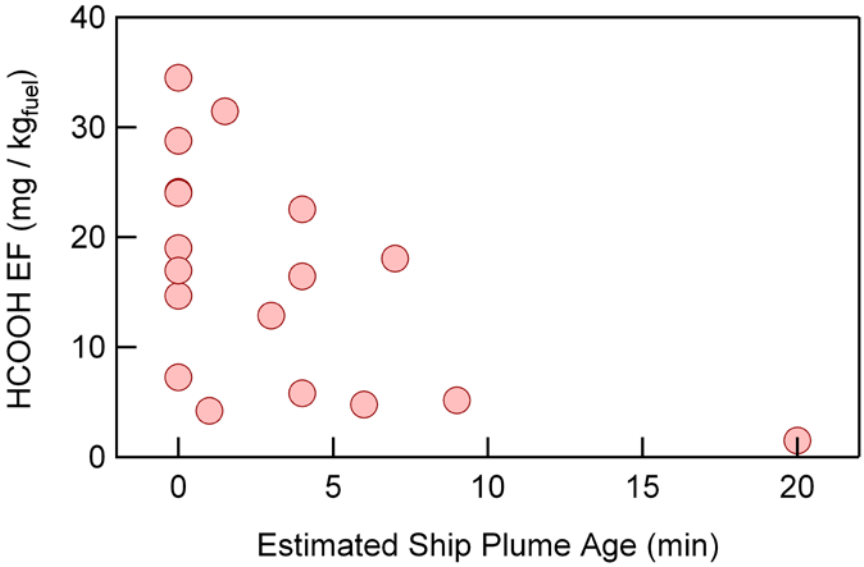

Figure 8-6: Dependence of the formic acid fuel-based emission factor on the estimated plume age.

8.5 Conclusions

The average fuel-based gas-phase organic acid emission factors for light duty gasoline vehicles display a strong dependence on the organic acid chain length, where formic acid emission factors are as high as 0.8 mg/kg$_{fuel}$ while the emission factors for gas-phase C4 or larger organic acids were observed to be less than 0.02 mg/kg$_{fuel}$. Measurements of the enhancement in organic acid mixing ratio following heating of the inlet air stream suggest that organic acids in primary vehicle exhaust are concentrated in the gas phase, a likely result of the acidity of primary aerosol particles. Finally, comparison of formic acid FBEFs between motor vehicles and ocean-going vessels (Fig. 7) indicates that motor vehicle emission factors are on average a factor of ten lower than those measured in ship emissions.

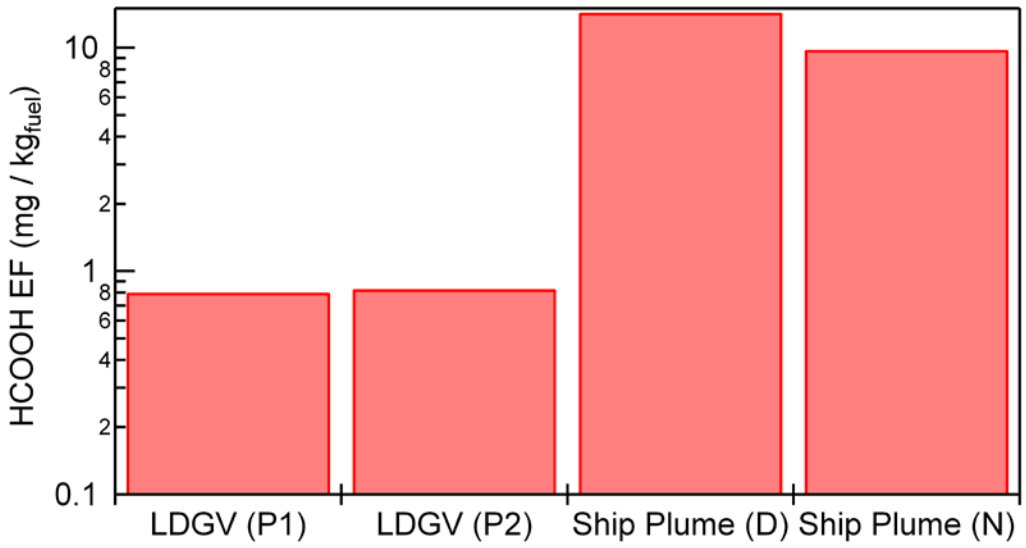

Figure 8-7: Comparison of formic acid fuel based emission factors between light duty gasoline vehicles, as measured at the CARB Haagen-Smit Laboratory with ocean-going vessel emissions as determined from field measurements in coastal California. P1 and P2 indicate the two main phases of the drive cycle and D and N indicate day and night, respectively.

9 REAL-TIME EMISSION FACTOR MEASUREMENTS OF ISOCYANIC ACID FROM LIGHT DUTY GASOLINE VEHICLES

9.1 Introduction

Laboratory investigations have shown that cyanate anions (NCO^-) can effectively modify protein structure and function through carbamylation of amino acid residuals.[138] Carbamylation of proteins by NCO^- has been implicated in several negative health effects ranging from cardiovascular and ocular impairments, to chronic diseases such as rheumatoid arthritis.[138-141] Recently, Roberts et al. reported the first atmospheric measurements of gas-phase isocyanic acid (HNCO), as well as showing that HNCO mixing ratios greater than 1 ppbv are high enough to cause protein carbamylation following accommodation and subsequent dissociation of HNCO into the blood stream.[139]

Real-time atmospheric measurements of HNCO mixing ratios are rare, thus limiting our ability to properly constrain HNCO sources and loss rates. The *in situ* measurements of Roberts et al. indicate that HNCO mixing ratios can exceed 200 pptv in air influenced by recent biomass burning, confirming laboratory investigations of HNCO production during the combustion and pyrolysis of nitrogen containing biomass (e.g. proteins).[142, 143] In the same publication, HNCO mixing ratios peaking at 100 pptv, and displaying strong diel variation, were reported for air sampled in Pasadena, CA during spring 2010. The sources of HNCO in Pasadena are less well understood, but have been hypothesized to be photochemical, potentially involving the oxidation of precursor amines and amides.[139, 144] Recently, Wentzell et al. reported HNCO mixing ratios as high as 990 pptv in Toronto, ON, where HNCO was observed to be highly correlated with benzene, suggesting a vehicular, fuel combustion source.[145] To the best of our knowledge, these are the only published measurements of atmospheric HNCO mixing ratios.

Laboratory efforts have focused on determining emission factors or ratios for HNCO from a variety of combustions sources. Roberts et al. reported the first measurements of HNCO emissions from controlled biomass burning experiments, where the HNCO/CO ratios ranged between 0.1-0.6% during flaming stages of combustion and dropped by a factor of 5-10 during the smoldering stages.[139] When scaled globally, biomass burning emissions of HNCO are estimated to be as large as 1.5 Tg yr^{-1}.[146] The atmospheric measurements of Wentzel et al. imply that vehicular emissions of HNCO are large, and could potentially surpass biomass burning emissions on a global scale. Wentzell et al. quantified HNCO emissions factors for a single light-duty diesel-powered engine, representative of light duty diesel-powered vehicles (LDDV) operating under 4 different steady-state driving modes,[145] showing fuel based HNCO emission factors ranging between 0.21-3.96 mg kg_{fuel}^{-1}. Further, HNCO emissions from diesel urea selective catalytic reduction (SCR) exhaust systems represent a potential HNCO source, which has yet to be fully characterized.[147]

To date, there are no direct determinations of emission factors for HNCO from light-duty gasoline-powered vehicles (LDGVs), despite the fact that in 2009 on-road gasoline vehicles accounted for the emission of 34,199 Gg of carbon monoxide (CO), an important precursor for HNCO, in the US as compared to 524 Gg of CO emitted from on-road diesel vehicles.[148] On-road gasoline-powered passenger cars and light-duty trucks accounted for 32,666 Gg of the

emitted CO, while diesel powered passenger cars and light-duty trucks specifically account for only 7 Gg of the total emitted CO.[148] Laboratory studies using FTIR to investigate the reactions of a tertiary gas mixture comprised of nitric oxide (NO), CO, and either hydrogen gas (H_2) or ammonia (NH_3) over precious metal catalysts have been used as proxy systems for LDGV engines and the associated catalytic converter systems. These laboratory measurements place an upper limit on the mixing ratios of HNCO emitted from LDGVs of 20 ppmv, the detection limit for the FTIR instrument used.[149] Mechanistically, these studies indicate that HNCO is formed in high yield when NO, CO, and either H_2 or NH_3 are reacted over precious metal catalysts (e.g., platinum, palladium, or rhodium) that are typically used in modern three-way catalytic converters (TWC).[150-153]

The production of HNCO on precious metal catalysts is proposed to occur through the reaction between surface bound hydrogen atoms and NCO, where NCO comes from surface reactions involving adsorbed NO and CO.[154] The reactions proceed as follows, where surface bound species are denoted by (*) and surface sites are neglected.

$$NO_{(g)} \rightleftharpoons {}^{*}NO \rightarrow {}^{*}N + {}^{*}O \quad \text{(R1)}$$

$$CO_{(g)} \rightleftharpoons {}^{*}CO \quad \text{(R2)}$$

$${}^{*}N + {}^{*}CO \rightleftharpoons {}^{*}NCO \quad \text{(R3)}$$

The surface bound hydrogen can arise from either the dissociation of H_2 (R4) or NH_3 (R5) on the catalyst surface.

$$H_{2(g)} \rightleftharpoons 2H^{*} \quad \text{(R4)}$$

$$NH_3(g) \rightarrow {}^{*}NH_3 \rightleftharpoons {}^{*}NH_2 + H^{*} \rightleftharpoons {}^{*}NH + 2H^{*} \rightleftharpoons {}^{*}N + 3H^{*} \quad \text{(R5)}$$

For platinum catalysts the production of HNCO commences at relatively low temperatures, ca. 150˚C, arising from reaction of NCO groups with adsorbed hydrogen.[152] As the catalyst temperature increases, H_2 produced by the engine is consumed, and the majority of the surface bound hydrogen is formed following NH_3 dissociation. For the palladium catalyst, the production of HNCO commences at 235 ˚C, with surface bound hydrogen forming primarily from NH_3.[152] The different behavior of the two metals has been attributed to the relative adsorption strengths of CO and NO adsorption on the surface of each catalyst.

The surface bound hydrogen atoms and NCO groups react to form HNCO, which desorbs from the surface as $HNCO_{(g)}$ (R6).

$$H^{*} + {}^{*}NCO \rightarrow HNCO_{(g)} \quad \text{(R6)}$$

For the lower temperature regimes and typical of platinum-based catalytic converters, the production of HNCO can be summarized as:

$$NO + CO + 1.5H_2 \rightarrow HNCO + H_2O \quad \text{(R7)}$$

while at higher temperature regimes and typical of palladium catalyst the generalized reaction is:

$$2NO + NH_3 + 5CO \rightarrow 3HNCO + 2CO_2 \quad \text{(R8)}$$

The highest HNCO yield for R7 is observed over a silicon supported platinum catalyst (Pt/SiO_2), peaking at 41% of the reacted nitrogen. The peak yield for HNCO from R8 over a silicon oxide supported platinum catalyst is 70% of the reacted nitrogen, with the yield over a silicon oxide supported palladium catalyst reaching 46% of the reacted nitrogen.

Despite the relatively high yields of HNCO from nitrogen on the catalyst surfaces present in a modern TWC, a rapid and complete hydrolysis of HNCO has been suggested to occur (R9) on the oxide washcoat of the TWC, effectively removing HNCO from the exhaust.[150-153]

$$HNCO + H_2O \rightarrow NH_3 + CO_2 \quad \text{(R9)}$$

These studies suggest that the water concentration in the engine exhaust of a typical LDGV is sufficiently high such that any HNCO formed on the catalyst will be completely hydrolyzed on the washcoat before the exhaust can exit through the pores of the catalytic converter.[150-153] If true, this would indicate that modern LDGVs would emit negligible concentrations of HNCO. However, while catalyst studies provide unique mechanistic information on the production and loss within an ideal catalytic converter, they do not provide constraints for the emission factors of HNCO from actual LDGVs and the associated range of catalytic converter functionality under a variety of real-world driving conditions.

Here, we report the first measurements of real-time, fuel-based HNCO emission factors from light duty gasoline vehicles. In this study, a representative fleet of eight LDGVs were driven under the California Unified driving cycle (UC) at the California Air Resources Board's (CARB) Haagen-Smit Laboratory (HSL), where HNCO, CO and CO_2 were detected in real-time in the diluted exhaust. The LDGVs were requisitioned by CARB from the current on-road vehicle fleet (Table 9-1). HNCO mixing ratios were determined via chemical ionization, time-of-flight mass spectrometry (CI-TOFMS) at 2 Hz, allowing for real-time measurement of HNCO mixing ratios throughout the drive cycle. In addition, the simultaneous measurement of CO and CO_2 allow for real-time fuel based emissions factors (FBEFs) to be calculated for the overall drive cycle, as well as for four specific phases of the UC as characterized by the catalytic converter temperature. The results indicate that HNCO production is highly dependent on the drive cycle and consequently on the efficiency with which the catalytic converter operates. This study establishes fuel based emissions factors for HNCO from LDGVs, while simultaneously providing a unique insight into the drive cycle dependency of HNCO emissions.

Table 9-1: Manufacturer, Model, and Year of the Eight Light Duty Gasoline Vehicles Tested

Manufacturer	Model	Year
Chevrolet	Cavalier	2001
Chevrolet	S-10	2002
Chrysler	Grand Cherokee	2002
Nissan	Pathfinder	2003
Toyota	Solara	2003
Toyota	Tacoma	2003
Ford	Taurus	1997
Ford	Windstar	1998

9.2 Experimental

9.2.1 Test Vehicle Selection and Operation

The eight LDGVs tested here met the current California vehicle emissions standards set by the LEV emission requirements. Before each day of testing, the eight LDGVs were stored overnight with a nominal cold soak engine temperature of 24 °C. The vehicles were then placed on a chassis dynamometer and driven according to the UC (Fig. 1A). The UC is representative of a typical twenty minute trip taken by a California driver and is more aggressive than the current federal test procedure urban drive cycle, FTP-75.[155] Each vehicle was driven under ambient conditions twice, with the exception of the Ford Windstar which was driven through the entire drive cycle only once due to an operation malfunction during the first day of testing.

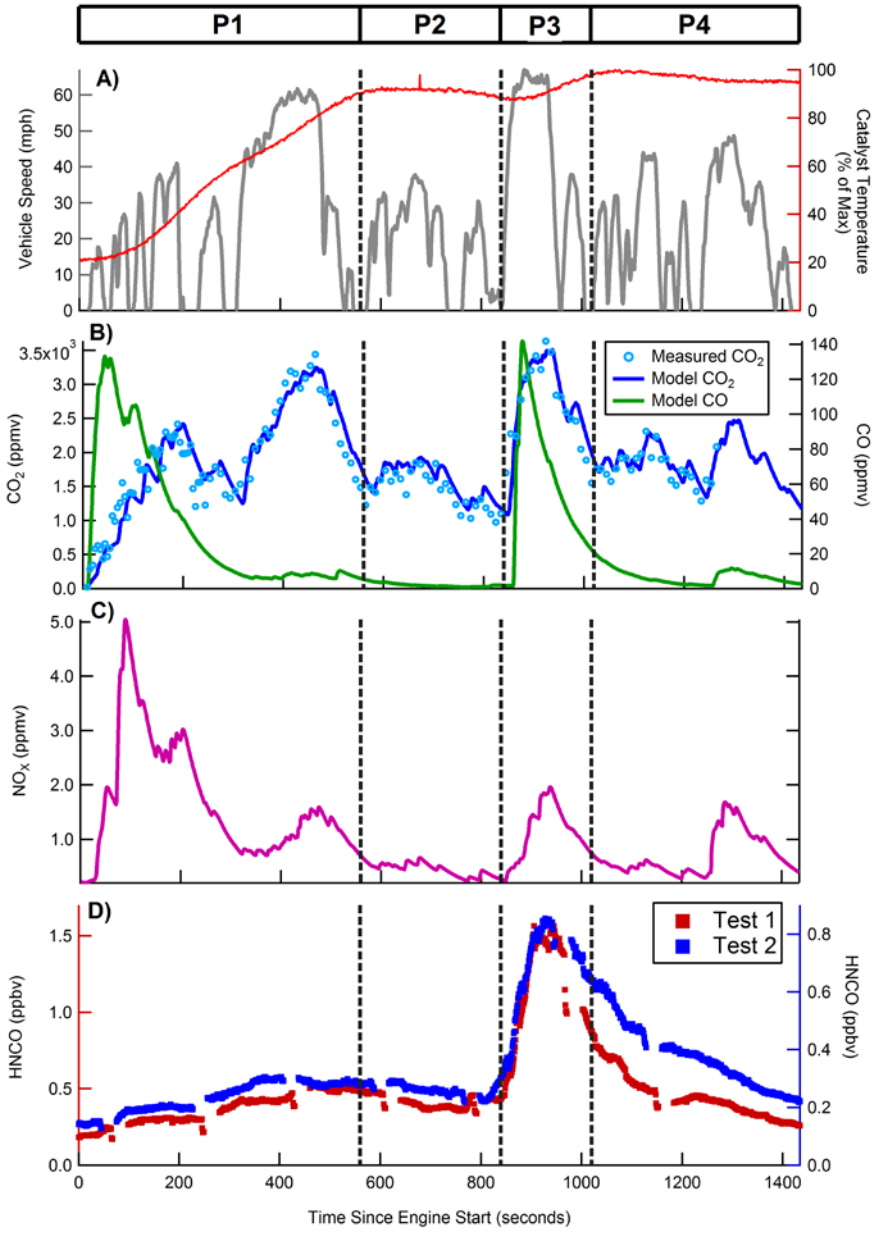

Figure 9-1: A) Vehicle speed (grey) and relative catalyst temperature (red) for the first Chevrolet Cavalier test with the four phases of the drive cycle depicted. Phase 1 (P1) is the cold start phase, Phase 2 (P2) is the first hot stabilized phase, Phase 3 (P3) is the hard acceleration phase, and Phase 4 (P4) is the second hot stabilized phase. B) Mixing ratios for modeled CO (green) as well as CO_2 measured (blue circles) and modeled (blue lines) after the secondary dilution system for the first Cavalier test. C) Mixing ratios for modeled NO_x (pink) after the secondary dilution system. D) Real-time post-SDS mixing ratios of HNCO for the Cavalier for both test 1 (red) and test 2 (blue). All gas concentration data has been time corrected to account for residence time in the dilution system.

9.2.2 Vehicle Exhaust Handling and Dilution System

The vehicle exhaust was sampled directly from the vehicle tailpipe and diluted in two stages prior to measurement. The exhaust dilution system has been described in detail elsewhere,[8] and is only summarized briefly here. The primary dilution stage consisted of a standard constant volume sampler (CVS), operated by CARB, which fed directly into a secondary stainless steel dilution system (SDS),[8] achieving a total dilution factor of ca. 80. Secondary dilution air passed through a pre-filter, activated carbon, and a high-efficiency particulate air (HEPA) filter. Following dilution in a turbulent mixing chamber the sample was aged for approximately 60 seconds in a 0.10-m^3 stainless steel residence time chamber (RTC) and then sub-sampled by the CI-TOFMS through a 2.24 meter long piece of perfluoroalkoxy (PFA) tubing with a 3.175 millimeter inner diameter. The transit time of the vehicle exhaust from tailpipe to instrument was ca. 80 seconds.

9.2.3 CIMS Measurement of HCNO

HNCO was detected in real-time using a chemical ionization time-of-flight mass spectrometer (CI-TOFMS). The instrument used here has been previously described for the detection of gas-phase formic acid[156] and details of acetate ion chemistry for the detection of HNCO can be found in Veres et al.[130] Here, we briefly describe the same instrument applied to the detection of gas-phase HNCO. The sample flow entering the CI-TOFMS ion-molecule reaction region (IMR) was restricted to 1.7 L min^{-1} using a critical orifice, with the remaining flow pulled through a sample bypass line. Utilizing acetate reagent ion chemistry, HNCO is detected as NCO^-, following negative ion proton transfer.[139] The acetate reagent ion was generated by mixing 10 sccm of ultra-high purity (UHP) nitrogen bubbled through a reservoir of acetic anhydride with 1.5 slpm of UHP N_2 and subsequently passing the mixture through a ^{210}Po ionization source (NRD P-2021) orthogonal to the IMR. The CI-TOFMS duty cycle was held at 66 kHz for the duration of the study, and raw spectra were time averaged and saved at a rate of 2 Hz.

The CI-TOFMS was calibrated twice daily at the start and finish of each testing run using a calibrated formic acid (HCOOH) permeation source (Kin-Tek, SRT-2, 21.6 ng min^{-1} at 50° C) as a relative reference compound. The sensitivity of the CI-TOFMS to HNCO, relative to HCOOH, is the largest source of uncertainty in the reported HNCO mixing ratios. Utilizing average-dipole-orientation (ADO) theory, the ion-molecule reaction rates were calculated and used to determine the relative sensitivity of the instrument to HNCO as compared to HCOOH.[157-159] In general the relative sensitivity is:

$$F_{HNCO} = \frac{C_{HNCO}}{C_{HCOOH}} = \frac{k_{HNCO}}{k_{HCOOH}} \quad \text{(E1)}$$

where F_{HNCO} is the relative sensitivity of the instrument to HNCO relative to HCOOH, C_{HNCO} and C_{HCOOH} are the respective calibration constants for HNCO and HCOOH, $k_{HNCO} = 1.77 \times 10^{-9}$ cm^3 $molecule^{-1}$ s^{-1} and $k_{HCOOH} = 1.60 \times 10^{-9}$ cm^3 $molecule^{-1}$ s^{-1}. The

mixing ratios of HNCO are then calculated as:

$$[HNCO]_{pptv} = \frac{[NCO^-]}{F_{HNCO} \times C_{HCOOH}} \quad \text{(E2)}$$

where $[NCO^-]$ is the measured ion signal for isocyanic acid and F_{HNCO}=1.11. A previous study performed using a similar chemical ionization system reported experimentally determined values for F_{HNCO} as large as 2.4.[130]

9.2.4 Measurements of NOx, CO and CO2 mixing ratios

Real-time mixing ratios of nitrogen oxides ($NO_x \equiv NO + NO_2$), CO, and CO_2 were measured in the CVS using a Horiba 7200-SLE. Because the HNCO measurements were made after the SDS+ RTC, the HNCO data is greatly smoothed relative to the measurements directly from the CVS. To facilitate comparison, measurements of gas-phase CO_2 were also made after the SDS by a LI-6262 CO_2/H_2O gas analyzer (LI-COR Inc., USA). The measurements taken by the LI-6262 were compared to the mixing ratio of gas-phase $CO_2^{\pm}$ measured by an Aerodyne High Resolution Time-of-Flight Aerosol Mass Spectrometer (HR-ToF-AMS) using the Peak Integration by Key Analysis (PIKA) 1.10H toolpak.[160] Good agreement between the CO_2 from the CVS and CO_2 from the HR-ToF-AMS, LI-6262, and SDS+RTC has been previously demonstrated.[161] Utilizing the CVS and post-SDS CO_2 mixing ratios as constraints, dilution and mixing in the SDS were modeled with a continuously mixed flow reactor model (Fig. 1B). The same model was applied to the concentrations of CO and NO_x measured in the CVS to give post-SDS mixing ratios for both CO and NO_x.

9.3 Results

9.3.1 Real-time Mixing Ratios

Based on the real-time catalytic converter temperature data for each vehicle, the UC cycle was sub-divided into four phases (Fig. 1A). In matching both vehicle speed and converter temperature data with the post-SDS gas-phase measurements, all gas-phase measurements were time adjusted by ca. 80 seconds to account for residence time in the dilution system. The first "cold start" phase is characterized by an increase in the catalytic converter temperature to a stable temperature (300 °C) at which the TWC should be operating efficiently. The second phase or "first hot stabilized" phase is characterized by a constant catalyst temperature (300 °C) that remains stable until reaching the third phase at ca. 840 seconds into the drive cycle. This third "hard acceleration" phase consists of vehicle acceleration from 0 to 65 miles per hour (mph) in approximately 40 seconds and is characterized by a subsequent rise in the average temperature of the catalytic converter (338 °C). The fourth and final "second hot stabilized" phase occurs as the car has come out of the hard acceleration and the catalytic converter temperature begins to stabilize again.

CO, CO_2, and NO_x concentrations in the post-SDS diluted exhaust for the first day of testing for the Cavalier are shown in Fig. 1B and Fig. 1C. The profiles for CO_2 and NO_x demonstrate a strong correlation with the drive cycle with increases in their respective mixing ratios corresponding to increases in vehicle speed and acceleration. The time trace of the CO concentration in the diluted exhaust gas depicts two significant spikes, the first at the start of the

drive cycle during the cold start phase when the catalytic converter is not yet sufficiently heated to efficiently convert the CO produced by the engine into CO_2, and a second occurring during the hard acceleration phase as would be expected for a vehicle entering a fuel rich state.[148]

Contrary to the literature-based *a priori* assumption of negligible HNCO emissions from LDGVs,[150-153] measureable and substantial HNCO mixing ratios were observed in the exhaust of all eight LDGVs tested. The median and mean mixing ratios of HNCO, CO, CO_2 and NO_x measured after dilution are presented in Table 9-2. The interquartile range is also reported to demonstrate the variability of emissions in each phase and over the course of the entire drive cycle. As an example, real-time post-SDS mixing ratios of HNCO are shown in Fig. 1D for the Chevrolet Cavalier. The concentration of HNCO steadily increases during the initial cold start phase of the UC and then reaches a local maximum 400-600 seconds after engine start. In the hard acceleration phase of the drive cycle the concentration of HNCO increases in lockstep with CO, reaching a maximum that directly follows peak acceleration. The maximum mixing ratios of HNCO in the post-SDS ranged from 0.37 ppbv to 13.65 ppbv depending on the vehicle. Following the hard acceleration, HNCO mixing ratios decay back toward their initial values through the hot stabilized phase of the drive cycle.

Table 9-2: Mean HNCO Emissions Factors and Mixing Ratios of HNCO, CO, CO_2, and NO_x for each vehicle test.

	Drive Cycle Phase	HNCO Emissions Factor (mg kgfuel-1)	HNCO (ppbv)	CO (ppmv)	CO_2 (%)	NO_x (ppmv)
Chevrolet Cavalier	Cold Run	0.427 (0.005) 0.375 (0.004)	0.36 (0.004) 0.24 (0.002)	36.72 (1.71) 31.8 (1.53)	0.263 (0.005) 0.192 (0.003)	1.74 (0.046) 1.328 (0.05)
	First Hot Run	0.559 (0.006) 0.512 (0.005)	0.41 (0.002) 0.26 (0.001)	2.18 (0.07) 1.86 (0.04)	0.226 (0.002) 0.157 (0.001)	0.447 (0.007) 0.304 (0.005)
	Hard Acceleration	0.91 (0.01) 0.747 (0.011)	1.12 (0.024) 0.68 (0.011)	60.12 (2.93) 74.91 (3.79)	0.376 (0.006) 0.272 (0.005)	1.124 (0.037) 0.601 (0.017)
	Second Hot Run	0.532 (0.008) 0.652 (0.01)	0.45 (0.007) 0.38 (0.006)	7.05 (0.21) 6.62 (0.21)	0.259 (0.002) 0.181 (0.001)	0.704 (0.019) 0.591 (0.02)
	All	0.55 (0.006) 0.542 (0.006)	0.49 (0.008) 0.34 (0.004)	24.03 (0.92) 23.8 (0.97)	0.266 (0.002) 0.19 (0.002)	1.09 (0.024) 0.809 (0.023)
Chevrolet S-10	Cold Run	0.297 (0.004) 0.281 (0.003)	0.21 (0.002) 0.19 (0.002)	14.07 (0.66) 22.38 (0.86)	0.232 (0.003) 0.212 (0.003)	0.266 (0.012) 0.327 (0.011)
	First Hot Run	0.393 (0.005) 0.387 (0.003)	0.23 (0.002) 0.22 (0.001)	2.6 (0.06) 3.43 (0.09)	0.176 (0.002) 0.172 (0.001)	0.063 (0.002) 0.119 (0.004)
	Hard Acceleration	1.208 (0.054) 0.683 (0.029)	1.37 (0.051) 0.74 (0.025)	141.18 (7.22) 94.91 (4.7)	0.317 (0.006) 0.303 (0.005)	0.061 (0.001) 0.202 (0.004)
	Second Hot Run	0.854 (0.024) 0.98 (0.009)	0.57 (0.015) 0.63 (0.007)	10.22 (0.46) 10.85 (0.25)	0.209 (0.002) 0.196 (0.001)	0.143 (0.008) 0.202 (0.006)
	All	0.62 (0.015) 0.586 (0.01)	0.46 (0.013) 0.39 (0.007)	26.7 (1.5) 24.37 (1)	0.222 (0.002) 0.208 (0.002)	0.165 (0.005) 0.234 (0.005)

Chrysler Grand Cherokee	Cold Run	0.587 (0.005) 0.441 (0.004)	0.39 (0.006) 0.27 (0.002)	27.91 (1.08) 28.75 (1.82)	0.197 (0.003) 0.183 (0.002)	1.551 (0.057) 1.179 (0.059)
	First Hot Run	0.776 (0.017) 0.676 (0.019)	0.38 (0.003) 0.32 (0.005)	11.52 (0.14) 6.44 (0.21)	0.158 (0.001) 0.149 (0.001)	0.375 (0.009) 0.33 (0.011)
	Hard Acceleration	3.084 (0.044) 1.722 (0.03)	2.78 (0.067) 1.47 (0.026)	65.02 (2) 53.98 (2.46)	0.271 (0.005) 0.261 (0.004)	2.787 (0.076) 2.004 (0.053)
	Second Hot Run	1.401 (0.031) 1.407 (0.019)	0.85 (0.018) 0.79 (0.01)	22.62 (0.35) 5.76 (0.19)	0.185 (0.001) 0.171 (0.001)	1.245 (0.021) 0.34 (0.015)
	All	1.217 (0.027) 0.974 (0.017)	0.82 (0.023) 0.58 (0.012)	27.67 (0.64) 20.82 (0.88)	0.192 (0.002) 0.18 (0.002)	1.37 (0.031) 0.861 (0.028)
Ford Taurus	Cold Run	0.306 (0.007) 0.408 (0.009)	0.25 (0.005) 0.31 (0.008)	31.66 (1.86) 59.83 (1.73)	0.242 (0.004) 0.231 (0.003)	2.806 (0.085) 2.374 (0.084)
	First Hot Run	0.937 (0.014) 0.94 (0.007)	0.54 (0.005) 0.57 (0.006)	5.98 (0.11) 13.95 (0.32)	0.18 (0.002) 0.181 (0.002)	0.267 (0.013) 0.199 (0.005)
	Hard Acceleration	6.33 (0.076) 1.285 (0.029)	7.22 (0.139) 1.24 (0.025)	72.03 (3.95) 41.33 (1.68)	0.344 (0.007) 0.303 (0.005)	1.578 (0.052) 1.652 (0.052)
	Second Hot Run	3.911 (0.104) 1.353 (0.013)	2.94 (0.074) 0.96 (0.008)	19.98 (0.29) 25.79 (0.26)	0.218 (0.002) 0.213 (0.002)	0.371 (0.011) 0.619 (0.011)
	All	2.39 (0.073) 0.948 (0.014)	1.96 (0.067) 0.66 (0.01)	28.47 (1.01) 38.15 (0.85)	0.233 (0.002) 0.222 (0.002)	1.42 (0.045) 1.323 (0.041)
Ford Windstar	Cold Run	0.324 (0.007)	0.25 (0.006)	41.49 (2.29)	0.237 (0.004)	2.076 (0.039)
	First Hot Run	0.643 (0.013)	0.42 (0.005)	2.3 (0.05)	0.201 (0.002)	0.694 (0.015)
	Hard Acceleration	1.295 (0.015)	1.36 (0.02)	54.71 (2.97)	0.318 (0.005)	2.586 (0.082)

	Second Hot Run	0.847 (0.016)	0.62 (0.011)	3.61 (0.17)	0.223 (0.001)	0.856 (0.019)
	All	0.686 (0.011)	0.53 (0.01)	24.24 (1.1)	0.233 (0.002)	1.493 (0.027)
Nissan Pathfinder	Cold Run	2.532 (0.089) 1.106 (0.029)	1.41 (0.053) 0.95 (0.029)	46.75 (1.09) 62.05 (1.12)	0.179 (0.003) 0.27 (0.005)	4.892 (0.073) 5.033 (0.081)
	First Hot Run	8.173 (0.084) 3.418 (0.018)	4.06 (0.065) 2.59 (0.012)	17.84 (0.32) 23.2 (0.27)	0.154 (0.001) 0.228 (0.002)	1.811 (0.028) 1.782 (0.037)
	Hard Acceleration	15.457 (0.397) 2.207 (0.057)	13.65 (0.328) 2.46 (0.007)	89.91 (3.26) 35.06 (0.53)	0.261 (0.004) 0.372 (0.006)	7.386 (0.213) 6.432 (0.18)
	Second Hot Run	11.727 (0.302) 2.333 (0.023)	7.02 (0.175) 1.99 (0.017)	25.24 (0.25) 25.96 (0.32)	0.175 (0.001) 0.261 (0.002)	2.8 (0.04) 2.666 (0.039)
	All	8.316 (0.182) 2.099 (0.029)	5.05 (0.127) 1.75 (0.022)	40.02 (0.84) 40.11 (0.65)	0.181 (0.002) 0.269 (0.003)	3.938 (0.063) 3.826 (0.06)
Toyota Solara	Cold Run	0.709 (0.009) 0.39 (0.003)	0.48 (0.002) 0.28 (0.002)	13.79 (0.66) 17.41 (0.79)	0.206 (0.003) 0.217 (0.003)	0.807 (0.035) 1.131 (0.05)
	First Hot Run	0.61 (0.008) 0.468 (0.005)	0.35 (0.003) 0.26 (0.002)	0.37 (0) 0.48 (0.01)	0.175 (0.001) 0.169 (0.002)	0.103 (0.002) 0.103 (0.002)
	Hard Acceleration	1.049 (0.019) 0.429 (0.009)	1.1 (0.026) 0.39 (0.003)	30.03 (1.77) 17.45 (1.01)	0.305 (0.005) 0.284 (0.005)	1.777 (0.095) 1.649 (0.083)
	Second Hot Run	0.652 (0.012) 0.392 (0.005)	0.42 (0.008) 0.25 (0.003)	1.48 (0.08) 1.16 (0.05)	0.197 (0.001) 0.193 (0.002)	0.201 (0.005) 0.267 (0.005)
	All	0.716 (0.007) 0.411 (0.003)	0.51 (0.007) 0.28 (0.002)	9.5 (0.42) 9.21 (0.39)	0.207 (0.002) 0.206 (0.002)	0.609 (0.023) 0.733 (0.026)
Toyota Tacoma	Cold Run	0.471 (0.008) 0.357 (0.005)	0.31 (0.003)	17.18 (0.93) 24.36 (1.16)	0.209 (0.003)	1.013 (0.046)

		0.25 (0.003)		0.209 (0.003)	1.063 (0.058)
First Hot Run	0.764 (0.004) 0.588 (0.005)	0.41 (0.003) 0.31 (0.002)	0.87 (0.03) 2.5 (0.04)	0.166 (0.001) 0.162 (0.002)	0.086 (0.004) 0.062 (0.002)
Hard Acceleration	0.763 (0.014) 0.419 (0.006)	0.65 (0.016) 0.37 (0.002)	2.74 (0.09) 3.12 (0.09)	0.274 (0.005) 0.262 (0.005)	1.073 (0.034) 0.591 (0.024)
Second Hot Run	0.563 (0.007) 0.474 (0.005)	0.36 (0.004) 0.28 (0.002)	0.82 (0.02) 1.12 (0.01)	0.19 (0.001) 0.18 (0.001)	0.181 (0.006) 0.239 (0.006)
All	0.604 (0.005) 0.453 (0.004)	0.38 (0.004) 0.28 (0.002)	7.41 (0.41) 10.63 (0.53)	0.201 (0.002) 0.196 (0.002)	0.589 (0.021) 0.56 (0.025)

9.3.2 Real-time HNCO fuel based emission factors

To capture the dependence of HNCO emissions on the vehicle drive cycle, we calculate fuel based emission factors (FBEFs) in real time for each of the eight LDGVs in two consecutive trials. For this work we define FBEFs for HNCO as the mass of HNCO (mg) emitted per kilogram of fuel burned by the LDGVs. The FBEFs were calculated as:

$$FBEF_{HNCO} = \frac{[HNCO]}{[CO_2]} \times \frac{MW_{CO_2}}{MW_C} \times W_C \qquad \text{(E3)}$$

where [HNCO] is the mass concentration of HNCO, $[CO_2]$ is the mass concentration of CO_2, MW_{CO_2} and MW_C are the molecular weights of CO_2 and carbon, and W_C is the mass fraction of carbon in the fuel, assumed to be 0.85.[31] The FBEFs are calculated under the assumption that the carbon present in the fuel is converted to CO_2 with unit efficiency, where the contributions from other carbon species are negligible. The mass concentrations of CO_2 were calculated using the real-time CO_2 measurements made by the HR-ToF-AMS (corrected for possible particle-phase CO_2^+ signal using the LI-6262) after the SDS.

Real-time determinations of the fuel based emission factors for the duration of the drive cycle are shown in Fig. 2 for three representative LDGVs on both test days considered. Calculated fuel based emission factors are not constant during the drive cycle, but rather can vary by as much as a factor of 10, peaking during the hard acceleration phase of each vehicle's drive cycle (Fig. 2). The differences in the FBEF between the two days of testing can be attributed to variations in HNCO production resulting from varying amounts of CO and NO_x, and is discussed in the following section. The average FBEF for each of the eight LDGVs are shown in Fig. 3 for the

four phases of the drive cycle as well as averaged for overall test runs. While the absolute value of the FBEF displays vehicle-to-vehicle variability, a similar dependence on the drive cycle is observed for all vehicles, where the FBEFs reach a maximum during the hard acceleration phase and the lowest FBEF is observed during the cold start phase. For the four phases of the UC, we compute fleet averaged HNCO FBEFs of: 0.41 (±0.03) mg kg_{fuel}^{-1} (Phase 1), 0.63 (±0.05) mg kg_{fuel}^{-1} (Phase 2), 1.52 (±0.45) mg kg_{fuel}^{-1} (Phase 3), and 1.08 (±0.26) mg kg_{fuel}^{-1} (Phase 4). The LDGV tested fleet averaged HNCO FBEF for the entire drive cycle is 0.82 ± 0.15 mg kg_{fuel}^{-1}. The overall drive cycle average was calculated as the mean of the HNCO FBEFs for all of the cars for both days of testing, with the exception of the Nissan Pathfinder.

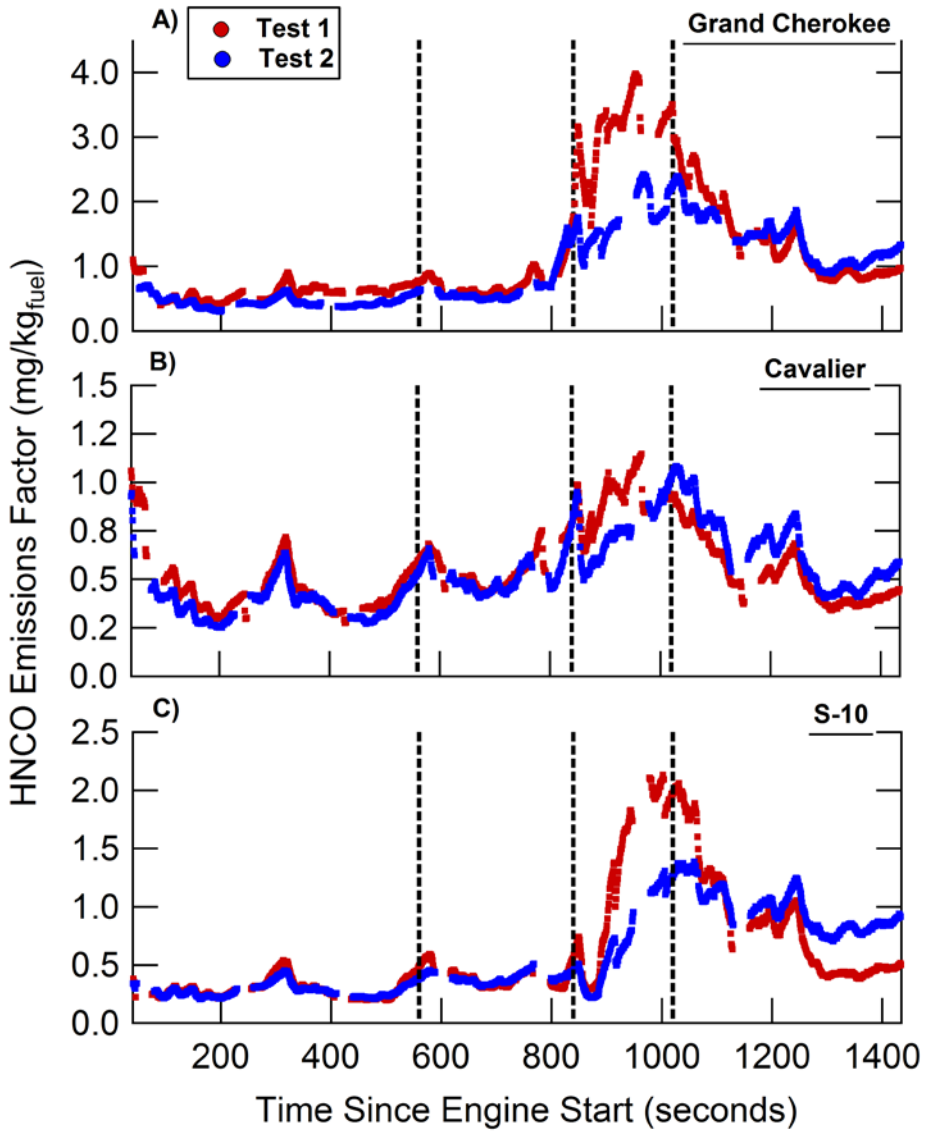

Figure 9-2: Fuel-based, real-time HNCO emissions factors for both test 1 (red) and test 2 (blue) for: A) the Chrysler Grand Cherokee, B) the Chevrolet Cavalier, and C) the Chevrolet S-10 Pickup. The dashed lines represent the divides between the four previously defined phases of the drive cycle.

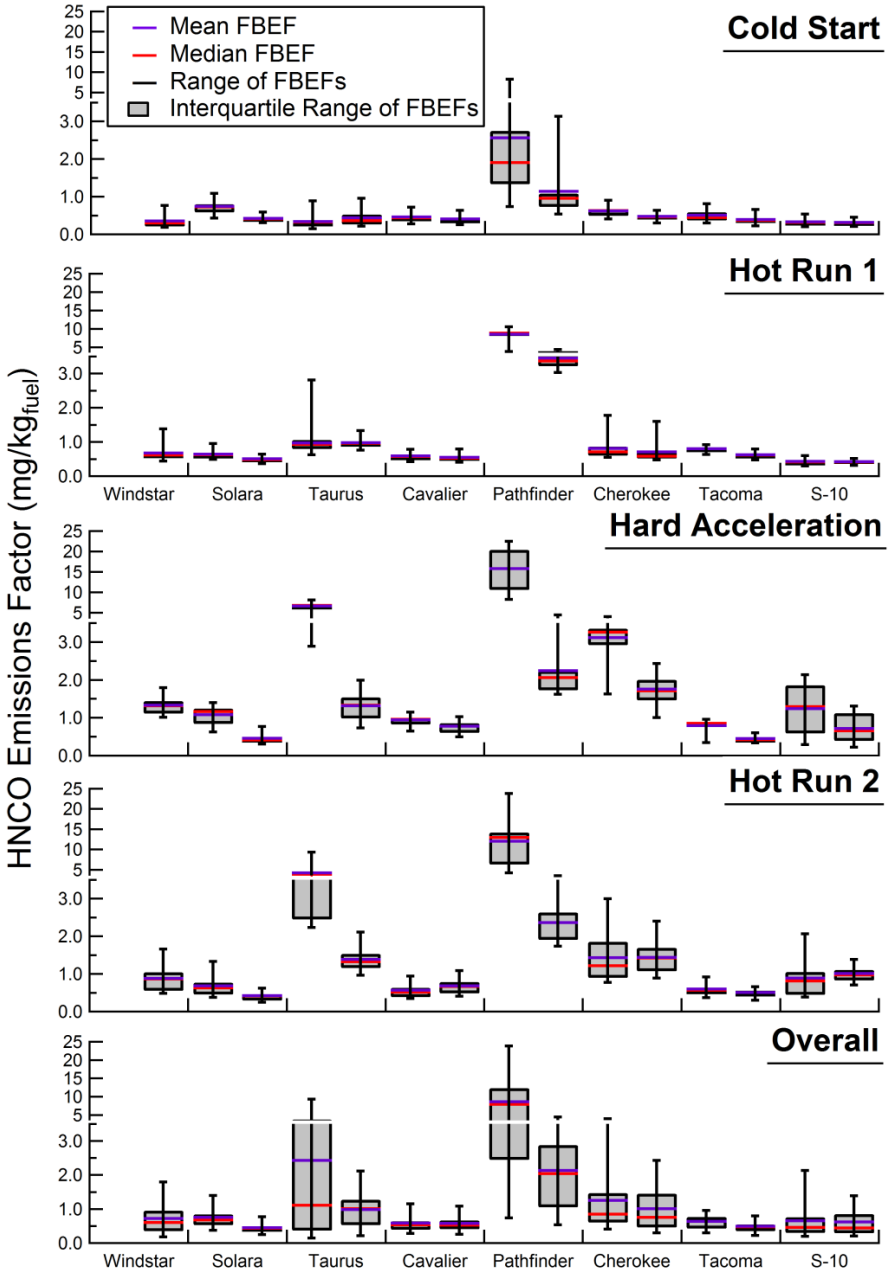

Figure 9-3: Median HNCO emissions factors (red) for both test 1 and test 2 of the eight light duty gasoline vehicles including mean FBEF (purple), the interquartile range, and the range of FBEF measured for: A) the cold start phase, B) the first hot stabilized phase, C) the hard acceleration phase, D) the second hot stabilized phase, and E) the overall test run. Fleet averages for the first test do not include contributions from the Pathfinder. Error bars represent the interquartile range.

The Nissan Pathfinder was excluded from the LDGV fleet average as the emissions were highly anomalous compared with the vehicle fleet, with elevated FBEFs (a factor of 5.4 larger on day 1 as compared with day 2) observed during all phases of the drive cycle during the first day of

testing. Further, on the second day of testing, the Pathfinder was observed to have maximum FBEF during the first hot stabilized phase and not the hard acceleration phase. At this time, we cannot confirm whether the Pathfinder itself or the measurement protocol caused the strong deviation from the fleet average state. If the Pathfinder is included, we compute fleet averaged HNCO FBEFs of the four phases as: 0.60 (±0.15) mg kg_{fuel}^{-1} (Phase 1), 1.32 (±0.52) mg kg_{fuel}^{-1} (Phase 2), 2.48 (±1.00) mg kg_{fuel}^{-1} (Phase 3), and 1.87 (±0.74) mg kg_{fuel}^{-1} (Phase 4). With the Pathfinder included, the tested fleet averaged HNCO FBEF for the entire drive cycle is 1.41 ± 0.52 mg kg_{fuel}^{-1}.

9.4 Discussion

9.4.1 Mechanisms of HNCO Production

The dependence of the HNCO emission factor on the UC provides further insight into the production mechanism of HNCO in the catalytic converter. The laboratory proxy-based studies on reactions of CO, NO, and either H_2 or NH_3 on precious metal catalysts have demonstrated that HNCO production is a complex function of the catalyst temperature and concentrations of CO, NO_x and hydrogen. As the vehicle is driven through the UC, the production of HNCO by the vehicle is expected to reflect real-time changes in each of these factors.

The fleet averaged HNCO FBEF during the cold start period of the drive cycle was 0.41 ± 0.03 mg kg_{fuel}^{-1}, a factor of 2 lower than the drive cycle average. During the cold start phase, the temperature of the catalytic converter steadily increases as the vehicle is driven through the UC cycle. The coincident increase in HNCO mixing ratio, and hence FBEF, during the cold start phase is consistent with the mechanisms illustrated in Reactions 1-8,[150-154] where the HNCO yield increases until the catalyst reaches an average temperature of 300°C (±82°C) at which point the yield of HNCO drops off as a result of limited CO coverage over the catalyst surface.[150] The local maximum in HNCO mixing ratio is achieved toward the end of the cold start phase and the FBEF decreases as the average catalytic converter temperature stabilizes at 300°C (±82°C).

As shown in Fig. 2 and 3, HNCO FBEFs are highest during the hard acceleration phase, with the fleet average FBEF 1.52 ± 0.45 mg kg_{fuel}^{-1}, a factor of 1.85 higher than the overall drive cycle average. This increase in HNCO emission is accompanied by a simultaneous increase in the concentration of CO in the exhaust, consistent with the LDGV entering into a fuel rich state as a result of the hard acceleration. When fuel rich, engine emissions have insufficient oxygen for complete conversion to CO_2, resulting in an increase in CO and the potential for a subsequent increase in the number of adsorbed CO on the precious metal catalyst surface. Previous work on model engine systems suggest a mechanism in which HNCO production is limited by the number of available adsorbed CO on the catalyst surface, with the formation of HNCO resulting from the hydrogenation of small concentrations of NCO groups under conditions of high CO coverage (R3 and R6).[150] With the increase in number of adsorbed CO on the catalyst during the hard acceleration, an increase in the yield of HNCO would be expected and is observed during our test runs.

During the second hot stabilized phase the vehicle ceases to operate under a fuel rich condition, leading to a decrease in CO emissions, and the catalyst returns to a steady-state temperature for efficient operation. Consequently, the concentration of adsorbed CO should decrease corresponding to a decrease in the yield of HNCO off the catalyst surface. This is consistent with the observed decrease in HNCO during the fourth phase of the drive cycle as the HNCO mixing ratios decline toward initial values. However, it is important to note that the production of HNCO is highly dependent not only on the CO concentration in the direct engine exhaust, but on the temperature of the catalytic converter denoted by suppressed HNCO production during the cold start phase, as well as the concentration of NO_x.

For many of the vehicles tested, NO_x and CO concentrations were not consistent between the two days of testing, permitting further assessment of the factors controlling HNCO production. For example, for the Chevrolet Cavalier there was a 45% decrease in the HNCO peak mixing ratio during the hard acceleration phase of the drive cycle on the second day of testing as compared to the first day of testing (1.56 ppbv as compared with 0.85 ppbv). This can be compared with the behavior of CO and NO_x during the same phase, with the mixing ratio of CO in the diluted vehicle exhaust being 25% larger (60 ppmv as compared with 75 ppmv), and the diluted NO_x mixing ratio being 46% smaller on the second day of testing (1.12 ppmv as compared with 0.60 ppmv). This result suggests that HNCO production for this vehicle was NO_x limited. In contrast, HNCO production from the Chevrolet S-10 during the hard acceleration phase appears to be CO limited. HNCO mixing ratios after the SDS were 50% lower (1.40 ppbv as compared with 0.70 ppbv) while diluted NO_x concentrations were 233% higher (0.06 ppmv as compared with 0.20 ppmv) on the second day of testing. The production of HNCO in the catalytic converter appears to be CO limited with the second day of testing not having adequate CO concentrations to facilitate the formation of NCO groups on the catalyst surface. Despite the higher NO_x concentrations on the second day of testing there was not a high enough concentration of adsorbed CO groups for efficient HNCO production.

The complexity of the HNCO production mechanism within the individual vehicles' catalytic converters and the dependence of the HNCO production rate on catalyst temperature, CO, and NO_x mixing ratios are illustrated in Fig. 4. The dependence of the production of HNCO on the temperature of the catalytic converter is observed with the minimal production of HNCO in the first cold start drive phase, despite high concentrations of both CO and NO_x. When the catalytic converter temperature is still cool, the production of HNCO is suppressed as CO and NO_x in the engine exhaust are not able to efficiently adsorb to the catalyst surface (R1-5) and thus inhibit the efficient formation of HNCO. However, when the catalyst is at an efficient operating temperature ($T > 300$ ˚C), high concentrations of both NO_x and CO are necessary to sustain a high yield of HNCO.

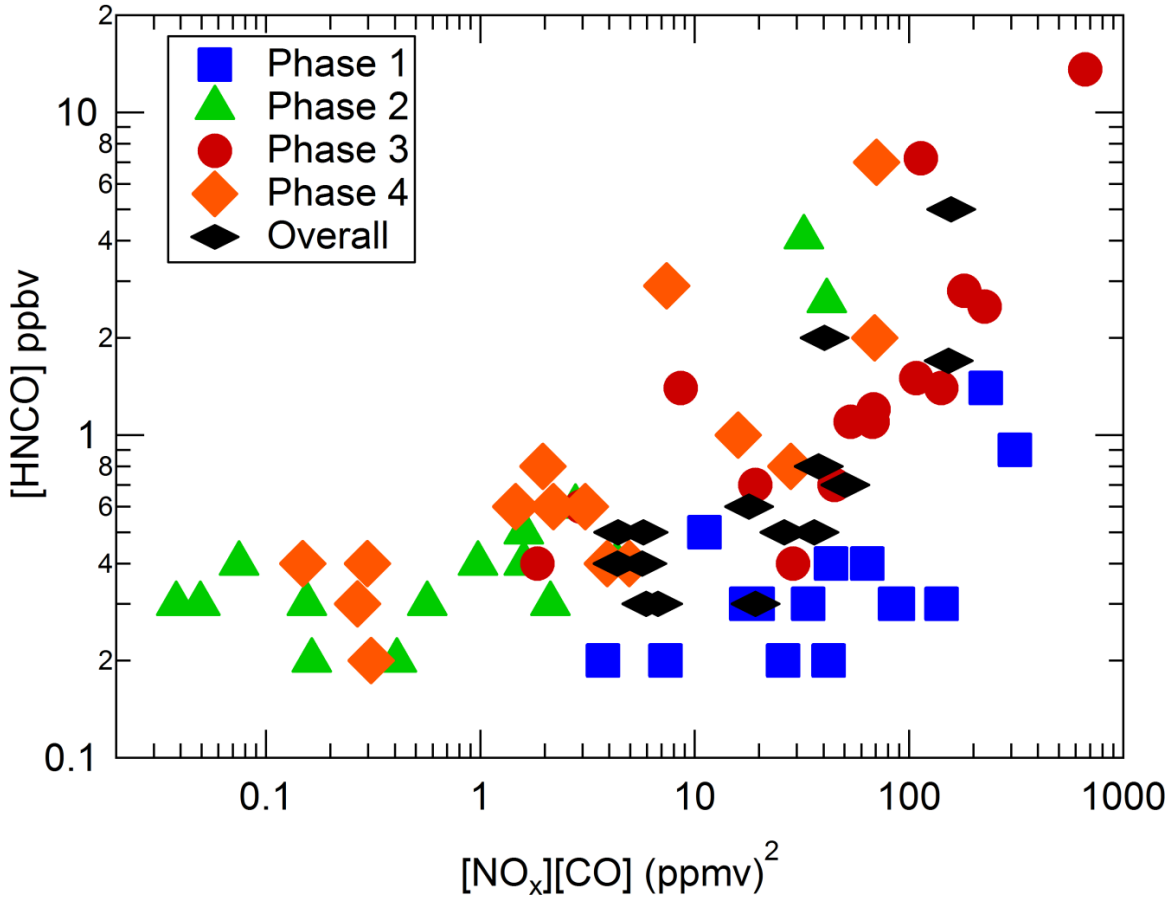

Figure 9-4: Dependence of the post-SDS average HNCO mixing ratios for the eight vehicles tested plotted vs. the product of the average loadings of NO_x and CO for both the first and second days of testing. The data are color-coded by drive phase shown in Fig. 1.

9.4.2 Comparison with previous studies HNCO vehicle emissions studies

The average fuel based emissions factors of HNCO for the LDGV fleet tested are shown in Fig. 5 alongside previously reported fuel based emissions factors for LDDVs.[145] Emission factors reported for the LDDVs were calculated from HNCO mixing ratios measured using a 2001 Volkswagen Jetta turbo diesel injection engine equipped with a diesel oxidation catalyst (DOC) run under four different steady-state driving modes.[145] The FBEF for LDGVs under the UC is approximately 3.9 times that of the LDDVs run under steady-state conditions assumed to be representative of the FTP-75 urban driving cycle (0.82 ± 0.15 mg kg_{fuel}^{-1}, vs. 0.21 ± 0.14 mg kg_{fuel}^{-1}, respectively). The precious metal catalysts in a typical diesel oxidation catalyst are usually either platinum or palladium,[145] similar to that of a TWC in the tested LDGVs, and we would expect HNCO production to have a strong dependence on the availability of adsorbed CO. Since the typical diesel engine operates under lean burn conditions the concentration of CO in the direct engine exhaust is significantly lower for LDDVs when compared to LDGVs. With the

higher direct CO emissions from the gasoline engine we would expect LDGVs to produce relatively higher concentrations of HNCO than LDDVs when driving under similar conditions assuming the converters are of a comparable size and oxide washcoat composition.

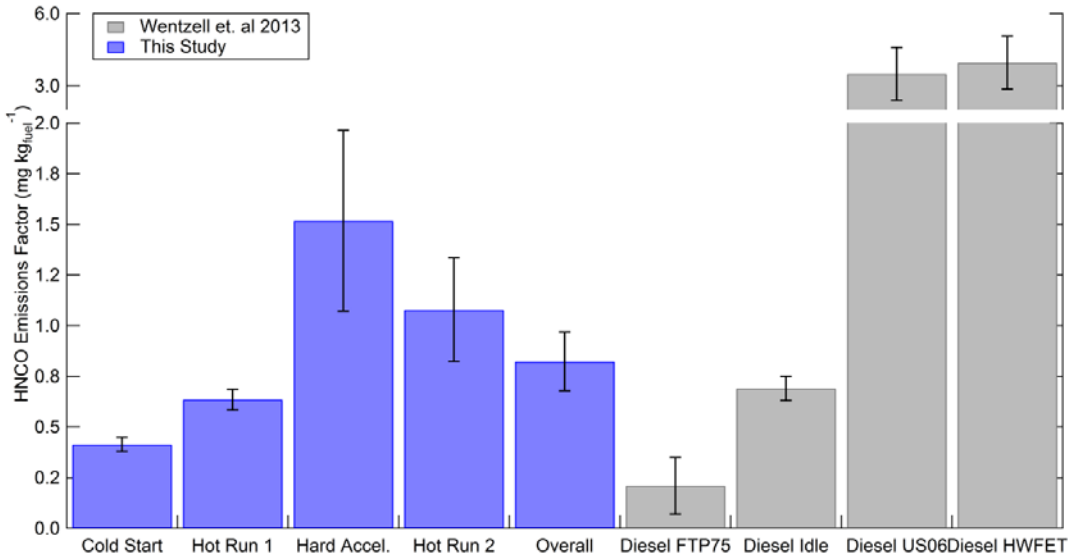

Figure 9-5: Comparison of the mean light duty gasoline vehicle HNCO emissions for the overall Unified Cycle (UC) and the four respective phases of the UC (blue) to the emission factors determined by Wentzel et al. for a light duty diesel engine operating under steady state conditions representative of the FTP75, USO6 and HWFET drive cycles and the engine running under idling conditions (grey).[8] Error bars represent standard deviations of the mean value reported. The y-axis is depicted with a split scale, the first from 0-2 mg kg_{fuel}^{-1} and second from 2-6 mg kg_{fuel}^{-1}.

The variability in the calculated FBEFs for the LDGVs throughout the drive cycle (Fig. 5) suggests that FBEFs determined under steady-state testing conditions may underestimate the true average HNCO emission factor in urban regions as they do not capture accelerations. The fleet averaged FBEF for the hard acceleration phase was 1.52 ± 0.44 mg kg_{fuel}^{-1} a factor of ca. 3.7 larger than that observed during the cold start (0.41 ± 0.03 mg kg_{fuel}^{-1}). As a result, the fleet average FBEF for the entire drive cycle (0.82 ± 0.15 mg kg_{fuel}^{-1}) is higher than that observed during the steady-state hot run phases. As such, calculating FBEFs from one representative engine state may not fully capture the range in HNCO production rates or accurately represent the typical emissions of HNCO in urban areas.

10 SUMMARY AND CONCLUSIONS

A sequence of measurements were conducted on the exhaust from light duty gasoline vehicles with the goal to better understand the volatility and partitioning mechanisms of the POA emissions at atmospherically relevant concentrations. Three main hypotheses were tested as a part of this effort:

1. The concentration of EC in the background dilution air changes the partitioning of individual organic compounds in the exhaust emitted from gasoline and diesel engines.

Result: This hypothesis is rejected because the action of EC was opposite to the expected trend based on simple adsorption theory of carbonyl species. EC added to the dilution air scavenged VOC precursors for carbonyl species which generally inhibited the production of individual carbonyl compounds in the exhaust. Increasing the EC concentrations decreased the partitioning of carbonyl compounds to the condensed phase via the classic adsorption mechanism.

2. The relative humidity of the background dilution air changes the partitioning of individual organic compounds in the exhaust emitted from gasoline and diesel engines.

Result: The measurements made during the project are consistent with this hypothesis. Increasing RH in the dilution air increased the total (=gas+particle phase) emissions rate of carbonyl species by providing larger aqueous reaction volumes for carbonyl production. The net effect was an increase in carbonyl emissions rates in the particle phase.

3. The OA in motor vehicle exhaust does not behave like a completely semi-volatile material when comparing to a base-case derived from reasonable dilution factors so that concentrations are at atmospherically relevant levels (10-30 $\mu g\ m^{-3}$).

Result: The measurements made during the project are consistent with this hypothesis. Evidence suggests that POA emissions from light duty gasoline vehicles are composed of intermediate volatility (motor oil) and low volatility (fuel combustion products) material. The low volatility material will not evaporate under realistic atmospheric conditions.

The following additional conclusions are offered based on the measurements and analysis conducted during the course of the project.

10.1 Real-time Black Carbon Emission Factor Measurements from Light Duty Vehicles

During September of 2011 a suite of real-time instruments was used to sample vehicle emissions at the California Air Resources Board Haagen-Schmidt facility in El Monte, CA. A fleet of 8 on-road, spark-ignition gasoline vehicles were tested on a chassis dynamometer and were driven on the Unified Drive Cycle (UC). The emissions were sampled into the facility's standard CVS tunnel and further diluted to atmospherically relevant levels (2-30 $\mu g/m^3$) in a custom secondary dilution system. The UC includes a cold start phase followed by a hot stabilized running phase. In addition, a light-duty gasoline LEV vehicle and ultra-low emission vehicle (ULEV), and a

light-duty diesel passenger vehicle and gasoline direct injection (GDI) vehicle were tested on a constant velocity driving cycle. A variety of instruments with response times ≥ 0.1 Hz were used to characterize how the emissions of the major PM components varied for the LEVs during a typical driving cycle. These measurements allowed for the determination of BC emission factors throughout the driving cycle, providing insights into the temporal variability of BC emission factors during different phases of a typical driving cycle. Emission of BC was much greater during the cold-start period relative to the hot running period, by factors of 3-20, likely reflecting differences in engine conditions. The average BC emission factor was 5.2 mg kg^{-1}. This is substantially smaller than mean and median emission factors measured for on-road vehicles. The average BC/TC (or EC/TC) ratio was 0.75 and was slightly larger during the cold start period compared to the hot running phase, indicating that the emitted particles were dominated by BC.

10.2 Gas-phase CO2 Subtraction for Improved Measurements of Organic Aerosol Mass Concentration and Oxidation Degree by Aerosol Mass Spectrometer

The Aerodyne Aerosol Mass Spectrometer (AMS) has been widely used for real-time characterization of the size-resolved chemical composition of aerosol particles. The first step in AMS sampling is the pre-concentration of aerosols while stripping away the gas-phase components which contributes to the high sensitivity of this instrument. Although the strength of the instrument lies in particle phase measurement, ion signals generated from gas-phase species can influence the interpretation of the particle-phase chemistry data. Methods were developed for subtracting the varying contributions of gas-phase carbon dioxide (CO_2) in the AMS spectra of aerosol particles, which is critical for determining the mass concentration and the oxygen-to-carbon (O/C) ratio of organic aerosol. The method has been demonstrated on a data set acquired from sampling of fresh and diluted vehicle emissions. Three different methods were tested: 1) co-located continuous gas phase CO_2 measurement coupled with periodic filter tests, 2) positive matrix factorization (PMF) analysis to separate gas-phase and particle phase signal of CO_2^+ at *m/z* 44, and 3) use of the particle time-of-flight (PTOF) size-resolved chemical information for separation of gas-phase and particle-phase signal at *m/z* 44. Our results indicate that these three different approaches yield internally consistent values for the gas/particle apportionment of *m/z* 44, but methods 2 and 3 require certain conditions to be met to yield reliable results. The methods presented are applicable to any situation where gas-phase components may influence the PM signal of interest.

10.3 Characterizing PM Emissions from Vehicles: Dynamometer Testing with a High Resolution Aerosol Mass Spectrometer

An Aerodyne High Resolution Time-of-Flight Aerosol Mass Spectrometer (HR-ToF-MS) was used to characterize the non-refractory organic and inorganic particulate matter (PM) emitted from light duty gasoline-powered vehicles at 10 second averaging and provided information on the real-time behavior of vehicle PM emissions. It was found that the mass loading of organic PM was strongly affected by the drive cycle conditions, such as accelerations or due to the cold-start phase, and although the vehicles responded in similar ways their overall loading could vary significantly by vehicle. The chemistry of vehicle organic PM emissions was extensively characterized and it was found to be influenced by overall PM mass loading, where the oxygen to carbon (O/C) ratio tended to increase at lower loading. The resulting averaged mass spectrum from all vehicles tested was also compared to those of hydrocarbon-like organic aerosol (HOA)

observed in ambient air and the agreement is very high. The results of these tests offer the vehicle emissions community a first time glimpse at the real-time chemical composition and variation of vehicle PM emissions for a variety of conditions and vehicle types at atmospherically relevant conditions and without chemical interferences from other primary or secondary aerosol sources.

10.4 Volatility of Primary Organic Aerosol Emitted from Light Duty Gasoline Vehicles

A partitioning model based on a single volatility distribution similar to motor oil roughly explains the median partitioning behavior of POA emitted from a fleet of 8 light duty gasoline motor vehicles but the error in the model fit is unacceptably large (R^2=0.52). A model incorporating two volatility distributions – one similar to motor oil and one composed largely of non-volatile material – explains the measured behavior of the POA volatility much more accurately (R^2=0.94). The two volatility distributions can be interpreted as motor oil with intermediate volatility and fuel combustion products with low volatility. Of the 8 vehicles in the test fleet, 4 vehicles emitted POA predominantly composed of motor oil and 4 vehicles emitted POA predominantly composed of fuel combustion products. Motor oil emissions were generally highest during the cold-start portion of the UC driving cycle with reduced emissions rates during the phases when the engine and emissions control equipment reached operating temperature. Emissions of POA associated with fuel combustion products were roughly equal during all segments of the driving cycle. A larger fleet of vehicles should be tested to determine accurate rates for motor oil and fuel combustion POA emissions for the fleet of light duty gasoline vehicles in California.

10.5 Effect of Dilution Air Temperature, Humidity, and Black Carbon Concentrations on the Gas-Particle Partitioning of Carbonyl Emissions from Gasoline-fueled Motor Vehicles

Organic carbon emissions from light duty gasoline vehicles diluted by a factor of ~60 and aged in the dark for 1.2 min continue to undergo chemical reactions that are influenced by changes to temperature, humidity, and the presence of background concentrations of black carbon in the dilution air. Total carbonyl emissions generally increased as relative humidity increased, suggesting production via an aqueous phase mechanism. Concentrations of total carbonyl emissions generally decreased as black carbon was added to the dilution air most likely because the black carbon scavenged the precursor species for carbonyl production. Temperature had a weak impact on total carbonyl production rates under the current experimental design. Concentrations of total (=gas+particle phase) carbonyls decreased in 2011 vs. 2002 for comparable vehicle fleets, most likely due to changes in summer blend gasoline composition in California.

10.6 Effect of Dilution Air Temperature, Humidity, and Black Carbon Concentrations on the Gas-Particle Partitioning of Carbonyl Emissions from Gasoline-fueled Motor Vehicles

Between 2011 and 2002, gas phase carbonyl emission rates from light duty gasoline vehicles decreased by 57% (from 4.8 mg/L to 2.1 mg/L) and the particle phase carbonyl emission rate increased by 133% (from 0.3 mg/L to 0.7 mg/L). Much of the trend for increasing particle-phase emissions is associated with additional transfer of gas-phase aliphatic species to the condensed phase. Particle-phase carbonyl species accounted for 28% of total OC in the current study under basecase conditions, compared to 18% of OC in 2002. Increasing RH from 55% to 85% increased particle-phase carbonyl concentrations by 43% and gas-phase carbonyl concentrations by 5%, consistent with the hypothesis of an aqueous phase production mechanism for carbonyl species. Increasing concentrations of black carbon in the dilution air decreased particle-phase carbonyl concentrations by 39% and gas-phase carbonyl concentrations by 33%, consistent with the hypothesis that the black carbon scavenges the carbonyl precursors, preventing them from entering the aqueous phase. Temperature perturbations up to 100^{o}C had little effect on the partitioning of carbonyl species, consistent with the hypothesis that these compounds do not partition to the condensed phase via classic absorption into an OC absorbing matrix.

10.7 On the Primary Emission of Organic Acids from Light Duty Gasoline Vehicles and Ocean-going Vessels

Organic acids comprise a significant fraction of secondary organic aerosol and contribute to the acidification of the aerosol phase. Despite the importance of organic acids in atmospheric chemistry, direct measurements of the source strengths for many organic acids are limited. Direct measurements of the fuel-based emission ratios of C1-C10 gas-phase organic acids from both light duty gasoline vehicles and ocean-going vessels were used to provide constraints on primary emissions of organic acids to the atmosphere. The average fuel-based gas-phase organic acid emission factors for light duty gasoline vehicles display a strong dependence on the organic acid chain length, where formic acid emission factors are as high as 0.8 mg/kg$_{fuel}$ while the emission factors for gas-phase C4 or larger organic acids were observed to be less than 0.02 mg/kg$_{fuel}$. Measurements of the enhancement in organic acid mixing ratio following heating of the inlet air stream suggest that organic acids in primary vehicle exhaust are concentrated in the gas phase, a likely result of the acidity of primary aerosol particles. Our observations, when compared with the magnitude of secondary organic acid production rates, suggest that primary emissions of organic acids contribute less than 1% (for formic acid) to global, annual average sources.

10.8 Real-time emission factor measurements of isocyanic acid from light duty gasoline vehicles

Exposure to gas-phase isocyanic acid (HNCO) has been associated with the development of atherosclerosis, cataracts and rheumatoid arthritis. Known sources of HNCO to the atmosphere include biomass burning, coal combustion, and light duty diesel engine emissions. Laboratory measurements using idealized three-way catalytic converters suggest that HNCO is produced at high yield, but efficiently hydrolyzed in the pores of the catalytic converter on the oxide washcoat, such that negligible HNCO emission from vehicles equipped with three-way catalytic converters is expected. However, this has not been verified for light duty gasoline vehicles operated under real world conditions. In the present study, the first measurements of real-time

emission factors of isocyanic acid from a representative fleet of eight light duty gasoline-powered vehicles (LDGVs) were presented. HNCO emissions were observed from all vehicles, in contrast to the idealized laboratory measurements. Fleet averaged HNCO emission factors, which depend strongly on the phase of the drive cycle; ranged from 0.41 ± 0.03 mg kg_{fuel}^{-1} during engine start to 1.52 ± 0.45 mg kg_{fuel}^{-1} during hard acceleration after the engine and catalytic converter were warm. The tested 8-car fleet average fuel based HNCO emission factor was 0.82 ± 0.15 mg kg_{fuel}^{-1}, within the range previously estimated for light duty diesel-powered vehicles (0.21-3.96 mg kg_{fuel}^{-1}). Our results suggest that HNCO emissions from LDGVs represent a significant emission source in urban areas that should be accounted for in global and regional models.

10.9 Future research

Measurements of POA emissions attributable to motor oil and fuel combustion are needed for a representative fleet of light duty gasoline vehicles in California. The 15 vehicles characterized to date suggest that emissions vary widely and a fleet of at least 100 vehicles should be considered in this analysis.

Discrepancies between POA emissions measurements made using AMS and traditional filter-based thermal optical measurements should be reconciled. A clearer understanding on this issue is needed to avoid misinterpretation of results in current and future studies.

11 REFERENCES

1. Shrivastava, M.K., et al., *Modeling semivolatile organic aerosol mass emissions from combustion systems.* Environmental Science & Technology, 2006. **40**(8): p. 2671-2677.
2. Kroll, J.H. and J.H. Seinfeld, *Chemistry of secondary organic aerosol: Formation and evolution of low-volatility organics in the atmosphere.* Atmospheric Environment, 2008. **42**(16): p. 3593-3624.
3. Volkamer, R., et al., *Secondary organic aerosol formation from anthropogenic air pollution: Rapid and higher than expected.* Geophysical Research Letters, 2006. **33**(17).
4. Grieshop, A.P., et al., *Constraining the Volatility Distribution and Gas-Particle Partitioning of Combustion Aerosols Using Isothermal Dilution and Thermodenuder Measurements.* Environmental Science & Technology, 2009. **43**(13): p. 4750-4756.
5. Jakober, C.A., et al., *Carbonyl emissions from gasoline and diesel motor vehicles.* Environmental Science & Technology, 2008. **42**(13): p. 4697-4703.
6. Kleeman, M.J., et al., *Lubricating oil and fuel contributions to particulate matter emissions from light-duty gasoline and heavy-duty diesel vehicles.* Environmental Science & Technology, 2008. **42**(1): p. 235-242.
7. Riddle, S.G., et al., *Size distribution of trace organic species emitted from light-duty gasoline vehicles.* Environmental Science & Technology, 2007. **41**(21): p. 7464-7471.
8. Robert, M.A., et al., *Size and composition distributions of particulate matter emissions: Part 1 - Light-duty gasoline vehicles.* Journal of the Air & Waste Management Association, 2007. **57**(12): p. 1414-1428.
9. Chen, J., et al., *Theoretical versus Observed Gas-Particle Partitioning of Carbonyl Emissions from Motor Vehicles.* Journal of the Air and Waste Management Association, 2010. **60**: p. 1237-1244.
10. Dockery, D.W., et al., *Association of air pollution with increased incidence of ventricular tachyarrhythmias recorded by implanted cardioverter defibrillators.* Environmental Health Perspectives, 2005. **113**(6): p. 670-674.
11. Watson, J.G., *Visibility: Science and regulation.* Journal of the Air & Waste Management Association, 2002. **52**(6): p. 628-713.
12. Bond, T.C., et al., *Bounding the role of black carbon in the climate system: A scientific assessment.* Journal of Geophysical Research: Atmospheres, 2013. **118**(11): p. 5380-5552.
13. Lohmann, U. and J. Feichter, *Global indirect aerosol effects: a review.* Atmospheric Chemistry and Physics, 2005. **5**: p. 715-737.
14. Board, C.A.R., *California Air Resources Board. LEV III PM: Technical Support Document; Development of Partiuclate Matter Mass Standards for Future Light-Duty Vehicles. Appendix P.* . 2012, P1-165; http://www.arb.ca.gov/regact/2012/leviighg2012/levappp.pdf.
15. Mohr, M., A.M. Forss, and U. Lehmann, *Particle emissions from diesel passenger cars equipped with a particle trap in comparison to other technologies.* Environmental Science & Technology, 2006. **40**(7): p. 2375-2383.
16. Graham, L., *Chemical characterization of emissions from advanced technology light-duty vehicles.* Atmospheric Environment, 2005. **39**(13): p. 2385-2398.

17. Agency, U.S.E.P., *Kansas City PM Characterization Study. Final Report, EPA420-R-08-009. Assessment and Standards Division Office of Transportation and Air Quality* U.S. Environmental Protection Agency Ann Arbor, MI, EPA Contract No. GS 10F-0036K, October 27, 2006, revised April 2008a by EPA staff; http://www.epa.gov/oms/emissionfactors-research/420r08009.pdf.
18. Fujita, E.M., et al., *Variations in Speciated Emissions from Spark-Ignition and Compression-Ignition Motor Vehicles in California's South Coast Air Basin.* Journal of the Air & Waste Management Association, 2007. **57**(6): p. 705-720.
19. Stipe, C.B., et al., *Inverted co-flow diffusion flame for producing soot.* Review of Scientific Instruments, 2005. **76**(2).
20. Langridge, J.M., et al., *Aircraft Instrument for Comprehensive Characterization of Aerosol Optical Properties, Part I: Wavelength-Dependent Optical Extinction and Its Relative Humidity Dependence Measured Using Cavity Ringdown Spectroscopy.* Aerosol Science and Technology, 2011. **45**(11): p. 1305-1318.
21. Lack, D.A., et al., *Aircraft Instrument for Comprehensive Characterization of Aerosol Optical Properties, Part 2: Black and Brown Carbon Absorption and Absorption Enhancement Measured with Photo Acoustic Spectroscopy.* Aerosol Science and Technology, 2012. **46**(5): p. 555-568.
22. Bond, T.C. and R.W. Bergstrom, *Light absorption by carbonaceous particles: An investigative review.* Aerosol Science and Technology, 2006. **40**(1): p. 27-67.
23. Cross, E.S., et al., *Soot Particle Studies—Instrument Inter-Comparison—Project Overview.* Aerosol Science and Technology, 2010. **44**(8): p. 592-611.
24. DeCarlo, P.F., et al., *Field-Deployable, High-Resolution, Time-of-Flight Aerosol Mass Spectrometer.* Analytical Chemistry, 2006. **78**(24): p. 8281-8289.
25. Allan, J.D., et al., *Quantitative sampling using an Aerodyne aerosol mass spectrometer - 1. Techniques of data interpretation and error analysis.* Journal of Geophysical Research-Atmospheres, 2003. **108**(D3).
26. McLafferty, F.W., and F. Turecek, *Interpretation of Mass Spectra*. 1993, Mill Valley, California.: University Science Books.
27. States, U., in *Exhaust gas analytical system, 2005; Code of Federal Regulations, Title 40, Chapter I, Subchapter C, Part 86, Subpart B, Section 86.111-94. 10.* .
28. Chow, J.C., et al., *The IMPROVE_A temperature protocol for thermal/optical carbon analysis: maintaining consistency with a long-term database.* Journal of the Air & Waste Management Association, 2007. **57**(9): p. 1014-1023.
29. Schauer, J.J., et al., *ACE-Asia intercomparison of a thermal-optical method for the determination of particle-phase organic and elemental carbon.* Environmental Science & Technology, 2003. **37**(5): p. 993-1001.
30. Chow, J.C., et al., *The IMPROVE-A temperature protocol for thermal/optical carbon analysis: maintaining consistency with a long-term database.* Journal of the Air & Waste Management Association, 2007. **57**(9): p. 1014-1023.
31. Kirchstetter, T.W., et al., *On-road measurement of fine particle and nitrogen oxide emissions from light- and heavy-duty motor vehicles.* Atmospheric Environment, 1999. **33**(18): p. 2955-2968.
32. Fujita, E.M., et al., *Variations in speciated emissions from spark-ignition and compression-ignition motor vehicles in California's south coast air basin.* Journal of the Air & Waste Management Association, 2007. **57**(6): p. 705-720.

33. Schauer, J.J., et al., *Impact of ambient temperatures and driving conditions on the chemical composition of particulate matter emissions from non-smoking gasoline-powered motor vehicles.* Aerosol Science and Technology, 2008. **42**(3): p. 210-223.
34. Kittelson, D.B., et al., *On-road and laboratory evaluation of combustion aerosols - Part 2: Summary of spark ignition engine results.* Journal of Aerosol Science, 2006. **37**(8): p. 931-949.
35. Agency, U.S.E.P., *Guidance on the Use of Models and Other Analyses for Demonstrating Attainment of Air Quality Goals for Ozone, PM2.5, and Regional Haze.* . EPA -454/B-07-002. Office of Air Quality Planning and Standards U.S. Environmental Protection Agency Research Triangle Park, NC, 2007; http://www.epa.gov/scram001/guidance/guide/final-03-pm-rh-guidance.pdf.
36. Cadle, S.H., et al., *Composition of light-duty motor vehicle exhaust particulate matter in the Denver, Colorado area.* Environmental Science & Technology, 1999. **33**(14): p. 2328-2339.
37. Zielinska, B., et al., *Emission Rates and Comparative Chemical Composition from Selected In-Use Diesel and Gasoline-Fueled Vehicles.* Journal of the Air & Waste Management Association, 2004. **54**(9): p. 1138-1150.
38. Durbin, T.D., et al., *Particulate emission rates from light-duty vehicles in the South Coast air quality management district.* Environmental Science & Technology, 1999. **33**(24): p. 4401-4406.
39. Lipsky, E.M. and A.L. Robinson, *Effects of dilution on fine particle mass and partitioning of semivolatile organics in diesel exhaust and wood smoke.* Environmental Science & Technology, 2006. **40**(1): p. 155-162.
40. Ning, Z., et al., *Emission factors of PM species based on freeway measurements and comparison with tunnel and dynamometer studies.* Atmospheric Environment, 2008. **42**(13): p. 3099-3114.
41. Strawa, A.W., et al., *Optical and physical properties of primary on-road vehicle particle emissions and their implications for climate change.* Journal of Aerosol Science, 2010. **41**(1): p. 36-50.
42. Grieshop, A.P., et al., *Fine particle emission factors from vehicles in a highway tunnel: Effects of fleet composition and season.* Atmospheric Environment, 2006. **40**: p. S287-S298.
43. Sonntag, D.B., et al., *Contribution of Lubricating Oil to Particulate Matter Emissions from Light-Duty Gasoline Vehicles in Kansas City.* Environmental Science & Technology, 2012. **46**(7): p. 4191-4199.
44. Rogge, W.F., et al., *Sources of fine organic aerosol .3. road dust, tire debris, and organometallic brake lining dust - roads as sources and sinks.* Environmental Science & Technology, 1993. **27**(9): p. 1892-1904.
45. Maricq, M.M., J.J. Szente, and K. Jahr, *The Impact of Ethanol Fuel Blends on PM Emissions from a Light-Duty GDI Vehicle.* Aerosol Science and Technology, 2012. **46**(5): p. 576-583.
46. Myung, C.-L., et al., *Comparative study of engine control strategies for particulate emissions from direct injection light-duty vehicle fueled with gasoline and liquid phase liquefied petroleum gas (LPG).* Fuel, 2012. **94**(1): p. 348-355.

47. Geller, M.D., et al., *Physicochemical and redox characteristics of particulate matter (PM) emitted from gasoline and diesel passenger cars.* Atmospheric Environment, 2006. **40**(36): p. 6988-7004.
48. Liggio, J., et al., *Are Emissions of Black Carbon from Gasoline Vehicles Underestimated? Insights from Near and On-Road Measurements.* Environmental Science & Technology, 2012. **46**(9): p. 4819-4828.
49. Park, S.S., et al., *Emission factors for high-emitting vehicles based on on-road measurements of individual vehicle exhaust with a mobile measurement platform.* Journal of the Air & Waste Management Association, 2011. **61**(10): p. 1046-1056.
50. Miguel, A.H., et al., *On-road emissions of particulate polycyclic aromatic hydrocarbons and black carbon from gasoline and diesel vehicles.* Environmental Science & Technology, 1998. **32**(4): p. 450-455.
51. Geller, V.D., et al., *Measurements of particle number and mass concentrations and size distributions in a tunnel environment.* Environmental Science & Technology, 2005. **39**(22): p. 8653-8663.
52. Co, R.L.P. *Polk Finds More Vehicles Scrapped than Added to Fleet.* . 2010 March 20, 2013]; Available from: https://www.polk.com/company/news/polk_finds_more_vehicles_scrapped_than_added_to_fleet.
53. Agency, U.S.E.P., *Light-Duty Automotive Technology, Carbon Dioxide Emissions, and Fuel Economy Trends: 1975 Through 2011. Final Report, EPA-420-R-12-001.* . Transportation and Climate Division, Office of Transportation and Air Quality, U.S. Environmental Protection Agency, March 2012.
54. Canagaratna, M.R., et al., *Chemical and microphysical characterization of ambient aerosols with the aerodyne aerosol mass spectrometer.* Mass Spectrometry Reviews, 2007. **26**(2): p. 185-222.
55. Jimenez, J.L., et al., *Ambient aerosol sampling using the Aerodyne Aerosol Mass Spectrometer.* Journal of Geophysical Research: Atmospheres, 2003. **108**(D7): p. 8425.
56. Allan, J.D., et al., *Technical Note: A generalised method for the extraction of chemically resolved mass spectra from Aerodyne aerosol mass spectrometer data.* Journal of Aerosol Science, 2004. **35**: p. 909-922.
57. Alfarra, M.R., et al., *Characterization of urban and regional organic aerosols in the lower Fraser Valley using two Aerodyne Aerosol Mass Spectrometers.* Atmospheric Environment, 2004. **38**: p. 5745–5758.
58. Allan, J.D., et al., *Quantitative sampling using an Aerodyne Aerosol Mass Spectrometer. Part 1: Techniques of data interpretation and error analysis.* Journal of Geophysical Research-Atmospheres, 2003. **108**(D3): p. 4090.
59. Herndon, S.C., et al., *Real-time measurements of SO2, H2CO, and CH4 emissions from in-use curbside passenger buses in New York City using a chase vehicle.* Environmental Science & Technology, 2005. **39**(20): p. 7984-7990.
60. Jayne, J.T., et al., *Development of an Aerosol Mass Spectrometer for Size and Composition Analysis of Submicron Particles.* Aerosol Science and Technology, 2000. **33**(1-2): p. 49-70.
61. Zhang, Q., et al., *Time- and size-resolved chemical composition of submicron particles in Pittsburgh: Implications for aerosol sources and processes.* J. Geophys. Res., 2005. **110**(D7): p. D07S09.

62. Zhang, Q., et al., *Insights into the Chemistry of New Particle Formation and Growth Events in Pittsburgh Based on Aerosol Mass Spectrometry.* Environmental Science & Technology, 2004. **38**(18): p. 4797-4809.
63. Aiken, A.C., P.F. DeCarlo, J.H. Kroll, D.R. Worsnop, J.A. Huffman, K. Docherty, I.M. Ulbrich, C. Mohr, J.R. Kimmel, D. Sueper, Q. Zhang, Y. Sun, A. Trimborn, M. Northway, P.J. Ziemann, M.R. Canagaratna, T.B. Onasch, R. Alfarra, A.S.H. Prevot, J. Dommen, J. Duplissy, A. Metzger, U. Baltensperger, and J.L. Jimenez, *O/C and OM/OC Ratios of Primary, Secondary, and Ambient Organic Aerosols with High Resolution Time-of-Flight Aerosol Mass Spectrometry.* Environmental Science & Technology, 2008. **42**: p. 4478–4485.
64. Setyan, A., Zhang, Q., Merkel, M., Knighton, W. B., Sun, Y., Song, C., Shilling, J. E., Onasch, T. B., Herndon, S. C., Worsnop, D. R., Fast, J. D., Zaveri, R. A., Berg, L. K., Wiedensohler, A., Flowers, B. A., Dubey, M. K., Subramanian, R., *Characterization of submicron particles influenced by mixed biogenic and anthropogenic emissions using high-resolution aerosol mass spectrometry: results from CARES.* Atmos. Chem. Phys., 2012. **12**(17): p. 8131-8156.
65. Paatero, P. and U. Tapper, *Positive matrix factorization: A non-negative factor model with optimal utilization of error estimates of data values.* Environmetrics, 1994. **5**: p. 111-126.
66. Kittelson, D.B., et al., *On-road and laboratory evaluation of combustion aerosols—Part 2:: Summary of spark ignition engine results.* Journal of Aerosol Science, 2006. **37**(8): p. 931-949.
67. Maricq, M.M. and H. Maldonado, *Directions for Combustion Engine Aerosol Measurement in the 21st Century.* Journal of the Air & Waste Management Association, 2010. **60**(10): p. 1165-1176.
68. Schneider, J., et al., *Mass spectrometric analysis and aerodynamic properties of various types of combustion-related aerosol particles.* International Journal of Mass Spectrometry, 2006. **258**(1–3): p. 37-49.
69. Tobias, H.J.B., D.E.; Ziemann, P.J., *Chemical Analysis of Diesel Engine Nanoparticles Using a Nano-DMA/Thermal Desorption Particle Beam Mass Spectrometer*. Environmental Science & Technology, 2001. **35**: p. 2233-2243.
70. Michael A. Robert, S.V., and Michael J. Kleeman, Christopher A. Jakober, *Size and Composition Distributions of Particulate Matter Emissions: Part 1— Light-Duty Gasoline Vehicles.* Journal of the Air & Waste Management Association, 2007. **57**: p. 1-15.
71. Zhang, Q., et al., *Understanding atmospheric organic aerosols via factor analysis of aerosol mass spectrometry: a review.* Anal. Bioanal Chem, 2011. **401**: p. 3045-3067.
72. Ulbrich, I.M., Canagaratna, M. R., Zhang, Q., Worsnop, D. R., and Jimenez, J. L., *Interpretation of organic components from Positive Matrix Factorization of aerosol mass spectrometric data.* Atmos. Chem. Phys., 2009. **9**(9): p. 2891-2918.
73. Zhang, Q., et al., *Hydrocarbon-like and oxygenated organic aerosols in Pittsburgh: Insights into sources and processes of organic aerosols.* Atmos. Chem. Phys., 2005. **5**: p. 3289-3311.
74. Mohr, C., et al., *Characterization of Primary Organic Aerosol Emissions from Meat Cooking, Trash Burning, and Motor Vehicles with High-Resolution Aerosol Mass*

Spectrometry and Comparison with Ambient and Chamber Observations. Environmental Science & Technology, 2009. **43**: p. 2443-2449.
75. Zhang, Q., et al., *Ubiquity and dominance of oxygenated species in organic aerosols in anthropogenically-influenced Northern Hemisphere midlatitudes.* Geophysical Research Letters, 2007. **34**(13): p. L13801.
76. Robinson, A.L., et al., *Rethinking Organic Aerosols: Semivolatile Emissions and Photochemical Aging.* Science, 2007. **315**(5816): p. 1259-1262.
77. Riddle, S.G., et al., *Large PAHs detected in fine particulate matter emitted from light-duty gasoline vehicles.* Atmospheric Environment, 2007. **41**(38): p. 8658-8668.
78. Bahreini, R., et al., *Gasoline emissions dominate over diesel in formation of secondary organic aerosol mass.* Geophys. Res. Lett., 2012. **39**(6): p. L06805.
79. Gentner, D.R., et al., *Elucidating secondary organic aerosol from diesel and gasoline vehicles through detailed characterization of organic carbon emissions.* Proceedings of the National Academy of Sciences, 2012. **109**(45): p. 18318-18323.
80. Canagaratna, M.R., et al., *Chase studies of particulate emissions from in-use New York city vehicles.* Aerosol Science & Technology, 2004. **38**: p. 555-573, 10.1080/02786820490465504.
81. Gross, D.S., et al., *Stability of single particle tracers for differentiating between heavy- and light-duty vehicle emissions.* Atmospheric Environment, 2005. **39**(16): p. 2889-2901.
82. Pierson, W.R., et al., *Real-world automotive emissions—Summary of studies in the Fort McHenry and Tuscarora mountain tunnels.* Atmospheric Environment, 1996. **30**(12): p. 2233-2256.
83. Ban-Weiss, G.A., et al., *Size-resolved particle number and volume emission factors for on-road gasoline and diesel motor vehicles.* Journal of Aerosol Science, 2010. **41**(1): p. 5-12.
84. Sun, Y.L., et al., *Characterization of near-Highway Submicron Aerosols in New York City with a High-Resolution Time-of-Flight Aerosol Mass Spectrometer.* Atmos. Chem. Phys. Discuss., 2011. **11**: p. 30719-30755.
85. Massoli, P., et al., *Pollution gradients and chemical characterization of particulate matter from vehicular traffic near major roadways: results from the 2009 Queens College Air Quality study in NYC.* Aerosol Sci. Tech. (submitted), 2011.
86. Canagaratna, M.R., et al., *Evolution of Vehicle Exhaust Particles in the Atmosphere.* Journal of the Air & Waste Management Association, 2010. **60**(10): p. 1192-1203.
87. Beddows, D.C.S. and R.M. Harrison, *Comparison of average particle number emission factors for heavy and light duty vehicles derived from rolling chassis dynamometer and field studies.* Atmospheric Environment, 2008. **42**(34): p. 7954-7966.
88. Schneider, J., et al., *Nucleation Particles in Diesel Exhaust: Composition Inferred from In Situ Mass Spectrometric Analysis.* Environmental Science & Technology, 2005. **39**(16): p. 6153-6161.
89. Robert, M.A., et al., *Size and Composition Distributions of Particulate Matter Emissions: Part 1—Light-Duty Gasoline Vehicles.* Journal of the Air & Waste Management Association, 2007. **57**(12): p. 1414-1428.
90. Baynard, T., et al., *Design and Application of a Pulsed Cavity Ring-Down Aerosol Extinction Spectrometer for Field Measurements.* Aerosol Science and Technology, 2007. **41**(4): p. 447-462.

91. Lack, D., et al., *Aerosol Absorption Measurement using Photoacoustic Spectroscopy: Sensitivity, Calibration, and Uncertainty Developments.* Aerosol Science & Technology, 2006. **40**: p. 697-708.
92. DeCarlo, P.F., et al., *Particle Morphology and Density Characterization by Combined Mobility and Aerodynamic Diameter Measurements. Part 1: Theory.* Aerosol Science and Technology, 2004. **38**(12): p. 1185-1205.
93. Middlebrook, A.M., et al., *Evaluation of Composition-Dependent Collection Efficiencies for the Aerodyne Aerosol Mass Spectrometer using Field Data.* Aerosol Science and Technology, 2012. **46**: p. 258–271.
94. Timko, M.T., et al., *Sampling Artifacts from Conductive Silicone Tubing.* Aerosol Science and Technology, 2009. **43**(9): p. 855-865.
95. Zhang, Q., et al., *Deconvolution and Quantification of Hydrocarbon-like and Oxygenated Organic Aerosols Based on Aerosol Mass Spectrometry.* Environmental Science & Technology, 2005. **39**(13): p. 4938-4952.
96. Jakober, C.A.M.A.R., S.G. Riddle, H. Destaillats, M. J. Charles, P.G. Green, M.J. Kleeman, *Carbonyl Emissions from Gasoline and Diesel Motor Vehicles.* Environmental Science & Technology, 2008. **42**(13): p. 4697-4703.
97. Lanz, V.A., et al., *Source apportionment of submicron organic aerosols at an urban site by factor analytical modelling of aerosol mass spectra.* Atmos. Chem. Phys., 2007. **7**(6): p. 1503-1522.
98. Lanz, V.A., et al., *Source Attribution of Submicron Organic Aerosols during Wintertime Inversions by Advanced Factor Analysis of Aerosol Mass Spectra.* Environmental Science & Technology, 2007. **42**(1): p. 214-220.
99. Hersey, S.P., et al., *The Pasadena Aerosol Characterization Observatory (PACO): chemical and physical analysis of the Western Los Angeles basin aerosol.* Atmos. Chem. Phys., 2011. **11**(15): p. 7417-7443.
100. Crippa, M., et al., *Wintertime aerosol chemical composition and source apportionment of the organic fraction in the metropolitan area of Paris.* Atmos. Chem. Phys., 2013. **13**(2): p. 961-981.
101. May, A.A., et al., *Gas-particle partitioning of primary organic aerosol emissions: (1) Gasoline vehicle exhaust.* Atmospheric Environment, 2013. **77**: p. 128-139.
102. Gundel, L.A., et al., *Direct determination of the phase distributions of semivolatile polycyclic aromatic-hydrocarbons using annular denuders.* Atmospheric Environment, 1995. **29**(14): p. 1719-1733.
103. Birch, M.E. and R.A. Cary, *Elemental carbon-based method for monitoring occupational exposures to particulate diesel exhaust.* Aerosol Science and Technology, 1996. **25**(3): p. 221-241.
104. NIOSH, ed. *NIOSH Manual of Analytical Methods*. 4 ed. 1996, National Institute for Occupational Safety and Health: Cincinnati, OH.
105. Karanasiou, A., et al., *On the quantification of atmospheric carbonate carbon by thermal/optical analysis protocols.* Atmospheric Measurement Techniques, 2011. **4**(11): p. 2409-2419.
106. EPA, *Analysis of Particulate Matter Emissions from Light-Duty Gasoline Vehicles in Kansas City*. 2008, United States Environmental Protection Agency.
107. Cappa, C.D., *A model of aerosol evaporation kinetics in a thermodenuder.* Atmospheric Measurement Techniques, 2010. **3**(3): p. 579-592.

108. Bond, T.C., et al., *A technology-based global inventory of black and organic carbon emissions from combustion.* Journal of Geophysical Research-Atmospheres, 2004. **109**(D14).
109. Hildemann, L.M., G.R. Markowski, and G.R. Cass, *Chemical-Composition of Emissions from Urban Sources of Fine Organic Aerosol.* Environmental Science & Technology, 1991. **25**(4): p. 744-759.
110. Schauer, J.J., et al., *Source apportionment of airborne particulate matter using organic compounds as tracers.* Atmospheric Environment, 1996. **30**(22): p. 3837-3855.
111. CARB, *Characterizatoin of Driving Patterns and Emissions from Light-Duty Vehicles in California, Final Report*. 1993, California Air Resources Board.
112. CARB, *California Phase 2 Reformulated Gasoline Specifications*. 1991, California Air Resources Board.
113. OEHHA, *Public Health Goal for Methyl Tertiary Butyl Ether (MTBE) in Drinking Water*, in *Executive Order D-5-99*. 1999, California EPA: Office of Environmental Health Hazard Assessment. p. 136.
114. McEnally, C.S. and L.D. Pfefferle, *The effects of dimethyl ether and ethanol on benzene and soot formation in ethylene nonpremixed flames.* Proceedings of the Combustion Institute, 2007. **31**: p. 603-610.
115. Healy, R.M., et al., *Effect of Relative Humidity on Gas/Particle Partitioning and Aerosol Mass Yield in the Photooxidation of p-Xylene.* Environmental Science & Technology, 2009. **43**(6): p. 1884-1889.
116. Blando, J.D. and B.J. Turpin, *Secondary organic aerosol formation in cloud and fog droplets: a literature evaluation of plausibility.* Atmospheric Environment, 2000. **34**(10): p. 1623-1632.
117. Cocker, D.R., et al., *The effect of water on gas-particle partitioning of secondary organic aerosol. Part I: alpha-pinene/ozone system.* Atmospheric Environment, 2001. **35**(35): p. 6049-6072.
118. Snoeyink, V.L. and R.S. Summers, *Adsorption of organic compounds.* Water quality and treatment, 1990. **5**.
119. Schauer, J.J., et al., *Measurement of emissions from air pollution sources. 5. C-1-C-32 organic compounds from gasoline-powered motor vehicles.* Environmental Science & Technology, 2002. **36**(6): p. 1169-1180.
120. Grosjean, D., E. Grosjean, and A.W. Gertler, *On-road emissions of carbonyls from light-duty and heavy-duty vehicles.* Environmental Science & Technology, 2001. **35**(1): p. 45-53.
121. Kean, A.J., et al., *On-road measurement of carbonyls in California light-duty vehicle emissions.* Environmental Science & Technology, 2001. **35**(21): p. 4198-4204.
122. Kristensson, A., et al., *Real-world traffic emission factors of gases and particles measured in a road tunnel in Stockholm, Sweden.* Atmospheric Environment, 2004. **38**(5): p. 657-673.
123. Roth, C.M., K.U. Goss, and R.P. Schwarzenbach, *Sorption of a diverse set of organic vapors to diesel soot and road tunnel aerosols.* Environmental Science & Technology, 2005. **39**(17): p. 6632-6637.
124. Keene, W.C. and J.N. Galloway, *The biogeochemical cycling of formic and acetic acids through the troposphere - An overview of current understanding.* Tellus B, 1988. **40**: p. 322-334.

125. Chebbi, A. and P. Carlier, *Carboxylic acids in the troposphere, occurrence, sources, and sinks: A review.* Atmospheric Environment, 1996. **30**(24): p. 4233-4249.
126. Khare, P., et al., *Atmospheric formic and acetic acids: An overview.* Reviews of Geophysics, 1999. **37**(2): p. 227-248.
127. Veres, P.R., et al., *Evidence of rapid production of organic acids in an urban air mass.* Geophysical Research Letters, 2011. **38**.
128. Lee, P.K.H., et al., *Identification of the major sources contributing to PM2.5 observed in Toronto.* Environmental Science & Technology, 2003. **37**(21): p. 4831-4840.
129. Kesselmeier, J., *Exchange of short-chain oxygenated volatile organic compounds (VOCs) between plants and the atmosphere: A compilation of field and laboratory studies.* Journal of Atmospheric Chemistry, 2001. **39**(3): p. 219-233.
130. Veres, P., et al., *Measurements of gas-phase inorganic and organic acids from biomass fires by negative-ion proton-transfer chemical-ionization mass spectrometry.* Journal of Geophysical Research-Atmospheres, 2010. **115**.
131. Kawamura, K. and I.R. Kaplan, *Motor Exhaust Emissions as a Primary Source for Dicarboxylic-Acids in Los-Angeles Ambient Air.* Environmental Science & Technology, 1987. **21**(1): p. 105-110.
132. Kawamura, K., L.L. Ng, and I.R. Kaplan, *Determination of Organic-Acids (C1-C10) in the Atmosphere, Motor Exhausts, and Engine Oils.* Environmental Science & Technology, 1985. **19**(11): p. 1082-1086.
133. Paulot, F., et al., *Importance of secondary sources in the atmospheric budgets of formic and acetic acids.* Atmospheric Chemistry and Physics, 2011. **11**(5): p. 1989-2013.
134. Talbot, R.W., et al., *Atmospheric Geochemistry of Formic and Acetic-Acids at a Mid-Latitude Temperate Site.* Journal of Geophysical Research-Atmospheres, 1988. **93**(D2): p. 1638-1652.
135. Bertram, T.H., et al., *A field-deployable, chemical ionization time-of-flight mass spectrometer.* Atmos. Meas. Tech., 2011. **4**: p. 1963-1987.
136. Veres, P., et al., *Measurements of gas-phase inorganic and organic acids from biomass fires by negative-ion proton-transfer chemical-ionization mass spectrometry.* Journal of Geophysical Research-Atmospheres, 2010. **115**: p. -.
137. Ryerson, T.B., et al., *The 2010 California Research at the Nexus of Air Quality and Climate Change (CalNex) field study.* Journal of Geophysical Research-Atmospheres, 2012. **submitted**.
138. Wang, Z., et al., *Protein carbamylation links inflammation, smoking, uremia and atherogenesis.* Nature Medicine, 2007. **13**(10): p. 1176-1184.
139. Roberts, J.M., et al., *Isocyanic acid in the atmosphere and its possible link to smoke-related health effects.* Proceedings of the National Academy of Sciences of the United States of America, 2011. **108**(22): p. 8966-8971.
140. Lee, C.K. and J.M. Manning, *Kinetics of the Carbamylation of the Amino Groups of Sickle Cell Hemoglobin by Cyanate.* Journal of Biological Chemistry, 1973. **248**(16): p. 5861-5865.
141. Mydel, P., et al., *Carbamylation-Dependent Activation of T Cells: A Novel Mechanism in the Pathogenesis of Autoimmune Arthritis.* The Journal of Immunology, 2010. **184**(12): p. 6882-6890.
142. Roberts, J.M., et al., *Measurement of HONO, HNCO, and other inorganic acids by negative-ion proton-transfer chemical-ionization mass spectrometry (NI-PT-CIMS):*

application to biomass burning emissions. Atmos. Meas. Tech. Discuss., 2010. **3**(1): p. 301-331.
143. Hansson, K.M., et al., *Formation of HNCO, HCN, and NH3 from the pyrolysis of bark and nitrogen-containing model compounds.* Combustion and Flame, 2004. **137**(3): p. 265-277.
144. Borduas, N., J.P.D. Abbatt, and J.G. Murphy, *Gas Phase Oxidation of Monoethanolamine (MEA) with OH Radical and Ozone: Kinetics, Products, and Particles.* Environmental Science & Technology, 2013. **47**(12): p. 6377-6383.
145. Wentzell, J.J.B., et al., *Measurements of Gas phase Acids in Diesel Exhaust: A Relevant Source of HNCO?* Environmental Science & Technology, 2013. **47**(14): p. 7663-7671.
146. Young, P.J., et al., *Isocyanic acid in a global chemistry transport model: Tropospheric distribution, budget, and identification of regions with potential health impacts.* Journal of Geophysical Research-Atmospheres, 2012. **117**.
147. Koebel, M. and M. Elsener, *Oxidation of diesel-generated volatile organic compounds in the selective catalytic reduction process.* Industrial & Engineering Chemistry Research, 1998. **37**(10): p. 3864-3868.
148. EPA, *Inventory of U.S. Greenhouse Gas Emissions and Sinks: 1990-2011*. 2013, Environmental Protection Agency.
149. Cant, N.W., D.C. Chambers, and I.O.Y. Liu, *The reduction of NO by CO in the presence of water vapour on supported platinum catalysts: formation of isocyanic acid (HNCO) and ammonia.* Applied Catalysis B-Environmental, 2003. **46**(3): p. 551-559.
150. Dümpelmann, R., N.W. Cant, and D.L. Trimm, *Formation of isocyanic acid during the reaction of mixtures of NO, CO and H2 over supported platinum catalysts.* Applied Catalysis B: Environmental, 1995. **6**(4): p. L291-L296.
151. Cant, N.W., et al., *Formation and reactions of isocyanic acid during the catalytic reduction of nitrogen oxides.* Topics in Catalysis, 2000. **10**(1-2): p. 13-20.
152. Chambers, D.C., D.E. Angove, and N.W. Cant, *The formation and hydrolysis of isocyanic acid during the reaction of NO, CO, and H-2 mixtures on supported platinum, palladium, and rhodium.* Journal of Catalysis, 2001. **204**(1): p. 11-22.
153. Cant, N.W., D.C. Chambers, and I.O.Y. Liu, *The formation of isocyanic acid during the reaction of NH3 with NO and excess CO over silica-supported platinum, palladium, and rhodium.* Journal of Catalysis, 2005. **231**(1): p. 201-212.
154. Cant, N.W., D.C. Chambers, and I.O.Y. Liu, *The formation of isocyanic acid and ammonia during the reduction of NO over supported platinum group metals.* Catalysis Today, 2004. **93-5**: p. 761-768.
155. Austen, T.C., et al., *Characterization of driving patterns and emissions from light-duty vehicles in California*. 1993, California Air Resources Board.
156. Bertram, T.H., et al., *A field-deployable, chemical ionization time-of-flight mass spectrometer.* Atmospheric Measurement Techniques, 2011. **4**(7): p. 1471-1479.
157. Paulot, F., et al., *Isoprene photooxidation: new insights into the production of acids and organic nitrates.* Atmospheric Chemistry and Physics, 2009. **9**(4): p. 1479-1501.
158. Bass, L., et al., *Ion-Polar Molecule Collisions - Modification of Average Dipole Orientation Theory - Cos-Theta Model.* Chemical Physics Letters, 1975. **34**(1): p. 119-122.
159. Su, T. and M.T. Bowers, *Theory of Ion-Polar Molecule Collisions - Comparison with Experimental Charge-Transfer Reactions of Rare-Gas Ions to Geometric Isomers of*

Difluorobenzene and Dichloroethylene. Journal of Chemical Physics, 1973. **58**(7): p. 3027-3037.
160. Aiken, A.C., et al., *O/C and OM/OC ratios of primary, secondary, and ambient organic aerosols with high-resolution time-of-flight aerosol mass spectrometry.* Environmental Science & Technology, 2008. **42**(12): p. 4478-4485.
161. Forestieri, S.D., et al., *Real-Time Black Carbon Emission Factor Measurements from Light Duty Vehicles.* Environmental Science & Technology, 2013.